UNIVERSITÀ
DEGLI STUDI
DI PADOVA

Sede Amministrativa: Università degli Studi di Padova

Dipartimento di Scienze Chimiche

CORSO DI DOTTORATO DI RICERCA IN: Scienze Molecolari
CURRICULUM: Scienze Farmaceutiche
CICLO: XXXI

Design, Synthesis and Characterization of Polycyclic and Heteropolycyclic Compounds as Biologically Active Agents

Coordinatore: Ch.mo Prof. Leonard Jan Prins
Supervisore: Prof.ssa Maria Grazia Ferlin

Dottorando: Matteo Dal Prà

A chi ha sempre creduto in me

Contents

Riassunto dell'attività svolta 1

Summary 5

Organization of the thesis 9

Introduction 11

CHAPTER 1

Synthesis and preliminary anti-inflammatory and anti-bacterial evaluation of some diflunisal aza-analogs 15

CHAPTER 2

In vitro and in vivo anticancer activity of anti-tubulin fluorinated 7-phenyl-pyrroloquinolinones 55

CHAPTER 3

Targeting RORs nuclear receptors by novel synthetic steroidal inverse agonists for autoimmune disorders 91

CHAPTER 4

In silico screening as a tool to identify new anticancer agents acting in the Notch pathway 137

CHAPTER 5

Rational design and synthesis of 2,3,4,9-tetrahydro-1H-β-carboline derivatives as trypanothione reductase inhibitors 161

Participation to congresses 195

Riassunto dell'attività svolta

L'attività di ricerca descritta in questa tesi di dottorato si inserisce all'interno di progetti avviati con diversi ricercatori presso Università sia italiane che estere e hanno come scopo principale l'identificazione, la sintesi e la validazione di nuove piccole molecole quali potenziali agenti farmacologici per il trattamento di diverse patologie: batteriche, antiparassitarie, tumorali e autoimmuni. I progetti presentano delle caratteristiche marcatamente multidisciplinari e questo ha permesso di estendere le mie esperienze ad ambiti non strettamente inerenti alla mia formazione curriculare e conseguentemente di acquisire consapevolezza della complessità della chimica farmaceutica nelle sue varie accezioni.

La mia principale attività è consistita nella progettazione e sintesi chimica di composti organici a struttura policiclica ed etero-policiclica applicando metodi di sintesi classici ed avanzati. La diversità dei progetti mi ha indotto ad affrontare e approfondire lo studio di nuove procedure di sintesi organica fondamentali per l'ottenimento di una grande varietà di strutture chimiche proposte come potenziali farmaci. Accanto allo studio per la progettazione dei percorsi sintetici, questa tesi di dottorato è contraddistinta dalla grande mole di lavoro sperimentale in laboratorio come si evince dall'elevato numero di composti intermedi e finali ottenuti e che sono stati purificati e compiutamente caratterizzati da un punto di vista chimico-fisico. Pertanto, anche le mie competenze riguardo l'uso di strumentazioni presenti e non nel Dipartimento di Scienze del Farmaco si sono notevolmente consolidate, in particolare ho potuto approfondire le tecniche di indagine spettroscopica più diffuse ed essenziali nell'ambito della chimica farmaceutica come la spettroscopia NMR e la spettrometria di massa. La maggior parte dei composti da me preparati in laboratorio sono già stati studiati anche per la loro attività biologica allo scopo di valutarne il potenziale farmacologico e per questo sono molto grato ai ricercatori con cui ho proficuamente collaborato.

Segue una breve descrizione dei risultati ottenuti nei vari capitoli.

Capitolo 1. Diflunisal, un noto farmaco antiinfiammatorio della categoria dei salicilati, è stato recentemente riproposto come agente in grado di sensibilizzare lo *Staphylococcus aureus* meticillino-resistente all'azione della meticillina. I principali problemi legati all'utilizzo di questo farmaco nella terapia antibiotica sono legati al meccanismo d'azione

antiinfiammatorio, che può condurre a lesioni gastrointestinali anche gravi, e alla scarsa solubilità in acqua. Per queste ragioni abbiamo progettato e sintetizzato degli aza-analoghi del diflunisal, seguendo una via sintetica che prevede l'ottenimento di intermedi ossazolici e l'applicazione della reazione di Diels-Alder per generare così una libreria di analoghi acidi idrossi-piridin-carbossilici variamente sostituiti. A seguito della valutazione biologica i composti sintetizzati non presentano attività citotossica ed alcuni di loro presentano interessanti proprietà antinfiammatorie e soprattutto antibatteriche, sensibilizzando i batteri *S. aureus*, *Streptococcus pyogenes*, *Enterococcus faecium* e *Pseudomonas aeruginosa* all'azione di alcuni antibiotici.

Capitolo 2. I 7-fenilpirrolochinolinoni (7-PPyQ) appartengono alla famiglia dei pirrolochinolinoni, una classe di composti che ha rivelato in anni recenti interessanti proprietà antitumorali. In particolare, alcuni derivati del 7-PPyQ agiscono come forti inibitori della polimerizzazione della tubulina e dimostrano grande affinità per il sito della colchicina. I dati ottenuti dallo studio di numerosi derivati hanno consentito la comprensione delle relazioni struttura-attività. Il problema principale di questi composti è dovuto alla scarsa stabilità metabolica in seguito ad ossidazioni multiple. Per questo motivo sono stati progettati e sintetizzati alcuni derivati inserendo l'atomo di fluoro in diverse posizioni allo scopo di esplorare l'influenza di questo elemento sull'attività biologica e sulla stabilità metabolica. La valutazione biologica comprende i test di citotossicità *in vitro* e antitumorale *in vivo* su modello murino di melanoma., saggi di inibizione della polimerizzazione della tubulina e ovviamente i test *in vitro* di stabilità metabolica.

Capitolo 3. Il recettore nucleare RORγt, un'isoforma del recettore orfano correlato ai recettori dell'acido retinoico ROR, è stato identificato come principale responsabile dell'attività e dello sviluppo dei linfociti T-helper 17 (T_H17), i quali sono implicati nella patogenesi di alcune malattie autoimmuni. Questo rende RORγt un bersaglio ideale per il trattamento di queste patologie. Esplorando la struttura dei ligandi steroidei naturali e sintetici di questo recettore e dei ligandi arotenoidi, è stata progettata una struttura ibrida come *lead compound* e generato una piccola libreria di analoghi, sfruttando in particolar modo le reazioni di Friedel-Crafts e di coupling di Suzuki. Saggi di citotossicità, attività estrogenica e modulazione dell'attività del recettore RORγt sono stati effettuati. I composti risultano essere meno potenti dell'acido ursolico, agonista inverso usato come riferimento, ma rappresentano un buon punto di partenza per lo sviluppo di nuovi agonisti inversi del recettore RORγt, a struttura steroidea.

Capitolo 4. L'attività descritta in questo capitolo è stata possibile grazie ad un periodo di 6 mesi trascorso presso il laboratorio di modellistica molecolare del professor Andrea Brancale presso Cardiff University (UK). Il recettore trans-membrana Notch e il suo sistema di *signalling* sono fattori chiave nello sviluppo e mantenimento dell'omeostasi in molti tessuti. Un'attività irregolare di questo sistema rappresenta uno dei principali *driver* nella patogenesi e progressione di molte forme tumorali, in particolar modo leucemiche. L'attività di Notch è fortemente dipendente dal contesto, infatti presenta caratteristiche sia di oncogene che di oncosoppressore. La sua modulazione rappresenta quindi una possibilità terapeutica concreta. Ad oggi, non esistono molecole in clinica che agiscono direttamente sul recettore Notch, per questo motivo prendendo in esame due diversi *binding sites*, è stato effettuato uno studio di modellistica molecolare adiuvato da simulazioni di docking per identificare nuovi possibili ligandi. Sono stati realizzati diversi studi di *virtual screening*, sia con approccio *structure-based* che *ligand-based*, e 62 molecole provenienti da diversi database commerciali, sono state selezionate per la valutazione biologica. Dai risultati ottenuti è stato possibile identificare due *hit compounds*, i quali verranno sottoposti a ulteriore indagine in futuri studi di *hit-to-lead optimization*.

Capitolo 5. La malattia di Chagas è una malattia tropicale negletta causata dal protozoo *Tripanosoma cruzi*. Attualmente, viene trattata mediante somministrazione di benznidazolo o nifurtimox, due vecchi agenti antiparassitari, che presentano molti effetti collaterali e limitata efficacia, soprattutto nella fase cronica dell'infezione. Un possibile bersaglio molecolare per il trattamento dell'infezione è rappresentato dall'enzima Tripanotione Reduttasi (TryR), responsabile della difesa del parassita contro lo stress ossidativo. L'inibizione di questo enzima incrementa la suscettibilità di *T. cruzi* nei confronti dei farmaci antiparassitari, probabilmente consentendo una riduzione del dosaggio e un maggiore successo della terapia. Uno *structure-based virtual screening* sulla struttura di TryR è stato effettuato confermando lo scaffold β-carbolinico come cruciale per la progettazione razionale di nuovi inibitori. La sintesi multi-step, comprendente reazione di Pictet-Spengler e coupling ammidico, è stata completata con successo per 7 derivati e al momento i composti sono sottoposti a valutazione biologica presso l'Universidad Metropolitana de Ciencias de la Educacion (UMCE), Santiago, Chile.

Summary

The research projects described in this thesis are part of numerous collaborations with different scientific groups of italian and foreign universities but all aim at identifying, synthesising and validating new chemical structures as potential pharmacological agents for the treatment of several diseases (bacterial, cancerous, autoimmune or parasitic). All the projects are extremely multidisciplinary, and this gave me the chance to extend my knowledge towards new subjects, not strictly related to my educational background and at the same time to understand the complexity of medicinal chemistry, in all its facets.

My principal task was to design and synthesise new chemical compounds with a polycyclic and hetero-polycyclic structure employing conventional and non-conventional synthetic methodologies. The high degree of diversity of these projects lead me to study and explore a considerable variety of chemical structures and functional groups, allowing me to learn and understand a very complex matter, but at the same time very fascinating, such as the organic chemistry applied to the pharmaceutical area.

Beside the more theoretical knowledges related to the synthesis planning, this thesis is also marked by the strong impact and effort due to the laboratory practical for the preparation and physico-chemical characterization of the synthesised derivatives, which allowed me to deepen the understanding of fundamental spectroscopic and spectrometric techniques such as NMR and mass spectrometry. Moreover, the biological evaluation of the synthesised compounds played a crucial role in all this works and I am very grateful to the researchers with whom I had the chance to collaborate.

A brief description of the major results presented in the various chapters follows.

Chapter 1. Diflunisal, an old anti-inflammatory drug with a salicylic structure, has been recently repurposed for its capacity of sensitising methicillin-resistant *Staphylococcus aureus* to the action of methicillin. The major drawbacks related to the use of this drug in the antibacterial therapy are related to the anti-inflammatory mechanism of action, which can lead to gastrointestinal lesions, and to the poor water solubility. For this reasons we designed and synthesised some aza-analogs of diflunisal, following a synthetic route involving the obtainment of key oxazole intermediates and which exploit the Diels-Alder reaction to generate a small library of hydroxy-pyridine-carboxylic acids, variously substituted. From the biological investigation, the synthesised derivatives showed no cytotoxic activity, but some of them presented interesting anti-inflammatory and anti-

bacterial properties, sensitising the bacteria *S. aureus*, *Streptococcus pyogenes*, *Enterococcus faecium* e *Pseudomonas aeruginosa* to the action of some common antibiotics.

Chapter 2. In the last ten years, we have been developing 7-phenyl-pyrroloquinolinones derivatives as a class of compounds which showed interesting anticancer properties. These compounds act as tubulin polymerization inhibitors and numerous derivatives have already been synthesised allowing the comprehension of the structure-activity relationships. The major problem of these compounds is their poor metabolic stability due to multiple oxidations. For this reason, we designed and synthesised some fluorinated derivatives to explore the effect of this element on the biological activity and on the metabolic stability. The biological evaluation includes *in vitro* cytotoxic activity, tubulin polymerization inhibition assays, metabolic stability test and two *in vivo* experiment on a murine model of melanoma.

Chapter 3. RORγt, an isoform of the retinoic acid-related orphan receptor gamma has been identified as the master regulator of T-helper 17 (T_H17) cell function and development, making it an attractive target for the treatment of autoimmune disorders. By exploring the structures of natural and synthetic steroidal ligands and of arotinoids ligands, we designed a hybrid structure as lead compound and we generated a small library of analogs, taking advantage of the Friedel-Crafts and Suzuki reactions. Cytotoxic assays, estrogenic activity and modulation of RORγt activity were evaluated. The compounds demonstrated to be less potent than ursolic acid used as reference, but still represent a good starting point in the development of RORγt inverse agonists with a steroidal scaffold.

Chapter 4. The work described in this chapter was performed during a 6-months research period spent in the molecular modelling laboratory of professor Andrea Brancale at Cardiff University (UK). The trans-membrane receptor Notch and its signalling system are key factors in the development and homeostasis maintenance of most tissues. An irregular activity of this system represents one of the principal driver in the pathogenesis and progression of cancer diseases, especially leukemia. Notch activity is highly context-dependent; indeed, it shows oncogenic and tumour-suppressor roles. Thus, its modulation represents a concrete therapeutic possibility, but still no molecules that directly interact with Notch receptor are proceeding in the clinical phases at the moment. For this reasons, we decided to take in consideration two different binding sites and to perform a molecular modelling study to identify new possible ligands. Different virtual screening study were

performed, both structure-based and ligand-based and at the end, 62 molecules from different commercial database were selected and purchased for the biological evaluation. From the biological screening, it was possible to identify two new hit compounds, which will be subject to further hit-to lead optimization studies.

Chapter 5. Chagas disease is a neglected tropical disorder caused by the protozoan *Trypanosoma cruzi.* The actual treatment consists in the administration of benznidazole or nifurtimox, two old anti-parasitic agents, which present several side effects and limited efficacy, especially in the chronic phase of the disease. An interesting molecular target for the treatment of the infection is represented by the enzyme Trypanothione reductase (TryR), which is responsible for the parasite's defence against oxidative stress. TryR inhibition increases the susceptibility of T. cruzi towards anti-parasitic drugs, probably allowing a reduction in the dosage and thus a major success of the therapy. A virtual screening study on the structure of TryR was performed, and again the β-carboline scaffold was confirmed as a key core for the rational design of new inhibitors. The multistep synthesis, involving Pictet-Spengler and amidic coupling reactions, of 7 derivatives was successfully completed, and the biological evaluation is ongoing at the Universidad Metropolitana de Ciencias de la Educacion (UMCE), Santiago, Chile.

Organization of the thesis

This thesis is organized in five chapters and each of them is related to a specific and self-standing medicinal chemistry topic. For this reason, this type of organization was preferred over a more traditional, monograph-style layout. Each chapter corresponds to an already published paper (Chapters 1 and 3), to a submitted paper (Chapter 2) or to a manuscript in preparation (Chapter 4-5) and represents a preliminary but relatively complete piece of research work. As medicinal chemistry is an interdisciplinary research, my contribution was mostly focused on the design, chemical synthesis and characterisation of all new derivatives, and in some cases on the molecular modelling sections. The fundamental contribution of the other participants to this research is acknowledged by their names as co-authors in each individual chapter. I hope the benefits of such organization outweigh its disadvantages.

Introduction

Medicinal chemistry still represents one of the most investigated and studied chemical sciences. The reason for the high interest in this field is the strong impact that it has on human health, providing new strategies and approaches to fight "new and old" diseases. The principal aim of medicinal chemistry is to discover new pharmaceutical agents which can be divided in two main families: small organic molecules, representing the largest part of all pharmacological entities and "biologics". Focusing on small organic molecules, medicinal chemistry by its nature is exceptionally multidisciplinary, requiring deep knowledge of organic chemistry and synthesis planning but always with the aim of finding compounds with a biological effect, thus also chemical biology, enzymology and structural biology expertise are fundamental.

In this thesis, I will present five different medicinal chemistry projects hoping to highlight how the chemical and biological efforts have to meet in order to reach a specific goal.

My personal contribution to all this work entitled "*Design, Synthesis and Characterization of Polycyclic and Heteropolycyclic Compounds as Biologically Active Agents*" was in the phases of *design*, *chemical synthesis and physico-chemical characterization*.

The adequate design of new potential biologically active compounds is essential, and several approaches have been identified and studied, furnishing important guidelines for the effectiveness of this first phase. In particular, a clever design is important because it helps reducing the time required to find a molecule with the potentiality to become a drug, a process which is known to be onerous and long-standing. One strategy to speed-up the drug discovery process is the so-called drug repurposing or repositioning, an approach which finds new uses for old drugs. This process consists in testing already approved drugs in order to find new potential pharmacological applications. This has the advantage that pharmacodynamic, pharmacokinetic and toxicity studies are usually already performed and available, conferring the chance of having a chemical entity as a starting point to develop new structures. In Chapter 1 (*Synthesis and preliminary anti-inflammatory and anti-bacterial evaluation of some diflunisal aza-analogs*), an example on how we decided to modify the structure of the NSAID diflunisal in order to develop new agents endowed with both anti-inflammatory and anti-bacterial properties, improved water solubility but devoid of cyclooxygenase activity, is given.

Another strategy to design new biologically active agents is to exploit the structure of natural compounds with known biological activity and modifying the chemical groups according to the results obtained by the biological evaluation in order to increase potency and efficacy. In this respect, the last effort of the ten-years research work on the development of anticancer 7-phenylpyrrolequinolinones is presented in Chapter 2 (*In vitro and in vivo anticancer activity of anti-tubulin fluorinated 7-phenyl-pyrroloquinolinones*). Furthermore, by means of a structure-based approach founded on hybridization of chemical structures, it is possible to mix structures of different known modulators for a specific target and to rationalize a new chemical entity with the potential to become a hit compound. In Chapter 3 (*Targeting RORs nuclear receptors by novel synthetic steroidal inverse agonists for autoimmune disorders*), there is an example on how we mix the structure of known steroidal natural ligands with arotinoids molecules to develop RORγ inverse agonists for the treatment of autoimmune disorders.

On the other hand, this strategies are not always working because often even a little modification on a chemical structure may be totally detrimental for the activity because the rationalization between chemical modifications and biological behaviour is difficult to predict. For this reason, in the recent years, the drug discovery process has started to rely on computational techniques and docking simulations in order to find new hit compounds in a fast but random way. These techniques are based on molecular docking which simulates and enables the prediction of the conformation and the interaction mode of a ligand with its target. One of the techniques which take advantage of molecular docking is virtual screening. Virtual screening is used to search libraries of small molecules, in a fastest and more economically way than high-throughput screening, in order to identify structures which are most likely to bind to the target. Different virtual screening approaches exist, but the most studied and performed are the Structure Based Virtual Screening (SBVS) and the Ligand-Based Virtual Screening (LBVS). The first uses the 3D structure of the target to filter a library of small molecules through molecular docking studies. The main disadvantage of this approach is that the crystal structure of the target has to be determined and although protein sequences are easily determined, only a minor percentage of all protein discovered have been crystallised. Due to this complication, homology modelling methods have been improved to predict the three-dimensional structure of proteins using their amino acid sequence.

On its part, ligand-based approach uses the 3D structure of a known determined ligand to filter a library of small molecules to find molecules with similar shape, electronic and sterical features. This might help in finding apparently dissimilar structures which may bind to the same target. Examples on how these techniques can be useful in the search for new molecular structures to target a specific protein or enzyme are given in Chapter 4 (*In silico screening as a tool to identify new anticancer agents acting in the Notch pathway*), which describes the work performed during a 6-month research period at the molecular modelling laboratory of professor Andrea Brancale at Cardiff University (UK). In Chapter 5 (*Rational design and synthesis of 2,3,4,9-tetrahydro-1H-β-carboline derivatives as trypanothione reductase inhibitors*) a molecular modelling study is described with the aim of rationally design new trypanothione reductase inhibitors for the treatment of Chagas disease.

Regarding the *chemical synthesis* part, in all the chapters that involve it, a remarkable attention was payed to *polycyclic* and *heteropolycyclic structures* which have always played a key role in medicinal chemistry. They can be usually divided in carbocyclic or heterocyclic systems, the former being totally composed by C atoms while the latter contain at least one heteroatom such as N, O, or S. Their importance have always been highlighted because the rigidity of a ring structure is able to maintain the binding groups in the correct position ensuring the "freezing" of the active conformation and reducing or eliminating the rotational freedom. Moreover, the minor loss of entropy freedom when a rigid cyclic structure bind to its target is always favourable. In the case of a more flexible acyclic drug when the binding process takes place, a significant loss in entropy freedom is paid because the small molecule can no longer adopt all the other explorable conformations. Furthermore, the cyclic system itself can participate in the binding process through the establishment of hydrophobic interactions or in the case of heterocycles also polar or ionic bonding. The presence of a heterocycle also influences and usually is beneficial for drug's aqueous solubility ensuring an appropriate balance between hydrophilicity and hydrophobicity which is vital for membrane crossing and solubility in gastrointestinal environment or blood.

CHAPTER 1

Synthesis and preliminary anti-inflammatory and anti-bacterial evaluation of some diflunisal aza-analogs[1]

Synopsis

Diflunisal, a classical nonsteroidal anti-inflammatory agent, has recently been repurposed for its anti-virulence properties against methicillin-resistant *Staphylococcus aureus*. The effective synthesis of some aza-analogs of the anti-inflammatory drug diflunisal was carried out following the route involving key oxazole intermediates to obtain *o*- and *m*-hydroxypyridinecarboxylic acid derivatives. The newly synthesized diflunisal aza-analogs did not exhibit cytotoxic activity up to 80 μM and some of them reported anti-inflammatory activities, damping the levels of pro-inflammatory cytokines and PGs induced by bacterial lipopolysaccharide in human primary macrophages. Ten of Diflunisal aza-analogs were found to have interesting antibacterial activity, sensitizing *S. aureus*, *Streptococcus pyogenes*, *Enterococcus faecium*, and *Pseudomonas aeruginosa* to the antibacterial effects of beta-lactam antibiotics and protein synthesis inhibitors.

Introduction

Antibiotic resistance is nowadays recognized as one of the most important threats to global human health and novel intervention strategies are required to cope or anticipate multiple mechanisms of drug resistance emerging in bacteria. Diflunisal, a well-known non-steroidal anti-inflammatory drug (NSAID), is currently used in many countries to treat painful conditions in patients suffering from rheumatoid arthritis and osteoarthritis,[1] but it has been recently repurposed as anti-virulent agent for the treatment of *Staphylococcus aureus* osteomyelitis.[2,3] The general anti-inflammatory mechanism of action of diflunisal has not been fully identified, but it has been demonstrated to act as prostaglandin synthetase inhibitor thus reducing prostaglandin levels at peripheral tissues

[1] Published as: Carta, D.; Brun, P.; Dal Prà, M.; Bernabè, G.; Castagliuolo, I.; Ferlin, M.G.; MedChemComm, 2018, 9, 1017-1032

and resulting in anti-inflammatory activity. Inhibition of prostaglandin synthetase, however, has been reported to increase rate of thrombotic events, myocardial infarction, and stroke following administration of diflunisal. Besides the cardiovascular adverse effects, administration of diflunisal has been associated with increased risk of bleeding, ulceration and perforation of stomach and intestine that, alike other NSAIDs, usually arise without any warning signs.

Diflunisal is a derivative of salicylic acid with a structure differing from the latter because of the presence of the 2,4-difluoro-phenyl substitution at 5 position. Although the aza-isosteres of salicylic acid, namely the *o*-hydroxy-pyridinecarboxylic acids[4] are generally less potent than salicylic acid itself, other pyridine derivatives such as flufenamic acid, niflumic acid and triflocin (Figure 1) were reported to have anti-inflammatory activity comparable to salicylic acid but with different metabolic properties and longer duration of the effects.

The renewed worldwide pharmacological interest for the multiple biological effects of diflunisal and our experience in the synthesis and study of hydroxy-pyridinecarboxylic acid derivatives (HP_{23} and HP_{24} in Figure 1)[5,6] prompted us to target the synthesis of some diflunisal aza-analogs and related pyridine compounds, all called diflunisal aza-analogs. Our aim was to identify new multi-target compounds endowed with both anti-inflammatory and antibacterial activities to treat human infections with improved pharmacokinetics and possibly reduced side effects. Thus, multi-target approach is remarkable in treatment of infections induced by multi-drug resistant bacteria as an alternative to currently used combination therapies.[7-9] Further, in a benzene ring, the switch of a C to a N atom, a classical isosteric modification,[10] generally makes the aza-derivatives more water soluble in comparison with the parent compound, in this case the insoluble diflunisal (diflunisal, LogP = 3.19 and the corresponding aza-analog, LogP = 2.28, see also solubility determination in the experimental section), and also, previous studies on 3-hydroxy-4-pyridinecarboxylic acids reported for carboxylic function pKa values of order of 1. All these features taken together might be a noteworthy improvement for drug formulations.

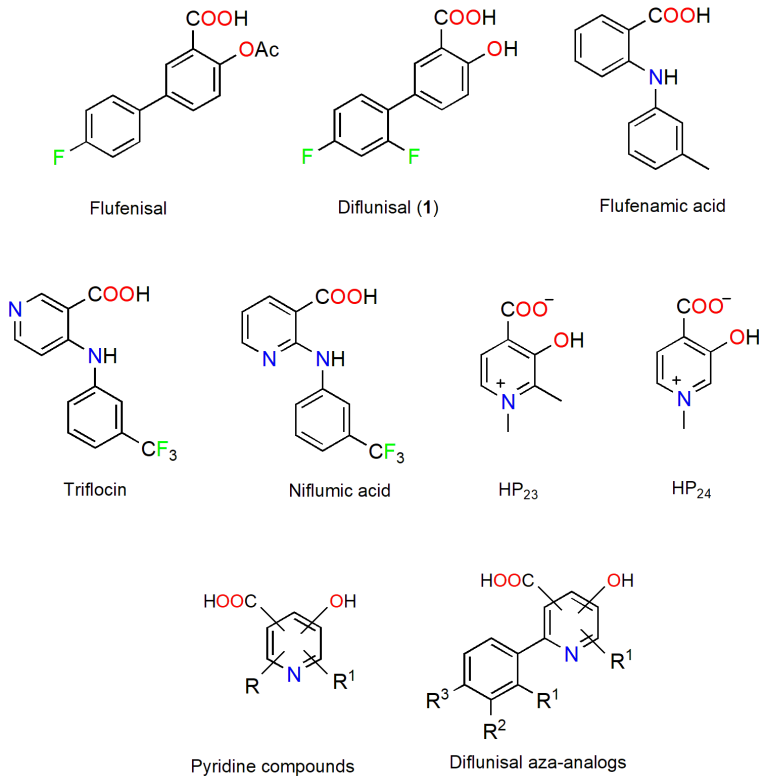

Figure 1. Structures of compounds mentioned in the text.

Results and Discussion

Chemical synthesis

Concerning the synthesis, we followed a shorter and efficient pathway different from the one implemented by some authors in 1971 for the preparation of Flufenisal aza-analogs (Figure 1).[11]

Oxazole derivatives have become increasingly important because of their use as intermediates for the preparation of new biological materials.[12] In the past we exploited the reactivity of oxazole as azadiene in intramolecular cycloaddition Diels–Alder reactions with a dienophile for obtaining several *o*-hydroxypyridinecarboxylic acid (HP) derivatives.[5] As known, the reaction between a 5-alkoxy-oxazole and an alkene proceeds through a bicyclic adduct intermediate that spontaneously but with different reaction times and amounts depending on 2 and 4 substitutions, transforms into the pyridine structure (Figure 2).[13]

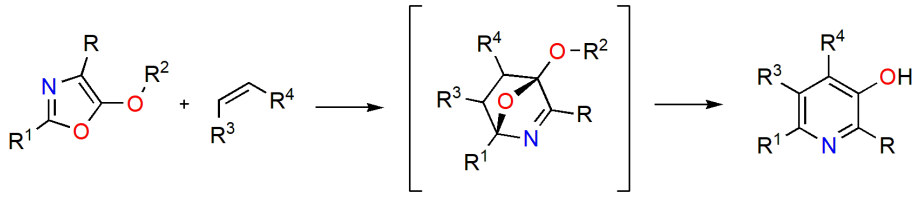

Figure 2. Oxazole synthesis of 3-hydroxy-4-pyridinecarboxylic acids.

Hence, for the synthesis of diflunisal aza-analogs we have repurposed the same route involving key oxazole intermediates.

Scheme 1. Synthesis of *o*- and *m*-hydroxypyridinecarboxylic acids derivatives **14** and **19-22**

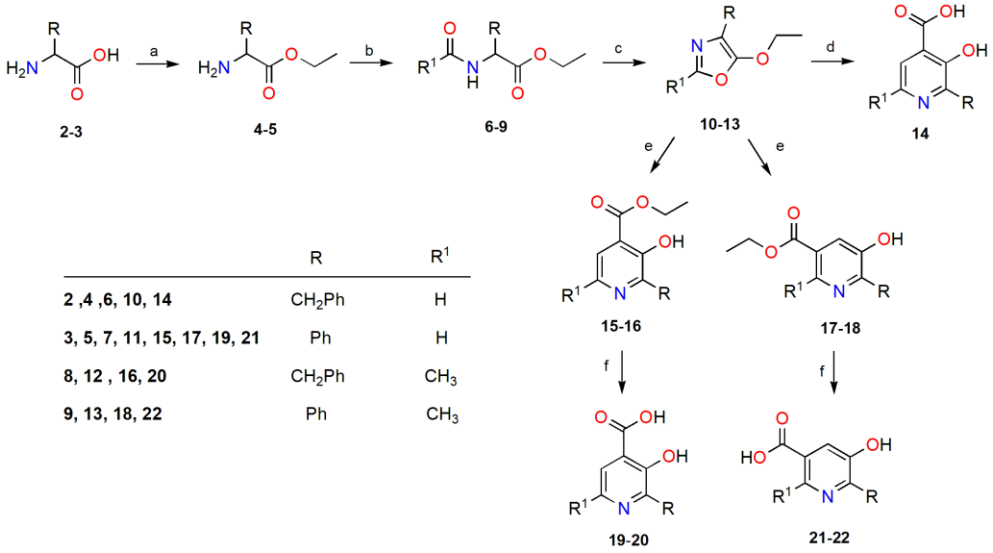

	R	R^1
2 ,4 ,6, 10, 14	CH_2Ph	H
3, 5, 7, 11, 15, 17, 19, 21	Ph	H
8, 12 , 16, 20	CH_2Ph	CH_3
9, 13, 18, 22	Ph	CH_3

Reagents and conditions: a) $SOCl_2$, abs EtOH, 80°C, 4 h, 95-99%; b) trimethyl-*o*-formate or trimethyl-*o*-acetate, ref., 3 h; 88-90% c) P_2O_5, Celite, MgO, $CHCl_3$, ref, 24 h, 73-96%; d) Acrylic acid, rt, 0.5 h, 30%; e) Ethyl acrylate, 100°C, 48 h, 20-35%; f) NaOH 10% aq, MeOH, ref.,4 h, 95-98%.

In Scheme 1, the key oxazoles **10-13** were obtained starting from amino acids phenyl-alanine **2** and phenyl-glycine **3** that were transformed into the respective ethyl ester hydrochlorides **4** and **5** by treatment with $SOCl_2$ in absolute ethanol at refluxing for 4 h, in almost quantitative yields. The esters **4** and **5** were reacted with trimethyl-*o*-formate or trimethyl-*o*-acetate at refluxing for 2 h to give the corresponding formyl and acetyl-derivatives **6, 7** and **8, 9** (88-90% yields).[14] Following a previously described procedure,[15] compounds **6-9** were submitted to a cyclization reaction carried out with P_2O_5, MgO in chloroform and in the presence of celite at refluxing for 24 h. After work

up of the reaction mixture, oxazole derivatives **10-13** were obtained in good yields (73-96%).

The next Diels–Alder reactions were performed with acrylic acid or ethyl acrylate to obtain HP compounds. Thus, 4-benzyl-oxazole derivative **10** was reacted with acrylic acid at room temperature to give the 2-benzyl-*o*-HP **14** (30% yield).[13] 4-Phenyl-oxazole derivative **11** was reacted with ethyl acrylate at 100 °C for 24-48 h[16] to give after separation by Flash Chromatography two 2-phenyl-isomers as ethyl esters: the *o*-HP derivative **15** (16%) and the *m*-HP derivative **17** (28%). The 2-methyl-4-benzyl-oxazole **12** by reacting with ethyl acrylate gave the corresponding ethyl ester *o*-HP derivative **16** (35%), while by the same reaction the 2-methyl-4-phenyl-oxazole **13** yielded the ethyl ester isomer *m*-HP **18** (19%). Finally, all the ethyl esters **15-18** were transformed into the corresponding acids by treatment with a mixture of 10% NaOH aqueous solution and methanol at reflux for 4 h furnishing the *o*- and *m*-HPs **19-22**, in almost quantitative yields.

Scheme 2. Synthesis of *o*- and *m*-hydroxypyridinecarboxylic acid derivatives **42-45** and **49-51**.

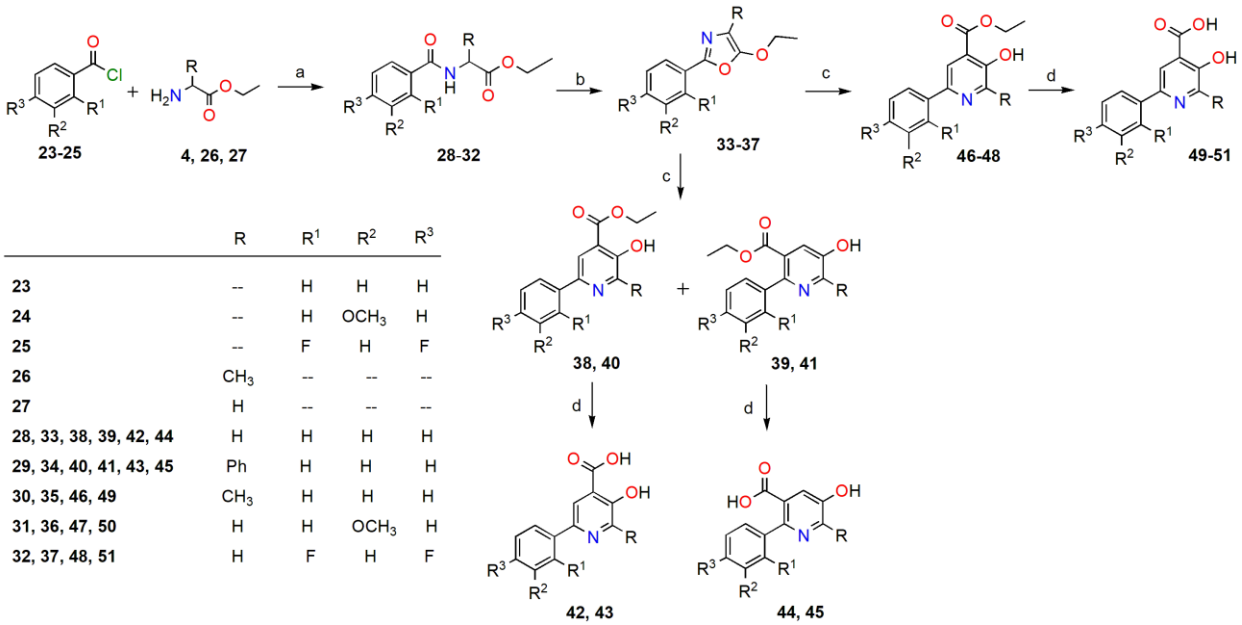

	R	R^1	R^2	R^3
23	--	H	H	H
24	--	H	OCH_3	H
25	--	F	H	F
26	CH_3	--	--	--
27	H	--	--	--
28, 33, 38, 39, 42, 44	H	H	H	H
29, 34, 40, 41, 43, 45	Ph	H	H	H
30, 35, 46, 49	CH_3	H	H	H
31, 36, 47, 50	H	H	OCH_3	H
32, 37, 48, 51	H	F	H	F

Reagents and conditions: a) Et_3N, CH_2Cl_2, rt, 1 h, 95-99%; b)1. PCl_5, Et_2O/diox., rt, 1 h; 2. 40°C, dark, 48 h, 50-90%; c) Ethyl acrylate, 100°C, 24-48 h, 20-40%; d) NaOH 10% aq, MeOH, ref., 4 h, 80-90%.

In Scheme 2, the phenylalanine ethyl ester **4** (Scheme 1) and the commercial ethyl glycine and alanine ethyl esters **26** and **27** were reacted with benzoyl chlorides derivatives

23-25 in CH_2Cl_2 at room temperature for 1 h to give amide derivatives **28-32** in almost quantitative yields (95-99%). All these last ones were submitted to a cyclisation reaction carried out in diethyl ether/dioxane 4:1 in the presence of an excess of dehydrating PCl_5 for 1 h. After removal of the solvents, the mixture was left at 40 °C in the dark for 48 h and oxazole derivatives **33-37** were obtained in high yields (50-90%).[17] The following Diels–Alder reactions with compounds **33-37** were all performed in the presence of ethyl acrylate[16] because with acrylic acid they did not work. Therefore, in all cases the ethyl esters of HP derivatives were obtained. As described in Scheme 2, the 2-phenyl-oxazole **33** by reacting with ethyl acrylate gave the two *o*- and *m*-isomers HP **38** and **39** respectively (15% and 21%). By the same way, also oxazole compound **34** gave the two isomer HPs **40** and **41** (11% and 31%). Whereas, oxazoles **35-37** provided only the ethyl esters of *o*-HPs **46-48.** Finally, all the ethyl esters of HPs **38-41** and **46-48** were transformed to HPs derivatives **42-45** and **49-51** by treatment with 10% NaOH methanol solution for 4 h (80-90% yields).

Scheme 3. Synthesis of 6,8-difluoro-4-hydroxyquinoline-3-carboxylic acid (**54**)

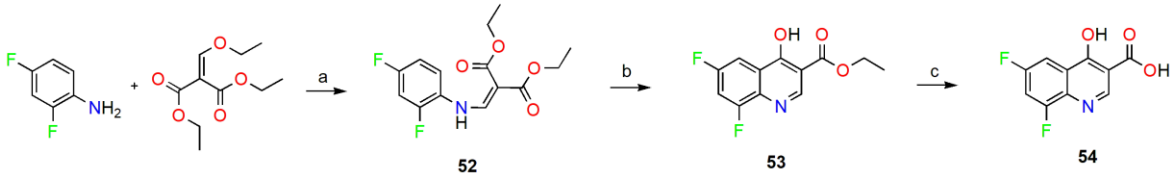

Reagents and conditions: a) 90°C, 3 h, 99%; b) boiling Ph_2O, 15 min., 60%; c) NaOH 10% aq, CH_3OH, ref., 4 h, 86.5%.

Scheme 3 describes the route carried on to obtain a quinoline compound showing the same structural elements as in diflunisal aza-analog **51** (Scheme 2) such as pyridine ring, the *o*-hydroxy-carboxylic acid groups and the two fluorine in meta position between them on an aromatic ring, although in a different arrangement. The starting 2,4-difluoroaniline was reacted with diethyl ethoxymethylenemalonate for 3 h at 90 °C to yield the condensed product **52** that submitted to thermal cyclisation in boiling diphenyl ether for 15 min gave the ethyl ester of the quinoline-4-hydroxy-3-carboxylic acid derivative **53** (60%).[18] As before, this last ethyl ester was hydrolyzed to the corresponding acid by treatment with 10% NaOH aqueous methanol solution (86.5%).

Scheme 4. Synthesis of N-methylated *o*-hydroxypyridinecarboxylic derivatives **55-57**.

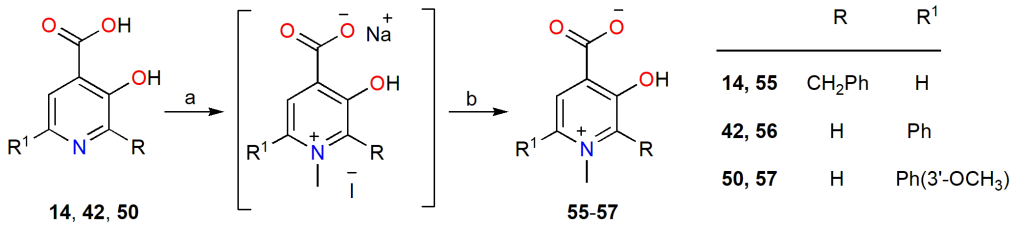

Reagents and conditions: a) CH_3I, DMF, NaOH 10%, ref., 24 h, 20-70%; b) H_2O_2, $CHCl_3$, H_2O, HCl 1M

As a final step, the diflunisal aza-analogs **14**, **42** and **50**, prepared as in the Schemes 1 and 2, were submitted to methylation with CH_3I in DMF and NaOH 10% aqueous solution at refluxing for 24 h (scheme 4). The scope for an *N*-alkylation was to get water soluble zwitterion compounds as previously found out for similar pyridine derivatives.[5] In all cases only 1*N*-methylated compounds were obtained as sodium and iodine salts. These intermediate salts were not isolated but were transformed directly into the zwitterions **55**–**57**. To do this, they were dissolved in water, treated with H_2O_2 and the iodine formed was removed by $CHCl_3$ extraction. The aqueous phase was acidified with 1 M HCl and the formed precipitate was subjected to reverse-phase flash chromatography to remove inorganics. In this way, pure zwitterion compounds **55**–**57** were obtained as proved by spectral evidence.

Biological activity

The cytotoxic activity of diflunisal aza-analogs was assessed on cultured human macrophages by the MTT assay. Compounds were tested at concentrations ranging from 10 nM to 100 µM and the calculated IC_{50} values are listed in Table 1. All the aza-analogs show minimal cytotoxic activity, with IC_{50} values generally higher than 80 µM whereas diflunisal reported a more evident cytotoxic activity (IC_{50} 53 µM).

Table 1. Cytotoxic activity of diflunisal aza-analogs assessed *in vitro* on human macrophages.

Compd	IC_{50} (μM)	Compd	IC_{50} (μM)
14	>100	**45**	92.1
19	>100	**49**	90.8
20	>100	**50**	88.6
21	>100	**51**	97.3
22	97.4	**54**	96.5
42	84.5	**55**	>100
43	81.2	**56**	91.4
44	87.9	**57**	95.0
diflunisal	53		

Diflunisal and aza-analogs were tested for anti-inflammatory activity by ELISA in cultured macrophages stimulated with lipopolysaccharide (LPS). Production of tumor necrosis factor (TNF)-α and interleukin (IL)-1β significantly increased in macrophages stimulated with LPS (404.1±23.22 pg/mL and 612.2±30.1 pg/mL, respectively) as compared with unstimulated macrophages (TNF-α: 75.6±10.4; IL-1β: 216.9±14.2; $P<0.02$). Compounds were tested at concentrations ranging from 10 nM to 10 μM and results are reported in Table 2 as the lowest concentration able to reduce by 25% the production of pro-inflammatory cytokines triggered by LPS. As reported, compounds **19**, **22**, **43**, **44**, and **45** significantly ($P<0.05$) reduced production of TNF-α and IL-1β at 10 μM, whereas the anti-inflammatory activity of compounds **51** and **54** was already evident at 1 μM. Likewise, in human macrophages LPS stimulation induced secretion of the chemokine interleukin (IL)-8 (544.0±29.7 pg/mL) as compared with unstimulated cells (176.9±2.6 pg/mL; $P<0.02$). Compounds **19**, **44**, **45**, **51**, and **54** significantly ($P<0.05$) reduced by at least 25% the production of IL-8 induced by LPS (Table 2). Unstimulated human macrophages produced low levels of PGs (56.0±3.6 pg/mL) which were significantly increased by LPS stimulation (632.9±31.7 pg/mL; $P<0.02$). As expected, diflunisal significantly reduced PGs production at 0.1 μM ($P<0.05$), whereas only compounds **43**, **51**, and **54** inhibited PGs release at 10 μM. All the other tested compounds did not report anti-inflammatory activity. No significant increase in pro-inflammatory cytokines or PGs production were observed in human macrophages incubated with diflunisal aza-analogs without LPS (data not shown).

Table 2. Anti-inflammatory activity of diflunisal aza-analogs evaluated by ELISA. Data are reported as the lowest concentration (μM) of compounds which significantly (P<0.05) reduced by at least 25% the levels of cytokines triggered by LPS stimulation. n.d.: the anti-inflammatory activity was not detected at the range 10 nM-10 μM. PGs: prostaglandins

Compd	TNF-α	IL-8	IL-1β	PGs
14	n.d.	n.d.	n.d.	n.d.
19	10	10	10	n.d.
20	n.d.	n.d.	n.d.	n.d.
21	n.d	n.d	n.d.	n.d.
22	10	n.d.	10	n.d.
42	n.d.	n.d.	n.d.	n.d.
43	10	n.d.	10	10
44	10	10	10	n.d.
45	10	10	10	n.d.
49	n.d.	n.d.	n.d.	n.d.
50	n.d.	n.d.	n.d.	n.d.
51	1	1	1	10
54	1	10	1	10
55	n.d.	n.d.	n.d.	n.d.
56	n.d.	n.d.	n.d.	n.d.
57	n.d.	n.d.	n.d.	n.d.
Diflunisal	n.d.	n.d.	n.d.	0.1

.

Up to 32 μM final concentration, diflunisal or aza-analogs alone did not report an intrinsic antibacterial activity, as expected. The highest final concentrations of DMSO or NaOH caused no significant bacterial growth inhibition (data not shown).

Diflunisal aza-analogs were then investigated for their ability to potentiate the antibacterial activity of antibiotics. In a first screening test, the minimum inhibitory concentration (MIC) of antibiotics against *S. aureus*, *S. pyogenes*, *K. pneumoniae*, *E. faecium*, *P. aeruginosa*, and *E. coli* was assessed, and antibiotic susceptibility was defined as per clinical breakpoints.[19]

As reported with diflunisal,[3] we tested diflunisal aza-analogs for their ability to potentiate the antibacterial activity, in combination with methicillin (MET), geneticin (GEN), ciprofloxacin (CPR), tetracycline (TET), and erythromycin (ERY) as representative antibiotics for different mechanism of actions. Bacterial strains were then incubated with each compound (final concentrations ranging 0.25 μM to 32 μM) in combination with antibiotics at sub-inhibitory concentration (MIC/4). Data were compared with bacteria incubated with antibiotics (MIC/4) alone. As reported in Table 3,

the diflunisal aza-analogs **19**, **21**, **22**, **43**, **44**, **45**, **51** and **54** significantly potentiated the antimicrobial activity of antibiotics in Gram-positive bacteria (*S. aureus*, *S. pyogenes*, *E. faecium*) and the effect was no evident in Gram-negative bacteria *K. pneumoniae* and *E. coli*, while interestingly in *P. aeruginosa* it was. In Gram-positive bacteria diflunisal aza-analogs reported the most important antibacterial effects when used in combination with MET, a *β*-lactam disrupting the synthesis of the peptidoglycan layer of bacterial cell wall, and with protein synthesis inhibitors (GEN, TET, ERY). On the contrary, the combination with CPR, which targets DNA gyrase, was ineffective. The same diflunisal aza-analogs increased inhibitory capacity against *P. aeruginosa* only when used in combination with CPR and ERY, antibiotics previously reported to interfere with virulence factors regulated by quorum sensing system.[20]

Table 3. Antibacterial activity of diflunisal aza-analogs in combination with antibiotics. Data are reported as minimum modulatory concentration (MMC, in μM, significative results are reported in red) of diflunisal aza-analog required to obtain significant (P<0.05) antibacterial activity in combination with sub-inhibitory concentration (MIC/4) of antibiotic. MET: methicillin; GEN: geneticin; CPR: ciprofloxacin; TET: tetracycline; ERY: erythromycin.

Activity against *Staphylococcus aureus* (MMC_4 μM)

Compd	MET	GEN	CPR	TET	ERY
14	>32	>32	>32	>32	>32
19	0.25	0.5	16	2	0.25
20	>32	>32	>32	>32	>32
21	0.5	2	>32	0.25	2
22	0.5	4	16	4	4
42	16	>32	16	>32	>32
43	4	8	16	2	2
44	8	16	>32	1	4
45	4	8	16	8	8
49	16	16	>32	16	>32
50	16	>32	>32	>32	>32
51	0.5	2	16	2	4
54	0.5	4	16	2	1
55	>32	>32	>32	>32	>32
56	>32	>32	>32	>32	>32
57	>32	>32	>32	>32	>32
diflunisal	8	>32	>32	>32	>32

Activity against *Streptococcus pyogenes* (MMC_4 μM)

Compd	MET	GEN	CPR	TET	ERY
14	>32	>32	>32	>32	>32
19	0.5	2	>32	1	2
20	>32	>32	>32	16	>32
21	1	8	>32	4	4
22	4	2	>32	4	4
42	16	16	>32	>32	>32
43	2	4	>32	8	4
44	1	2	>32	2	4
45	1	2	>32	4	8
49	>32	>32	>32	>32	>32
50	>32	>32	>32	>32	>32
51	2	8	>32	8	4
54	1	4	>32	4	8
55	>32	>32	>32	>32	>32
56	>32	>32	>32	>32	>32
57	>32	>32	>32	>32	>32
diflunisal	16	>32	>32	>32	>32

Activity against *Klebsiella pneumoniae* (MMC_4 μM)

Compd	MET	GEN	CPR	TET	ERY
14	>32	>32	>32	>32	>32
19	>32	>32	>32	>32	>32
20	>32	>32	>32	>32	>32
21	>32	>32	>32	>32	>32
22	>32	>32	>32	>32	>32
42	>32	>32	>32	>32	>32
43	>32	>32	>32	>32	>32
44	>32	>32	>32	>32	>32
45	>32	>32	>32	>32	>32
49	>32	>32	>32	>32	>32
50	>32	>32	>32	>32	>32
51	>32	>32	>32	>32	>32
54	>32	>32	>32	>32	>32
55	>32	>32	>32	>32	>32
56	>32	>32	>32	>32	>32
57	>32	>32	>32	>32	>32
diflunisal	>32	>32	>32	>32	>32

Activity against *Enterococcus faecium* (MMC_4 µM)

Compd	MET	GEN	CPR	TET	ERY
14	>32	>32	>32	>32	>32
19	1	4	>32	2	4
20	>32	>32	>32	>32	>32
21	0.5	8	>32	1	4
22	0.5	8	>32	1	4
42	>32	>32	>32	>32	>32
43	2	8	>32	2	2
44	2	8	>32	4	2
45	1	4	>32	2	2
49	>32	>32	>32	>32	>32
50	16	>32	>32	>32	>32
51	0.25	4	>32	4	4
54	0.25	4	>32	4	4
55	>32	>32	>32	>32	>32
56	>32	>32	>32	>32	>32
57	>32	>32	>32	>32	>32
diflunisal	16	>32	>32	>32	>32

Activity against *Pseudomonas aeruginosa* (MMC_4 µM)

Compd	MET	GEN	CPR	TET	ERY
14	>32	>32	>32	>32	>32
19	8	>32	4	>32	4
20	>32	>32	>32	>32	>32
21	16	>32	4	>32	4
22	16	>32	4	>32	4
42	>32	>32	>32	>32	>32
43	8	>32	8	>32	8
44	16	>32	8	>32	8
45	16	>32	4	>32	8
49	>32	>32	>32	>32	>32
50	>32	>32	>32	>32	>32
51	8	>32	4	>32	4
54	8	>32	4	>32	4
55	>32	>32	>32	>32	>32
56	>32	>32	>32	>32	>32
57	>32	>32	>32	>32	>32
diflunisal	>32	>32	>32	>32	>32

Activity against *Escherichia coli* (MMC_4 μM)

Compd	MET	GEN	CPR	TET	ERY
14	>32	>32	>32	>32	>32
19	>32	>32	>32	>32	>32
20	>32	>32	>32	>32	>32
21	>32	>32	>32	>32	>32
22	>32	>32	>32	>32	>32
42	>32	>32	>32	>32	>32
43	>32	>32	>32	>32	>32
44	>32	>32	>32	>32	>32
45	>32	>32	>32	>32	>32
49	>32	>32	>32	>32	>32
50	>32	>32	>32	>32	>32
51	>32	>32	>32	>32	>32
54	>32	>32	>32	>32	>32
55	>32	>32	>32	>32	>32
56	>32	>32	>32	>32	>32
57	>32	>32	>32	>32	>32
diflunisal	>32	>32	>32	>32	>32

Conclusion

Following the multi-target approach in treatment of infections induced by multi-drug resistant bacteria, in this study we investigated the anti-inflammatory and antibacterial properties of some newly synthesized aza-analogs of the known diflunisal, taken as reference compound. Regarding the anti-inflammatory activity, diflunisal was confirmed to inhibit production of PGs while in our experiments, it did not influence pro-inflammatory cytokines TNF-α, IL-8, and IL-1β, in LPS stimulated macrophages. On the contrary, except for compounds **43**, **51** and **54,** diflunisal aza-analogs lost the inhibitory activity against prostaglandin synthetase but some of them (**19**, **22**, **44** and **45)** revealed interesting anti-inflammatory effects probably acting on the NF-κB pathway (Table 2). This way of aza-analogs action might result advantageous by reducing gastrointestinal adverse effects. Nevertheless, **51** and **54** reported the best anti-inflammatory activity since at concentration ranging 1-10 μM reduced the levels of both cytokines and PGs in human macrophages. However, their effects on PGs were 100 folds less than diflunisal (0.1 μM). From a SAR point of view, it is possible to affirm that the presence of fluorine atoms on

the phenyl moiety is crucial for a wide anti-inflammatory activity. The most interesting results were observed when we studied the antibacterial activity of diflunisal aza-analogs in combination with common antibiotics. Our results (Table 3) clearly reported that some diflunisal aza-analogs (**19**, **21**, **22**, **43**, **44**, **45**, **51**, and **54**) significantly potentiated the antimicrobial activity of antibiotics targeting the synthesis of peptidoglycan or proteins in tested Gram-positive bacteria and to a lesser extent in *P. aeruginosa* whereas no intrinsic antibacterial activities were observed when compounds were tested alone. The fluorine compounds **51** and **54** were again the most effective, reporting low values of minimum modulatory concentration (range 0.25-16 μM). Important antibacterial activities were observed also for compounds **21** and **22** although they lack both fluorine atoms and the specific salicylic acid structure. The observed synergistic effects could be explained by several mechanisms such as alterations in superficial properties of bacteria induced by aza-analogs. Moreover, compelling evidences reported that bi-aryl compounds interfere with the bacterial quorum sensing, a signaling mechanism controlling bacterial phenotype through the exchange of autoinducer peptides (AIPs).[3] We hypothesize that, since the AIPs regulate bacterial virulence and survival,[21] the use of the here pyridine compounds lowered the dose of antibiotics required for the antibacterial effects likely reducing side effects and the selective pressure in the emergence of new resistant bacteria.[22] In this perspective, and taking in account that the almost pyridine derivatives are more water soluble than the corresponding phenyl compounds (see diflunisal, LogP = 3.19 and the aza-analog **51,** LogP = 2.28, ESI) and less cytotoxic than diflunisal (Table 1), they represent a promising chemo type for the development of new multi-target agents able to sensitize bacteria to co-administered antibiotics.

Experimental section

Chemistry

^{1}H NMR spectra were determined on Bruker 300 and 400 MHz spectrometers, with the solvents indicated; chemical shifts are reported in δ (ppm) downfield from tetramethylsilane as internal reference. Coupling constants are given in hertz. In the case of multiplets, chemical shifts were measured starting from the approximate center. Integrals were satisfactorily in line with those expected based on compound structure. Mass spectra were obtained on a Mat 112 Varian Mat Bremen (70 eV) mass spectrometer

and Applied Biosystems Mariner System 5220 LC/MS (nozzle potential 140 eV). Column flash chromatography was performed on Merck silica gel (250−400 mesh ASTM); chemical reactions were monitored by analytical thin-layer chromatography (TLC) on Merck silica gel 60 F-254 glass plates. Solutions were concentrated on a rotary evaporator under reduced pressure. The purity of new tested compounds was checked by HPLC using the instrument HPLC SHIMADZU model LC-10 AT-VP, with detector UV-Vis A-VP. The analysis was performed with a flow of 1 mL/min, a C-18 column of dimensions 250 mm x 4.6 mm, a particle size of 5 mm, and a loop of 10 µL. The detector was set at 254 nm. The mobile phase consisted of phase A (Milli-Q H_2O, 18.0 MU, TFA 0.05%) and phase B (MeCN). Gradient elution was performed as reported: 0 min, % B = 0; 3 min, % B = 0; 33 min, % B = 30; 38 min, % B = 30; 39 min, % B = 0; 45 min, % B = 0. Starting materials were purchased from Sigma-Aldrich and Alfa Aesar, and solvents were from Carlo Erba, Fluka and Lab-Scan.

General Procedure for the Synthesis of aminoacidic derivatives (**4-5**). As a typical procedure, the synthesis of ethyl 2-amino-3-phenylpropanoate hydrochloride **4** is described in detail. Into a round-bottomed flask, 25 g (151 mmol) of phenylalanine (**2**) were suspended in absolute ethanol (150 mL). 13 mL (181 mmol) of $SOCl_2$ were added dropwise, under stirring at 0°C. The mixture was then refluxed for 4 h, being monitored by TLC analysis (eluent BuOH/CH_3COOH/H_2O, 3:1:1). At the end of the reaction, $SOCl_2$ was evaporated in a N_2 chamber and the mixture was left at room temperature overnight, leading to the formation of a white precipitate. The precipitate was filtered and dried to obtain 33.31 g of ester derivative.

Ethyl 2-amino-3-phenylpropanoate hydrochloride (**4**).

Yield 96%; R_f = 0.45 (eluent BuOH/CH_3COOH/H_2O, 3:1:1); ^{1}H NMR (300 MHz, $CDCl_3$): δ 7.29 (m, 5H, H-2',H-3',H-4',H-5'and H-6'), 4.13 (q, J = 6.75 Hz, 2H, OCH_2CH_3), 4,36 (s_b, 1H, H-2), 3.39 (m, J = 5.53 Hz, 2H, CH_2), 1.89 (s_b, 2H, NH_2), 1.18 (t, J = 6.93 Hz, 3H, OCH_2CH_3) ppm.

Ethyl 2-amino-2-phenylacetate hydrochloride (**5**).

Compound **5** was prepared as for compound **4** by reacting commercial 2-phenyl glycine (**3**) (15.0 g, 99.23 mmol) and $SOCl_2$ (14.2 mL, 119,08 mmol) in absolute ethanol. The reaction was monitored by TLC analysis (eluent BuOH/CH_3COOH/H_2O, 3:1:1) and at the end of the workup procedure, 21.40 g of a brownish solid were obtained. Yield 99%; R*f*: 0.58 (eluent BuOH/CH_3COOH/H_2O, 3:1:1); ^{1}H NMR (300 MHz, $CDCl_3$): δ 7.53 (m, 2H,

H-2'and H-6'), 7.36 (m, 2H, H-3'and H-5'), 7.35 (m, 1H, H-4'), 5.11 (s_b, 1H, H-2), 4.15 (q, J = 7.4 Hz, 2H, OCH_2CH_3), 1.89 (s_b, 2H, NH_2), 1.16 (t, J = 7.11 Hz, 3H, OCH_2CH_3) ppm.

General Procedure for the Synthesis of amide derivatives (**6-9**). As a typical procedure, the synthesis of ethyl 2-(formyl-amino)-3-phenylpropanoate **6** is described in detail. 5 g (21.76 mmol) of compound **4** were mixed with 7.16 mL (65.30 mmol) of trimethyl orthoformate and refluxed for 2 h. The reaction was monitored by TLC analysis (eluent *n*-hexane/ethyl acetate 1:1). At the end of the reaction, the mixture was cooled to room temperature and the solvents evaporated to yield 5.503 g of a brownish oil.

Ethyl 2-(formyl-amino)-3-phenylpropanoate (**6**).

Yield 88%; R*f*: 0.56 (eluent *n*-hexane/ethyl acetate 1:1); ^{1}H NMR (300 MHz, $CDCl_3$): δ 8.14 (s, 1H, CHO), 7.2 (m, 5H, H-2', H-3', H-4', H-5'and H-6'), 6.38 (d, J = 5.83 Hz ,1H, NH), 4.63 (t, J = 5.86, 1H, CH), 4.2 (q, J = 7.15 Hz, 2H, OCH_2CH_3), 3.14 (q_b, J = 2.97, 2H, H-3), 1.25 ppm (t, J = 7.13 Hz, 3H, OCH_2CH_3) ppm.

Ethyl 2-(formyl-amino)-2-phenylacetate (**7**).

Compound **7** was prepared as for compound **6** by reacting previously synthesized compound **5** (5.0 g, 23.18 mmol) with trimethyl orthoformate (7.62 mL, 69.54 mmol), yielding 4.82 g of a brown oil. Yield 92%; R*f*: 0.41 (eluent *n*-hexane/ethyl acetate 1:1); ^{1}H NMR (300 MHz, $CDCl_3$): δ 8.11 (s, 1H, CHO), 7.26 (m, 5H, H-2', H-3', H-4', H-5'and H-6'), 6.9 (d, J = 5.47 Hz, 1H, NH), 5.5 (d, J = 7.55 Hz, 1H, H-2), 4.1 (q, J = 7.18 Hz, 2H, OCH_2CH_3), 1.19 (t, J = 7.14 Hz, 3H, OCH_2CH_3) ppm.

Ethyl 2-(acetyl-amino)-3-phenylpropanoate (**8**).

Compound **8** was prepared as for compound **6** by reacting previously synthesized compound **4** (5.0 g, 21.76 mmol) with trimethyl orthoacetate (8.21 mL, 65.30 mmol), yielding 5.08 g of a brownish residue. Yield 92%; R*f*: 0.34 (eluent *n*-hexane/ethyl acetate 1:1); ^{1}H NMR (300 MHz, $CDCl_3$): δ 7.28 (m, 3H, H-2', H-4'and H-6'), 7.1 (m, 2H, H-3'and H-5'), 5.99 (d, J = 6.83 Hz, 1H, NH), 4.2 (q, J = 7.15 Hz, 2H, OCH_2CH_3), 4.85 (dd, J = 7.78 Hz and J = 5.84 Hz, 1H, H-2), 3.14 (q_{br}, J = 2.97, 2H, H-3), 1.97 (s, 3H, $COCH_3$), 1.24 (t, J = 7.14 Hz, 3H, OCH_2CH_3) ppm.

Ethyl 2-(acetyl-amino)-2-phenylacetate (**9**).

Compound **9** was prepared as for compound **6** by reacting previously synthesized compound **5** (5.0 g, 23.18 mmol) with trimethyl orthoacetate (8.85 mL, 69.54 mmol), yielding 4.63 g of a transparent oil. Yield 90%; R*f*: 0.41 (eluent *n*-hexane/ethyl acetate 1:1); ^{1}H NMR (300 MHz, $CDCl_3$): δ 7.26 (m, 5H, H-2', H-3', H-4', H-5' and H-6'), 6.67

(d, J = 6.78 Hz, 1H, NH), 5.5 (d, J = 7.37 Hz, 1H, H-2), 4.12 (q, J = 7.15 Hz, 2H, OCH_2CH_3), 1.93 (s, 3H, $COCH_3$), 1.12 (t, J = 7.14 Hz, 3H, OCH_2CH_3) ppm.

General Procedure for the Synthesis of oxazole derivatives (**10-13**). As a typical procedure, the synthesis of 4-benzyl-5-ethoxyoxazole **10** is described in detail. Into a 500-mL round-bottomed flask, 5.17 g (19.13 mmol) of celite $(CaO)_3 \cdot Al_2O_3$ and 5.17 g (128.18 mmol) of MgO are suspended in 150 mL of chloroform. With stirring, 17.18 g (120.53 mmol) of P_2O_5 are added quickly to the suspension. 5.50 g (24.87 mmol) of compound **6** were dissolved in 5 mL of chloroform and added dropwise to the mixture at room temperature. The mixture was refluxed for 24 h under N_2 atmosphere and monitored by TLC analysis (eluent *n*-hexane/ethyl acetate 1:1). At the end of the reaction, the mixture was cooled to room temperature and neutralized with a saturated $NaHCO_3$ solution, until pH = 7. The mixture was then extracted with chloroform and the combined organic layers dried over sodium sulphate and evaporated under vacuum.

4-Benzyl-5-ethoxyoxazole (**10**).

Yield 77%; R*f*: 0.76 (eluent *n*-hexane/ethyl acetate 1:1); ^{1}H NMR (300 MHz, $CDCl_3$): δ 7.38 (s, 1H, H-2), 7.27 (m, 5H, H-2', H-3', H-4', H-5'and H-6'), 4.12 (q, J = 7.08 Hz, 2H, OCH_2CH_3), 3.75 (s, 2H, CH_2), 1.31 (t, J = 7.08 Hz, 3H, OCH_2CH_3) ppm.

5-Ethoxy-4-phenyloxazole (**11**).

Compound **11** was prepared as for compound **10** by reacting compound **7** (4.83 g, 23.32 mmol) with 4.49 g (17.94 mmol) of celite $(CaO)_3 \cdot Al_2O_3$, 4.48 g (120.18 mmol) of MgO and 14.87 g (113 mmol) of P_2O_5, yielding 4.23 g of a brown-orange semi-solid residue. Yield 96%; R*f*: 0.77 (eluent *n*-hexane/ethyl acetate 1:1); ^{1}H NMR (400 MHz, $CDCl_3$): δ 7.87 (m, 2H, H-2'and H-6'), 7.50 (s, 1H, H-2), 7.42 (m, 2H, H-3'and H-5'), 7.25 (dd, J = 7.45 Hz e J = 1.29Hz, 1H, H-4'), 4.38 (q, J = 7.08 Hz, 2H, OCH_2CH_3), 1.48 (t, J = 7.08 Hz, 3H, OCH_2CH_3) ppm.

4-Benzyl-5-ethoxy-2-methyloxazole (**12**).

Compound **12** was prepared as for compound **10** by reacting compound **8** (5.09 g, 21.62 mmol) with 4.49 g (17.94 mmol) of celite $(CaO)_3 \cdot Al_2O_3$, 4.48 g (120.18 mmol) of MgO and 14.87 g (113 mmol) of P_2O_5, yielding 2.07 g of a brown-orange semi-solid residue. Yield 44%; R*f*: 0.70 (eluent *n*-hexane/ethyl acetate 1:1); ^{1}H NMR (300 MHz, $CDCl_3$): δ 7.27 (m, 4H, H-2', H-3', H-5'and H-6'), 7.19 (m, 1H, H-4'), 4.07 (q, J = 7.10 Hz, 2H, OCH_2CH_3), 3.74 (s, 2H, CH_2), 2.30 (s, 3H, CH_3), 1.24 (t, J = 7.14 Hz, 3H, OCH_2CH_3) ppm.

5-Ethoxy-2-methyl-4-phenyloxazole (**13**).

Compound **13** was prepared as for compound **10** by reacting compound **9** (3.00 g, 13.56 mmol) with 2.82 g (10.43 mmol) of celite $(CaO)_3 \cdot Al_2O_3$, 2.83 g (69.88 mmol) of MgO and 9.33 g (65.70 mmol) of P_2O_5, yielding 2.02 g of a brown-orange semi-solid residue. Yield 73%; R*f*: 0.80 (eluent *n*-hexane/ethyl acetate 1:1); ^{1}H NMR (300 MHz, $CDCl_3$): δ 7.79 (m, 2H, H-2'and H-6'), 7.35 (m, 2H, H-3'and H-5'), 7.22 (m, 1H, H-4'), 4.32 (q, J = 7.09 Hz, 2H, OCH_2CH_3), 2.40 (s, 3H, CH_3), 1.45 (t, J = 7.08 Hz, 3H, OCH_2CH_3) ppm.

Synthesis of 2-benzyl-3-hydroxypyridine-4-carboxylic acid (**14**).

4 g (19.7 mmol) of compound **10** were mixed with 2.81 mL (56 mmol) of acrylic acid at room temperature. After 10 minutes, a precipitate formed at the bottom of the flask. The precipitate was filtered under vacuum, washed with acetone and dried to obtain 1.43 g of hydroxypyridine-4-carboxylic acid **14**. Yield 32 %; R*f*: 0.64 (eluent BuOH/CH_3COOH/H_2O, 3:1:1); mp = 314-315 °C; ^{1}H NMR (400 MHz, D_2O/NaOD): δ 7.23 (m, J = 6.96 Hz, 1H, H-6), 7.11 (m, 2H, H-2'and H-6'), 7.01 (m, 3H, H-3', H-4'and H-5'), 6.77 (d, J = 4.84 Hz, 1H, H-5), 3.88 (s, 2H, CH_2) ppm; ^{13}C NMR (101 MHz, D_2O/NaOD): δ 177.90 (*C*OOH), 168.38 (*C*OH), 152.77 (C2), 141.07 (C4), 136.46 (C1'), 131.30 (C6), 128.73 (C3'and C5'), 128.43 (C2' and C6'), 125.79 (C4'), 120.42 (C5), 37.26 (CH_2) ppm; IR (KBr): ν = 3423.00 (OH, bounded), 3068.10 (CH, aromatic), 2433.78 (CO-OH, bounded), 2137.88 (intermolecular H bond), 1680.00 (C=O), 1474.31 (C=N), 1474.31 (CH_2), 1230.52 and 1192.17 (C-OH); UV-Vis (H_2O, 0.05% NaOH): 316.46 nm; fluorescence (H_2O, 0.05% NaOH): λ_{exc} = 316 nm, λ_{ems} = 431.96 nm; HRMS (ESI-MS, 140 eV): m/z $[M+H]^+$ calculated for $C_{13}H_{12}NO_3^+$, 230.0812; found, 230.0870; calculated for $C_{13}H_{11}NNaO_3^+$, 252.0631; found, 252.0682; RP-C18 HPLC: t_R = 8.61 min, 96.16 %.

General Procedure for the Synthesis of pyridine derivatives (**15-18**). As a typical procedure, the synthesis of the mixture composed by ethyl 3-hydroxy-2-phenylpyridine-4-carboxylate **15** and ethyl 5-hydroxy-6-phenylpyridine-3-carboxylate **17** is described in detail. Into a sealed tube, 1.0 g (5.29 mmol) of oxazole derivative **11** were mixed with 0.634 mL (5.81 mmol) of ethyl acrylate, and the mixture was stirred at 100°C for 48 h. The reaction was monitored by TLC analysis (eluent *n*-hexane/ethyl acetate 8:2), and at the end of the reaction, two fluorescent spots appeared. The excess ethyl acrylate was evaporated, and the mixture separated by Flash-column chromatography (silica gel, *n*-hexane/ethyl acetate 8:2), to yield 0.208 g of derivative **15** and 0.350 g of derivative **17**.

Ethyl 3-hydroxy-2-phenylpyridine-4-carboxylate (**15**).

Yield 16%; R*f*: 0.56 (eluent *n*-hexane/ethyl acetate 8:2); ^{1}H NMR (400 MHz, $CDCl_3$): δ 11.10 (s, 1H, OH), 8.31 (d, J = 5.00 Hz, 1H, H-6), 8.02 (m, 2H, H-2'and H-6'), 7.62 (d, J = 5.00 Hz, 1H, H-5), 7.47 (m, 2H, H-3'and H-5'), 7.41 (m, 1H, H-4'), 4.48 (q, J = 7.14 Hz, 2H, OCH_2CH_3), 1.45 (t, J = 7.12 Hz, 3H, OCH_2CH_3) ppm; ^{13}C NMR (101 MHz, $CDCl_3$): δ 169.55 ($COOCH_2CH_3$), 154.06 (C2), 149.05 (C3), 139.84 (C6), 136.77 (C1'), 129.21 (C2'and C6'), 128.79 (C4'), 128.08 (C3'and C5'), 120.79 (C5), 118.68 (C4), 62.46 (OCH_2CH_3), 14.08 (OCH_2CH_3) ppm.

Ethyl 5-hydroxy-6-phenylpyridine-3-carboxylate (**17**).

Yield 28%; R*f*: 0.23 (eluent *n*-hexane/ethyl acetate 8:2);^{1}H NMR (400 MHz, $CDCl_3$): δ 8.88 (d, J = 1.76 Hz, 1H, H-2), 7.86 (d, J = 1.80, 1H, H-4), 7.81 (m, 2H, H-2' and H-6'), 7.52 (m, 2H, H-3'and H-5'), 7.47 (m, 1H, H-4'), 5.90 (s_b, 1H, OH), 4.42 (q, J = 7.13 Hz, 2H, OCH_2CH_3), 1.42 (t, J = 7.14 Hz, 3H, OCH_2CH_3) ppm; ^{13}C NMR (101 MHz, $CDCl_3$): δ 165.13 ($COOCH_2CH_3$), 149.64 (C6), 149.35 (C5), 142.99 (C2), 135.78 (C1'), 129.63 (C4'), 129.17 (C2'and C6'), 128.67 (C3'and C5'), 126.33 (C3), 124.41 (C4), 61.49 (OCH_2CH_3), 14.28 (OCH_2CH_3) ppm.

Ethyl 2-benzyl-3-hydroxy-6-methylpyridine-4-carboxylate (**16**).

Compound **16** was prepared as for compound **15** by reacting oxazole derivative **12** (1.0 g, 4.60 mmol) with ethyl acrylate (0.552 mL, 5.06 mmol). After 48 h, the excess ethyl acrylate was evaporated, and the crude product was purified by Flash-column chromatography (silica gel, *n*-hexane/ethyl acetate 9:1) yielding 0.439 g of pyridinic ester derivative. Yield 35%; R*f*: 0.40 (eluent *n*-hexane/ethyl acetate 9:1); ^{1}H NMR (400 MHz, $CDCl_3$): δ 10.45 (s_b, 1H, OH), 7.41 (m, 2H, H-2'and H-6'), 7.38 (s, 1H, H-5), 7.29 (m, 2H, H-3'and H-5'), 7.20 (m, 1H, H-4'), 4.42 (q, J = 7.14 Hz, 2H, OCH_2CH_3), 4.27 (s, 2H, CH_2), 2.54 (s, 3H, CH_3), 1.43 (t, J = 7.14 Hz, 3H, OCH_2CH_3) ppm; ^{13}C NMR (101 MHz, $CDCl_3$): δ 169.31 ($COOCH_2CH_3$), 151.66 (C3), 151.05 (C2), 147.54 (C6), 139.15 (C1'), 129.03 (C2'and C6'), 128.23 (C3'and C5'), 126.10 (C4'), 119.15 (C5), 118.17 (C4), 62.12 (OCH_2CH_3), 38.89 (CH_2), 23.45 (CH_3), 14.09 (OCH_2CH_3) ppm.

Ethyl 5-hydroxy-2-methyl-6-phenylpyridine-3-carboxylate (**18**).

Compound **18** was prepared as for compound **15** by reacting oxazole derivative **13** (1.0 g, 4.92 mmol) with ethyl acrylate (0.590 mL, 5.41 mmol). After 48 h, the excess ethyl acrylate was evaporated, and the crude product was purified by Flash-column chromatography (silica gel, *n*-hexane/ethyl acetate 9:1) yielding 0.239 g of pyridinic ester derivative. Yield 19%; R*f*: 0.41 (eluent *n*-hexane/ethyl acetate 9:1); ^{1}H NMR (300 MHz, $CDCl_3$): δ 7.81 (s, 1H, H-4), 7.80 (m, 2H, H-2'and H-6'), 7.51 (m, 2H, H-3'and H-5'),

7.45 (m, 1H, H-4'), 5.50 (s_b, 1H, OH), 4.40 (q, J = 7.14 Hz, 2H, OCH_2CH_3), 2.82 (s, 3H, CH_3), 1.43 (t, J = 7.12 Hz, 3H, OCH_2CH_3) ppm; ^{13}C NMR (75 MHz, $CDCl_3$): δ 166.29 ($COOCH_2CH_3$), 149.27 (C2), 147.78 (C6), 147.41 (C5), 135.88 (C1'), 129.39 (C4'), 129.08 (C3'and C5'), 128.74 (C2'and C6'), 126.10 (C3), 125.04 (C4), 61.32 (OCH_2CH_3), 23.95 (CH_3), 14.27 (OCH_2CH_3) ppm.

General Procedure for the Synthesis of pyridine-carboxylic acid derivatives (**19-22**). As a typical procedure, the synthesis of 3-hydroxy-2-phenylpyridine-4-carboxylic acid **19** is described in detail. Into 50-mL round-bottomed flask, compound **15** (0.272 g) is dissolved in 5 mL of MeOH and 3 mL of 10% NaOH solution were added. The mixture was refluxed for 4 h and monitored by TLC analysis (eluent $BuOH/CH_3COOH/H_2O$, 3:1:1). At the end of the reaction, MeOH was removed under vacuum and the water layer was acidified with HCl 10% to obtain a precipitate corresponding to the pyridine-4-carboxylic acid derivative **19**. The precipitate was filtered and dried to yield 0.236 g of a white solid.

3-Hydroxy-2-phenylpyridine-4-carboxylic acid (**19**).

Yield 98%; R*f*: 0.69 (eluent $BuOH/CH_3COOH/H_2O$, 3:1:1); mp = 310-311°C; ^1H NMR (400MHz, D_2O/NaOD): δ 7.59 (m, J = 6.96 Hz, 2H, H-2'and H-6'), 7.53 (d, J = 4.76 Hz, 1H, H-6), 7.39 (m, J = 7.38 Hz, J = 1.41 Hz, 2H, H-3'and H-5'), 7.31 (m, J = 7.36 Hz e J = 1.38 Hz, 1H, H-4'), 7.00 (d, J = 4.76 Hz, 1H, H-5) ppm; ^{13}C NMR (101 MHz, D_2O/NaOD): δ 177.88 (C-4), 157.71 (C-2), 150.69 (C-3), 140.08 (C-4), 138.71 (C-1'), 131.84 (C-6), 128.99 (C-2'and C-6'), 128.05 (C-3'and C-5'), 127.30 (C-4'), 121.23 (C-5) ppm; IR (KBr): $\tilde{\nu}$ (cm^{-1}) = 3462.05 (OH, bounded), 3106.95 (CH, aromatic), 2445.37 (CO-OH, bounded), 2059.46 (intermolecular H bond), 1670.32 (C=O), 1534.71 (C=N), 1401.54 (C-OH), 1239.16 and 1277.69 (C-OH); UV-Vis (H_2O, 0.05% NaOH): 341.19 nm; fluorescence (H_2O, 0.05% NaOH): λ_{exc} = 342 nm, λ_{ems} = 456.06 nm; HRMS (ESI-MS, 140 eV): m/z $[M+H]^+$ calculated for $C_{12}H_{10}NO_3^+$, 216.0655; found, 216.0756; calculated for $C_{12}H_9NNaO_3^+$, 238.0475; found, 238.0531; RP-C18 HPLC: t_R = 7.00 min, 99 %.

2-Benzyl-3-hydroxy-6-methylpyridine-4-carboxylic acid (**20**).

Compound **20** was prepared as for compound **19** by reacting compound **16** (0.439 g) with 10% NaOH solution (3 mL) to obtain 0.374 g of a white solid. Yield 95%; R*f*: 0.75 (eluent $BuOH/CH_3COOH/H_2O$, 3:1:1); mp = 241-244°C; ^1H NMR (400 MHz, D_2O/NaOD): δ 6.95 (m, 2H, H-2'and H-6'), 6.85 (m, 3H, H-3', H-4'and H-5'), 6.49 (s, 1H, H-3), 3.71 (s, 2H, CH_2), 1.88 (s, 3H, CH_3) ppm; ^{13}C NMR (101 MHz, D_2O/NaOD): δ

177.85 (*C*OOH), 168.35 (C3), 155.39 (C2), 151.16 (C6), 141.13 (C4), 139.74 (C1'), 137.25 (C4'), 128.30 (C2'and C6'), 125.70 (C-3'and C5'), 119.73 (C5), 37.53 (CH_2), 21.24 (CH_3) ppm; IR (KBr): $\tilde{\nu}$ (cm^{-1})= 3412.41 (OH, bonded), 3082.88 (CH, aromatic), 2553.89 (CO-OH, bonded), 2083.48 (intermolecular H bond), 1670.19 (C=O), 1542.41 (C=N), 1352.43 (C-OH), 1279.59 and 1279.59 (C-OH); UV-Vis (H_2O, 0.05% NaOH): 213.83 nm, 327.30 nm; fluorescence (H_2O, 0.05% NaOH): λ_{exc} = 342 nm, λ_{ems} = 429 nm; HRMS (ESI-MS, 140 eV): m/z $[M+H]^+$ calculated for $C_{14}H_{14}NO_3^+$, 244.0968; found, 244.1124; calculated for $C_{14}H_{13}NNaO_3^+$, 266.0788; found, 266.0905; RP-C18 HPLC: t_R = 8.39 min, 98.63 %.

5-Hydroxy-6-phenylpyridine-3-carboxylic acid (**21**).

Compound **21** was prepared as for compound **19** by reacting compound **17** (0.350 g) with 10% NaOH solution (3 mL) to obtain 0.294 g of a white solid. Yield 95%; R*f*: 0.86 (eluent BuOH/CH_3COOH/H_2O, 3:1:1); mp = 312-314°C; ^{1}H NMR (300 MHz, D_2O/NaOD): δ 8.18 (d, J = 1.78 Hz, 1H, H-2), 7.16 (d, J = 1.81 Hz, 1H, H-4), 7.11 (m, 2H, H-2'and H-6'), 6.92 (m, 2H, H-3'and H-5'), 6.72 (m, 1H, H-4') ppm; ^{13}C NMR (75 MHz, D_2O/NaOD): δ 169.13 (*C*OOH), 150.12 (C2), 148.28 (C6), 140.19 (C2), 138.28 (C1'), 128.63 (C4'), 128.19 (C3'and C5'), 127.67 (C2'and C6'), 120.71 (C4), 119.31 (C3) ppm; IR (KBr): $\tilde{\nu}$ (cm^{-1})= 3601.23(OH bonded), 3000.00 (CH, aromatic), 1686.23 (C=O), 1559.75 (C=N), 1382.02 (C-OH), 1301.64 and 1221.59 (C-OH); UV-Vis (H_2O, 0.05% NaOH): 341.5; fluorescence (H_2O, 0.05% NaOH): λ_{exc} = 342 nm, λ_{ems} = 448.49 nm; HRMS (ESI-MS, 140 eV): m/z $[M+H]^+$ calculated for $C_{12}H_{10}NO_3^+$, 216.0655; found, 216.0734; calculated for $C_{12}H_9NNaO_3^+$, 238.0475; found, 238.0559; RP-C18 HPLC: t_R = 10.10 min, 95.55 %.

5-Hydroxy-2-methyl-6-phenylpyridine-3-carboxylic acid (**22**).

Compound **22** was prepared as for compound **19** by reacting compound **18** (0.095 g) with 10% NaOH solution (3 mL) to obtain 0.083 g of a yellowish solid. Yield 98%; R*f*: 0.65 (eluent BuOH/CH_3COOH/H_2O, 3:1:1); mp = 308-309°C; ^{1}H NMR (300 MHz, D_2O/NaOD): δ 7.31 (m, 2H, H-2'and H-6'), 7.20 (m, 2H, H-3'and H-5'), 7.13 (m, 1H, H-4'), 6.74 (s, 1H, H-4), 2.12 (s, 3H, CH_3) ppm; ^{13}C NMR (75 MHz, D_2O/NaOD): δ 175.28 (*C*OOH), 168.28 (C3), 151.29 (C2), 147.88 (C6), 139.27 (C4), 135.28 (C1'), 129.03 (C2'and C6'), 127.87 (C3'and C5'), 127.41 (C4'), 125.61 (C5), 19.40 (CH_3) ppm; IR (KBr): $\tilde{\nu}$ (cm^{-1})= 3611.16 (OH bonded), 3000.00 (CH, aromatic), 1676.44 (C=O), 1553.14 (C=N), 1360.09 (C-OH), 1311.14 and 1229.51 (C-OH); UV-Vis (H_2O, 0.05% NaOH): 336 nm; fluorescence (H_2O, 0.05% NaOH): λ_{exc} = 336 nm, λ_{ems} = 445 nm;

HRMS (ESI-MS, 140 eV): m/z $[M+H]^+$ calculated for $C_{13}H_{12}NO_3^+$, 230.0812; found, 230.0843; calculated for $C_{13}H_{11}NNaO_3^+$, 252.0631; found, 252.0615; RP-C18 HPLC: t_R = 11.12 min, 96.64 %.

General Procedure for the Synthesis of amide derivatives (**28-32**). As a typical procedure, the synthesis of ethyl 2-(benzamido) acetate **28** is described in detail. 1.40 g (10.03 mmol) of compound **27** were suspended in 30 mL of DCM, and then 3.07 mL (22 mmol) of Et_3N were added. The mixture was cooled to 0°C and then 1.280 mL (11 mmol) of benzoyl chloride were added dropwise. The mixture was stirred for 1 h and monitored by TLC analysis (eluent *n*-hexane/ethyl acetate 1:1). At the end of the reaction, 25 mL of water were added, and the mixture extracted with DCM. The organic layers were dried over sodium sulphate, filtered and evaporated. The obtained residue was dissolved with a mixture *n*-hexane/ethyl acetate 1:1, and the obtain precipitate was filtered. The filtrate was evaporated to dryness to yield 2.02 g of a yellow solid.

Ethyl 2-(benzamido) acetate (**28**).

Yield 97.6%; R*f*: 0.52 (eluent *n*-hexane/ethyl acetate 1:1); ^{1}H NMR (300 MHz, $CDCl_3$): δ 7.81 (m, 2H, H-2'and H-6'), 7.51 (m, 2H, H-3'and H-5'), 7.45 (m, 1H, H-4'), 6.67 (s_{br}, 1H, NH), 4.26 (q, J = 7.15 Hz, 2H, OCH_2CH_3), 4.24 (d, J = 5.09 Hz, 2H, H-2), 1.31 (t, J = 7.13 Hz, 3H, OCH_2CH_3) ppm.

Ethyl 2-(benzamido)-2-phenylacetate (**29**).

Compound **29** was prepared as for compound **28** by reacting compound **5** (1.40 g, 6.49 mmol) with Et_3N (2.0 mL, 13.63 mmol) and benzoyl chloride (0.829 mL, 7.14 mmol) to yield 1.838 g of a white solid. Yield 99%; R*f*: 0.29 (eluent *n*-hexane/ethyl acetate 8:2); ^{1}H NMR (300 MHz, $CDCl_3$): δ 7.82 (m, 2H, H-2'and H-6'), 7.5 (m, 2H, H-2''and H-6''), 7.45 (m, 4H, H-3', H-5', H-3''and H-5''), 7.36 (m, 2H, H-4'and H-4''), 7.16 (d, J = 6.38, 1H, NH), 5.76 (d, J = 7.04 Hz, 1H, H-2), 4.26 (q, J = 7.15 Hz, 2H, OCH_2CH_3), 1.24 (t, J = 7.13, 3H, OCH_2CH_3) ppm.

Ethyl 2-(benzamido) propanoate (**30**).

Compound **30** was prepared as for compound **28** by reacting compound **26** (1.53 g, 10 mmol) with Et_3N (3.06 mL, 22 mmol) and benzoyl chloride (1.28 mL, 11 mmol) to yield 2.212 g of a yellow solid. Yield 99%; R*f*: 0.70 (eluent *n*-hexane/ethyl acetate 9:1); ^{1}H NMR (300 MHz, $CDCl_3$): δ 7.78 (m, 2H, H-2'and H-6'), 7.46 (m, 2H, H-3'and H-5'), 7.45 (m, 1H, H-4'), 6.86 (d, J = 6.54, 1H, NH), 4.74 (quin, J = 7.17 Hz, 1H, H-2), 4.23 (q, J = 7.14 Hz, 2H, OCH_2CH_3), 1.49 (d, J = 7.15, 3H, CH_3), 1.27 (t, J = 7.13, 3H, OCH_2CH_3) ppm.

Ethyl 2-(3-methoxybenzamido) acetate (**31**).

Compound **31** was prepared as for compound **28** by reacting compound **27** (1.40 g, 10 mmol) with Et_3N (3.06 mL, 22 mmol) and 3-methoxybenzoyl chloride (1.55 mL, 11 mmol) to yield 2.320 g of an orange solid. Yield 99%; R*f*: 0.48 (eluent *n*-hexane/ethyl acetate 1:1); ^{1}H NMR (300 MHz, $CDCl_3$): δ 7.81 (m, 2H, H-2'and H-6'), 7.51 (m, 2H, H-3'and H-5'), 6.9 (m, 1H, H-4'), 6.7 (s_{br}, 1H, NH), 4.25 (q, J = 7.16 Hz, 2H, OCH_2CH_3), 4.21 (d, J = 4.97 Hz, 2H, H-2), 3.73 (s, 3H, OCH_3), 1.31 (t, J = 7.14 Hz, 3H, OCH_2CH_3) ppm.

Ethyl 2-(2,4-difluorobenzamido) acetate (**32**).

Compound **32** was prepared as for compound **28** by reacting compound **27** (1.40 g, 10 mmol) with Et_3N (3.06 mL, 22 mmol) and 2,4-difluorobenzoyl chloride (1.35 mL, 11 mmol) to yield 2.420 g of a yellowish solid. Yield 99 %; R*f* = 0.60 (eluent *n*-hexane/ethyl acetate 1:1); ^{1}H NMR (300 MHz, $CDCl_3$) δ 8.13 (m, *J* H-F = 8.9, *J* H-H = 6.6 Hz, 1H, H-3'), 7.24 (s, 1H, NH), 7.03 – 6.96 (m, *J* H-F = 7.68 Hz, *J* H-H = 1.33 Hz, 1H, H-5'), 6.89 (m, *J* H-F = 11.9, *J* H-H = 8.5, 1H, H-6'), 4.28 (q, *J* = 7.15 Hz, 2H, OCH_2CH_3), 4.25 (dd, *J* = 4.95 Hz, *J* = 1.24 Hz, 2H, H-2), 1.31 (t, *J* = 7.1 Hz, 3H, OCH_2CH_3) ppm.

General Procedure for the Synthesis of oxazole derivatives (**33-37**). As a typical procedure, the synthesis of 5-ethoxy-2-phenyloxazole **33** is described in detail. 1.00 g (4.82 mmol) of compound **28** was dissolved in a mixture of dioxane/ethyl ether 1:4. At room temperature, with stirring, 1.00 g (4.82 mmol) of PCl_5 was added to the solution. The mixture was stirred for 1 h and then, the solvents were evaporated. The obtained residue was left in the dark at 40°C for 48 h. Then, the mixture was cooled to 0°C and PCl_5 was neutralized with a saturated solution of $NaHCO_3$. The mixture was extracted with chloroform and the combined organic layers dried and evaporated in vacuo, to obtain 0.817 g a red liquid.

5-Ethoxy-2-phenyloxazole (**33**).

Yield 98%; R*f* = 0.61 (eluent *n*-hexane/ethyl acetate 1:1); ^{1}H NMR (300 MHz, $CDCl_3$): δ 7.32 (m, 2H, H-2'and H-6'), 7.58 (m, 2H, H-3'and H-5'), 7.45 (m, 1H, H-4'), 6.87 (s, 1H, H-4), 4.37 (q, J = 7.05 Hz, 2H, OCH_2CH_3), 1.54 (t, J = 7.01 Hz, 3H, OCH_2CH_3) ppm.

5-Ethoxy-2,4-diphenyloxazole (**34**).

Compound **34** was prepared as for compound **33** by reacting compound **29** (1.00 g, 3.53 mmol) with PCl_5 (0.74 g, 3.53 mmol) to obtain 0.918 g of a red liquid. Yield 95 %; R*f* = 0.76 (eluent *n*-hexane/ethyl acetate 8:2); ^{1}H NMR (300 MHz, $CDCl_3$): δ 8.01 (m, 2H, H-

2'and H-6'), 7.93 (m, 2H, H-2''and H-6''), 7.44 (m, 6H, H-3', H-5', H-3'', H-5'', H-4', H-4''), 4.44 (q, J = 7.08 Hz, 2H, OCH_2CH_3), 1.52 (t, J = 7.08, 3H, OCH_2CH_3) ppm.

5-Ethoxy-4-methyl-2-phenyloxazole (**35**).

Compound **35** was prepared as for compound **33** by reacting compound **30** (2.21 g, 11.12 mmol) with PCl_5 (2.32 g, 11.12 mmol) to obtain 2.160 g of a red liquid. Yield 97 %; R*f* = 0.84 (eluent *n*-hexane/ethyl acetate 1:1); ^{1}H NMR (300 MHz, $CDCl_3$): δ 8.38 (m, 2H, H-2'and H-6'), 7.59 (m, 2H, H-3'and H-5'), 7.53 (m, 1H, H-4'), 4.40 (q, J = 7.08 Hz, 2H, OCH_2CH_3), 2.41 (s, 3H, CH_3), 1.27 (t, J = 7.13, 3H, OCH_2CH_3) ppm.

5-Ethoxy-2-(3-methoxyphenyl)oxazole (**36**).

Compound **36** was prepared as for compound **33** by reacting compound **31** (2.32 g, 9.79 mmol) with PCl_5 (2.04 g, 9.79 mmol) to obtain 2.05 g of a red liquid. Yield 95 %; R*f* = 0.52 (eluent *n*-hexane/ethyl acetate 1:1); ^{1}H NMR (300 MHz, $CDCl_3$): δ 8.04 (s, 1H, H-2'), 7.77 (d, J = 7.72 Hz, 1H, H-6'), 7.47 (t, J = 7.87, 1H, H-5'), 7.2 (d, J = 6.42 Hz, 1H, H-4'), 6.69 (s, 1H, H-4), 4.38 (q, J = 7.14 Hz, 2H, OCH_2CH_3), 3.69 (s, 3H, OCH_3), 1.55 (t, J = 6.77 Hz, 3H, OCH_2CH_3) ppm.

5-ethoxy-2-(2,4-difluorophenyl)oxazole (**37**).

Compound **37** was prepared as for compound **33** by reacting compound **32** (0.949 g, 3.90 mmol) with PCl_5 (0.812 g, 3.90 mmol) to obtain 0.456 g of a red liquid. Yield 52 %; R*f* = 0.81 (eluent *n*-hexane/ethyl acetate 1:1); ^{1}H NMR (300 MHz, $CDCl_3$): δ 7.90 (m, *J* H-F = 12.16 Hz, *J* H-H = 6.10 Hz, 1H, H-3'), 6.95 – 6.84 (m, 2H, H-5' and H-6'), 6.26 (s, 1H, H-4), 4.26 (q, *J* = 7.07 Hz, 2H, OCH_2CH_3), 1.47 (t, *J* = 7.06 Hz, 3H, OCH_2CH_3) ppm.

General procedure for the synthesis of pyridine derivatives (**38**–**41** and **46**–**48**). The synthesis of derivatives **38**–**41** and **46**–**48** follows the general procedure reported for the preparation of derivatives (**15**–**18**).

Synthesis of ethyl 5-hydroxy-2-phenylpyridine-4-carboxylate (**38**) *and of ethyl 5-hydroxy-2-phenylpyridine-3-carboxylate* (**39**).

Compounds **38** and **39** were prepared as described for compound **15** by reacting 0.817 g (4.32 mmol) of the oxazole derivative **33** with 0.520 mL (4.75 mmol) of ethyl acrylate to yield a crude product consisting of the two isomers **38** and **39**. The two isomers were separated by Flash-column chromatography (silica gel, *n*-hexane/ethyl acetate 1:1) to obtain 0.160 g of a yellow oil (**38**) and 0.224 g of a yellow solid (**39**). Compound **38**: Yield 15%; R*f* = 0.84 (eluent *n*-hexane/ethyl acetate 1:1); ^{1}H NMR (300 MHz, $CDCl_3$): δ 10.34 (s, 1H, OH), 8.57 (d, J = 0.69 Hz, 1H, H-6), 8.05 (d, J = 0.66 Hz, 1H, H-3), 7.94 (m, 2H, H-2'and H-6'), 7.46 (m, 2H, H-3'and H-5'), 7.38 (m, 1H, H-4'), 4.50 (q, J = 7.14

Hz, 2H, OCH_2CH_3), 1.47 ppm (t, J = 7.12 Hz, 3H, OCH_2CH_3); ^{13}C NMR (75 MHz, $CDCl_3$): δ 168.86 (*C*$OOCH_2CH_3$), 154.68 (C2), 148.78 (C5), 141.40 (C6), 138.25 (C1'), 128.80 (C3'and C5'), 128.51 (C4'), 126.33 (C2'and C6'), 119.18 (C4), 118.42 (C3), 62.51 (O*C*H_2CH_3), 14.15 (OCH_2*C*H_3) ppm; Compound **39**: Yield 21%; R*f* = 0.48 (eluent *n*-hexane/ethyl acetate 1:1); ^1H NMR (400 MHz, $CDCl_3$): δ 8.88 (d, J = 1.76 Hz, 1H, H-6), 7.86 (d, J = 1.76 Hz, 1H, H-4), 7.80 (m, 2H, H-2' e H-6'), 7.50 (m, 2H, H-3' and H-5'), 7.47 (m, 1H, H-4'), 5.86 (s_{br}, 1H, OH), 4.42 (q, J = 7.13 Hz, 2H, OCH_2CH_3), 1.42 (t, J = 7.14 Hz, 3H, OCH_2CH_3) ppm; ^{13}C NMR (101 MHz, $CDCl_3$): δ 169.79 (*C*$OOCH_2CH_3$), 150.27 (C2), 148.27 (C5), 142.95 (C6), 135.82 (C1'), 129.83 (C4'), 129.21 (C3'and C5'), 128.72 (C2'and C6'), 124.51 (C4), 119.27 (C1'), 61.47 (O*C*H_2CH_3), 14.55 (OCH_2*C*H_3) ppm.

Synthesis of ethyl 3-hydroxy-2,6-diphenylpyridine-4-carboxylate (**40**) *and of ethyl 5-hydroxy-2,6-diphenylpyridine-3-carboxylate* (**41**).

Compounds **40** and **41** were prepared as described for compound **15** by reacting 0.890 g (3.35 mmol) of the oxazole derivative **34** with 0.400 mL (3.69 mmol) of ethyl acrylate to yield a crude product consisting of the two isomers. The two isomers were separated by Flash-column chromatography (silica gel, *n*-hexane/ethyl acetate 8:2) to obtain 0.117 g of a yellow semi-solid compound (**40**) and 0.335 g of a yellowish solid (**41**). Compound **40**: Yield 11%; R*f* = 0.67 (eluent *n*-hexane/ethyl acetate 8:2); ^1H NMR (400 MHz, $CDCl_3$): δ 11.17 (s_b, 1H, OH), 8.23 (m, 2H, H-2''and H-6''), 8.11 (s, 1H, H-5), 8.10 (m, 2H, H-2'and H-6'), 7.53 (m, 2H, H-3'' and H-5''), 7.50 (m, 2H, H-3'and H-5'), 7.48 (m, 1H, H-4'), 7.41 (m, 1H, H-4''), 4.54 (q, J = 7.14 Hz, 2H, OCH_2CH_3), 1.52 (t, J = 7.14 Hz, 3H, OCH_2CH_3) ppm; ^{13}C NMR (101 MHz, $CDCl_3$): δ 169.69 (*C*$OOCH_2CH_3$), 153.19 (OH), 147.97 (C6), 147.56 (C2), 138.66 (C1''), 137.07 (C1'), 129.54 (C2'and C6'), 129.46 (C2''and C6''), 128.82 (C4'), 128.70 (C3''and C5''), 128.36 (C4''), 126.33 (C2''and C6''), 119.47 (C4), 117.29 (C5), 62.55 (O*C*H_2CH_3), 14.17 (OCH_2*C*H_3) ppm. Compound **41**: Yield 31%; R*f* = 0.16 (eluent *n*-hexane/ethyl acetate 8:2); ^1H NMR (300 MHz, $CDCl_3$): δ 8.02 (s, 1H, H-4), 8.01 (m, 2H, H-2'and H-6'), 7.94 (m, 2H, H-2''and H-6''), 7.53 (m, 2H, H-3''and H-5''), 7.46 (m, 2H, H-3'and H-5'), 7.45 (m, 1H, H-4''), 7.43 (m, 1H, H-4'), 4.16 (q, J = 7.17 Hz, 2H, OCH_2CH_3), 1.26 (t, J = 7.13 Hz, 3H, OCH_2CH_3) ppm; ^{13}C NMR (75 MHz, $CDCl_3$): δ 171.06 (*C*$OOCH_2CH_3$), 167.38 (*C*OH), 150.19 (C2), 149.27 (C6), 140.17 (C3), 136.63 (C1'), 135.92 (C1''), 128.76 (C4'), 128.72 (C2'and C6'), 128.56 (C3'and C5'), 128.25 (C3''and C5''), 128.12 (C4''), 127.97 (C2''and C6''), 127.23 (C4), 61.42 (O*C*H_2CH_3), 14.02 (OCH_2*C*H_3) ppm.

Ethyl 3-hydroxy-2-methyl-6-phenylpyridine-4-carboxylate (**46**).

Compound **46** was prepared as for compound **15** by reacting oxazole derivative **35** (0.790 g, 3.89 mmol) with ethyl acrylate (0.451 mL, 4,28 mmol). After 48 h, the excess ethyl acrylate was evaporated, and the crude product was purified by Flash-column chromatography (silica gel, *n*-hexane/ethyl acetate 1:1) yielding 0.350 g of pyridinic ester derivative. Yield 35%; R*f*: 0.91 (eluent *n*-hexane/ethyl acetate 1:1); ^{1}H NMR (400 MHz, $CDCl_3$): δ 10.64 (s, 1H, OH), 7.96 (m, 2H, H-2' and H-6'), 7.92 (d, J = 0.48 Hz, 1H, H-3), 7.47 (m, 2H, H-3' and H-5'), 7.38 (m, 1H, H-4'), 4.50 (q, J = 7.13 Hz, 2H, OCH_2CH_3), 2.64 (s, J = 0.34, 3H, CH_3), 1.48 ppm (t, J = 7.14 Hz, 3H, OCH_2CH_3); ^{13}C NMR (101 MHz, $CDCl_3$): δ 169.52 ($COOCH_2CH_3$), 153.15 (C2), 150.13 (C5), 147.27 (C6), 138.96 (C1'), 128.68 (C3' and C5'), 128.10 (C4'), 126.31 (C2'and C6'), 117.56 (C4), 116.16 (C3), 62.28 (OCH_2CH_3), 19.34 (CH_3), 14.15 (OCH_2CH_3) ppm.

Ethyl 5-hydroxy-2-(3-methoxyphenyl)pyridine-4-carboxylate (**47**).

Compound **47** was prepared as for compound **15** by reacting oxazole derivative **36** (2.05 g, 9.35 mmol) with ethyl acrylate (1.12 mL, 10,28 mmol). After 48 h, the excess ethyl acrylate was evaporated, and the crude product was purified by Flash-column chromatography (silica gel, *n*-hexane/ethyl acetate 1:1) yielding 0.410 g of pyridinic ester derivative. Yield 16%; R*f*: 0.87 (eluent *n*-hexane/ethyl acetate 1:1); ^{1}H NMR (400 MHz, $CDCl_3$): δ 10.34 (s, 1H, OH), 8.56 (d, J = 0.56 Hz, 1H, H-6), 8.05 (d, J = 0.52 Hz, 1H, H-3), 7.54 (m, 1H, H-6'), 7.50 (m, 1H, H-2'), 7.37 (t, J = 7.98 Hz, 1H, H-5'), 6.93 (ddd, J = 8.17, J = 2.06 e J = 0.90 Hz, 1H, H-4'), 4.49 (q, J = 7.14 Hz, 2H, OCH_2CH_3), 3.89 (s, 3H, OCH_3), 1.47 (t, J = 7.14 Hz, 3H, OCH_2CH_3) ppm; ^{13}C NMR (101 MHz, $CDCl_3$): δ 168.84 ($COOCH_2CH_3$), 160.14 ($COCH_3$), 154.78 (C2), 148.49 (C5), 141.28 (C6), 139.71 (C1'), 129.79 (C5'), 119.09 (C4), 118.58 (C3), 114.37 (C4'), 111.75 (C6'), 62.53 (OCH_3 e OCH_2CH_3), 14.16 (OCH_2CH_3) ppm.

Ethyl 2-(2,4-difluorophenyl)-5-hydroxypyridine-4-carboxylate (**48**).

Compound **48** was prepared as for compound **15** by reacting oxazole derivative **37** (0.215 g, 0.884 mmol) with ethyl acrylate (0.243 mL, 0.972 mmol). After 48 h, the excess ethyl acrylate was evaporated, and the crude product was purified by Flash-column chromatography (silica gel, *n*-hexane/ethyl acetate 8:2) yielding 0.043 g of pyridinic ester derivative. Yield 20%; Rf = 0.73 (eluent *n*-hexane/ethyl acetate 8:2); ^{1}H NMR (300 MHz, $CDCl_3$): δ 8.68 (s, 1H, H-6), 8.34 (d, *J* = 1.5 Hz, 1H, H-3), 8.23 (td, *J* = 8.5, 6.5 Hz, 1H, H-3'), 8.04 (td, *J* = 8.8, 6.6 Hz, 1H, H-6'), 6.99 – 6.92 (m, 1H, H-5'), 4.32 (q, *J* = 7.1 Hz, 2H, OCH_2CH_3), 1.23 (t, *J* = 7.1 Hz, 3H, OCH_2CH_3) ppm; ^{13}C NMR (101 MHz, $CDCl_3$): δ

168.14 ppm ($COOCH_2CH_3$), 162.99 (dd, J = 243.70 Hz, J = 8.90 Hz, C4'), 158.50 (d, J = 3.00 Hz, C2), 158.36 (dd, J = 248.72 Hz, J = 7.99 Hz, C2'), 147.27 (C5), 141.88 (C6), 137.72 (dd, J = 13.21 Hz, J = 3.89 Hz, C6'), 132.01 (dd, J = 9.00 Hz, J = 4.95 Hz, C5'), 123.69 (dd, J = 5.00 Hz, C3), 116.14 (d, J = 1.90 Hz, C4), 112.64 (dd, J = 21.60 Hz, J = 3.39 Hz, C5'), 105.13 (t, J = 26.50 Hz, C3'), 62.51 (OCH_3 e OCH_2CH_3), 14.15 (OCH_2CH_3) ppm.

General procedure for the synthesis of pyridine carboxylic acid derivatives (**42**–**45** *and* **49**–**51**). The synthesis of derivatives **42**–**45** and **49**–**51** follows the general procedure reported for the preparation of derivatives (**19–22**).

5-Hydroxy-2-phenylpyridine-4-carboxylic acid (**42**).

Compound **42** was prepared as for compound **19** by reacting compound **38** (0.160 g) with 10% NaOH solution (3 mL) to obtain 0.112 g of a brownish solid. Yield 70%; R*f*: 0.69 (eluent $BuOH/CH_3COOH/H_2O$, 3:1:1); mp = 314-315°C; ^{1}H NMR (300 MHz, DMSO): δ 8.47 (s, 1H, H-6), 8.09 (s, 1H, H-3), 7.98 (m, J = 7.96 Hz, 2H, H-2'and H-6'), 7.47 (m, J = 7.58 Hz, 2H, H-3'and H-5'), 7.39 (m, J = 7.07 Hz e J = 2.06 Hz, 1H, H-4') ppm; ^{13}C NMR (75 MHz, DMSO): δ 182.45 (*C*OOH), 154.92 (C2), 146.69 (C5), 144.69 (C4), 140.18 (C6), 137.66 (C1'), 128.77 (C3'and C5'), 128.30 (C4'), 125.79 (C2'and C6'), 119.07 (C3) ppm; IR (KBr): ṽ (cm^{-1})= 3432.40 (OH, bounded), 3029.21 (CH, aromatic), 2395.47 (CO-OH, bounded), 2115.97 (intermolecular H bond), 1647.32 (C=O), 1545.63 (C=N), 1492.63 (C-OH), 1259.66 and 1283.33 (C-OH); UV-Vis (H_2O, 0.05% NaOH): 254.33, 337.27 nm; fluorescence (H_2O, 0.05% NaOH): λ_{exc} = 337 nm, λ_{ems} = 445 nm; HRMS (ESI-MS, 140 eV): m/z $[M+H]^+$ calculated for $C_{12}H_{10}NO_3^+$, 216.0655; found, 216.0670; calculated for $C_{12}H_9NNaO_3^+$, 238.0475; found, 238.0483; RP-C18 HPLC: t_R = 7.69 min, 97 %.

3-Hydroxy-2,6-diphenylpyridine-4-carboxylic acid (**43**).

Compound **43** was prepared as for compound **19** by reacting compound **40** (0.117 g) with 10% NaOH solution (3 mL) to obtain 0.104 g of a yellowish solid. Yield 98%; R*f*: 0.81 (eluent $BuOH/CH_3COOH/H_2O$, 3:1:1); mp = 119-120°C; ^{1}H NMR (300 MHz, D_2O/NaOD): δ 7.58 (m, J = 7.88 Hz, 2H, H-2''and H-6''), 7.53 (m, J = 7.59 Hz, 2H, H-2'and H-6'), 7.28 (s, 1H, H-5), 7.24 (m, 2H, H-3''and H-5''), 7.23 (m, 2H, H-3'and H-5'), 7.17 (m, 1H, H-4''), 7.12 ppm (m, 1H, H-4'); ^{13}C NMR (75 MHz, D_2O/NaOD): δ 177.61 (*C*OOH), 168.30 (*C*OH), 157.65 (C6), 150.60 (C2), 140.24 (C4), 139.93 (C1''), 139.47 (C1'), 129.03 (C3''and C5''), 128.68 (C3''and C5''), 128.16 (C3'and C5'), 127.88 (C2'and C6'), 127.28 (C4''), 127.06 (C4'), 119.08 (C5) ppm; UV-Vis (H_2O,

0.05% NaOH): 224.86, 360.23 nm; fluorescence (H_2O, 0.05% NaOH): λ_{exc} = 360 nm, λ_{ems} = 455 nm; HRMS (ESI-MS, 140 eV): m/z $[M+H]^+$ calculated for $C_{18}H_{14}NO_3^+$, 292.0968; found, 292.1117; calculated for $C_{18}H_{13}NNaO_3^+$, 314.0788; found, 314.0863; RP-C18 HPLC: t_R = 17.07 min, 98 %.

5-Hydroxy-2-phenylpyridine-3-carboxylic acid (**44**).

Compound **44** was prepared as for compound **19** by reacting compound **39** (0.224 g) with 10% NaOH solution (3 mL) to obtain 0.226 g of a brown solid. Yield 98%; R*f*: 0.72 (eluent BuOH/CH_3COOH/H_2O, 3:1:1); mp = 312-314°C; ^{1}H NMR (400 MHz, D_2O/NaOD): δ 7.69 (s, 1H, H-6), 7.54 (m, J = 7.24 Hz, 2H, H-2'and H-6'), 7.35 (s, 1H, H-4), 7.27 (m, J = 7.66 Hz, 2H, H-3'and H-5'), 7.15 (m, J = 7.36 Hz, 1H, H-4') ppm; ^{13}C NMR (101 MHz, D_2O/NaOD): δ 176.60 (*C*OOH), 159.78 (C5), 142.64 (C2), 140.52 (C1'), 139.77 (C6), 129.14 (C3'and C5'), 127.19 (C4'), 125.38 (C2'and C6'), 120.84 (C4), 119.70 (C3) ppm; IR (KBr): $\tilde{\nu}$ (cm^{-1})= 3560.20 (OH,),3000.00 (CH, aromatic), 1656.54 (C=O), 1543.56 (C=N), 1399.83 (C-OH), 1259.23 and 1212.69 (C-OH); UV-Vis (H_2O, 0.05% NaOH): 253.49, 337.39 nm; fluorescence (H_2O, 0.05% NaOH): λ_{exc} = 337 nm, λ_{ems} = 428.93 nm; HRMS (ESI-MS, 140 eV): m/z $[M+H]^+$ calculated for $C_{12}H_{10}NO_3^+$, 216.0655; found, 216.0736; calculated for $C_{12}H_9NNaO_3^+$, 238.0475; found, 238.0555; RP-C18 HPLC: t_R = 7.67 min, 95.2 %.

5-Hydroxy-2,6-diphenylpyridine-3-carboxylic acid (**45**).

Compound **45** was prepared as for compound **19** by reacting compound **41** (0.335 g) with 10% NaOH solution (3 mL) to obtain 0.293 g of a brown solid. Yield 96%; R*f*: 0.94 (eluent BuOH/CH_3COOH/H_2O, 3:1:1); mp = 149-151°C; ^{1}H NMR (300 MHz, D_2O/NaOD): δ 7.23 (m, J = 8.09 Hz, 2H, H-2'and H-6'), 7.11 (m, J = 8.24 Hz, 2H, H-2''and H-6''), 6.95 (m, 2H, H-3'and H-5'), 6.80 (m, 2H, H-3''and H-5''), 6.73 (m, 1H, H-4''), 6.72 (m, 1H, H-4'), 6.44 (s, 1H, H-4) ppm; ^{13}C NMR (75 MHz, D_2O/NaOD): δ 177.66 (COOH), 165.34 (C5), 151.28 (C2), 150.27 (C6), 136.27 (C1'), 135.92 (C1''), 129.98 (C2'and C6'), 128.48 (C3'and C5'), 128.44 (C2''and C6''), 128.15 (C3''and C5''), 128.11 (C4'), 128.02 (C4''), 127.36 (C3), 125.26 (C4) ppm; UV-Vis (H_2O, 0.05% NaOH): 329.44 nm; fluorescence (H_2O, 0.05% NaOH): λ_{exc} = 329 nm, λ_{ems} = 437.67 nm; HRMS (ESI-MS, 140 eV): m/z $[M+H]^+$ calculated for $C_{18}H_{14}NO_3^+$, 292.0968; found, 292.1080; calculated for $C_{18}H_{13}NNaO_3^+$, 314.0788; found, 314.0933; RP-C18 HPLC: t_R = 12.84 min, 99 %.

3-Hydroxy-2-methyl-6-phenylpyridine-4-carboxylic acid (**49**).

Compound **49** was prepared as for compound **19** by reacting compound **46** (0.350 g) with

10% NaOH solution (3 mL) to obtain 0.302 g of a yellow solid. Yield 96%; R*f*: 0.74 (eluent BuOH/CH_3COOH/H_2O, 3:1:1); mp = 300-302°C; ^{1}H NMR (400 MHz, D_2O/NaOD): δ 7.28 (m, J = 7.16 Hz, 2H, H-2' and H-6'), 7.02 (m, J = 7.66 Hz, 2H, H-3'and H-5'), 6.95 (d, J = 0.40 Hz, 1H, H-3), 6.91 (m, J = 7.94 Hz, J = 1.24 Hz, 1H, H-4'), 1.93 (s, J = 0.23, 3H, CH_3) ppm; ^{13}C NMR (101 MHz, D_2O/NaOD): δ 177.36 (*C*OOH), 168.29 (C5), 157.82 (C2), 151.67 (C6), 139.34 (C4), 134.83 (C1'), 128.64 (C3'and C5'), 126.94 (C4'), 125.63 (C2'and C6'), 112.89 (C3), 19.35 (CH_3) ppm; IR (KBr): $\tilde{\nu}$ (cm^{-1})= 3503.88 (OH, bounded), 3074 (CH, aromatic), 2607.89 (CO-OH, bounded), 2048.53 (intermolecular H bond), 1670.21 (C=O), 1534.17 (C=N), 1458.46 (CH_3); UV-Vis (H_2O, 0.05% NaOH): 253.72 nm, 342.10 nm; fluorescence (H_2O, 0.05% NaOH): λ_{exc} = 342 nm, λ_{ems} = 451.96 nm; HRMS (ESI-MS, 140 eV): m/z $[M+H]^+$ calculated for $C_{13}H_{12}NO_3^+$, 230.0812; found, 230.0854; calculated for $C_{13}H_{11}NNaO_3^+$, 252.0631; found, 252.0672; RP-C18 HPLC: t_R = 7.50 min, 98.8 %.

5-hydroxy-2-(3-methoxyphenyl)pyridine-4-carboxylic acid (**50**).

Compound **50** was prepared as for compound **19** by reacting compound **47** (0.417 g) with 10% NaOH solution (3 mL) to obtain 0.334 g of a yellow solid. Yield 91%; R*f*: 0.87 (eluent BuOH/CH_3COOH/H_2O, 3:1:1); mp = 240°C; ^{1}H NMR (400 MHz, D_2O/NaOD): δ 7.50 (s, 1H, H-6), 7.15 (s, 1H, H-3), 6.89 (m, 2H, H-2' and H-6'), 6.80 (m, 1H, H-5'), 6.42 (m, J = 6.92 Hz, J = 2.24 Hz, 1H, H-4'), 6.36 ppm (s, 3H, OCH_3); ^{13}C NMR (101 MHz, D_2O/NaOD): δ 176.45 (*C*OOH), 168.33 (C3'), 160.22 (C2), 158.81 (C5), 142.83 (C6), 140.81 (C4), 135.77 (C1'), 129.89 (C5'), 119.97 (C3), 118.27 (C2'), 112.59 (C4'), 110.76 (C6'), 55.27 (OCH_3) ppm; UV-Vis (H_2O, 0.05% NaOH): 219.79, 257.44, 340.04 nm; fluorescence (H_2O, 0.05% NaOH): λ_{exc} = 342 nm, λ_{ems} = 455 nm; HRMS (ESI-MS, 140 eV): m/z $[M+H]^+$ calculated for $C_{13}H_{12}NO_4^+$, 246.0761; found, 246.0841; calculated for $C_{13}H_{11}NNaO_4^+$, 268.0580; found, 268.0604; RP-C18 HPLC: t_R = 8.87 min, 98.8 %.

2-(2,4-Difluorophenyl)-5-hydroxypyridine-4-carboxylic acid (**51**).

Compound **51** was prepared as for compound **19** by reacting compound **48** (0.043 g) with 10% NaOH solution (3 mL) to obtain 0.037 g of a yellow solid. Yield 97%; R*f* = 0.71 (eluent BuOH/CH_3COOH/H_2O, 3:1:1); ^{1}H NMR (400 MHz, D_2O/NaOD): δ 7.76 (d, *J* = 0.5 Hz, 1H, H-6), 7.44 (m, *J* H-H = 8.86 Hz, *J* H-F = 6.72 Hz, 1H, H-3'), 7.27 (dd, *J* = 2.1 Hz, *J* = 0.5 Hz 1H, H-3), 6.90 (m, H-4H' and H-6') ppm; ^{13}C NMR (101 MHz, D_2O/NaOD): δ 104.13 (t, *J* = 26.40 Hz, C3'), 111.54 (dd, *J* = 21.30 Hz, *J* = 3.38 Hz, C5'), 122.59 (d, *J* = 4.99 Hz, C3), 123.83 (dd, *J* = 13.11 Hz, *J* = 3.91 Hz, C1'), 131.01 (dd, *J* = 8.98 Hz, J = 4.65 Hz, C6'), 136.22 (d, *J* = 1.82 Hz, C4), 142.78 (C6), 159.26

(dd, *J* = 249.82 Hz, *J* = 7.88 Hz, C2'), 159.60 (dd, *J* = 249.82 Hz, *J* = 7.88 Hz, C2'), 161.89 (dd, *J* = 242.82 Hz, *J* = 8.80 Hz, C4'), 168.40 (C5), 176.71 (COOH) ppm; UV-vis (H_2O, 0.05% NaOH) : λmax = 250.11, 330.46 nm; fluorescence λ_{exc}= 342 nm, λ_{ems} = 433.03 nm; HRMS (ESI-MS, 140 eV): m/z $[M+H]^+$ calculated for $C_{12}H_8F_2NO_3^+$, 252.0467; found, 252.0520; calculated for $C_{12}H_7F_2NNaO_3^+$, 274.0286; found, 274.0337; RP-C18 HPLC: t_R = 10.59 min, 98.83 %.

Synthesis of diethyl 2-((2,4-difluorophenylamino)methylene)malonate (**52**).

Into a 100-mL round bottomed flask, 1.00 g (7.74 mmol) of 2,4-difluoroaniline are mixed with 1.565 mL (7.74 mmol) of diethyl 2-(ethoxymethylene)malonate. The mixture was stirred at 90 °C for 3 h and the reaction was monitored by TLC analysis (eluent *n*-hexane/ethyl acetate 1:1). At the end of the reaction, the mixture was evaporated under vacuum to obtain 2.32 g of condensation product. Yield 99%; R*f*: 0.78 (eluent *n*-hexane/ethyl acetate 1:1); ^{1}H NMR (300 MHz, $CDCl_3$): δ 11.00 (d, J = 13.24 Hz, 2H, N-H), 8.14 (d, J = 13.46 Hz, 1H, C-H), 7.24 (ddt, J = 5.39 Hz, J = 9.49 Hz, 1H, H-3), 6.92 (m, J = 6.99 Hz, 2H, H-5 and H-6), 4.28 (ddq, J = 7.12 Hz, 4H, OCH_2CH_3), 1.38 (ddt, J = 7.12 Hz, 6H, OCH_2CH_3) ppm.

Synthesis of ethyl 6,8-difluoro-4-hydroxyquinoline-3-carboxylate (**53**).

In a two-necked round-bottomed flask, 15 mL of diphenyl ether were heated to boiling. An amount of 2.32 g of derivative **52** were then added portion wise, and the resulting mixture was refluxed for 15 min. After cooling to room temperature, a precipitate started to precipitate from the mixture. The separated precipitate was collected by filtration and washed many times with diethyl ether and dried, obtaining 1.460 g of a pink solid. Yield 60%; R*f*: 0.48 (eluent chloroform/MeOH 95:5); ^{1}H NMR (400 MHz, DMSO-d_6): δ 8.40 (s, 1H, H-2), 7.81 (m, J = 10.96 Hz, J = 2.76 Hz, 1H, H-7), 7.66 (m, J = 9.07 Hz, J = 1.46, 1H, H-5), 4.23 (q, J = 7.09 Hz, 2H, OCH_2CH_3), 1.28 ppm (t, J = 7.10 Hz, 3H, OCH_2CH_3); ^{13}C NMR (101 MHz, DMSO-d_6): δ 172.03 (dd, J = 2.85 Hz, *C*OH), 164.80 (*C*$OOCH_2CH_3$), 158.39 (dd, J = 245.59 Hz, J = 11.29 Hz, C8), 152.83 (dd, J = 253.18 Hz, J = 12.24 Hz, C6), 145.23 (C2), 129.96 (dd, J = 7.22 Hz, J = 1.47 Hz, C4a), 126.14 (dd, J = 12.75 Hz, J = 2.02 Hz, C8a), 110.31 (C3), 108.16 (dd, J = 29.17 Hz, J = 21.14 Hz, C7), 106.50 (dd, J = 22.83 Hz, J = 4.22 Hz, C5), 62.32 (OCH_2CH_3), 14.72 (OCH_2CH_3) ppm.

Synthesis of 6,8-difluoro-4-hydroxyquinoline-3-carboxylic acid (**54**).

Into 50-mL round-bottomed flask, compound **53** (1.00 g) was dissolved in 5 mL of MeOH and 3 mL of 10% NaOH solution were added. The mixture was refluxed for 4 h and monitored by TLC analysis (eluent chloroform/MeOH, 95:5). At the end of the

reaction, MeOH was removed under vacuum and the water layer was acidified with HCl 10% to obtain a precipitate corresponding to the carboxylic acid derivative **54**. The precipitate was filtered and dried to yield 0.865 g of a white solid. Yield 87%; R*f*: 0.11 (eluent chloroform/MeOH 95:5); mp = 284-285°C; ^{1}H NMR (400 MHz, DMSO-d_6): δ 14.73 (s_{br}, 1H, OH), 13.87 (s_{br}, 1H, COOH), 8.63 (s, 1H, H-2), 8.00 (m, J = 9.90 Hz, J = 2.76 Hz, 1H, H-7), 7.78 (m, J = 8.74 Hz, J = 2.74 Hz, J = 1.54 Hz, 1H, H-5) ppm; ^{13}C NMR (101 MHz, DMSO-d_6): δ 177.33 ppm (dd, J = 3.06 Hz, OH), 166.12 (*C*OOH), 159.14 (dd, J = 247.78 Hz, J = 11.22 Hz, C8), 153.11 (dd, J = 254.91 Hz, J = 12.78 Hz, C6), 145.44 (C2), 127.19 (dd, J = 9.19 Hz, J = 2.10 Hz, C4a), 126.73 (dd, J = 14.18 Hz, J = 2.36 Hz, C8a), 109.66 (dd, J = 29.73 Hz, J = 21.13 Hz, C3), 108.45 (C3), 106.04 (dd, J = 23.16 Hz, J = 4.19 Hz, C5) ppm; IR (KBr): ṽ (cm^{-1})= 1690.00 (C=O), 1490.20 (C=N), 1389.89 (C-OH), 1315.54 and 1284.36 (C-OH), 1119.33 (C-F); UV-Vis (H_2O, 0.05% NaOH): 228.28 nm, 303.90 nm; HRMS (ESI-MS, 140 eV): m/z $[M+H]^+$ calculated for $C_{10}H_6F_2NO_3^+$, 226.031; found, 226.0414; calculated for $C_{10}H_5F_2NNaO_3^+$, 248.013; found, 248.0232; RP-C18 HPLC: t_R = 9.75 min, 97.04 %.

General procedure for the synthesis of N-methylated derivatives (**55-57**). As a typical procedure, the synthesis of 2-benzyl-3-hydroxy-1-methylpyridin-1-ium-4-carboxylate **55** is described in detail. 0.200 g (0.872 mmol) of compound **14** were dissolved in 4 mL of DMF. The resulting suspension was stirred at room temperature and 10% NaOH (7.5 ml) was added drop-wise until complete dissolution of the solid was obtained (pH 9-10). Methyl iodide, 0.163 g (2.62 mmol, d=2.28 g ml^{-1}) was added under stirring and the mixture was heated to 150°C for 24 h and monitored by TLC analysis (eluent CH_3CN/H_2O, 1:1). Once the starting material disappeared, the solvent was removed under reduced pressure obtaining a coloured solid which was dissolved in boiling water (50 mL) and added of 5% H_2O_2 (1 mL). Then, the iodine was exhaustively extracted with $CHCl_3$ (5×15 mL) in a separating funnel. The mixture was separated, and the aqueous phase was acidified with HCl 1M to obtain the precipitation of the desired methylated compound, which was filtered and dried. The crude product was purified by Biotage Isolera Spektra Flash-column chromatography (RP-C18, eluent CH_3CN/H_2O, 1:1) to yield 0.071 g of a yellow solid.

2-Benzyl-3-hydroxy-1-methylpyridin-1-ium-4-carboxylate (**55**).

Yield 36%; R*f*: 0.36 (eluent CH_3CN/H_2O, 1:1); mp = 260-262°C; ^{1}H NMR (300 MHz, D_2O/NaOD): δ 7.36 (m, J = 6.03 Hz, 1H, H-6), 7.16 (m, 2H, H-3'and H-5'), 7.13 (m, 1H, H-4'), 7.10 (m, 1H, H-5), 6.97 (m, 2H, H-2'and H-6'), 4.24 (s, 2H, CH_2), 3.72 (s, 3H,

CH_3) ppm; ^{13}C NMR (75 MHz, D_2O/NaOD): δ 174.75 (C4), 168.33 (C3), 148.15 (C2), 141.96 (C4), 135.91 (C1'), 128.93 (C3'and C5'), 128.29 (C6), 127.87 (C2'and C6'), 126.79 (C4'), 121.48 (C5), 45.34 (CH_3), 37.45 (CH_2) ppm; IR (KBr): ṽ (cm^{-1})= 3422.04 (OH, bonded), 3086.09 (CH, aromatic), 1653.88 (C=O), 1474.71 (C=N), 1376.11 (C-OH), 1302.11 and 1246.64 (C-OH); UV-Vis (H_2O, 0.05% NaOH): 214.31, 321.85 nm; HRMS (ESI-MS, 140 eV): m/z $[M+H]^+$ calculated for $C_{14}H_{13}NO_3^+$, 244.0968; found, 244.1166; calculated for $C_{14}H_{12}NNaO_3^+$, 266.0788; found, 266.0927; RP-C18 HPLC: t_R = 8.70 min, 97.7 %.

2-Phenyl-5-hydroxy-1-methylpyridin-1-ium-4-carboxylate (**56**).

Compound **56** was prepared as for compound **55** by reacting compound **38** (0.045 g) with CH_3I (0.039 mL) to obtain 0.037 g of a yellow solid. Yield 70%; R*f*: 0.43 (eluent CH_3CN/H_2O, 1:1); mp = 165°C; ^1H NMR (300 MHz, D_2O/NaOD): δ 7.68 (s, 1H, H-6), 7.49 (m, 3H, H-3', H-4'and H-5'), 7.40 (m, 2H, H-2' and H-6'), 7.29 (s, 1H, H-3), 3.82 (s, 3H, CH_3) ppm; ^{13}C NMR (75 MHz, D_2O/NaOD): δ 182.45 (*C*OOH), 154.92 (C2), 146.69 (C5), 144.69 (C4), 140.18 (C6), 137.66 (C1'), 128.77 (C3'and C5'), 128.30 (C4'), 125.79 (C2'and C6'), 119.07 (C3) ppm; IR (KBr): ṽ (cm^{-1})= 3422.37 (OH, bonded), 2980.59 (CH, aromatic), 2775.42 (CH_3), 2446.10 (CO-OH, bonded), 1647.96 (C=O), 1458.47 (C=N), 1354.99 (C-OH), 1299.27 and 1262.20 (C-OH); UV-Vis (H_2O, 0.05% NaOH): 326.87 nm; HRMS (ESI-MS, 140 eV): m/z $[M+H]^+$ calculated for $C_{13}H_{12}NO_3^+$, 230.0812; found, 230.0934; calculated for $C_{13}H_{11}NNaO_3^+$, 252.0631; found, 252.0750; RP-C18 HPLC: t_R = 6.52 min, 97.9 %.

5-Hydroxy-2-(3'-methoxyphenyl)-1-methylpyridin-1-ium-4-carboxylate (**57**).

Compound **57** was prepared as for compound **55** by reacting compound **41** (0.122 g) with CH_3I (0.093 mL) to obtain 0.059 g of an orange solid. Yield 46%; R*f*: 0.40 (eluent CH_3CN/H_2O, 1:1); mp = 140-143°C; ^1H NMR (300 MHz, D_2O/NaOD): δ 7.55 (s, 1H, H-6), 7.28 (t, J = 8.02 Hz, 1H, H-5'), 7.14 (s, 1H, H-3), 6.94 (dd, J = 8.18 Hz, J = 2.28 Hz, 1H, H-4'), 6.88 (m, J = 1.5Hz, 1H, H-6'), 6.85 (m, 1H, H-2'), 3.68 (s, 3H, CH_3), 3.64 (s, 3H, OCH_3) ppm; ^{13}C NMR (75 MHz, D_2O/NaOD): δ 173.72 (*C*OOH), 164.27 (C5), 161.24 (C3'), 154.23 (C2), 140.11 (C4), 139.43 (C5), 139.27 (C1'), 129.08 (C5'), 127.78 (C2'), 126.94 (C6'), 121.72 (C3), 120.76 (C4'), 62.74 (OCH_3), 48.25 (CH_3) ppm; IR (KBr): ṽ (cm^{-1})= 3412.41 (OH, bonded), 3082.88 (CH, aromatic), 2553.89 (CO-OH, bonded), 2083.48 (intermolecular H bond), 1670.19 (C=O), 1542.41 (C=N), 1352.43 (C-OH), 1279.59 (C-OH), 1279.59 and 1229.93 (C-O-C); UV-Vis (H_2O, 0.05% NaOH): 216.14, 325.17 nm; HRMS (ESI-MS, 140 eV): m/z $[M+H]^+$ calculated for $C_{14}H_{14}NO_4^+$,

260.0917; found, 260.1043; calculated for $C_{14}H_{13}NNaO_3^+$, 282.0737; found, 282.0879; RP-C18 HPLC: t_R = 7.57 min, 95.9 %.

Solubility in water of compound 51

Five standard solutions of 2-(2,4-difluorophenyl)-5-hydroxypyridine-4-carboxylic acid (**51**) of concentration within the range $1\text{-}4\cdot10^{-5}$ M were prepared by diluting with water a 10^{-4} M mother solution in water. The absorbance of each solution was measured at 250 nm, which corresponds to a plateau region in the UV absorption spectrum of **4** and plotted against concentration. Linear regression analysis of the data points yielded this equation: y = 13405x – 0.0333. The obtained curve was used to interpolate the concentration of an aqueous saturated solution of **51** prepared by vigorously stirring **51** (2.5 mg) in water (2 mL) for 16 h, a time considered sufficient to reach equilibrium. The clear supernatant (200 μL) was diluted with water (3 mL) and the absorbance of the resulting solution measured at 250 nm. Three repetitions of this experiment yielded an average value of A = 0.256 ± 0.00015, from which a concentration of (2.15 ± 0.003) 10^{-5} M was interpolated using the calibration curve. Correcting for the dilution factor, a solubility of (3.44 ± 0.0046) 10^{-4} mol/L is obtained.

Biology

Isolation and culture of human monocyte derived macrophages

Human macrophages were differentiated from peripheral blood mononuclear cells (PBMCs) obtained from buffy-coat preparations of whole human blood. The buffy-coat was mixed at a ratio of 1:1 (vol/vol) with sterile RPMI 1640 Medium (Gibco; Life Technologies, Monza, Italy) and layered over Ficoll-Paque PLUS (GE Healthcare; Sigma, Milan, Italy). After centrifugation (1200 rpm, 30 min, at 20°C without brake), PBMCs were separated by collecting the ring of cells located at the interface of the two phases. Cells were washed by centrifugation (1600 rpm, 10 min) in sterile RMPI 1640 medium, pooled, resuspended in RPMI 1640 supplemented with 1% penicillin-streptomycin and 10% FBS (all provided by Life Technologies), and counted. PBMCs were seeded ($3x10^5$ cells/well) on 96-well tissue-culture plates (Corning, Sigma) and cultured for 3 h in a 5% CO_2, humidified, 37°C incubator. Floating cells consisting mainly lymphocytes were then removed by aspiration. Attached cells were extensively washed with RPMI 1640 and differentiated in mature macrophages by incubation for 10 days with complete medium supplemented with recombinant human granulocyte-

macrophage colony-stimulating factor (rh GM-CSF, 2 ng/ml; ImmunoTools; Friesoythe, Germany). The culture medium was renewed every 3 days.

Cytotoxic assay

Diflunisal was dissolved in dimethylsulfoxide (DMSO; Sigma); aza-analogs of diflunisal were dissolved in 5N NaOH to obtain a stock solution of 100 mM. Compounds were then diluted in sterile water. For the cytotoxic assay, mature macrophages were treated for 24 h with compounds at final concentrations ranging 0 - 100 μM. Controls received the highest final DMSO and NaOH concentrations used. Treatments were removed, and cells cultured for additional 48 h. Then MTT solution (50 μg/100 μL; Sigma) was added. Cells were incubated for 4 h at 37°C and formazan crystals were then solubilized in 100 μL of SDS 10% w/vol, HCl 0.01 N. The absorbance was recorded 16 h later at 590 nm using a micro plate reader (Sunrise; Tecan, Switzerland). IC_{50} values were determined in three separate experiments, each one performed in duplicate.

Cytokines and prostaglandins measurement

Differentiated macrophages were incubated in serum-free media for 24 h with compounds at final concentrations ranging 0 - 10 μM with or without 100 ng/ml lipopolysaccharide (LPS from *Salmonella enterica* serotype typhimurium; Sigma). At the end of incubation, conditioned media was collected and stored at -80°C. Levels of TNF-α, IL-8, and IL-1β were measured in the conditioned media using commercially available enzyme-linked immunosorbent assay kits (ELISA, Affymetrix eBioscience; Prodotti Gianni, Milan, Italy) and developed using 3,3',5,5'-tetrametilbenzidina (TMB). Optical densities were measured at 450 nm using a micro plate reader (Sunrise). The sensitivity of the assays ranged 5 to 15 pg/ml. PGs were screened in the conditioned medium using the Prostaglandin Screening ELISA kit (Cayman Chemical; Vinci-Biochem, Vinci, Italy). The sensitivity of the assay was of approximately 30 pg/mL. All experiments were performed in triplicate.

Bacterial strains and antibiotics

Staphylococcus aureus ATCC 33592, *Streptococcus pyogenes* ATCC 14289, *Klebsiella pneumoniae* ATCC 13883, *Enterococcus faecium* ATCC 700221, *Pseudomonas aeruginosa* ATCC BAA-2108, and *Escherichia coli* ATCC 43894 were purchased from ATCC (LGC Standards; Milan, Italy) and cultured at 37°C in Mueller-Hinton broth (MHB) or agar. Methicillin (MET), geneticin (GEN), ciprofloxacin (CPR), tetracycline (TET), erythromycin (ERY) were purchased from Sigma and dissolved in sterile water.

Antimicrobial susceptibility test

The antimicrobial activities of antibiotics, diflunisal, and aza-analogs of diflunisal were tested through the determination of the minimum inhibitory concentration (MIC) standardized by the Clinical and Laboratory Standards Institute.[23] The bacterial inoculum was growth in 10 mL of MHB at 37°C for 16 h. Concentration of bacteria was adjusted to 0.5 McFarland. Bacteria were diluted in MHB and dispensed in 96-well microtiter plates (final bacterial concentration $1x10^4$ CFU/well). Tested compounds were added at final concentrations ranging 0.25 μM to 32 μM and plates were incubated at 37°C for 16 h. Plates were at first visually inspected. Bacterial growth was recorded using a micro plate reader (Sunrise) by quantifying adsorption at 620 nm. In addition, bacteria were diluted and used to inoculate MH agar plates. Not inoculated control wells, wells inoculated without compounds, and wells inoculated and incubated with the highest final DMSO and NaOH concentrations were included in each test. All experiments were performed at least in triplicate.

Assessment of interaction of antibiotics and diflunisal aza-analogs

In a separate set of experiments, the antimicrobial activity of diflunisal and aza-analogs were evaluated in combination with sub-inhibitory concentrations (MIC/4) of antibiotics. Experiments were performed as described above and bacterial growth was monitored by recording adsorption at 620 nm and by counting bacterial colonies growth on MH agar plates. The inhibitor activity was reported as minimum modulatory concentration (MMC_4), as means the lowest concentrations of aza-analog required to achieve the antibacterial activity in combination with the sub-inhibitory concentration (MIC/4) of the antibiotic.[24] All experiments were performed at least in triplicate.

Statistical analysis

Data were analyzed by two-way analysis of variance (ANOVA) followed by Bonferroni multiple comparison post hoc test using GraphPad Prism (version 6.0). *P* values <0.05 were considered statistically significant.

Acknowledgements

Synthesis by D. Carta, M. Dal Prà, M.G. Ferlin and biological evaluation by P. Brun, G. Bernabè, I. Castagliuolo were supported by financial grants from the University of Padova, Italy.

References

[1] C. Stone, C. Van Arman, V. Lotti, D. Minsker, E. Risley, W. Bagdon, D. Bokelman, R. Jensen, B. Mendlowski, C. Tate, H. Peck, R. Zwickley, S. McKinney, Pharmacology and toxicology of diflunisal., Br. J. Clin. Pharmacol. 4 (1977) 19S–29S. doi:10.1111/j.1365-2125.1977.tb04510.x.; R.N. Brogden, R.C. Heel, G.E. Pakes, T.M. Speight, G.S. Avery, Diflunisal: A Review of its Pharmacological Properties and Therapeutic Use in Pain and Musculoskeletal Strains and Sprains and Pain in Osteoarthritis, Drugs. 19 (1980) 84–106. doi:10.2165/00003495-198019020-00002.

[2] A.S. Hendrix, T.J. Spoonmore, A.D. Wilde, N.E. Putnam, N.D. Hammer, D.J. Snyder, S.A. Guelcher, E.P. Skaar, J.E. Cassat, Repurposing the nonsteroidal anti-inflammatory drug diflunisal as an osteoprotective, antivirulence therapy for Staphylococcus aureus osteomyelitis, Antimicrob. Agents Chemother. 60 (2016) 5322–5330. doi:10.1128/AAC.00834-16.

[3] V. Khodaverdian, M. Pesho, B. Truitt, L. Bollinger, P. Patel, S. Nithianantham, G. Yu, E. Delaney, E. Jankowsky, M. Shoham, Discovery of antivirulence agents against methicillin-resistant Staphylococcus aureus., Antimicrob. Agents Chemother. 57 (2013) 3645–52. doi:10.1128/AAC.00269-13.

[4] D. Williams, T. Lemke, *Foye's principles of medicinal chemistry*. Philadelphia: Lippincott Williams & Wilkins. 2002.

[5] P. Brun, A. Dean, V. Di Marco, P. Surajit, I. Castagliuolo, D. Carta, M.G. Ferlin, Peroxisome proliferator-activated receptor-γ mediates the anti-inflammatory effect of 3-hydroxy-4-pyridinecarboxylic acid derivatives: Synthesis and biological evaluation, Eur. J. Med. Chem. 62 (2013) 486–497. doi:10.1016/j.ejmech.2013.01.024.

[6] F.N. Penas, D. Carta, G. Dmytrenko, G.A. Mirkin, C.P. Modenutti, Á.C. Cevey, M.J. Rada, M.G. Ferlin, M.E. Sales, N.B. Goren, Treatment with a new peroxisome proliferator-activated receptor gamma agonist, pyridinecarboxylic acid derivative, increases angiogenesis and reduces inflammatory mediators in the heart of Trypanosoma cruzi-infected mice, Front. Immunol. 8 (2017). doi:10.3389/fimmu.2017.01738.

[7] D.C. Swinney, J. Anthony, How were new medicines discovered?, Nat. Rev. Drug Discov. 10 (2011) 507–519. doi:10.1038/nrd3480.

[8] L.M. Espinoza-Fonseca, The benefits of the multi-target approach in drug design and discovery, Bioorganic Med. Chem. 14 (2006) 896–897. doi:10.1016/j.bmc.2005.09.011.

[9] J.N. Pendleton, S.P. Gorman, B.F. Gilmore, Clinical relevance of the ESKAPE pathogens, Expert Rev. Anti. Infect. Ther. 11 (2013) 297–308. doi:10.1586/eri.13.12.

[10] G.A. Patani, E.J. LaVoie, Bioisosterism: A rational approach in drug design, Chem. Rev. 96 (1996) 3147–3176. doi:10.1021/cr950066q.

[11] G.L. Walford, H. Jones, T.Y. Shen, Aza Analogs of 5-(Para Fluorophenyl)Salicylic Acid, J. Med. Chem. 14 (1971) 339–343. doi:Doi 10.1021/Jm00286a017.

[12] H.Z. Zhang, Z.L. Zhao, C.H. Zhou, Recent advance in oxazole-based medicinal chemistry, Eur. J. Med. Chem. 144 (2018) 444–492. doi:10.1016/j.ejmech.2017.12.044.

[13] J.I. Levin, L.M. Laakso, Oxazole Diels–Alder Reactions, in: Oxazoles Synth. React. Spectrosc. Part A, John Wiley & Sons, Inc., Hoboken, NJ, USA, 2003: pp. 417–472. doi:10.1002/0471428035.ch3.

[14] T. Chancellor, C. Morton, A Facile Procedure for the Synthesis of *N* -Formyl Amino Acid Esters, Synthesis (Stuttg). 1994 (1994) 1023–1025. doi:10.1055/s-1994-25628.

[15] R.G.F. Giles, C.P. Taylor, Synthesis of a protected 2-ethoxy-3-hydroxyethylfuran and its regioselectivity as a Diels – Alder diene on reaction with 3 , 5-dimethoxydehydrobenzene, Arkivoc. (2002) 149–165.

[16] K. E. Benenato, A. L. Choy, M. R.Hale, P. Hill, V. Marone, M. Miller (Astrazeneca, UK), Hydroxamic acid derivatives as gram-negative antibacterial agents, WO2010/100475 A1, 2010.

[17] D. J. Collins, T. C. Hughes, W.M. Johnson, Regiospecific Syntheses of the Monomethylated 3-Phenyldihydro-1,2,4-triazin-6(1H)-ones**,** Aust. J. Chem. 1996, 463-468.

[18] G.X. Li, Z.Q. Liu, X.Y. Luo, Dichloro-4-quinolinol-3-carboxylic acid: Synthesis and antioxidant abilities to scavenge radicals and to protect methyl linoleate and DNA, Eur. J. Med. Chem. 45 (2010) 1821–1827. doi:10.1016/j.ejmech.2010.01.018.

[19] European Committee on Antimicrobial Susceptibility Testing. 2013. Breakpoint tables for interpretation of MICs and zone diameters, version 3.1, 2013. http://www.eucast.org/fileadmin/src/media/PDFs/EUCAST_files/Breakpoint_tables/Breakpoint_table_v_3.1.pdf

[20] M.E. Skindersoe, M. Alhede, R. Phipps, L. Yang, P.O. Jensen, T.B. Rasmussen, T. Bjarnsholt, T. Tolker-Nielsen, N. Høiby, M. Givskov, Effects of antibiotics on quorum sensing in Pseudomonas aeruginosa, Antimicrob. Agents Chemother. 52 (2008) 3648–3663. doi:10.1128/AAC.01230-07.

[21] K. Reuter, A. Steinbach, V. Helms, Interfering with bacterial quorum sensing, Perspect. Medicin. Chem. 8 (2016) 1–15. doi:10.4137/PMc.s13209.

[22] C.A. Deryke, Y.L. Su, J.L. Kuti, D.P. Nicolau, Optimising dosing strategies of antibacterials utilising pharmacodynamic principles: Impact on the development of resistance, Drugs. 66 (2006) 1–14. doi:10.2165/00003495-200666010-00001.

[23] CLSI, Methods for Dilution Antimicrobial Susceptibility Tests for Bacteria that Grow Aerobically, Approved Standard, 9th ed., CLSI document M07-A9. Clinical and Laboratory Standards Institute, 950 West Valley Road, Suite 2500, Wayne, Pennsylvania 19087, USA, 2012**.**

[24] F. Fontaine, A. Hequet, A.S. Voisin-Chiret, A. Bouillon, A. Lesnard, T. Cresteil, C. Jolivalt, S. Rault, First identification of boronic species as novel potential inhibitors of the Staphylococcus aureus NorA efflux pump, J. Med. Chem. 57 (2014) 2536–2548. doi:10.1021/jm401808n.

CHAPTER 2

In vitro and in vivo anticancer activity of anti-tubulin fluorinated 7-phenyl-pyrroloquinolinones

Synopsis

Tricycle 7-phenyl-pyrroloquinolinones (7-PPyQs) are a class of compounds that have showed interesting *in vitro* and *in vivo* antiproliferative activity acting as tubulin polymerization inhibitors. Despite the excellent pharmacodynamic, 7-PPyQs suffer from poor metabolic stability, due to oxidative metabolism and consequently have a low half-life. The design and synthesis of some fluorinated 7-PPyQs derivatives were accomplished in order to improve metabolic stability and understand the effects of H-F isosterism on the biological activity. Of the new synthesized compounds, potent cytotoxicity (low and sub-nanomolar GI_{50} values) was observed for some of them, in both leukemic and solid tumor cell lines. Experiments carried out with derivatives **12** and **15**, in a mouse syngeneic model demonstrated high antitumor activity, which significantly reduced the tumor mass at doses four times lower than that required for combretastatin-4-phosphate (CA-4P) used as reference compound. Metabolic stability studies of the newly synthesized compounds were performed to assess the role of fluorine substitution towards oxidative metabolism.

Introduction

Antimitotic compounds are one of the most employed and effective agents for the inhibition of cancer growth. The general mechanism of action is the inhibition of microtubules polymerization dynamics which induces the mitotic arrest and the apoptosis process.[1] The most important advantage of this class of antitumor drugs over other classical chemotherapeutic agents, is that they do not interfere or damage the DNA macromolecule and, therefore, do not cause any cell genome mutations. However, even the most clinically effective antimitotics such as taxanes and Vinca alkaloids, suffer from two major drawbacks: development of resistance within tumor cells and neurological toxicity. Therefore, during the past few decades, efforts to identify novel microtubule inhibitors have produced dozens of microtubule targeting compounds, some of which are

in clinical and preclinical trials. They are either natural (like colchicine or flavones) or synthetic small molecules (Figure 1). A synthetic class that generated our interest is the class of 2-phenylquinolinones (2-PQs) which are structurally derived from the flavone nucleus by isosteric substitution of the cyclic oxygen with a nitrogen atom. Compared to flavone derivatives, 2-PQs showed a more selective mechanism of action, inhibiting tubulin polymerization and presented a higher antiproliferative activity.[2,3]

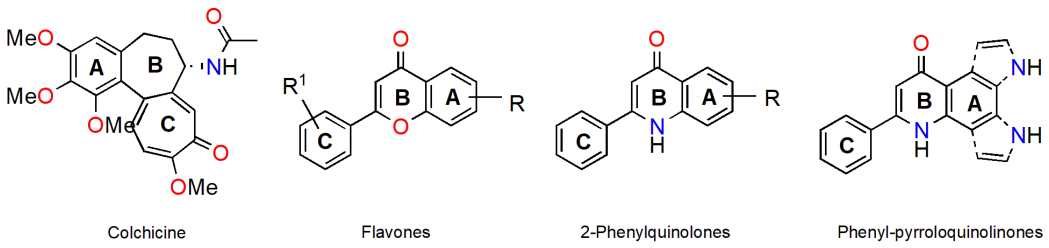

Figure 1. Chemical structures of colchicine, flavones, 2-phenylquinolinones and phenyl-pyrroloquinolinones

In the last decades we have been determined in the development of tricyclic pyrroloquinolinones (PyQs) which showed interesting *in vitro* and *in vivo* antiproliferative activity acting as tubulin polymerization inhibitors by binding at the colchicine site into β-tubulin.[4-6] Several 7-PPy-[3,2-f]-Qs derivatives of various geometry and variously substituted were synthesized and biologically evaluated providing relevant structure-activity relationships (SARs) that let us establish the essential structural elements for an effective cytotoxic activity (Figure 2). Briefly, the crucial structural elements for the best antiproliferative activity are the [3,2-f] geometry of the pyrroloquinolinone core, the phenyl ring at position 7 and the carbonyl group at position 9. The only portion of the molecule that tolerates substituents is position 3. In the past, we demonstrated how to modulate the potency of 7-PPyQ derivatives by suitable substitution with alkyl and acyl substituents.[7,8]

Recently, SARs were also confirmed by docking studies of a series of 7-PPyQs in the site of colchicine into β-tubulin, in which a key hydrogen bond interaction between quinolinonic NH and Val236 was disclosed.[7,8] Notably, their binding mode is compatible with a competitive mechanism of action at the colchicine site.

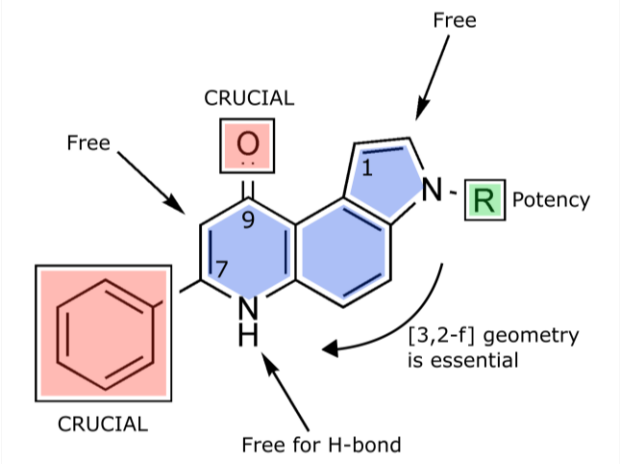

Figure 2. Structure-Activity Relationships of 7-PPyQs

Structural optimization efforts produced highly antiproliferative phenyl-pyrroloquinolinones (PPyQs) acting at nanomolar and sub-nanomolar concentrations by an apoptotic mechanism against a broad spectrum of human tumour cell lines. Overcoming resistance for taxol and vincristine, no or poor cytotoxicity in non-tumour cell lines and a worthy synergism with conventional chemotherapeutic agents in inhibiting leukemia cell proliferation were also observed and studied.[7-9] Despite their promising potency and efficacy, preliminary studies on *in vitro* metabolic stability of 3*N*-alkyl-7-PPyQs showed poor metabolic profile characterized by fast multiple oxidations and a low half-life (data not shown).

The introduction of fluorine in organic molecules drug candidates has become a common practice in modern small-molecule drug discovery. The presence of the small and electronegative fluorine generally is able to modulate all aspects of molecular properties, including drug potency, physical chemistry and pharmacokinetics. Indeed, several examples are reported in the literature in which H-F isosterism was able to improve the duration of action and the drug potency, to allow the establishment of new polar interactions and ameliorate metabolic stability.[10]

In order to investigate the effects of H-F isosterism on the metabolic and biological properties of 7-PPyQs, we designed and synthesized compounds **12-14**, monofluoro-phenyl derivatives of 3*N*-ethyl 7-PPyQ **20** and compounds **15** and **19**, monofluoro-derivatives of the 3*N*-benzoyl-7-PPyQ **21**, respectively. Previously, both compounds **20** and **21** showed promising *in vitro* biological properties: nanomolar and sub-nanomolar anticancer activity against a broad panel of human cancer cell lines, poor cytotoxicity in human non-tumor cell lines, antiproliferative activity in resistant cell lines.[6-9] Biological

investigations with novel fluoro-derivatives including *in vitro* cellular cytotoxicity, tubulin inhibition assays and *in vivo* experiments on a melanoma mouse model were performed. *In vitro* studies to get preliminary information on metabolic stability of the fluorine derivatives allowed us to obtain more insights on how fluorine substitution affects the metabolism and pharmacodynamics of original compounds.

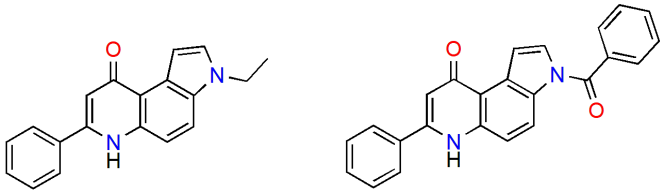

Figure 3. Structures of previously synthesised derivatives **20** and **21**

Results and Discussion

Chemistry

The synthetic four-step pathway leading to 7-PPyQ compounds is described in Scheme 1. Firstly, commercially available 5-nitroindole was subjected to *N*-alkylation and acylation reactions using appropriate halogenated compounds to obtain the nitro indole derivatives **1-3**. The catalytic reduction (Pd/C 10%, H_2 at atmospheric pressure, ethyl acetate) of intermediate **1** and (Pt/C 10%, H_2 at atmospheric pressure, ethyl acetate) of intermediates **2** and **3** gave the corresponding aminoindoles **4-6** in almost quantitative yields. Compound **4** was reacted with commercial ethyl-2-, -3- and -4-fluoro benzoyl-acetate, compound **5** with ethyl-3-fluoro benzoyl acetate, while compound **6** with ethyl benzoyl acetate. All the reactions were carried out in absolute ethanol at reflux in the presence of a catalytic amount of acetic acid, yielding the acrylate derivatives as crude material **7-11**. These had to be purified by silica gel column chromatography before being submitted to thermal cyclization in boiling diphenyl ether (250 °C) to obtain the final products **12-15** in good yields. Compound **11** cyclized but in the meantime lost the 2-fluoro-benzoyl moiety giving the known 7-PPyQ **16**. For this reason, in order to obtain the 3*N*-fluorobenzoyl 7-PPyQ **19** (Scheme 2), compound **16** was directly reacted with 2-fluorobenzoyl chloride **17** in DMF in the presence of NaH obtaining two products: the main reaction product was identified as the isomeric ester **18** (73%) and the desired 3-amide compound **19** with lower yield (22%).

Scheme 1. Synthesis of fluorinated 7-PPyQs derivatives **12-15**

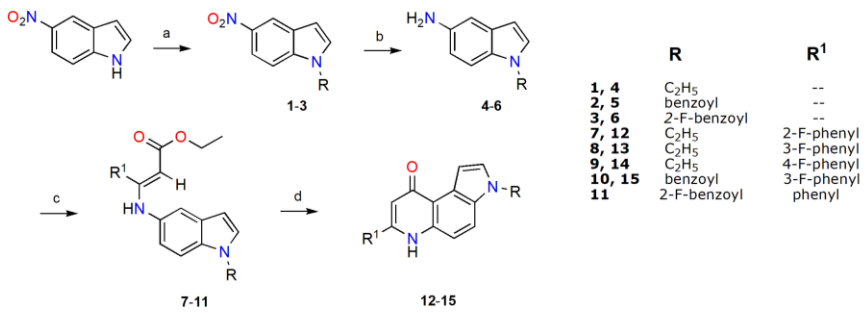

Reagents and conditions: a) NaH, Bromoethane, DMF, 50°C, 6h, 99% (**1**) or benzoyl chloride, 2-fluoro-benzoyl chloride, py, DMAP, rt, 24h, 54% (**2**,**3**); b) H_2, Pd/C 10%, EtOAc, 50°C, 12 h, 98% (**4**) or H_2, Pt/C 10%, EtOAc, rt, 2h, 84% (**5**,**6**); c) ethyl (2-fluorobenzoyl)acetate (**7**), ethyl (3-fluorobenzoyl)acetate (**8**,**10**), ethyl (4-fluorobenzoyl)acetate (**9**), ethyl benzoylacetate (**11**), AcOH, drierite, abs EtOH, 100°C, 24h, 35-70%; d) Ph_2O, 250°C, 15 min, 27-56%.

Scheme 2. Synthesis of fluorinated 7-PPyQs derivative **19**

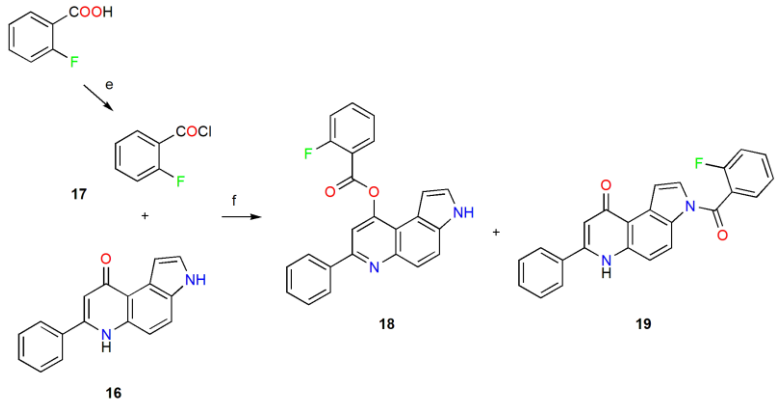

Reagents and conditions: e) $SOCl_2$, DCM, 80°C, 2h, 80%; f) NaH, DMF, rt, 30 min., 73% (**18**), 22% (**19**)

Biology

In vitro antiproliferative activities

The new compounds were designed to obtain additional SAR information by introducing a fluorine atom at various positions (*ortho*-, *meta*-, *para*-) of 7-phenyl ring in parent compound **20** and at *meta*-position of 7-phenyl ring and *ortho*-position of *N*-benzoyl substituent of parent compound **21**. Evaluation of antiproliferative activities of **12**-**15** and **19** was performed with the 3-(4,5-dimethylthiazol-2-yl)-2,5- diphenyltetrazolium bromide (MTT) assay against a panel of 11 human tumour cell lines (DND41, Jurkat, HL-60, RS4;11, MCF-7, MDA-MB-231, MDA-MB-468, HeLa, A375, A2058, HT-29). The

results are expressed as concentrations that inhibit cell growth by 50% (GI_{50} values) and are presented in Table 1. As reference compound CA-4 was also added. From the cytotoxicity data reported in the Table, some noteworthy considerations can be made with respect to reference compounds **20** and **21**. Regarding compounds **12**-**14**, it is clear that the fluorine substitution at *ortho*- (**12**) and *meta*-position (**13**) of 7-phenyl ring is well-tolerated and actually increases the cytotoxic effect in most tumour cell lines. In particular, both compounds **12** and **13** are effective in most cases at sub-nanomolar concentrations. The same cannot be said for compound **14** in which the H-F substitution at *para*-position resulted in a decrease of the cytotoxic power, compared to parent compound **20**. This result was unexpected and probably the reason for this behaviour may reside on the electronic effect impaired to the system by *para*-fluoro substitution. Also compounds **15** and **19** demonstrated to be less potent than parent compound **21**, even though, especially for compound **15**, the GI_{50}s values are still remarkable and in the nanomolar range.

Table 1. *In vitro* cell growth inhibitory effects of compounds **12**-**15** and **19**-**21**.

GI_{50} (nM)[a] ± SE

Compd	DND41	Jurkat	HL-60	RS4;11	MCF-7	MDA-MB-231	MDA-MB-468	HeLa	A375	A2058	HT-29
12	0.26± 0.088	0.19± 0.01	0.17± 0.07	0.09± 0.005	246.6± 12.0	1459± 137.0	22.3± 2.2	1.2± 0.1	15.5± 1.5	4.8± 0.2	1.1± 0.2
13	0.13± 0.020	0.11± 0.02	0.08± 0.002	0.07± 0.006	52.7± 10.7	25.8± 11.2	15.0± 1.1	0.7± 0.05	11.4± 2.0	3.5± 0.4	0.9± 0.1
14	476.7± 128.1	333.5± 12.1	1440± 42.4	293.3± 61.7	51.3± 9.9	206± 8.3	43.0± 12.6	340± 18.4	69.8± 5.9	1180± 90.7	447± 12.0
15	10.2± 0.160	32.4± 2.2	15.1± 0.090	56±12	103± 50	476± 43	871± 60	13.3± 0.9	n.d.	n.d.	402± 37.
19	240.0± 15.3	53.7± 20.2	276.0± 20.9	119.7± 25.4	1082± 24.9	3031± 340.4	70± 15.7	9.3± 1.1	332± 13.6	322± 12.5	26.6± 2.0
20[b]	n.d.	0.5± 0.2	0.5± 0.2	2± 0.3	40± 10	n.d.	n.d.	11± 8	n.d.	n.d.	32± 1.2
21[b]	n.d.	16± 6	2± 0.8	0.3± 0.1	0.2± 0.1	n.d.	n.d.	0.2± 0.04	n.d.	n.d.	0.1± 0.08
CA-4[c]	n.d.	5.0± 0.6	n.d.	0.8± 0.2	n.d.	n.d.	n.d.	4.0± 1.0	n.d.	n.d.	3100± 100

[a] Results are expressed as compound concentration required to inhibit tumour cell proliferation by 50%. Data are expressed as the mean ± SE from the dose-response curves of at least three independent experiments. n d: not determined;[b] Data taken from [6]; [c] Data taken from [8].

Evaluation of cytotoxicity of compounds 12, 13 and 15 in human non-cancer cells

To obtain a preliminary indication of the cytotoxic potential of these derivatives in normal human cells, three of the most active compounds (**12**, **13** and **15**) were evaluated *in vitro* against peripheral blood lymphocytes (PBL) from healthy donors (Table 2). All the three compounds showed a very low activity in quiescent lymphocytes (GI_{50}>20 μM), while in the presence of the mitogenic stimulus phytohematoaglutinin (PHA), the GI_{50} was slightly decreased, although substantially remaining in the higher micromolar range. Notably, these values were almost 10000-30000 times higher than that observed against the lymphoblastic cell lines Jurkat, DND-41 and CEM (Tables 1 and 3). These results indicate that these compounds are endowed with a modest inhibitory effect in primary lymphocytes, as previously observed for other antimitotic derivatives developed by our group.[7-8]

Table 2. Cytotoxicity of compounds **12**, **13** and **15** on human peripheral blood lymphocytes (PBL)

GI_{50} (μM)[a] ± SEM

	12	**13**	**15**
$PBL_{resting}$[b]	28.0±2.3	31.3±10.3	45.6±6.3
PBL_{PHA}[c]	15.2±6.9	10.8±3.8	17.6±3.9

[a] Compound concentration required to reduce cell growth inhibition by 50%; [b] PBL not stimulated with PHA; [c] PBL stimulated with PHA; Values are the mean ± SEM for three separate experiments.

Effect of compounds 12, 13 and 15 on multidrug resistant cells

To investigate whether these derivatives are substrates of drug efflux pumps, compounds **12**, **13** and **15** were tested against $CEM^{Vbl\text{-}100}$ cells that are a multidrug-resistant line selective against vinblastine and that overexpress P-glycoprotein (P-gp).[5] This membrane protein acts as a drug efflux pump and exhibits resistance to a wide variety of structurally unrelated anticancer drugs and other compounds. As shown in Table 3, all the compounds exhibited cytotoxic activity in the CEM^{Vbl100} cell line that was even higher than their activity against the parental line, suggesting that these derivatives are not substrates for P-gp.

Table 3. Cytotoxicity of **12**, **13** and **15** on multidrug resistant cells CEM^{Vbl100}

GI_{50} (nM)[a] ± SEM

	CEM^{wt}	**CEM^{Vbl100}**
12	3.1±0.2	1.1±0.4
13	2.2±0.3	0.8±0.3
15	44±6	36±10

[a] Compound concentration required to reduce cell growth inhibition by 50%; Values are the mean ± SEM for three separate experiments.

Inhibition of tubulin polymerization and colchicine binding

To evaluate the tubulin interaction properties of the new compounds, we investigated their effects on the inhibition of tubulin polymerization and on the binding of [^{3}H]colchicine to tubulin (Table 4).[11-13] For comparison, CA-4 was examined in contemporaneous experiments as a reference compound. Among the test compounds, **12**, **13** and **15** strongly inhibited tubulin assembly with IC_{50} below 1 μM (0.96, 0.78 and 0.38 μM, respectively) being **12** and **13** slightly higher than that obtained for the reference compounds CA-4 (IC_{50} = 0.64 μM) whereas compound **15** showed the highest activity also in comparison with CA-4. These results with tubulin correlate well with the growth inhibitory effects exhibited by these compounds indicating that their antiproliferative activity derives mostly from an interaction with tubulin.

The other compounds also inhibited tubulin assembly with a low IC_{50} values in the range of 1.3-3.7 μM. All compounds inhibited the binding of [^{3}H]colchicine to tubulin, with the best activity occurring with **12**, **13** and **15**, but none approached CSA-4 in its potency as an inhibitor of colchicine binding.

Table 4. Inhibition of tubulin polymerization and colchicine binding

Compound	**Inhibition of tubulin assembly**	**Inhibition of colchicine binding**
	IC_{50} (μM) ± SD[a]	**% Inhibition ± SD[b]**
12	0.96±0.08	77±3
13	0.78±0.03	83±5
14	3.7± 0.4	12±4
15	0.38±0.9	70±0.8
19	1.3±0.07	34±4
20	0.57±0.02	73±0.7

21	0.89±0.04	70±2
CA-4[c]	0.64±0.1	100±2

[a] Inhibition of tubulin polymerization. Tubulin was at 10 μM.

[b] Inhibition of [^{3}H]colchicine binding. Tubulin and colchicine were at 1 and 5 μM, respectively.

[c] Data taken from [6]

Influence of test compound 12 on the cell cycle

As representative of the new library of fluorinated 7-PPyQs, compound **12** was selected for further biological investigations. The effect on cell cycle progression was examined by flow cytometry in two melanoma cell lines (A375 and A2058) (Figure 4, Panels A and B). After a 24 h treatment, **12** evaluated at the concentration of 50 and 100 nM induced a strong G2/M arrest already at the lowest concentration used in both cell lines. A concomitant reduction of both the S and G1 phases was also observed. In order to determine whether **12** was able to block cells at the mitotic phase (M), cells were stained with an immunofluorescent antibody to p-histone H3, a well-known mitotic marker, as well as PI, and analyzed by flow cytometry. As shown in Figure 4 (Panel C), HeLa cells arrested in M phase by treatment with **12** are readily distinguished from G2 cells by the higher level of p-histone H3. In particular, treatment with **12** induced an increase in the percentage of mitotic cells from the about 1.5% observed in untreated cells to about 10% and 44 % with 50 and 100 nM concentrations, respectively.

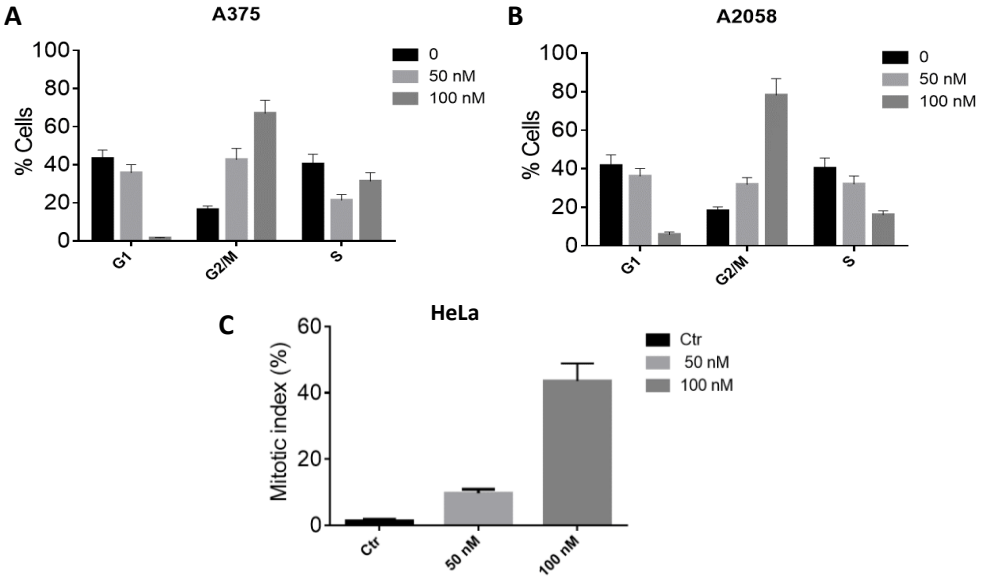

Figure 4. Percentage of cells in each phase of the cell cycle in A375 cells (Panel A) and A2058 (Panel B) treated with compounds **12** at the indicated concentrations for 24 h. Cells were fixed and labelled with PI

and analyzed by flow cytometry as described in the Experimental Section. Data are represented as mean of two independent experiments ± SEM. Panel C: Mitotic index evaluated in Hela cells with compound **12** after 24 h of treatment.

We also studied the association between **12**-induced G2/M arrest and alterations in G2/M regulatory protein expression in HeLa cells. As shown in Figure 5, compound **12** caused, an increase in cyclin B1 expression after 24 h in a concentration-dependent manner, and 48 h, indicating an activation of the mitotic checkpoint following drug exposure.

This effect was confirmed by a reduction in the expression of phosphatase cdc25c at 24 h, followed by a disappearance in its expression at 48 h. This was associated with the appearance of slower migrating forms of phosphatase cdc25c indicative of cdc25c phosphorylation. The phosphorylation of cdc25c directly stimulates its phosphatase activity, and this is necessary to activate cdc2/cyclin B on entry into mitosis.[14,15] We also observed a decrease of the phosphorylated form of cdc2 kinase, in particular after the 48 h treatment.

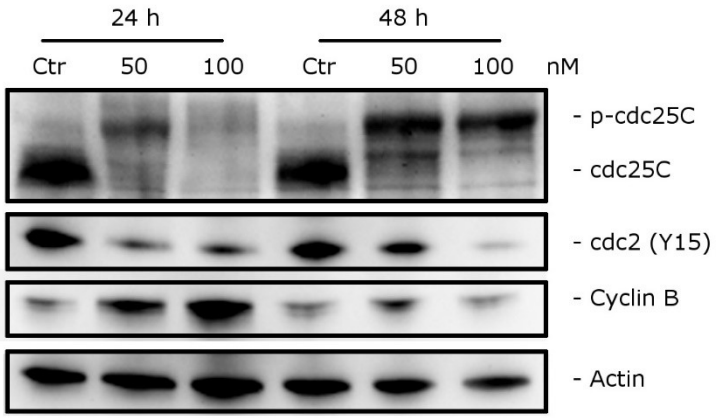

Figure 5. Effect of compound **12** on cell cycle checkpoint proteins. HeLa cells were treated for 24 or 48 h with the indicated concentrations of **12**. The cells were harvested and lysed for detection of the expression of the indicated protein by western blot analysis. To confirm equal protein loading, each membrane was stripped and re-probed with anti-γ-tubulin antibody.

Compound 12 induce apoptosis in HeLa cells

To evaluate the mode of cell death induced by test compound, we performed a bi-parametric cytofluorimetric analysis using propidium iodide (PI) and annexin-V-FITC, which stain DNA and phosphatidylserine (PS) residues, respectively.[16,17] We used Hela cells, in which we evaluated the effects of compound **12**. As shown in Figure 6 the

B

compound induced apoptosis in a time and concentration dependent manner, even at the lower concentration used (10 nM).

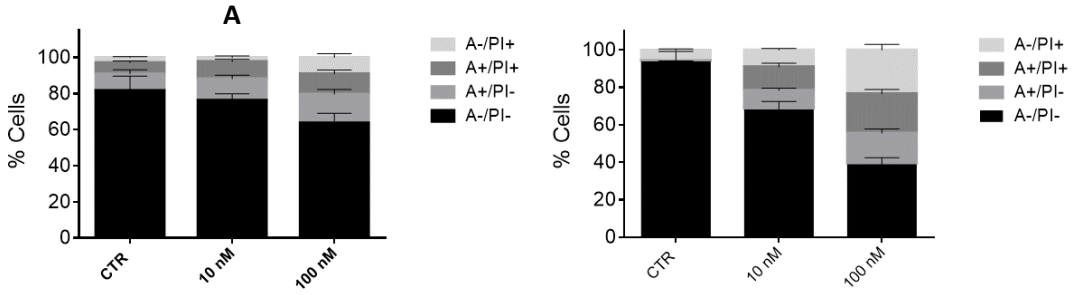

Figure 6. Flow cytometric analysis of apoptotic cells after treatment of HeLa (Panels A and B) cells with compound **12** at the indicated concentrations after incubation for 24 h (A) or 48 h (B). The cells were harvested and labeled with annexin-V-FITC and PI and analyzed by flow cytometry. Data are represented as mean±SEM of three independent experiments.

Compound 12 induced mitochondrial depolarization and reactive oxygen species (ROS) production

Mitochondria play an essential role in the propagation of apoptosis.[18,19] It is well established that, at an early stage, apoptotic stimuli alter the mitochondrial transmembrane potential ($\Delta\psi_{mt}$). $\Delta\psi_{mt}$ was monitored by the fluorescence of the dye JC-1.[20] HeLa cells treated with compound **12** (10-100 nM) showed a time-dependent increase in the percentage of cells with low $\Delta\psi_{mt}$ (Figure 7, Panel A). The depolarization of the mitochondrial membrane is associated with the appearance of annexin-V positivity in the treated cells when they are in an early apoptotic stage. In fact, the dissipation of $\Delta\psi_{mt}$ is characteristic of apoptosis and has been observed with both microtubule stabilizing and destabilizing agents, including other derivatives, in different cell types. [21-24] It is well known that mitochondrial membrane depolarization is associated with the mitochondrial production of ROS.[25,26] Therefore, we investigated whether ROS production increased after treatment with the test compounds. We utilized the fluorescence indicator 2,7-dichlorodihydrofluorescein diacetate (H_2-DCFDA).[27] As shown in Figure 7 (Panel B) compound **12** induced significant production of ROS starting at 12-24 h of treatment at 100 nM, in good agreement with the mitochondrial depolarization described above.

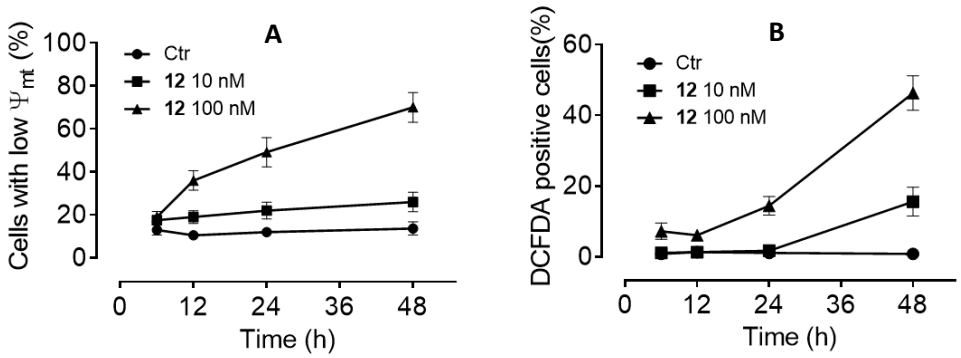

Figure 7. Assessment of mitochondrial membrane potential ($\Delta\psi_{mt}$) after treatment of HeLa (Panel A) cells with compound **12**. Cells were treated with the indicated concentration of compound for 6 h, 12 h, 24 and 48 h and then stained with the fluorescent probe JC-1 for analysis of mitochondrial potential. Cells were then analyzed by flow cytometry as described in the experimental section. Data are represented as mean±SEM of three independent experiments. Panel B. Assessment of ROS production after treatment of HeLa cells with the compound **12**. Cells were treated with the indicated concentration of compound for 6 h, 12 h, 24 h, and 48 h and then stained with H_2-DCFDA for the evaluation of ROS levels. Cells were then analyzed by flow cytometry as described in the experimental section. Data are represented as mean ± SEM of three independent experiments.

Compound 12 induced casp-3 and PARP activation and caused a decrease in the expression of anti-apoptotic proteins

As shown in Figure 7, compound **12** in HeLa cells caused a concentration and time-dependent increase of the cleaved fragment of caspase-3 and concomitantly the cleavage of poly (ADP-Ribose) polymerase (PARP), confirming its pro-apoptotic activity.

We also investigated the expression of anti-apoptotic proteins, such as Bcl-2 and Mcl-1. Bcl-2 plays a major role in controlling apoptosis through the regulation of mitochondrial processes and the release of mitochondrial proapoptotic molecules that are important for the cell death pathway.[28-30] Our results (Figure 8) showed that the expression of the anti-apoptotic protein Bcl-2 was significantly decreased after a 48 h treatment at both concentration used (50 and 100 nM). The decrease in expression of Mcl-1 was even greater.

Interestingly, as observed for other antimitotics, we observed after treatment with **12** a significant increase of the expression of the phosphohistone H2AX, a well know marker of DNA damage. In this contest it is worthwhile to note that prolonged mitotic arrest may induce DNA damage that ultimately lead to apoptosis.

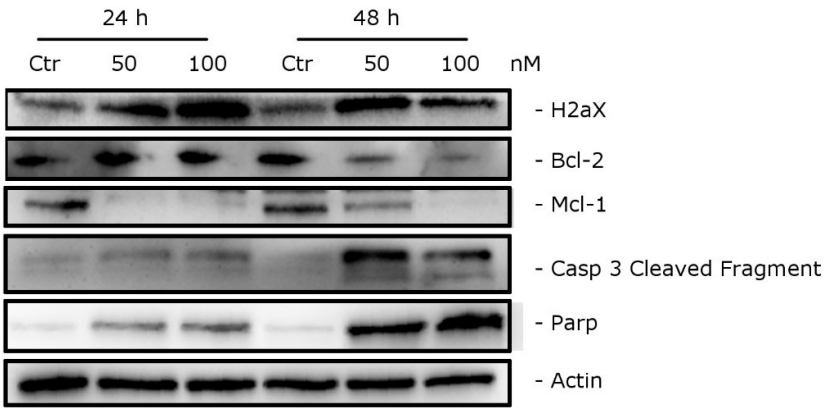

Figure 8. Western blot analysis of Bcl-2, Mcl-1, Casp3 cleaved fragment and PARP after treatment of HeLa cells with **12** at the indicated concentrations and for the indicated times. To confirm equal protein loading, each membrane was stripped and re-probed with anti-γ-tubulin antibody.

Evaluation of antitumor activity of compound 12 and 15 *in vivo*

To determine the *in vivo* antitumor activity of **12** and **15**, a syngeneic murine model was used, represented by the BL6-B16 mouse melanoma cell line. Preliminary *in vitro* experiments were carried out to evaluate the cytotoxicity of these compounds in the murine tumor cell line. The GI_{50} obtained after 72 h was 10 ± 4 nM and 18 ± 6 nM, respectively. BL6-B16 cells were injected subcutaneously in syngeneic C57BL/6 mice. Once the tumor reached a measurable size (about 100 mm^3), mice were randomly assigned to different experimental groups and treated intraperitoneally every other day with vehicle (DMSO), the two compounds (at doses of 7.5 or 3 mg/kg) or with Combretastatin 4-A phosphate (CA-4P) (at 30 mg/kg) as reference compound.

As shown in Figure 9, both compounds **12** and **15** caused a similar and significant reduction in the growth of BL6-B16 melanoma cells at the dose of 7.5 mg/kg (60% for **12** and 58.4% for **15**) in comparison with vehicle-treated group. Also, at the dose of 3 mg/kg we observed a significant reduction of the tumor mass only for compound **12** (28.6%), whereas compound **15** did not reach statistical significance (16.7%). Notably, treatment with the reference compound CA-4P at 30 mg/kg caused only a small reduction in tumor volume (31.3 %) if compared with both compounds **12** and **15** at 7.5 mg/kg. Under the safety/tolerability point of view, no significant variation in body weight occurred in animals treated with **12** and **15** at the higher concentration (data not shown).

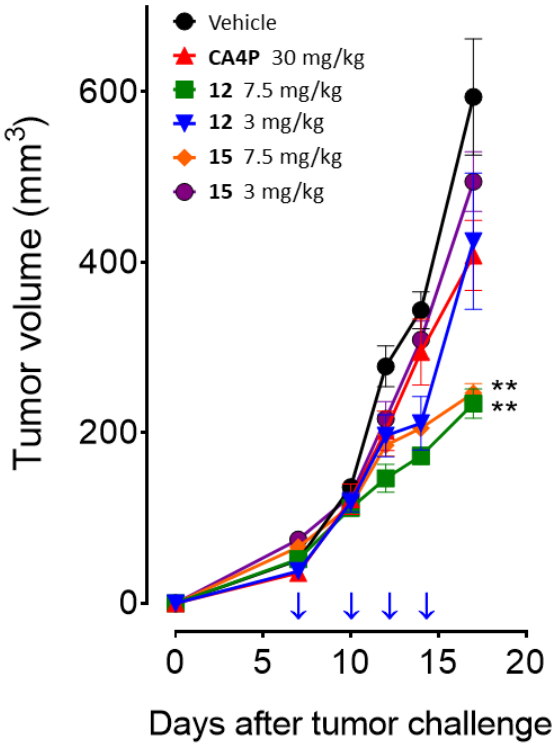

Figure 9. Inhibition of mouse allograft growth *in vivo* by compounds **12** and **15**. Male C57BL/6 mice were injected subcutaneously at their dorsal region with 10^7 BL6-B16 murine melanoma cells. Tumor-bearing mice were administered the vehicle, as control, or 7.5 and 3.0 mg/kg of **12** and **15** or CA-4P as reference compound at the dose of 30 mg/kg. Injections were given intraperitoneally at the days indicated by the arrows. Arrows indicate times of administration. Data are presented as mean ± SEM of tumor volume at each time point for 5 animals per group. **p<0.01 *vs*. control.

Metabolic stability of compounds 12-15, 19, 20 and 21 in human liver microsomes

Liver microsomal oxidation and hydrolysis represent major routes of drug metabolism in mammals, including humans.[31] *In vitro* studies were therefore carried out to retrieve preliminary information on the stability of newly synthesised fluorinated derivatives in comparison with reference compound **20** and **21**. Experiments were performed to understand if fluorine substitution conferred resistance to oxidative and hydrolytic metabolism by human liver microsomes. As shown in Figure 10, all fluorinated compounds **12-14** (10 μM), as their parent compound **20**, were not stable in human liver microsomes (0.5 mg/mL) with less than 20% compound remaining after 60 min incubation at 37°C.

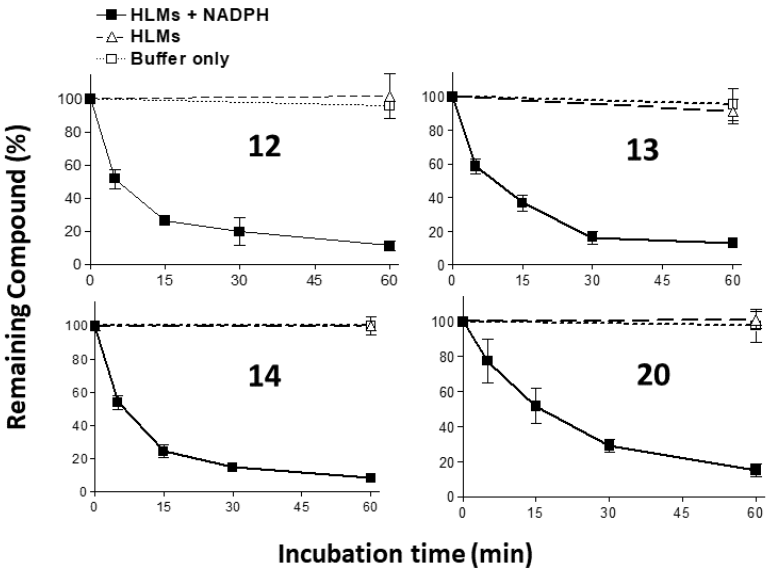

Figure 10. Assessment of metabolic stability of **12**-**14** and **20** in human liver microsomal incubations. Each compound (10 µM) was incubated at 37°C with HLMs (0.5 mg/mL; -Δ-), HLMs plus 1 mM NADPH (-■-), or buffer only (0.1 M KH_2PO_4, pH 7.4; -□-). Incubation time points were 0, 5, 15, 30 and 60 min ("HLMs"), or 0 and 60 min ("HLMs plus NADPH" and "buffer only"). The data are expressed as percentage of parent compound remaining at each time compared with time 0 min and represent the mean ± SD of n = 3 independent determinations. Error bars smaller than the symbols are not visible. Depletion half-lives in incubation mixture containing HLMs and NADPH were 21.6, 21.3, 18.1 and 22.4 min for **12**, **13**, **14** and **20**, respectively.

Interestingly, fluorinated derivatives **15** and **19** of 3*N*-benzoyl derivative **21** were relatively stable and with the co-presence of the cytochrome P450- and flavin monooxygenase cofactor NADPH being irrelevant. (Figure 11). Collectively, these findings suggest that fluorinated and non-fluorinated 3*N*-ethyl-PPyQ derivatives (**12**-**14** and **20**) are very susceptible to oxidative and hydrolytic metabolism, and this is reflected on poor half-lives (about 20 minutes for all derivatives) while for compounds **15**, **19** and **21**, the benzoyl substituent confers resistance to metabolic pathways, with the fluorine substitution being not a decisive factor.

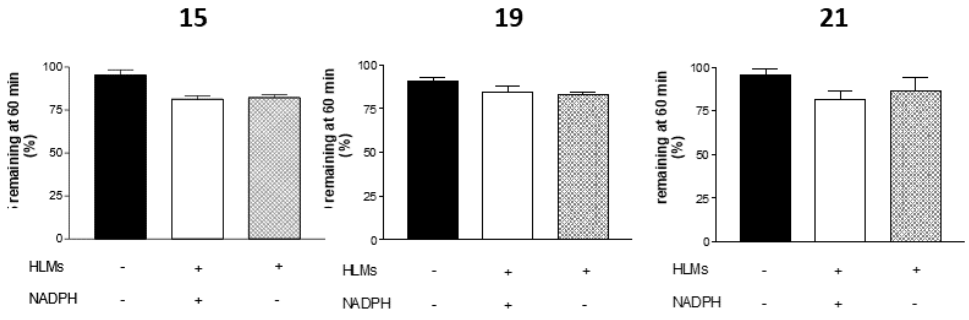

Figure 11. Assessment of metabolic stability of **15**, **19** and **21** in human liver microsomal incubations. Each compound (10 µM) was incubated at 37°C with HLMs (1 mg/mL), HLMs plus 1 mM NADPH, or buffer

only (0.1 M KH_2PO_4, pH 7.4), for 0 or 60 min. Each bar represents the percentage (mean ± SD; n = 3) of compound remaining at 60 min, compared with time 0 min.

Conclusion

A small library of novel fluorinated derivatives of 7-PPyQ was synthesised with the aim to obtain additional information on the *in vitro* and *in vivo* cytotoxic profile and on the metabolic stability towards human liver microsomes.

The chemical series included final compounds **12**-**14**, 7-phenyl *ortho*-, *meta*-, *para*-fluoro-substituted derivatives of 3*N*-ethyl-PPyQ **20**; compound **15**, 7-phenyl *meta*-fluoro-substituted derivative of 3*N*-benzoyl-PPyQ **21**, and compound **19**, 3*N*-benzoyl-*ortho*-fluoro-substituted derivative of 3*N*-benzoyl-PPyQ **21**. Most compounds showed remarkable antiproliferative activity against a panel of 11 tumour cell lines, with GI_{50} values in the nanomolar or sub-nanomolar range, with the best activities obtained for *N*-ethyl derivatives **12** and **13** and *N*-benzoyl derivative **15**. In the case of compounds **12** and **13**, the *ortho*- and *meta*-fluoro substitution demonstrated to be favourable for the cytotoxic profile, leading to an increase in the antiproliferative potency in comparison with parent compound **20**. On the other hand, the *para*-fluoro-substituted derivative **14** showed a significant reduction in activity compared to compound **20**, meaning that substitution at *para* position of 7-phenyl ring is unfavourable for an optimal antiproliferative effect.

Regarding 3*N*-benzoyl derivatives, compound **15** showed a slightly inferior cytotoxicity compared to parent compound **21**, but still in the low nanomolar range demonstrating again that, in general, oxygenated substitutions at the 3 position are positive for the maintenance of an excellent anticancer activity. In addition, the three best-performing compounds **12**, **13** and **15** showed only a modest inhibitory effect in non-cancer primary lymphocytes with GI_{50} values almost 10000-30000 times higher than that observed against the rapidly proliferating lymphoblastic cell lines and were also able to overcome resistance on multidrug resistant cells. Deeper investigations on the mechanism of action confirmed the strong inhibition of tubulin polymerization and agreed with the growth inhibitory effects exhibited by these compounds. In view of the excellent findings obtained with the *in vitro* biological screening, compounds **12** and **15**, as representatives of 3*N*-ethyl- and 3*N*-benzoyl-PPyQ sub-families, were evaluated *in vivo* in a syngeneic murine model with the BL6-B16 mouse melanoma cell line, using CA-4P at 30 mg/kg

dosage as reference treatment. Both compounds **12** and **15** caused a similar, remarkable reduction of about 60% in the growth of BL6-B16 melanoma cells, already at the dose of 7.5 mg/kg in comparison with vehicle-treated group. Notably, treatment with the reference compound CA-4P at 30 mg/kg caused only a small reduction in tumor volume (31.3 %), indicating that our compounds have better *in-vivo* anticancer activity, even with a four-time lower dose. These results clearly show the potentialities of 7-PPyQ class in the chemotherapeutic field. Furthermore, *in vitro* metabolic stability studies indicated that fluorinated compounds **12-14** as their parent compound **20**, were not stable in human liver microsomes with less than 20% compound remaining after 60 min of treatment. This suggests that even though the fluorine substitution was able to improve the pharmacodynamic properties of derivatives **12** and **13**, its effects on metabolic stability were not significant. Interestingly, compound **15** and its cognate compound **21** were relatively stable in the tested conditions. In this case, it seems that the benzoyl substituent contributes more in the resistance to metabolic pathways than the fluorine substitution.
Overall, these recent studies provide further insights in the medicinal chemistry of potent anticancer 7-PPyQs and contribute to extend the comprehension of the biological significance of this class of compounds.

Experimental section

Chemistry

Melting points were determined on a Buchi M-560 capillary melting point apparatus and are uncorrected. ^{1}H NMR spectra were determined on Bruker 300 and 400 MHz spectrometers, with the solvents indicated; chemical shifts are reported in δ (ppm) downfield from tetramethylsilane as internal reference. Coupling constants are given in hertz. In the case of multiplets, chemical shifts were measured starting from the approximate centre. Integrals were satisfactorily in line with those expected based on compound structure. Mass spectra were obtained on a Mat 112 Varian Mat Bremen (70 eV) mass spectrometer and Applied Biosystems Mariner System 5220 LC/MS (nozzle potential 140 eV). Column flash chromatography was performed on Merck silica gel (250−400 mesh ASTM); chemical reactions were monitored by analytical thin-layer chromatography (TLC) on Merck silica gel 60 F-254 glass plates. The purity of new tested compounds was checked by HPLC using the instrument HPLC VARIAN ProStar

model 210, with detector DAD VARIAN ProStar 335. The analysis was performed with a flow of 1 mL/min, a C-18 column of dimensions 250 mm X 4.6 mm, a particle size of 5 mm, and a loop of 10 mL. The detector was set at 300 nm. The mobile phase consisted of phase A (Milli-Q H_2O, 18.0 MU, TFA 0.05%) and phase B (95% MeCN, 5% phase A). Gradient elution was performed as reported: 0 min, % B = 10; 0 and 20 min, % B = 90; 25 min, % ; B = 90; 26 min, % B = 10; 31 min, % B = 10.

Starting materials were purchased from Sigma-Aldrich and Alfa Aesar, and solvents were from Carlo Erba, Fluka and Lab-Scan. DMSO was obtained anhydrous by distillation under vacuum and stored on molecular sieves.

1-Ethyl-5-nitro-1H-indole (**1**).

Into a two-necked 100 mL round-bottomed flask, 0.666 g (27.75 mmol) of NaH, 60% dispersion in mineral oil, was placed and washed with toluene (3 × 10 mL). With stirring, a solution of commercial 5-nitroindole, 1.500 g (9.25 mmol), in 5 mL of anhydrous DMF, was dropped into the flask, and the initial yellow colour changed to red with the formation of H_2 gas. After 40 min at room temperature, the mixture was cooled to 0°C and 2.00 mL (26.61 mmol, d=1.46 g/mL) of bromoethane was dropped into the flask and 0.050 g of NaI were added to the mixture. The reaction was monitored by TLC analysis (eluent toluene/n-hexane/ethyl acetate, 1:1:1). At the end of the reaction, 25 mL of water was added, and the solvent was evaporated under reduced pressure, leaving a residue, which was extracted with ethyl acetate (3 × 30 mL). The organic phase, washed with water, brine, and dried over anhydrous Na_2SO_4, was concentrated under vacuum giving 1.69 g of a yellow solid. Yield: 99 %; R*f*: 0.63 (Toluene/n-Hexane/Ethyl acetate, 1:1:1); ^{1}H NMR (300 MHz, DMSO-d_6): δ 7.74 (d, J = 2.1 Hz, 1H, H-4), 7.20 (dd, J = 9.0, 2.1 Hz, 1H, H-6), 6.87 (m, 2H, H-7 e H-3), 5.93 (d, J = 3.3 Hz, 1H, H-2), 3.47 (q, J = 7.1 Hz, 2H, CH_2), 0.55 (t, J = 7.1 Hz, 3H, CH_3), ppm; HRMS (ESI-MS, 140 eV): m/z $[M+H]^+$ calculated for $C_{10}H_{11}N_2O_2^+$, 191.2035; found, 191.1859.

(5-Nitro-1H-indol-1-yl)(phenyl)methanone (**2**).

Into a 50 mL round-bottomed flask, a solution of 5-nitroindole 0,500 g (3.08 mmol, 1 eq.) in 20 mL of CH_2Cl_2 was treated with DMAP (0.692 g, 6.17 mmol, 2 eq.) and pyridine (0.500 mL, 6.17 mmol, 2 eq.). The mixture was cooled to 0°C and a solution of benzoyl chloride in CH_2Cl_2 (0.716 mL, 6.17 mmol, 2 eq.) was dropped into the flask. The reaction mixture was stirred at room temperature for 24h. The reaction was monitored by TLC analysis (eluent CH_2Cl_2/petroleum ether/EtOAc, 3:6.5:0.5). At the end, the reaction was

quenched by adding a solution of HCl 0.5 M and the aqueous phase was extracted with CH_2Cl_2 (3 x 50 mL). The combined organic extracts were dried over $MgSO_4$, concentrated under vacuo, dissolved filtered through SiO_2 (eluent CH_2Cl_2/petroleum ether/EtOAc, 3:6.5:0.5) giving a pale-yellow solid (0.443 g, 1.67 mmol, 54%). Yield = 54 %; R*f*: 0.61 (eluent CH_2Cl_2/petroleum ether/EtOAc, 3:6.5:0.5); ^{1}H NMR (300 MHz, $CDCl_3$) δ 8.53 (d, *J* = 2.2 Hz, 1H, H-4), 8.49 (d, *J* = 9.1 Hz, 1H, H-7), 8.27 (dd, *J* = 9.1, 2.3 Hz, 1H, H-6), 7.80 – 7.73 (m, 2H, H-2' and H-6'), 7.67 (ddd, *J* = 6.6, 3.9, 1.4 Hz, 1H, H-4'), 7.57 (ddd, *J* = 6.6, 4.5, 1.3 Hz, 2H, H-3' and H-5'), 7.50 (d, *J* = 3.8 Hz, 1H, H-2), 6.77 (dd, *J* = 3.8, 0.5 Hz, 1H, H-3) ppm; HRMS (ESI-MS, 140 eV): m/z $[M+H]^+$ calculated for $C_{15}H_{11}N_2O_3^+$, 267.0764; found, 267.0745.

(2-fluorophenyl)(5-nitro-1H-indol-1-yl)methanone (**3**).

Into a 50 mL round-bottomed flask, a solution of 5-nitroindole 0.500 g (3.08 mmol, 1 eq.) in 20 mL of CH_2Cl_2 was treated with DMAP (0.692 g, 6.17 mmol, 2 eq.) and pyridine (0.500 mL, 6.17 mmol, 2 eq.). The mixture was cooled to 0°C and a solution of 2-fluoro-benzoyl chloride (**17**) in CH_2Cl_2 (0.978 g, 6.17 mmol, 2 eq.) was dropped into the flask. The reaction mixture was stirred at room temperature for 24h. The reaction was monitored by TLC analysis (eluent CH_2Cl_2/petroleum ether/EtOAc, 3:6.5:0.5). At the end, the reaction was quenched by adding a solution of HCl 0.5 M and the aqueous phase was extracted with CH_2Cl_2 (3 x 50 mL). The combined organic extracts were dried over $MgSO_4$, concentrated under vacuo, dissolved, filtered through SiO_2 (eluent CH_2Cl_2/petroleum ether/EtOAc, 3:6.5:0.5) giving a yellow solid (0.543 g, 1.90 mmol, 62%). Yield = 62 %; R*f*: 0.61 (eluent CH_2Cl_2/petroleum ether/EtOAc, 3:6.5:0.5); ^{1}H NMR (300 MHz, $CDCl_3$) δ 8.71 (1H, dd, *J* = 2.0, 1.9 Hz), 8.24 (1H, dd, *J* = 8.8, 1.9 Hz), 7.99 (1H, m, *J* = 8.8, 0.5 Hz), 7.82 (1H, m, *J* = 8.7 Hz), 7.73 (1H, m, *J* = 8.1, 1.5, Hz), 7.51 (1H, m, *J* = 8.3, 7.4 Hz), 7.44 (1H, m, *J* = 8.3, 1.3 Hz), 7.32 (1H, dd, *J* = 8.1, 7.4), 6.88 (1H, m, *J* = 8.7, 2.0 Hz) ppm; HRMS (ESI-MS, 140 eV): m/z $[M+H]^+$ calculated for $C_{15}H_{10}FN_2O_3^+$, 285.0670; found, 285.0618.

1-Ethyl-1H-indol-5-amine (**4**).

Into a two-necked flask, previously dried in an oven, about 0.300 g of Pd/C 10% and approximately 50 mL of ethyl acetate were placed. After connecting the flask to an elastomer balloon containing hydrogen gas, the mixture was stirred at room temperature for 1 h in order to saturate the suspension of Pd/C with hydrogen. Then, 1.69 g (8.90 mmol) of derivative 1 in 15 mL of ethyl acetate was added dropwise to the suspension, and the mixture was stirred under hydrogen at atmospheric pressure and heated by means

of an oil bath at 50-60 °C monitoring the progress of the reaction by TLC analysis (ethyl acetate/toluene/*n*-hexane, 1:1:1). At the end of the reaction, the mixture was filtered through a celite pad, and the solution was concentrated under vacuum to give 1.40 g of amine. Yield: 98.2 %; R*f*: 0.28 (toluene/*n*-hexane/ethyl acetate, 1:1:1); ^{1}H NMR (300 MHz, DMSO-d_6): δ 7.16 (m, 2H, H-3 e H-7), 6.69 (d, J = 2.28 Hz, 1H, H-4), 6.54 (dd, J = 8.5, 2.28 Hz, 1H, H-6), 6.15 (d, J = 3.05 Hz, 1H, H-2), 4.48 (s br, 2H, NH_2), 4.06 (q, J = 7.3 Hz, 2H, CH_2), 1.55 (t, J = 7.3 Hz, 3H, CH_3) ppm; HRMS (ESI-MS, 140 eV): m/z $[M+H]^+$ calculated for $C_{10}H_{13}N_2^+$, 161.2231; found, 161.1593.

(5-Amino-1H-indol-1-yl)(phenyl)methanone (**5**).

Into a 50 mL round-bottomed flask, 1-benzoyl-5-nitroindole 0.443 g (1.67 mmol) was dissolved in 30 mL of EtOAc. Pt/C catalyst (65 mg, 15% p/p) was added under N_2 atmosphere and then the mixture was treated with H_2 for 75 min at room temperature. The catalyst was removed by filtration on a celite pad and the solution was concentrated under vacuum. The product was purified by silica gel chromatographic column (eluent CH_2Cl_2/EtOAc, 9:1), yielding 0.331 g of a pure yellow solid. Yield = 84%; R*f*: 0.43 (eluent CH_2Cl_2/EtOAc, 9:1); ^{1}H NMR (300 MHz, $CDCl_3$) δ 8.12 (d, *J* = 8.7 Hz, 1H, H-7), 7.66 – 7.58 (m, 2H, H-2' and H-6'), 7.52 – 7.38 (m, 3H, H-3', H-4' and H-5'), 7.11 (d, *J* = 3.7 Hz, 1H, H-2), 6.85 – 6.80 (m, 1H, H-3), 6.72 (dd, *J* = 8.7, 2.2 Hz, 1H, H-6), 6.38 (dd, *J* = 3.7, 0.6 Hz, 1H, H-3), 3.06 (s, 2H, NH_2) ppm; HRMS (ESI-MS, 140 eV): m/z $[M+H]^+$ calculated for $C_{15}H_{13}N_2O^+$, 237.1022; found, 237.1043.

(5-Amino-1H-indol-1-yl)(2-fluorophenyl)methanone (**6**).

Into a 50 mL round-bottomed flask, 0.375 g of compound **3** (1.32 mmol) were dissolved in 25 mL of EtOAc. Pt/C catalyst (60 mg, 15% p/p) was added under N_2 atmosphere and then the mixture was treated with H_2 for 75 min at room temperature. The catalyst was removed by filtration on a celite pad and the solution was concentrated under vacuum. The product was purified by silica gel chromatographic column (eluent CH_2Cl_2/EtOAc, 9:1), yielding 0.293 g of a solid. Yield = 87 %; R*f*: 0.40 (eluent CH_2Cl_2/EtOAc, 9:1); ^{1}H NMR (300 MHz, $CDCl_3$) δ 7.84 (1H, m, *J* = 8.1, 1.5 Hz), 7.56 (1H, dd, *J* = 8.3, 7.4 Hz), 7.63 (1H, dt, *J* = 8.2, 0.5 Hz), 7.42 (1H, m, *J* = 8.3, 1.4 Hz), 7.44 (1H, m, *J* = 8.3, 0.4 Hz), 7.33 (1H, dd, *J* = 8.1, 7.4 Hz), 7.30 (1H, m, *J* = 1.9, 0.4 Hz), 6.52 (1H, m, *J* = 8.2, 2.0 Hz), 6.33 (1H, dd, *J* = 8.3, 1.9 Hz), 3.01 (s, 2H, NH_2) ppm; HRMS (ESI-MS, 140 eV): m/z $[M+H]^+$ calculated for $C_{15}H_{12}FN_2O^+$, 255.0928; found, 255.0912.

General Procedure for the Synthesis of acrylate derivatives **7**-**11**. As a typical procedure, the synthesis of acrylate derivative **7** is described in detail. In a 100 mL round-bottomed

flask, 0.700 g (4.37 mmol) of 3-ethyl aminoindole **4** were dissolved in 10 mL of absolute ethanol. 0.5 mL of glacial acetic acid, 0.100 g of drierite and 1.84 g (8.74 mmol) of ethyl 3-(2-fluorophenyl)-3-oxopropanoate dissolved in 2 mL of absolute ethanol were added to the solution. The mixture was refluxed for about 48 h, the reaction being monitored by TLC analysis (*n*-hexane/ethyl acetate, 1:1). At the end of the reaction, the mixture was cooled and filtered to remove the drierite; the resulting solution was evaporated to dryness under vacuum and the residue (2.47 g) purified by silica gel chromatography (d = 3 cm, l = 35 cm, 230−400 mesh, eluent *n*-hexane/ethyl acetate, 1:1) to yield 1.01 g of a brown solid.

(E,Z)-Ethyl 3-(1-ethyl-1H-indol-5-ylamino)-3-(2-fluorophenyl)acrylate (**7**).

Yield: 63 %; R*f*: 0.47 (*n*-hexane/ethyl acetate, 1:1); ^{1}H NMR (400 MHz, DMSO-d_6): δ 10.72 (s, 1H, NH), 7.58 (m, J = 7.84, 5.37, 1.35 Hz, 1H, H-6'), 7.44 (m, J = 8.31, 7.41, 1.35 Hz, 1H, H-5'), 7.37 (d, J = 9.08 Hz, 1H, H-7), 7.30 (d, J = 3.15 Hz, 1H, H-2), 7.23 (m, J = 7.84, 7.41, 1.38 Hz, 1H, H-4'), 6.95 (m, J = 8.29, 5.31, 1.57, 1H, H-3'), 6.94 (m, J = 2.08 Hz, 1H, H-4), 6.65 (dd, J = 8.71, 2.08 Hz, 1H, H-6), 6.27 (dd, J = 3.19, 0.69 Hz, 1H, H-3), 4.83 (s, 1H, C*H*COOCH$_2$CH$_3$), 4.16 (q, J = 6.92 Hz, 2H, COOC*H*$_2$CH$_3$), 3.84 (q, J = 7.64 Hz, 2H, NC*H*$_2$CH$_3$), 1.25 (t, J = 6.92 Hz, 3H, COOCH$_2$C*H*$_3$), 1.13 (t, J = 7.67 Hz, 3H, NCH$_2$C*H*$_3$), ppm; HRMS (ESI-MS, 140 eV): m/z $[M+H]^+$ calculated for $C_{21}H_{22}FN_2O_2^+$, 353.1660; found, 353.1688.

(E,Z)-Ethyl 3-(1-ethyl-1H-indol-5-ylamino)-3-(3-fluorophenyl)acrylate (**8**).

Compound **8** was prepared as for compound **7** by reacting 1.84 g (8.74 mmol) of ethyl 3-(3-fluorophenyl)-3-oxopropanoate with 0.700 g (4.37 mmol) of previously prepared compound **4**, yielding 2,76 g of crude product, which was purified by silica gel column chromatography (d = 3 cm, l = 35 cm, 230−400 mesh, eluent *n*-hexane/ethyl acetate, 1:1) to yield 1.07 g of a brown solid. Yield: 67 %; R*f*: 0.47 (*n*-hexane/ethyl acetate, 1:1); ^{1}H NMR (400 MHz, DMSO-d_6): δ 10.68 (s, 1H, NH), 7.46 (m, J = 7.75, 1.52 Hz, 1H, H-6'), 7.44 (m, J = 8.21, 7.73, 1H, H-5'), 7.37 (d, J = 9.08 Hz, 1H, H-7), 7.30 (d, J = 3.15 Hz, 1H, H-2), 7.19 (m, 1H, H-2'), 7.14 (m, 1H, H-4'), 6.94 (m, J = 2.08 Hz, 1H, H-4), 6.65 (dd, J = 8.71, 2.08 Hz, 1H, H-6), 6.23 (dd, J = 3.19, 0.69 Hz, 1H, H-3), 4.89 (s, 1H, C*H*COOCH$_2$CH$_3$), 4.12 (q, J = 6.92 Hz, 2H, COOC*H*$_2$CH$_3$), 3.83 (q, J = 7.64 Hz, 2H, NC*H*$_2$CH$_3$), 1.25 (t, J = 6.92 Hz, 3H, COOCH$_2$C*H*$_3$), 1.18 (t, J = 7.67 Hz, 3H, NCH$_2$C*H*$_3$) ppm; HRMS (ESI-MS, 140 eV): m/z $[M+H]^+$ calculated for $C_{21}H_{22}FN_2O_2^+$, 353.1660; found, 353.1645.

(E,Z)-Ethyl 3-(1-ethyl-1H-indol-5-ylamino)-3-(4-fluorophenyl)acrylate (**9**).

Compound **9** was prepared as for compound **7** by reacting 1.84 g (8.74 mmol) of ethyl 3-(4-fluorophenyl)-3-oxopropanoate with 0.700 g (4.37 mmol) of previously prepared compound **4**, yielding 2,60 g of crude product, which was purified by silica gel column chromatography (d = 3 cm, l = 35 cm, 230−400 mesh, eluent *n*-hexane/ethyl acetate, 1:1) to yield 1.12 g of a yellow solid. Yield: 70 %; R*f*: 0.69 (*n*-hexane/ethyl acetate, 1:1); ^{1}H NMR (400 MHz, DMSO-d_6): δ 10.44 (s, 1H, NH), 7.97 (m, J = 5.65, 3.27, 2H, H-2' and H-6'), 7.44 (m, J = 8.90, 3.25, 2.20 Hz, 2H, H-3' and H-5'), 7.35 (d, J = 9.08 Hz, 1H, H-7), 7.29 (d, J = 3.15 Hz, 1H, H-2), 6.98 (m, J = 2.08 Hz, 1H, H-4), 6.66 (dd, J = 8.71, 2.08 Hz, 1H, H-6), 6.28 (dd, J = 3.19, 0.69 Hz, 1H, H-3), 4.85 (s, 1H, C*H*COOCH$_2$CH$_3$), 4.14 (q, J = 6.92 Hz, 2H, COOC*H$_2$*CH$_3$), 3.76 (q, J = 7.64 Hz, 2H, NC*H$_2$*CH$_3$), 1.24 (t, J = 6.92 Hz, 3H, COOCH$_2$C*H$_3$*), 1.14 (t, J = 7.67 Hz, 3H, NCH$_2$C*H$_3$*) ppm; HRMS (ESI-MS, 140 eV): m/z $[M+H]^+$ calculated for $C_{21}H_{22}FN_2O_2^+$, 353.1660; found, 353.1656.

(E,Z)-Ethyl-3-[(1-benzoylindol-5-ylamino]-3-(3-fluorophenyl)prop-2-enoate (**10**).

Compound **10** was prepared as for compound **7** by reacting 0.660 mL (3.66 mmol) of ethyl 3-(3-fluorophenyl)-3-oxopropanoate with 0.864 g (3.66 mmol) of previously prepared compound **5**, yielding 1,85 g of crude product, which was purified by silica gel column chromatography (d = 3 cm, l = 35 cm, 230−400 mesh, eluent petroleum ether/acetone 85:15) to yield 0.540 g of a yellow solid. Yield: 35 %; R*f*: 0.69 (eluent petroleum ether/acetone 85:15); ^{1}H NMR (300 MHz, DMSO) δ 10.23 (s, 1H, NH), 8.06 (d, *J* = 8.8 Hz, 1H, H-7), 7.70 (m, 2H, H-2'' and H-6''), 7.65 (dt, *J* = 2.8, 2.0 Hz, 1H, H-4'), 7.60 – 7.52 (m, 2H, H-3'' and H-5''), 7.40 – 7.31 (m, 1H, H-2'), 7.29 (d, *J* = 3.8 Hz, 1H, H-4), 7.24 – 7.15 (m, 3H, H-4'', H-5' and H-6'), 7.07 (d, *J* = 2.1 Hz, 1H, H-2), 6.84 (dd, *J* = 8.8, 2.2 Hz, 1H, H-6), 6.56 (d, *J* = 3.4 Hz, 1H, H-3), 5.00 (s, 1H, C*H*COOCH$_2$CH$_3$), 4.15 (q, *J* = 7.1 Hz, 2H, COOC*H$_2$*CH$_3$), 1.24 (t, *J* = 7.1 Hz, 3H, COOCH$_2$C*H$_3$*) ppm; HRMS (ESI-MS, 140 eV): m/z $[M+H]^+$ calculated for $C_{26}H_{22}FN_2O_3^+$, 429.1605; found, 429.1612.

(E,Z)-Ethyl-3-[(2-fluoro-1-benzoylindol-5-ylamino]-3-phenyl-prop-2-enoate (**11**).

Compound **11** was prepared as for compound **7** by reacting 0.869 mL (5.11 mmol) of ethyl-benzoyl-acetate with 0.866 g (3.41 mmol) of previously prepared compound **6**, yielding 1,65 g of crude product, which was purified by silica gel column chromatography (d = 3 cm, l = 35 cm, 230−400 mesh, eluent petroleum ether/acetone 85:15) to yield 0.456 g of a yellow solid. Yield: 31 %; R*f*: 0.77 (eluent petroleum ether/acetone 90:10); ^{1}H NMR (300 MHz, DMSO) δ 10.29(s, 1H, NH), 8.01 (d, *J* = 8.1 Hz, 1H, H-7), 7.65 (m, 2H, H-2' and H-6'), 7.57 (dt, *J* = 2.8, 2.0 Hz, 1H, H-4''), 7.60 –

7.58 (m, 2H, H-3' and H-5'), 7.40 – 7.38 (m, 1H, H-2''), 7.28 (d, *J* = 3.2 Hz, 1H, H-4), 7.23 – 7.10 (m, 3H, H-4', H-5'' and H-6''), 7.02 (d, *J* = 2.1 Hz, 1H, H-2), 6.80 (dd, *J* = 8.8, 2.21 Hz, 1H, H-6), 6.66 (d, *J* = 3.3 Hz, 1H, H-3), 5.02 (s, 1H, C*H*$COOCH_2CH_3$), 4.12 (q, *J* = 7.0 Hz, 2H, $COOCH_2CH_3$), 1.26 (t, *J* = 7.0 Hz, 3H, $COOCH_2CH_3$) ppm; HRMS (ESI-MS, 140 eV): m/z $[M+H]^+$ calculated for $C_{26}H_{22}FN_2O_3^+$, 429.1609; found, 429.1626.

General Procedure for the Synthesis of Phenylpyrroloquinolinones **12-15**. As a typical procedure, the synthesis of the phenylpyrroloquinolinone derivative **12** is described in detail. In a two-necked round-bottomed flask, 7 mL of diphenyl ether was heated to boiling. An amount of 1.03 g (2.8 mmol) of acrylate derivative **7** was then added, and the resulting mixture was refluxed for 15 min. After cooling to room temperature, an amount of 20 mL of diethyl ether was added, and the mixture was left for 12 h. Then the separated precipitate was collected by filtration and washed many times with diethyl ether. The crude product (0.530 g) was purified by Flash column chromatography (eluent chloroform/methanol, 9:1), obtaining 0.220 g of final pure compound.

3-Ethyl-7-(2-fluorophenyl)-3H-pyrrolo[3,2-f]quinolin-9(6H)-one (**12**).

Yield: 26 %; R*f*: 0.53 (light blue fluorescent spot, chloroform/methanol 9:1); ^{1}H-NMR (400 MHz, DMSO-d_6) δ 11.64 (s, 1H, NH), 7.93 (d, J = 9.06 Hz, 1H, H-4), 7.90 – 7.85 (m, 2H, H-1 and H-6'), 7.69 – 7.51 (m, 4H, H-2, H-3', H-5' and H-5), 7.51 (m, 1H, H-4'), 6.39 (s, 1H, H-8), 4.32 (q, J = 6.51 Hz, 2H, NCH_2CH_3), 1.41 (t, J = 6.51 Hz, 3H, NCH_2CH_3) ppm; ^{13}C-NMR (101 MHz, DMSO-d_6) δ 178.38 ppm (C-9), 154.54 (C-6), 141.98 (d, J=246.83 Hz, C-2'), 133.12 (d, J=21.52 Hz, C-1'), 132.26 (C-3a), 131.85 (C-7), 131.42 (C-5a), 130.75 (C-2), 129.78 (d J=20.97 Hz, C-3' and C-5'), 129.36 (d, J=3.24 Hz, C-4'), 128.90 (d, J=7.94 Hz, C-6'), 128.14 (C-9b), 118.46 (C-9a), 116.49 (C-4), 116.27 (C-5), 109.03 (C-8), 104.52 (C-1), 41.38 (NCH_2CH_3),c16.74 (NCH_2CH_3) ppm; IR (KBr): ν= 3422.38 (NH), 3022 (aromatic C-H), 2901.12 (aliphatic C-H), 1608.38 (C=O), 1509.10 (C=C), 1228.67 (C-F) cm^{-}1; UV-Vis (H_2O): 273 nm (A = 0.473 mAU), 342 nm (A = 0.297 mAU); fluorescence (H_2O): λ_{exc} = 342 nm, λ_{ems} = 484.02 nm; ESI-MS: m/z $[M+H]^+$ calculated for $C_{19}H_{16}FN_2O^+$, 307.1241; found, 307.1287; RP-C18 HPLC: t_R = 13.27 min, 95.07%

3-Ethyl-7-(3-fluorophenyl)-3H-pyrrolo[3,2-f]quinolin-9(6H)-one (**13**).

Compound **13** was prepared as described for compound **12** by reacting 1.07g (2.92 mmol) of the appropriate phenyl-acrylate derivative **8** to yield 0.836 g of a raw solid which was purified by Flash column chromatography (eluent chloroform/methanol, 9:1) to yield

0.332 g of final compound. Yield: 37 %; R*f*: 0.53 (light blue fluorescent spot, chloroform/methanol, 9:1); mp = 303°C; ^{1}H-NMR (400 MHz, DMSO-d_6) δ 8.00 (dd, 1H, J=9.35 Hz and J=0.70 Hz, H-4), 7.67 (dd, 1H, J=2.92 Hz and J=0.72 Hz, H-1), 7.59 (d, 1H, J=9.35 Hz, H-5), 7.57 (m, 5H, H-2', H-4', H-5', H-6'), 7.57 (m, 1H, H-2), 6.04 (s, 1H, H-8), 4.37 (q, 2H, J=7.20 Hz, NCH_2CH_3), 1.42 (t, 3H, J=7.20 Hz, NCH_2CH_3) ppm; ^{13}C-NMR (101MHz, DMSO-d_6) δ: 178.25 (C-9), 163.27 (d, J=247.72 Hz, C-3'), 137.97 (C-3a), 135.83 (C-5a), 131.92 (d, J=7.93 Hz, C-1'), 131.43 (C-7), 129.69 (d, J= 3.14 Hz, C-4'), 128.61 (d, J=21.24 Hz, C-2' and C-6'), 124.36 (C-2 and C-9b), 123.85 (d, J=7.36 Hz, C-5'), 118.59 (C-9a), 116.42 (C-4), 113.78 (C-8), 108.67 (C-5), 104.68 (C-1), 41.50 (NCH_2CH_3), 16.82 (NCH_2CH_3) ppm; IR (KBr): ν= 3427.83 (NH), 3027 (aromatic C-H), 2928.07 (aliphatic C-H), 1602.79 (C=O), 1508.25 (C=C), 1222.76 (C-F) cm^{-}1; UV-Vis (H_2O): 273 nm (A = 0.326 mAU), 344 nm (A = 0.202 mAU); fluorescence (H_2O): λ_{exc} = 344 nm, λ_{ems} = 492.98 nm; ESI-MS: m/z $[M+H]^+$ calculated for $C_{19}H_{16}FN_2O^+$, 307.1241; found, 307.1264; RP-C18 HPLC: t_R = 13.15 min, 96.25%.

3-Ethyl-7-(4-fluorophenyl)-3H-pyrrolo[3,2-f]quinolin-9(6H)-one (**14**).

Compound **14** was prepared as described for compound **12** by reacting 1.12 g (3.05 mmol) of the appropriate phenylacrylate derivative **9** to yield 0.340 g of a raw solid which was purified by Flash column chromatography (eluent chloroform/methanol, 9:1) to yield 0.320 g of final compound. Yield: 39 %; R*f*: 0.59 (light blue fluorescent spot, chloroform/methanol, 9:1); mp = 308°C; ^{1}H-NMR (400 MHz, DMSO-d_6) δ 11.66 (s, 1H, NH), 7.93 (m, J = 5.46, 3.24 Hz, 2H, H-2' and H-6'), 7.90 (d, J=8.96 Hz, 1H, H-4), 7.57 (d, J = 8.92 Hz, 1H, H-5), 7.52 (d, J = 2.66 Hz, 1H, H-1), 7.50 (d, J = 2.82 Hz, 1H, H-2), 7.42 (m, J = 8.86, 3.19, 2.19 Hz, 2H, H-3' and H-5'), 6.47 (s, 1H, H-8), 4.32 (q, J = 7.21 Hz, 2H, NCH_2CH_3), 1.41 (t, J = 7.22 Hz, 3H, NCH_2CH_3) ppm; ^{13}C-NMR (101 MHz, DMSO-d_6) δ 178.69 (C-9), 163.97 (d, J=247.32 Hz, C-4'), 147.32 (C-7), 137.21 (C-5a), 131.91 (C-3a), 130.51 (d, J=8.63 Hz, C-2' and C-6'), 128.91 (C-2), 123.90 (C-9a and C-9b), 118.74 (d, J=2.31 Hz, C-1'), 116.73 (d, J=21.80 Hz, C-3' and C-5'), 116.33 (C-4), 113.13 (C-5), 109.02 (C-8), 104.59 (C-1), 41.43 (NCH_2CH_3), 16.78 (NCH_2CH_3) ppm; IR (KBr): ν= 3422.31 (NH), 3078 (aliphatic C-H), 2930.57 (aliphatic C-H), 1609.22 (C=O), 1508.23 (C=C), 1220.20 cm^{-1} (C-F); UV-Vis (H_2O): 269 nm (A = 0.248 mAU), 352.97 nm (A = 0.165 mAU); fluorescence (H_2O): λ_{exc} = 352.97 nm, λ_{ems} = 484.02 nm; HRMS (ESI-MS, 140 eV): m/z $[M+H]^+$ calculated for $C_{19}H_{16}FN_2O^+$, 307.1241; found, 307.1272; RP-C18 HPLC: t_R = 12.95 min, 97.05%.

3-Benzoyl-7-(3-fluorophenyl)-6H-pyrrolo[3,2-f]quinolin-9-one (**15**).

Compound **15** was prepared as described for compound **12** by reacting 0.150g (3.05 mmol) of the appropriate phenyl-acrylate derivative **10** to yield 0.080 g of final compound. Yield: 56 %; R*f*: 0.59 (light blue fluorescent spot, chloroform/methanol, 9:1); mp = 318°C; ^{1}H NMR (300 MHz, DMSO) δ 6.51 (s, 1H, H-8), 7.43 (t, *J* = 8.5 Hz, 1H), 7.52 (d, *J* = 3.6 Hz, 1H), 7.68 – 7.60 (m, 3H, H-3', H-4' and H-5') 7.87 – 7.70 (m, 7H, H-2', H-6',), 8.61 (d, *J* = 9.1 Hz, 1H, H-4), 11.90 (s, 1H, NH) ppm; ^{13}C NMR (101 MHz, DMSO-d_6) δ 179.80 (CO), 165.20 (NCO), 163.04 (d, J=248.16 Hz, C-3'), 135.57 (C-3a), 135.12 (C-5a), 133.65 (C-7), 130.64 (C-4''), 130.12 (d, J=7.91 Hz, C-1'), 129.99 (d, J= 3.28 Hz, C-4'), 129.96 (C-3'' and C-5''), 128.11 (d, J=21.24 Hz, C-2' and C-6'), 127.64 (C-2'' and C-6''), 124.19 (C-2 and C-9b), 124.02 (d, J=7.32 Hz, C-5'), 120.45 (C-4), 120.14 (C-9a), 117.02 (C-5), 110.41 (C-1), 107.03 (C-8) ppm; UV-Vis (H_2O): 275 nm (A = 0.568 mAU); fluorescence (H_2O): λ_{exc} = 275 nm, λ_{ems} = 541 nm; HRMS (ESI-MS, 140 eV): m/z $[M+H]^+$ calculated for $C_{24}H_{16}FN_2O_2^+$, 383.1190; found, 383.1175; RP-C18 HPLC: t_R = 20.50 min, 95.62%.

2-fluorobenzoyl chloride (**17**).

2.0 g of 2-fluorobenzoic acid (14.27 mmol) are placed in a 50 mL round-bottomed flask and 7 mL of thionyl chloride were added. The mixture was refluxed at 80°C for 2 h, concentrated under reduced pressure and the residue was co-evaporated with toluene (10 mL) 3 times to obtain 0.910 g of a yellow oil. The compound was used for the next step without further purification. Yield = 40 %; ^{1}H NMR signals were compatible with data reported in literature.

Synthesis of 7-phenyl-3H-pyrrolo[3,2-f]quinolin-9-yl 2-fluorobenzoate (**18**) and *3-(2-fluorobenzoyl)-7-phenyl-6H-pyrrolo[3,2-f]quinolin-9-one* (**19**).

Into a two-necked 50 mL round-bottomed flask, 0.060 g (2.54 mmol, 3 eq.) of NaH, 60% dispersion in mineral oil, was placed and washed with toluene (3 x 10 mL). With stirring, a solution of 7-phenyl- 3H,6H-pyrrolo[3,2-f]quinolin-9-one (**16**), (prepared as previously reported)[4] 0.220 g (0.85 mmol, 1 eq.) in 7 mL of anhydrous DMF, was dropped into the flask. After 40 min at room temperature, a solution of 2-fluorobenzoyl chloride, 0.40 g (2.54 mmol, 3 eq.) in 2 mL dry DMF, was added, and the reaction mixture was stirred for 2 h. The reaction was monitored by TLC analysis (eluent chloroform/methanol, 9:1). At the end of the reaction, 25 mL of water were added, and then extracted with EtOAc (3 x 50 mL). The combined organic phases were washed with water and brine, dried over anhydrous Na_2SO_4 and concentrated under vacuum to yield a crude brown solid (1.44 g). This crude product was purified with Flash column chromatography

(chloroform/methanol, 9:1), yielding 0.236 g of compound **18** and 0.070 g of desired compound **19**. Compound **18**: Yield 73 %; R*f*: 0.70 (light blue fluorescent spot, chloroform/methanol, 9:1); mp = 324°C; ^{1}H NMR (400 MHz, DMSO-d_6) δ 11.90 (s, 1H, NH), 8.46 (t, J=6.86 Hz, H-4), 8.34 (m, 1H, H-6''), 8.17 (d, 1H, J=9.19 Hz, H-5), 8.02 (m, 2H, H-2' and H-6'), 7.86 (d, 1H, J=3.21 Hz, H-2), 7.75 - 7.85 (m, 3H, H-3'', H-4'' and H-5''), 7.71 (m, 2H, H-3' and H-5'), 7.70 (m, 1H, H-4'), 7.67 (s, 1H, H-8), 7.42 (dd, 1H, J=2.99 Hz and J=0.65 Hz, H-1) ppm; ^{13}C NMR (101 MHz, DMSO-d_6) δ 176.63 (CO), 169.98 (C-9), 164.62 (d, J=245.27 Hz, C-2''), 151.15 (C-7), 138.72 (d, J=21.62 Hz, C-1''), 137.87 (C-5a), 133.62 (d, J=7.82 Hz, C-4''), 132.61 (C-1'), 132.58 (C-3a), 132.12 (C-4'), 131.44 (d, J=7.47 Hz, C-6''), 130.95 (C-2), 129.94 (d, J=2.61 Hz, C-5''), 129.83 (C-3' and C-5'), 129.05 (C-2' and C-6'), 120.68 (C-9b), 120.13 (C-4), 118.24 (d, J=21.82 Hz, C-3''), 114.10 (C-9a), 113.22 (C-5), 105.40 (C-1), 105.19 (C-8) ppm; IR (KBr): ν= 3301 cm^{-1} (NH), 3024.54 cm^{-1} (aromatic C-H), 2961.89 cm^{-1} (aliphatic C-H), 1458.09cm^{-1} (C=C), 1736.10cm^{-1} (COO), 1239.51cm^{-1} (C-F); UV-Vis (H_2O): 269 nm (A = 0.640), 376 nm (A = 0.393); fluorescence (H_2O): λ_{exc} = 376 nm, λ_{em} = 473.93 nm; HRMS (ESI-MS, 140 eV): m/z $[M+H]^+$ calculated for $C_{24}H_{16}FN_2O_2^+$, 383.119; found, 383.1261; RP-C18 HPLC: t_R = 15.44 min, 98 %; Compound **19**: Yield: 22%; R*f*: 0.60 (light blue fluorescent spot, chloroform/methanol, 9:1); mp = 163°C; ^{1}H NMR (400 MHz, DMSO-d_6) δ 11.95 (m, 1H, NH), 8.65 (d, J = 9.12 Hz, 1H, H-4), 7.87 (m, 2H, H-2' and H-6'), 7.86 (m, 1H, H-5''), 7.82 (m, J = 2.95 Hz, 1H, H-2), 7.80 (m, J = 2.84 Hz, 1H, H-1), 7.74 (m, 1H, H-4'), 7.60 (m, 2H, H-3' and H-5'), 7.50 (d, J = 9.12 Hz, 1H, H-5), 7.46 (m, 1H, H-3''), 7.39 (m, J = 1.60 Hz, 1H, H-6''), 7.26 (m, 1H, H-4''), 6.45 (s, 1H, H-8) ppm; ^{13}C NMR (101 MHz, DMSO-d_6) δ 178.50 (CO), 164.93 (NCO), 160.27 (C-7), 158.93 (d, J=249.32, C-2''), 149.44 (C-5a), 140.27 (d, J=22.78 Hz, C-1''), 139.14 (C-3a), 135.17 (d, J=8.76 Hz, C-4''), 134.48 (C-1), 134.24 (C-4'), 132.34 (d, J=1.30 Hz, C-5''), 130.71 (d, J=7.82 Hz, C-6''), 129.52 (C-3' and C-5'), 128.51 (C-2), 127.94 (C-2' and C-6'), 120.54 (C-9b), 120.54 (C-4), 119.84 (C-9a), 117.25 (d, J=23.04 Hz, C-3''), 116,56 (C-5), 111.16 (C-1), 109.12 (C-8) ppm; IR (KBr): ν = 3430.03 cm^{-1} (NH), 3067.39 cm^{-1} (aromatic C-H), 2964 cm^{-1} (aliphatic C-H), 1687 cm^{-1} (C=O), 1547cm^{-1} (C=C), 1351.18cm^{-1} (C-F); UV-Vis (H_2O): 280 nm (A = 0.989), 346.42 nm (A = 0.803); Fluorescence (H_2O): λ_{exc}=346.42 nm, λ_{em}=500.00 nm; HRMS (ESI-MS, 140 eV): m/z $[M+H]^+$ calculated for $C_{24}H_{16}FN_2O_2^+$, 383.119; found, 383.1261; RP-C18 HPLC: t_R = 15.24 min, 96.5 %.

Biology

Cell growth conditions and antiproliferative assay

Human T-cell leukemia (Jurkat and CEM), human B-cell leukemia (RS4;11) and human myeloid leukemia (Kasumi-1) cells were grown in RPMI-1640 medium (Gibco, Milano, Italy). Breast adenocarcinoma (MDA-MB-231), human cervix carcinoma (HeLa), non-small cell lung adenocarcinoma (A549), human melanoma cells (A375 and A2058) and human colon adenocarcinoma (HT-29) cells were grown in DMEM medium (Gibco, Milano, Italy), all supplemented with 115 units/mL penicillin G (Gibco, Milano, Italy), 115 μg/mL streptomycin (Invitrogen, Milano, Italy), and 10% fetal bovine serum (Invitrogen, Milano, Italy). Stock solutions (10 mM) of the different compounds were obtained by dissolving them in DMSO. Individual wells of a 96-well tissue culture microtiter plate were inoculated with 100 µL of complete medium containing 8×10^3 cells. The plates were incubated at 37 °C in a humidified 5% CO_2 incubator for 18 h prior to the experiments. After medium removal, a 100 µL aliquot of fresh medium containing the test compound at a varying concentration was added to each well in triplicate and incubated at 37 °C for 72 h. Cell viability was assayed by the (3-(4, 5-dimethylthiazol-2-yl)-2,5-diphenyltetrazolium bromide test as previously described.[22] The GI_{50} was defined as the compound concentration required to inhibit cell proliferation by 50%. $CEM^{Vbl\text{-}100}$ cells are a multidrug-resistant line selected against vinblastine and were a kind gift of Dr. G. Arancia (Istituto Superiore di Sanità, Rome, Italy). They were grown in RPMI-1640 medium supplemented with 100 ng/mL of vinblastine. Peripheral blood lymphocytes (PBL) from healthy donors were obtained by separation on a Lymphoprep (Fresenius KABI Norge AS) gradient. After extensive washing, cells were resuspended (1.0×10^6 cells/mL) in RPMI-1640 with 10% fetal bovine serum and incubated overnight. For cytotoxicity evaluations in proliferating PBL cultures, non-adherent cells were resuspended at 5×10^5 cells/mL in growth medium containing 2.5 μg/mL PHA (Irvine Scientific). Different concentrations of the test compounds were added, and viability was determined 72 h later by the MTT test. For cytotoxicity evaluations in resting PBL cultures, non-adherent cells were resuspended (5×10^5 cells/mL) and treated for 72 h with the test compounds, as described above.

Effects on tubulin polymerization and on colchicine binding to tubulin

To evaluate the effect of the compounds on tubulin assembly *in vitro,*[12] varying concentrations of compounds were preincubated with 10 µM bovine brain tubulin in 0.8

M monosodium glutamate (from a 2 M stock solution adjusted to pH 6.6 with HCl) for 15 min at 30 ˚C and then cooled to 0 ˚C. After addition of 0.4 mM GTP (final concentration), the mixtures were transferred to 0 °C cuvettes in a recording spectrophotometer equipped with an electronic temperature controller and warmed to 30 °C. Tubulin assembly was followed turbidimetrically at 350 nm. The IC_{50} was defined as the compound concentration that inhibited the extent of assembly by 50% after a 20 min incubation. The ability of the test compounds to inhibit colchicine binding to tubulin was measured as described,[13] with the reaction mixtures containing 1 μM tubulin, 5 μM [^{3}H]colchicine and 1 or 5 μM test compound.

Flow cytometric analysis of cell cycle distribution

5×10^5 HeLa cells were treated with different concentrations of the test compounds for 24 h. After the incubation period, the cells were collected, centrifuged, and fixed with ice-cold ethanol (70%). The cells were then treated with lysis buffer containing RNase A and 0.1% Triton X-100 and stained with PI. Samples were analyzed on a Cytomic FC500 flow cytometer (Beckman Coulter). DNA histograms were analyzed using MultiCycle for Windows (Phoenix Flow Systems).

Apoptosis assay

Cell death was determined by flow cytometry of cells double stained with annexin V/FITC and PI. The Coulter Cytomics FC500 (Beckman Coulter) was used to measure the surface exposure of PS on apoptotic cells according to the manufacturer's instructions (Annexin-V Fluos, Roche Diagnostics).

Analysis of mitochondrial potential and ROS

The mitochondrial membrane potential was measured with the lipophilic cation JC-1 (Molecular Probes, Eugene, OR, USA), while the production of ROS was followed by flow cytometry using the fluorescent dyes H_2DCFDA (Molecular Probes), as previously described.[23]

Western blot analysis

HeLa cells were incubated in the presence of **12** and, after different times, were collected, centrifuged, and washed two times with ice cold phosphate buffered saline (PBS). The pellet was then resuspended in lysis buffer. After the cells were lysed on ice for 30 min, lysates were centrifuged at 15000 x g at 4 °C for 10 min. The protein concentration in the supernatant was determined using the BCA protein assay reagents (Pierce, Italy). Equal amounts of protein (10 μg) were resolved using sodium dodecyl sulfate-polyacrylamide

gel electrophoresis (SDS-PAGE) (Criterion Precast, BioRad, Italy) and transferred to a PVDF Hybond-P membrane (GE Healthcare). Membranes were blocked with a bovine serum albumin solution (5% in Tween PBS 1X), and the membranes being gently rotated overnight at 4 °C. Membranes were then incubated with primary antibodies against Bcl-2, PARP, caspase-3, H2AX, cdc25c, cyclin B, p-cdc2^{Tyr15}, Mcl-1 (all from Cell Signaling) and γ-tubulin (Sigma-Aldrich) for 2 h at room temperature. Membranes were next incubated with peroxidase labeled secondary antibodies for 60 min. All membranes were visualized using ECL Select (GE Healthcare), and images were acquired using an Uvitec-Alliance imaging system (Uvitec, Cambridge, UK). To ensure equal protein loading, each membrane was stripped and reprobed with anti-actin antibody.

***In vivo* animal studies**

Animal experiments were approved by our local animal ethics committee (OPBA, Organismo Preposto al Benessere degli Animali, Università degli Studi di Brescia, Italy) and were executed in accordance with national guidelines and regulations. Procedures involving animals and their care conformed with institutional guidelines that comply with national and international laws and policies (EEC Council Directive 86/609, OJ L 358, 12 December 1987) and with "ARRIVE" guidelines (Animals in Research Reporting *In Vivo* Experiments). Six weeks old C57BL/6 mice (Envigo) were injected subcutaneously into the dorsolateral flank with 2.5x10^5 BL6-B16 murine melanoma cells in 200 µL-total volume of PBS. When tumors were palpable, animals were treated intraperitoneally every other day with different doses of test compounds dissolved in 50 µL of DMSO. Tumors were measured in two dimensions, and tumor volume was calculated according to the formula V=(D x d^2)/2, where D and d are the major and minor perpendicular tumor diameters, respectively.

Evaluation of the metabolic stability of compounds 12-15 and 19 in human liver microsomes

Incubation procedure. Compounds (final concentration, 10 mM) were incubated in a medium (final volume, 0.2 mL) containing 0.1 M KH_2PO4 (pH 7.4) and 1.0 mg/mL of pooled mixed gender human liver microsomes (Xenotech LLC, Lenexa, USA; HLMs), in the absence or presence of 1 mM NADPH (Sigma- Aldrich). Control incubations were performed in the absence of both HLMs and NADPH (buffer only-incubations). The reactions were started by adding the microsomes following a 3-min thermal equilibration at 37°C, conducted at 37°C for different time periods (i.e. 0, 15, 30 and 60 min), and

terminated by adding 0.1 mL of ice-cold acetonitrile. Samples were then centrifuged (4°C) at 20,000 g for 10 min, and aliquots of the supernatants were analyzed by HPLC with fluorescence detection, as described below.

HPLC analysis. The chromatographic system consisted of a Hewlett-Packard 1100 HPLC system (Agilent Technologies Inc., formerly Hewlett-Packard, Palo Alto, USA) equipped with a degasser, a quaternary pump, an autosampler, a column oven, and a fluorescence detector; chromatographic data were collected and integrated using the Agilent ChemStation software. Chromatographic conditions were as follows: column, Agilent Zorbax SB C18 (4.6x75 mm, 3.5 mm); mobile phase, 0.1% HCOOH in H_2O (solvent A) and 0.1% HCOOH in acetonitrile (solvent B); elution program, isocratic elution with 95% solvent A for 2 min, linear gradient from 5 to 40% solvent B in 8 min, followed by a further linear gradient from 40 to 60% solvent B in 2 min, and an isocratic elution with 60% solvent B for 7 min; post-run time, 5 min; flow rate, 1.0 mL/min; injection volume, 50 mL; column temperature, 30° C; detection, fluorescence (excitation wavelength, 344 nm; emission wavelength, 493 nm).

Acknowledgements

Synthesis by M. Dal Prà, D. Carta, M.G. Ferlin, *in vitro* evaluation by R. Bortolozzi, G. Viola, E. Hamel, *in vivo* evaluation by R. Ronca, metabolic stability studies by V. Di Paolo, L. Quintieri were supported by financial grants from University of Padova, Italy.

References

[1] R.J. Van Vuuren, M.H. Visagie, A.E. Theron, A.M. Joubert, Antimitotic drugs in the treatment of cancer, Cancer Chemother. Pharmacol. 76 (2015) 1101–1112. doi:10.1007/s00280-015-2903-8.

[2] Y. Xia, Z.Y. Yang, P. Xia, K.F. Bastow, Y. Tachibana, S.C. Kuo, E. Hamel, T. Hackl, K.H. Lee, Antitumor agents. 181. Synthesis and biological evaluation of 6,7,2',3',4'-substituted-1,2,3,4-tetrahydro-2-phenyl-4-quinolones as a new class of antimitotic antitumor agents, J. Med. Chem. 41 (1998) 1155–1162. doi:10.1021/jm9707479.

[3] L. Li, H.K. Wang, S.C. Kuo, W. Tian-Shung, D. Lednicer, C.M. Lin, E. Hamel, K.H. Lee, Antitumor Agents. 150. 2′,3′,4′,5′,5,6,7-Substituted 2-Phenyl-4-

quinolones and Related Compounds: Their Synthesis, Cytotoxicity, and Inhibition of Tubulin Polymerization, J. Med. Chem. 37 (1994) 1126–1135. doi:10.1021/jm00034a010.

[4] V. Gasparotto, I. Castagliuolo, G. Chiarelotto, V. Pezzi, D. Montanaro, P. Brun, G. Palù, G. Viola, M.G. Ferlin, Synthesis and biological activity of 7-phenyl-6,9-dihydro-3H-pyrrolo[3,2-f]quinolin-9-ones: a new class of antimitotic agents devoid of aromatase activity., J. Med. Chem. 49 (2006) 1910–5. doi:10.1021/jm0510676.

[5] V. Gasparotto, I. Castagliuolo, M.G. Ferlin, 3-Substituted 7-phenyl-pyrroloquinolinones show potent cytotoxic activity in human cancer cell lines, J. Med. Chem. 50 (2007) 5509–5513. doi:10.1021/jm070534b.

[6] M.G. Ferlin, R. Bortolozzi, P. Brun, I. Castagliuolo, E. Hamel, G. Basso, G. Viola, Synthesis and in vitro evaluation of 3H-pyrrolo[3,2-f]-quinolin-9-one derivatives that show potent and selective anti-leukemic activity, ChemMedChem. 5 (2010) 1373–1385. doi:10.1002/cmdc.201000180.

[7] D. Carta, R. Bortolozzi, E. Hamel, G. Basso, S. Moro, G. Viola, M.G. Ferlin, Novel 3-Substituted 7-Phenylpyrrolo[3,2-f]quinolin-9(6H)-ones as Single Entities with Multitarget Antiproliferative Activity, J. Med. Chem. 58 (2015) 7991–8010. doi:10.1021/acs.jmedchem.5b00805.

[8] D. Carta, R. Bortolozzi, M. Sturlese, V. Salmaso, E. Hamel, G. Basso, L. Calderan, L. Quintieri, S. Moro, G. Viola, M.G. Ferlin, Synthesis, structure-activity relationships and biological evaluation of 7-phenyl-pyrroloquinolinone 3-amide derivatives as potent antimitotic agents, Eur. J. Med. Chem. 127 (2017) 643–660. doi:10.1016/j.ejmech.2016.10.026.

[9] R. Bortolozzi, E. Mattiuzzo, M. Dal Pra, M. Sturlese, S. Moro, E. Hamel, D. Carta, G. Viola, M.G. Ferlin, Targeting tubulin polymerization by novel 7-aryl-pyrroloquinolinones: Synthesis, biological activity and SARs, Eur. J. Med. Chem. 143 (2018) 244–258. doi:10.1016/j.ejmech.2017.11.038.

[10] W.K. Hagmann, The many roles for fluorine in medicinal chemistry, J. Med. Chem. 51 (2008) 4359–4369. doi:10.1021/jm800219f.

[11] R. Romagnoli, P.G. Baraldi, M.K. Salvador, F. Prencipe, V. Bertolasi, M. Cancellieri, A. Brancale, E. Hamel, I. Castagliuolo, F. Consolaro, E. Porcù, G. Basso, G. Viola, Synthesis, antimitotic and antivascular activity of 1-(3',4', 5'-

trimethoxybenzoyl)-3-arylamino-5-amino-1,2,4-triazoles, J. Med. Chem. 57 (2014) 6795–6808. doi:10.1021/jm5008193.

[12] E. Hamel, Evaluation of antimitotic agents by quantitative comparisons of their effects on the polymerization of purified tubulin, Cell Biochem. Biophys. 38 (2003) 1–21. doi:10.1385/CBB:38:1:1.

[13] P. Verdier-Pinard, J.Y. Lai, H.D. Yoo, J. Yu, B. Marquez, D.G. Nagle, M. Nambu, J.D. White, J.R. Falck, W.H. Gerwick, B.W. Day, E. Hamel, Structure-activity analysis of the interaction of curacin A, the potent colchicine site antimitotic agent, with tubulin and effects of analogs on the growth of MCF-7 breast cancer cells., Mol. Pharmacol. 53 (1998) 62–76. doi:10.1124/mol.53.1.62.

[14] B.A.A. Weaver, D.W. Cleveland, Decoding the links between mitosis, cancer, and chemotherapy: The mitotic checkpoint, adaptation, and cell death, Cancer Cell. 8 (2005) 7–12. doi:10.1016/j.ccr.2005.06.011.

[15] P.R. Clarke, L.A. Allan, Cell-cycle control in the face of damage - a matter of life or death, Trends Cell Biol. 19 (2009) 89–98. doi:10.1016/j.tcb.2008.12.003.

[16] I. Vitale, A. Antoccia, C. Cenciarelli, P. Crateri, S. Meschini, G. Arancia, C. Pisano, C. Tanzarella, Combretastatin CA-4 and combretastatin derivative induce mitotic catastrophe dependent on spindle checkpoint and caspase-3 activation in non-small cell lung cancer cells, Apoptosis. 12 (2007) 155–166. doi:10.1007/s10495-006-0491-0.

[17] C. Cenciarelli, C. Tanzarella, I. Vitale, C. Pisano, P. Crateri, S. Meschini, G. Arancia, A. Antoccia, The tubulin-depolymerising agent combretastatin-4 induces ectopic aster assembly and mitotic catastrophe in lung cancer cells H460, Apoptosis. 13 (2008) 659–669. doi:10.1007/s10495-008-0200-2.

[18] Y. Tsujimoto, S. Shimizu, Role of the mitochondrial membrane permeability transition in cell death, Apoptosis. 12 (2007) 835–840. doi:10.1007/s10495-006-0525-7.

[19] S. Xiong, T. Mu, G. Wang, X. Jiang, Mitochondria-mediated apoptosis in mammals., Protein Cell. 5 (2014) 737–49. doi:10.1007/s13238-014-0089-1.

[20] E. Lugli, L. Troiano, A. Cossarizza, Polychromatic analysis of mitochondrial membrane potential using JC-1., Curr. Protoc. Cytom. Chapter 7 (2007) Unit7.32. doi:10.1002/0471142956.cy0732s41.

[21] A. Rovini, A. Savry, D. Braguer, M. Carré, Microtubule-targeted agents: When mitochondria become essential to chemotherapy, Biochim. Biophys. Acta - Bioenerg. 1807 (2011) 679–688. doi:10.1016/j.bbabio.2011.01.001.

[22] R. Romagnoli, P.G. Baraldi, C. Lopez-Cara, D. Preti, M. Aghazadeh Tabrizi, J. Balzarini, M. Bassetto, A. Brancale, X.H. Fu, Y. Gao, J. Li, S.Z. Zhang, E. Hamel, R. Bortolozzi, G. Basso, G. Viola, Concise Synthesis and Biological Evaluation of 2-Aroyl-5-Amino Benzo[b]thiophene Derivatives As a Novel Class of Potent Antimitotic Agents, J. Med. Chem. 56 (2013) 9296–9309. doi:10.1021/jm4013938.

[23] R. Romagnoli, P.G. Baraldi, M.K. Salvador, F. Prencipe, C. Lopez-Cara, S. Schiaffino Ortega, A. Brancale, E. Hamel, I. Castagliuolo, S. Mitola, R. Ronca, R. Bortolozzi, E. Porcuì, G. Basso, G. Viola, Design, Synthesis, in Vitro, and in Vivo Anticancer and Antiangiogenic Activity of Novel 3-Arylaminobenzofuran Derivatives Targeting the Colchicine Site on Tubulin, J. Med. Chem. 58 (2015) 3209–3222. doi:10.1021/acs.jmedchem.5b00155.

[24] N. Zamzami, P. Marchetti, M. Castedo, D. Decaudin, A. Macho, T. Hirsch, S.A. Susin, P.X. Petit, B. Mignotte, G. Kroemer, Sequential reduction of mitochondrial transmembrane potential and generation of reactive oxygen species in early programmed cell death., J. Exp. Med. 182 (1995) 367–77. doi:10.1084/jem.182.2.367.

[25] J. Cai, D.P. Jones, Superoxide in apoptosis. Mitochondrial generation triggered by cytochrome c loss, J. Biol. Chem. 273 (1998) 11401–11404. doi:10.1074/jbc.273.19.11401.

[26] H. Nohl, L. Gille, K. Staniek, Intracellular generation of reactive oxygen species by mitochondria, Biochem. Pharmacol. 69 (2005) 719–723. doi:10.1016/j.bcp.2004.12.002.

[27] G. Rothe, G. Valet, Flow cytometric analysis of respiratory burst activity in phagocytes with hydroethidine and 2',7'-dichlorofluorescin., J. Leukoc. Biol. 47 (1990) 440–448. http://www.ncbi.nlm.nih.gov/pubmed/2159514 (accessed September 20, 2017).

[28] M.E. Harley, L.A. Allan, H.S. Sanderson, P.R. Clarke, Phosphorylation of Mcl-1 by CDK1-cyclin B1 initiates its Cdc20-dependent destruction during mitotic arrest, EMBO J. 29 (2010) 2407–2420. doi:10.1038/emboj.2010.112.

[29] I.E. Wertz, S. Kusam, C. Lam, T. Okamoto, W. Sandoval, D.J. Anderson, E. Helgason, J.A. Ernst, M. Eby, J. Liu, L.D. Belmont, J.S. Kaminker, K.M. O'Rourke, K. Pujara, P.B. Kohli, A.R. Johnson, M.L. Chiu, J.R. Lill, P.K. Jackson, W.J. Fairbrother, S. Seshagiri, M.J.C. Ludlam, K.G. Leong, E.C. Dueber, H. Maecker, D.C.S. Huang, V.M. Dixit, Sensitivity to antitubulin chemotherapeutics is regulated by MCL1 and FBW7, Nature. 471 (2011) 110–114. doi:10.1038/nature09779.

[30] M.D. Haschka, C. Soratroi, S. Kirschnek, G. Häcker, R. Hilbe, S. Geley, A. Villunger, L.L. Fava, The NOXA-MCL1-BIM axis defines lifespan on extended mitotic arrest, Nat. Commun. 6 (2015) 6891. doi:10.1038/ncomms7891.

[31] A. Parkinson, B.W. Ogilvie, Biotransformation of xenobiotics, in casarett &Doull's toxicology (Klaassen CD ed). The Basic Science of Poisons, seventh ed., McGraw-Hill, New York, 2008, pp. 161e304. 25].

CHAPTER 3

Targeting RORs nuclear receptors by novel synthetic steroidal inverse agonists for autoimmune disorders[1]

Synopsys

Designing novel inverse agonists of NR RORγt still represents a challenge for the pharmaceutical community to develop therapeutics for treating immune diseases. By exploring the structure of NRs natural ligands, the representative arotinoid ligands and RORs specific ligands share some chemical homologies which can be exploited to design a novel molecular structure characterized by a polycyclic core bearing a polar head and a hydrophobic tail. Compound MG 2778 (**8**), a cyclopenta[a]phenanthrene derivative, was identified as lead compound which was chemically modified at position 2 in order to obtain a small library for preliminary SARs. Cell viability and estrogenic activity of compounds **7**, **8**, **19a**, **30**, **31** and **32** were evaluated to attest selectivity. The selected **7**, **8**, **19a** and **31** compounds were assayed in a Gal4 UAS-Luc co-transfection system in order to determine their ability to modulate RORγt activity in a cellular environment. They were evaluated as inverse agonists taken ursolic acid as reference compound. The potency of compounds was lower than that of ursolic acid, but their efficacy was similar. Compound **19a** was the most active, significantly reducing RORγt activity at low micromolar concentrations.

Introduction

Background

Nuclear receptors (NRs) form a family of transcription factors that are composed of

[1] Published as: Dal Prà, M; Carta, D.; Szabadkai, G.; Suman, M.; Frión-Herrera, Y.; Paccagnella, N.; Castellani, G.; De Martin, S.; Ferlin, M.G.; Biorg Med Chem, 2018, 26, 1686-1704

modular protein structures with DNA- and ligand-binding domains (DBDs and LBDs). The DBDs confer gene target site specificity, whereas LBDs serve as control switches for NR function. In each case the overall fold of the LBD is conserved, and the ligand is bound entirely within the protein, completing the core as the protein refolds around it.[1] It was shown that despite the chemical diversity of the natural nuclear receptor ligands, their volumes are highly conserved.[2] Examples of NRs ligands are reported in Figure 1.

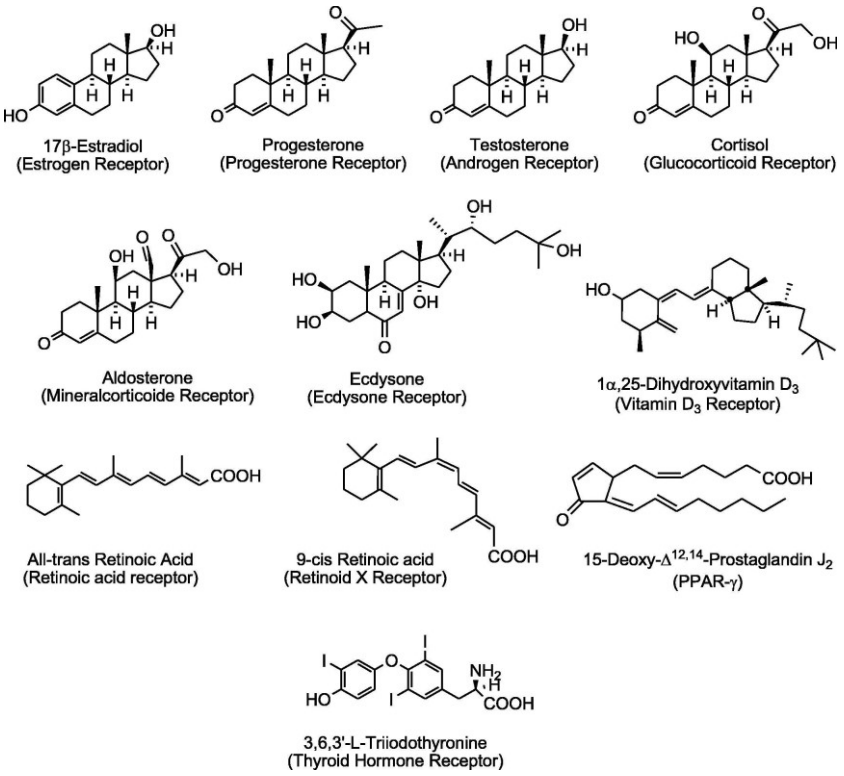

Figure 1. The natural ligands of nuclear receptors[2]

For many NRs, both endogenous and synthetic small molecule ligands bind to small pockets within the LBDs, resulting in conformational changes that regulate transcriptional activity. This property of NRs has proven to be a rich source as targets for developing of therapeutics for a myriad of human diseases, ranging from inflammatory diseases and cancer to endocrine and metabolic diseases.[3]

The retinoic acid nuclear receptors subfamily includes RARα, RARβ and RARγ and it is evolutionarily closed to the retinoic acid receptor-related orphan receptors subfamily, which is constituted by RORα, RORβ and RORγ or RORc. RORγt is a splice variant of RORγ and is encoded by a single gene called RORc. RORγt is selectively expressed in thymocytes (T cells) and appears to drive the activation and differentiation of CD4+ and

CD8+ cells into IL17-producing T helper cells (T_H17) and cytotoxic T cells (Tc17). T_H17 and Tc17 are effector cells that promote inflammation, adaptive immunity, and autoimmunity by producing IL17 and other inflammatory cytokines such as IL21. Both synthetic and putative endogenous agonists of RORγt have been shown to increase the basal activity of RORγt enhancing T_H17 cell proliferation. Among the various transcriptional regulators RORγ is a uniquely tractable drug target for manipulating T_H17 cell development and function in the context of autoimmune diseases.[4] The RORγt LBD is an ideal domain to target via small molecules. Small molecules targeting RORs come in at least two types: inverse agonists, which block ROR-dependent transcriptional activity; and agonists, which enhance the transactivation of RORs.[5]

Since the discovery of the first small molecule T0901317[6,8,9] (Table 1), many RORγt ligands with agonistic and inverse agonistic activity have been disclosed in the literature.[7,10] Using the T0901317 scaffold as a lead compound, a series of synthetic RORγ inverse agonists have been developed, including SR1001, SR1555, and SR2211.[6-11] Some structurally complex natural products, such as digoxin and ursolic acid have also been reported to be RORγ inverse agonists.[15,16] Dan Littman's group, who discovered the crucial role for RORγt in T_H17 cells, identified the cardiac glycoside digoxin as a specific inhibitor for RORγt transcriptional activity using a chemical library screening.[15] They confirmed that digoxin inhibited murine T_H17 cell differentiation without affecting other T cell lineages, and it was efficient in a mouse EAE model. Digoxin was also identified in a random screening campaign, as an inhibitor of mouse and human T_H17 cell differentiation, and the crystal structure of the LBD of RORγt in complex with digoxin at 2.2 A° resolution has been solved. (Fig. 2). [15,17]

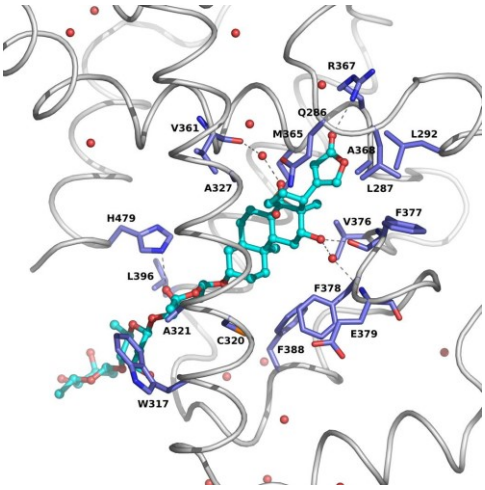

Figure 2. Digoxin binding mode in the RORγt ligand binding domain.[15]

Ursolic acid, another natural product, was also found in a compound library screening as an inhibitor of RORγt.[16] Importantly, both digoxin and ursolic acid have cholesterol-like chemical structures, which might account for their similar action on the NR.

Recently, a team at Genentech identified N-isobutyl-N-((5-(4-(methylsulfonyl) phenyl)thiophen-2-yl)methyl)-1-phenylmethanesulfonamide (named Gnt1 in Table 1 for reasons of brevity) as a RORγt inverse agonist via a biochemical screening campaign.[20] Although the development of RORγt inverse agonists has shown significant promise,[21,22] the development of new RORγt selective modulators with therapeutic potential still remains an urgent need.

Wang et al.[23] first reported that the natural products 7α-hydroxycholesterol[17] and 24S-hydroxycholesterol[19] were inverse agonists (i.e. functional antagonists) of RORγ and RORγ that suppressed transcriptional activities in hepatocytes. Oxysterols are well known natural ligands for the related NR including the liver X receptor (LXR), therefore their interaction with the LBDs of RORs was not surprising.[24] Most small molecule inhibitors and drugs are based on cyclic systems, which leads to a stiffening of the molecule, resulting in enhanced target affinity due to less entropy loss upon binding. The structural homology of NRs suggested to evaluate ligands for other class of receptors as possible cognate compounds that opportunely modified could switch their target classes becoming specific RARs/RORs agonists or inverse agonists.

Table 1. Structure of some RORs ligands[7]

Name	Structure	Receptor preferences	Ligand type	Ref.
T0901317	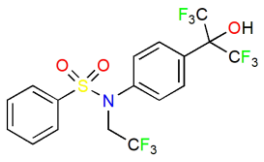	RORα, RORγ, LXRα, LXRβ, PXR, FXR, other	RORs: inverse agonist LXRS, PXR, FXR: agonist	8;9
SR1001	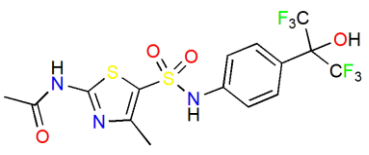	RORα RORγ	Inverse agonist	11

SR2211	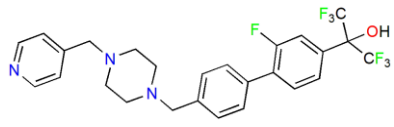	RORγ	Inverse agonist	12
Digoxin	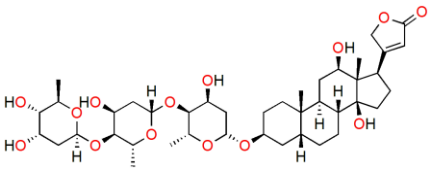	RORγ	Inverse agonist	15
Ursolic acid	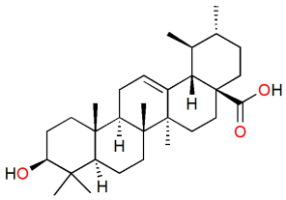	RORγ	Inverse agonist	16
Gnt1	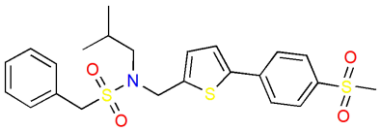	RORγ	Inverse agonist	20
7α-Hydroxy cholesterol	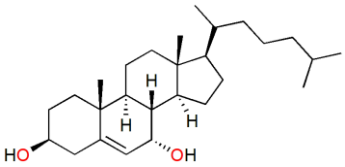	RORα RORγ	Inverse agonist	17
24S-Hydroxy cholesterol	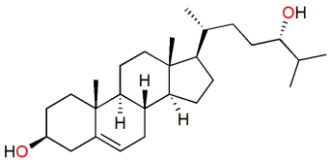	RORα RORγ	Inverse agonist	19

Designing a lead compound

Looking through the NRs superfamily and the chemical variety of the ligands scaffolds (polyenes, polycyclic compounds, aromatic or aliphatic rings, eicosanoids, oxysterols) (Figure 1), it could seem very unlikely that a novel RORγ inverse agonist lead candidate could be designed. However, we decide to explore the possibility to target RORγt receptor with a novel lead candidate, characterized by a cyclopenta[a]phenanthrene

scaffold. The design of a novel RORγ inverse agonist lead candidate was rationalized by means of a structure-based approach founded on hybridization of chemical structures, which mix the features of RORγ natural ligands (cholesterol-like derivatives, digoxin, ursolic acid) with the features of representative arotinoids. The term arotinoid referred to synthetic molecules which bear the retinoic acid carbon skeleton but with a more rigid aryl-based scaffold (Figure 3).[24] This choice was made because RARs and RORs receptors are evolutionarily closed and shared sequence homology.[6]

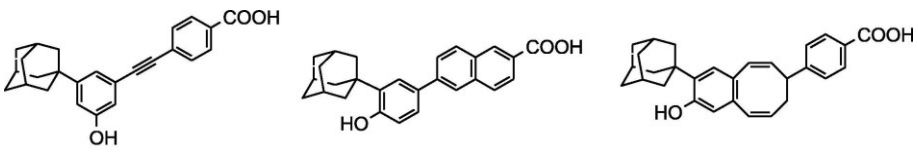

20.7 CD437 CD153

Figure 3. Arotinoids selective ligands

The envisaged novel RORs inverse agonist may result then conceptually defined by the following attributes:

1) A central polycyclic fused structure is present in other natural ligands of different classes of NRs assuring a suitable molecular volume to fulfil the LBD of the ROR receptors. The conservation of volumes among the natural ligands of nuclear receptors is likely to be a useful criterion in the design of high-affinity analogs.[2] It serves as a linker and supporting structure for the other fundamental chemical functions necessary for delivering the biological activity of the compound.
2) An aromatic ring as usually represented in arotinoids[24]
3) A large lipophilic scaffold (cyclic, polycyclic or poly methylated scaffold) mimicking the cyclic RA function or other bulky substituents connected to the polycyclic linker
4) A polar terminus corresponding to or mimicking the RA and ursolic acid acidic function (COOH or any of the known bioisosters or derivatives)
5) A hydroxylic function, as represented in arotinoids, cholesterol-like ligands and ursolic acid

The molecular structure of a lead compound might be the tetracycle MG 2778 or **8** as shown in Figure 4.

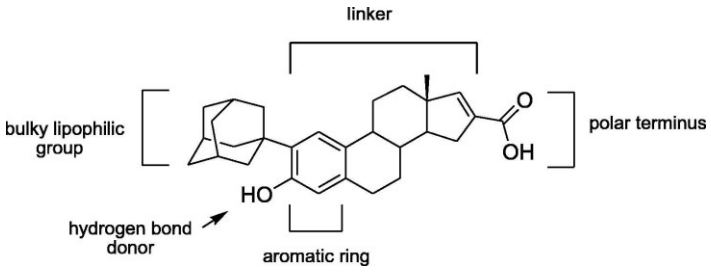

Figure 4. Lead structure of MG 2778 (**8**)

The early objective was to develop an efficient synthetic path for obtaining the proposed compound as described in Figure 4 (MG 2778). MG 2778 is a cyclopenta[a]phenanthrene derivative bearing an adamanthyl group at 2 position. This large group in position 2 was placed also because it was found to be effective in reducing hormonal effects of estrone and estradiol analogs in non-feminizing neuroprotective agents and so preventing estrogen receptor binding.[25] It also has an α-β-unsaturated carboxylic group at 16 and a phenolic hydroxyl at position 3. Next, with the aim to obtain preliminary SARs, a small series of analogs modified at position 2 of the polycyclic nucleus with groups other than adamanthyl but maintaining the lipophilic and bulky features was planned, since a suitable substitution at this position is considered significant for giving selectivity. To synthesize 2-substituted analogs we adopted methods such as Friedel-Crafts alkylation, acylation and Suzuki-Miyaura cross-coupling reactions on aromatic ring. Six compounds (**7**, **8**, **19a**, **30**-**32**) were tested for cytotoxicity and estrogen receptor activity. The selected four non-cytotoxic compounds (**7**, **8**, **19a**, **31**) were assayed in a Gal4 UAS-Luc co-transfection system in order to determine their ability to modulate RORγt activity in a cellular environment. They were evaluated as inverse agonists taken ursolic acid as reference compound.[26]

Results and Discussion

Docking simulations of MG 2778 (8) in RORγt LBD

We further employed molecular modelling analysis to simulate MG 2778 (**8**) binding in the RORγt binding pocket. We selected the crystal structure of RORγt in complex with one of the best-known inverse agonists, digoxin (PDB code 3B0W).[27] Computer docking

simulation of compound **8** was performed using Maestro 10.5 Glide software SP precision.

Figure 5 shows the binding mode of the most favoured pose of compound **8** in the presumptive binding site in comparison with digoxin. We found that compound **8** could be readily accommodate in the pocket. Moreover, RORγt shows a binding pocket mostly characterized by hydrophobic residues (Leu-287, Leu-292, Trp-317, Cys-320, Ala-321, Ala-327, Val-361, Met-365, Ala-368, Val-376, Phe-377, Phe-378, Phe-388, Leu-396) which suggests a binding interaction mode mainly characterised by hydrophobic interactions. No direct interaction between compound **8** and the residues responsible for digoxin binding was found.[15] However, even if the molecular volume of compound **8** is smaller than that of digoxin, it is possible that the bulky substituent in position 2 of the cyclopenta[a]phenanthrene core (which occupies the position of the first sugar ring in digoxin) might be sufficient to disturb the polar interactions observed in the agonist-bound RORγt LBD, involving His-479, Tyr-502 and Phe-506 which would be important to stabilize the active conformation of helix H12.[15,17]

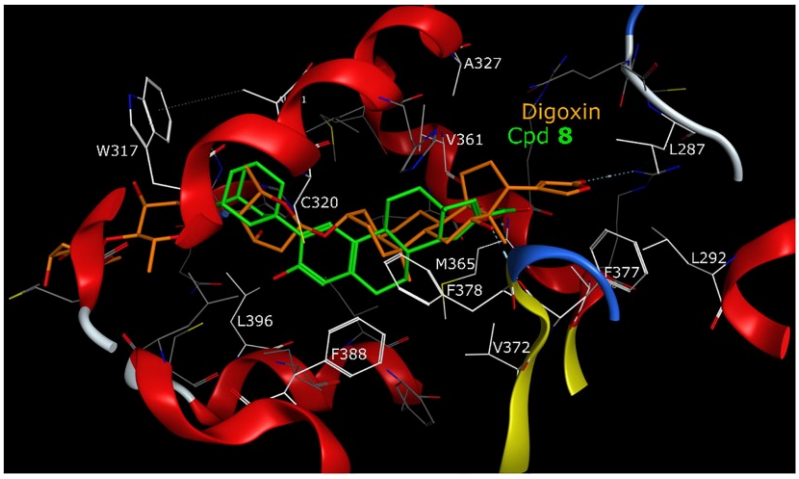

Figure 5. Comparison of the crystallographic structure of digoxin (in orange) in complex with RORγt ligand binding domain (Protein Data Bank code 3B0W) and the energetically most favourable pose of compound **8** (in green) obtained by molecular docking simulation. Hydrophobic residues are shown in white. Hydrogen atoms are omitted.

Chemistry

The synthetic work has been organized into four schemes that describe the optimized synthetic pathways as a result of trials to improve yields and purity of reaction products. The schemes report the routes carrying to final compounds for the synthesis of which the

pre-formed polycyclic scaffold 3-hydroxyestra-1,3,5(10)-triene-17-one (estrone) was selected as starting material. In all cases, the early protection of phenolic OH was necessary to prevent unresolvable mixtures formation along the pathway. Scheme 1 and 2 describe two alternative routes to obtain compound **8** (named MG 2778) by performing the same reactions in a different order. For this purpose, intermediate **1** was obtained from the starting commercial estrone by alkylating with CH_3I in the presence of Bu_4NI and NaOH 10% in CH_2Cl_2 at 70° C (99% yield).[28] As previously reported,[29] compound **1** was submitted to a Friedel-Crafts reaction conducted with adamanthanol, BF_3 Et_2O in hexane for 4 h. The reaction proved to be highly regiospecific yielding only the 2-adamanthyl substituted compound **2** (95% yield). The following 16-C methoxycarbonylation reaction[30] was carried out with dimethyl carbonate, NaH at refluxing (85° C) for 3h yielding compound **3** (93% yield). In order to form the 16-17 double bond, at first the 17-carbonyl group was reduced to secondary alcohol **4** by a chemo-selective reaction with $NaBH_4$[31] in a mixture of THF/CH_3OH 9:1 for 1 h at room temperature (90% yield). The obtained alcohol **4** was mesylated with MsCl in anhydrous CH_2Cl_2[32] giving the intermediate ester 17-methylsulfonate **5**, which by treatment with DBU in benzene[32] for 6h at 60°C and after Flash Chromatography purification, furnished the precursor intermediate **6** (60% yield).

The last step to produce the designed compound **8** was attempted with various hydrolytic methods and most of them failed. Among all, the treatment with, MeOH, NaOH 2M, in CH_2Cl_2[33] for 96 h gave the acid derivative **7** by 95% yield and only the method involving the use of $NaSCH_3$ in NMP at refluxing for 9h[34] was successful in giving the desired compound **8** with a yield of 56%.

Scheme 1. Synthesis of compound **8**

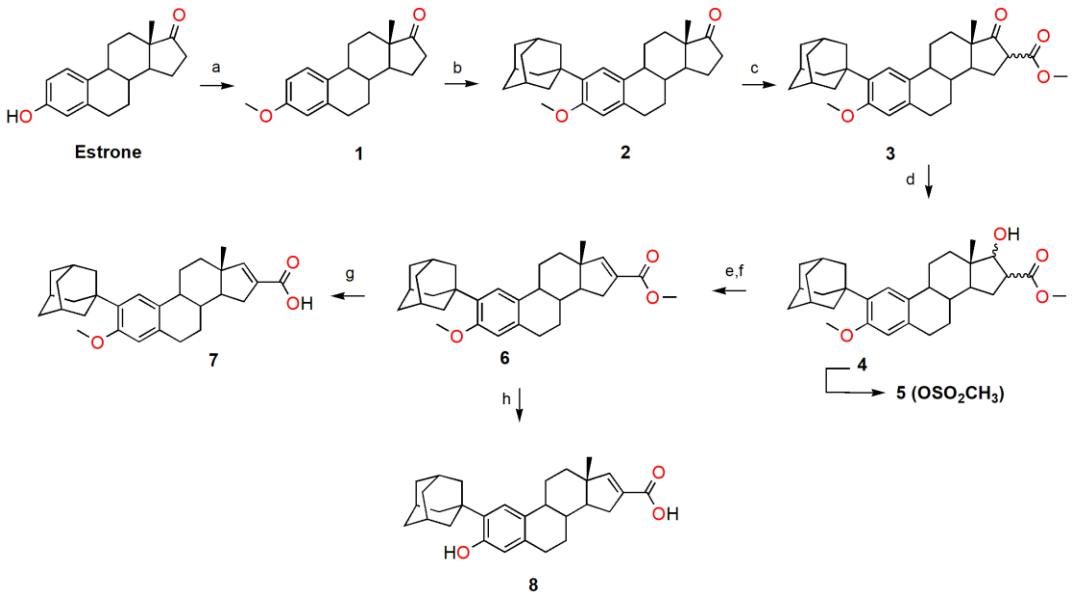

Reagents and conditions: a) CH_3I, $Bu_4N^+I^-$, CH_2Cl_2, NaOH 10%, ref., 3h, 99%; b) 1-adamantanol, BF_3Et_2O, hexane, 4h, 95%; c) $C_3H_6O_3$, NaH, ref., 3h, 93%; d) $NaBH_4$, THF/CH_3OH 9:1, 1h, 90%; e) MsCl, Et_3N, anhydrous CH_2Cl_2; f) DBU, C_6H_6, ref., 6h, 60%; g) NaOH, MeOH, CH_2Cl_2, 96 h, 90%; h) $NaSCH_3$, NMP, ref., 9h, 56%.

In Scheme 2, the route to compound **8** was set up in an attempt to improve the work up of reaction mixtures. Indeed, through the previous Scheme 1, with compounds bearing the 2-adamanthyl substitution the procedure resulted difficult. Thus, the adamanthyl moiety was inserted at the end of the pathway. Henceforward, compound **1** was transformed into the 16-methoxycarbonylated derivative **9**[30] (93%) that was reduced to the 17-hydroxylic derivative **10**[31] (60%). Then, the last was mesylated to compound **11** and this reacting with DBU produced the precursor compound **12**[32] (84%) showing the 16-17 double bond. At this point, the introduction of the adamanthyl group again produced only compound **6** but unfortunately with low yields (12%).[29] Evidently, the presence of the 16-17 double bond provoked the formation of byproducts in the F-C reaction. Following, compound **6** gave the described acid **8** by reacting with $NaSCH_3$ and NMP at reflux.[34] Accordingly, by comparing the two synthetic pathways (scheme 1 and 2), it was concluded that by the pathway in scheme 2 the scope to facilitate the synthetic work was achieved, but despite the laborious work up, the pathway in scheme 1 was undoubtedly the more advantageous because of the higher yields.

Scheme 2. An alternative pathway for the synthesis of compound **8**

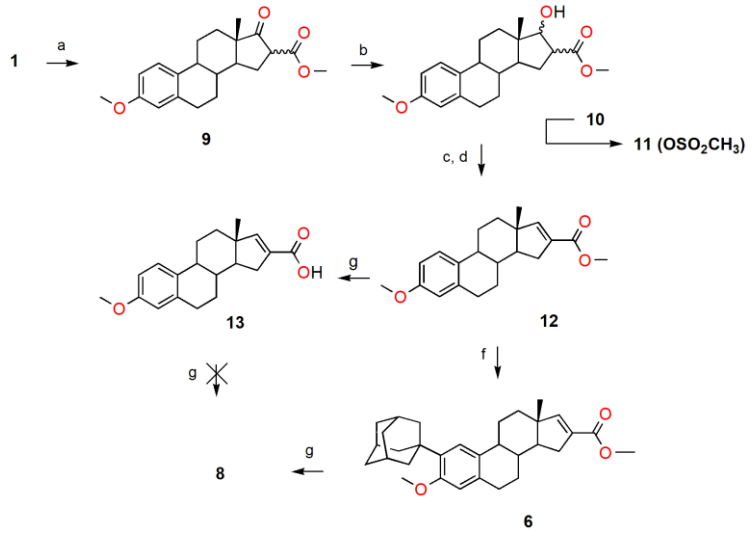

Reagents and conditions: a) $C_3H_6O_3$, NaH, ref., 3h, 95%; b) $NaBH_4$, THF/CH_3OH 9:1, 1h, 60%; c) MsCl, Et_3N, anhydrous CH_2Cl_2, 84%; d) DBU, C_6H_6, ref., 6h, 99%; e) NaOH, MeOH, CH_2Cl_2, 96 h, 90%; f) 1-adamanthanol, BF_3Et_2O, hexane, 4h, 12%; g) $NaSCH_3$, NMP, ref., 5h, 32%.

Next, in view of the synthesis of various 2-substituted analogs of **8**, the synthetic work has proceeded with an assessment of the reactivity of 3-methoxylated estrone **1** towards the Friedel-Crafts (F-C) acylation and the Suzuky-Miyaura (S-M) cross-coupling reaction. For this purpose, following the above useful pathway and carrying out the same kind of reactions as in Scheme 1, Scheme 3 describes the synthesis of 2-benzoyl-compound **14**. The 3-methoxy-estrone **1** was submitted to the F-C reaction with benzoyl chloride in the presence of $AlCl_3$ in CH_2Cl_2 at 0°C for 3 h.[35] In this case, a mixture of three compounds was obtained that were separated by Flash Chromatography. As expected, due to the more electron-rich position 2, the 2-benzoyl-3-methoxy-derivative **14a** was retrieved in greater amount (58%), but also the 4-benzoyl-methoxy isomer **14b** (31%) and in lesser amount the 2-benzoyl-3-hydroxy derivative **14c** (2%) were obtained. The last formed due to the demethylating property of reaction conditions. Compound **14a** was then transformed into the 16-methoxycarbonylated derivative **15** (33%)[30] before being selectively reduced to the 17-hydroxylic_compound **16** by $NaBH_4$ (97%).[31] This compound was first mesylated and thereafter by treatment with DBU, compound **18** (17-H)[32] showing the 16-17 double bond, was obtained (21%). Finally, compound **18** was reacted with $NaSCH_3$ in DMF[34] for 1 h when at this time the starting compound disappeared on monitoring the reaction progress by TLC. After work-up of the reaction mixture, the raw material was purified by Flash Chromatography giving three

compounds, identified as **19a**, **b** and **c**. Unfortunately, the desired compound **19a** was present in lesser amount (25%), **19b** (37,5%) and **19c** (37%). The different reactivity of benzoyl compound **18** in comparison with compound **6** (schemes 1 and 2) towards $NaSCH_3$ has not been understood. In this case, the F-C acylation reaction of 3-methoxy-estrone, as for some reported alkylation[35] other than with adamanthanol, was proved not to be a regiospecific reaction. Therefore, it is possible to conclude that the lack of region specificity of F-C acylation towards position 2 together with the low yields of compound **19a** might represent a drawback for the future synthesis of novel 2-substituted analogs.

Scheme 3. Synthesis of compound **19a**

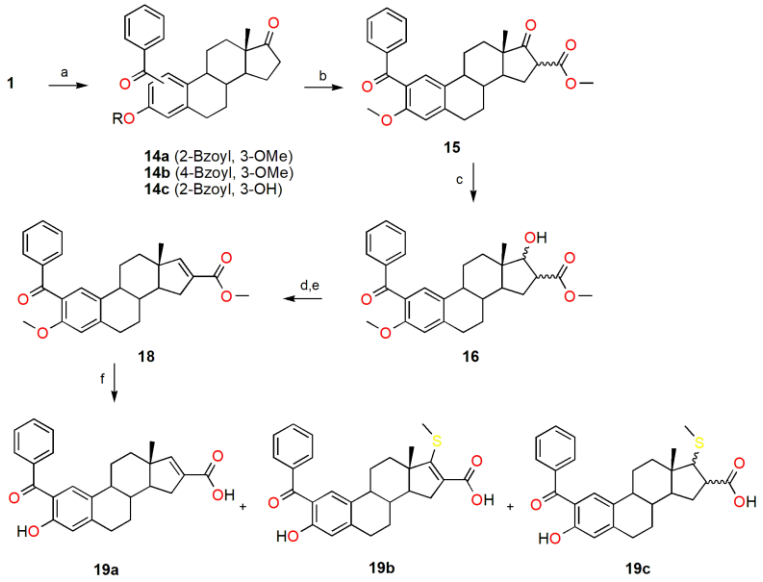

Reagents and conditions: a) benzoyl chloride, $AlCl_3$, anhydrous DCM, 3h, 91%; b) $C_3H_6O_3$, NaH, rif., 3h, 31%; c) $NaBH_4$, THF/CH_3OH 9:1, 0.5 h, 94%; d) MsCl, Et_3N, anhydrous CH_2Cl_2; e) DBU, C_6H_6, rif., 5h, 21%; f) $NaSCH_3$, DMF, 1h., 63%.

It is known that the Suzuki-Miyaura cross-coupling reaction[36] is a robust method to obtain a variety of aromatic derivatives because of the large amount of commercially available boronic acids, therefore it was planned to study also the possibility to obtain novel 2-substituted analogs by this kind of cross-coupling. In scheme 4, the synthesis of three novel 2-substituted compounds by this method is reported.

Preliminary results suggested an optimal pathway where the starting estrone was protected as benzyl ether, easily removable later in the path, giving compound **20** (BzCl, Bu_4NI) (99%)[28] that was then transformed into the 16-methoxycarbonylated derivative **21**, as before (81%).[30] This was first selectively reduced with $NaBH_4$ to the

corresponding alcohol **22** (68%).[31] After mesylation of 17-hydroxy (**23**) and the next treatment with DBU, compound **24** was obtained (54%). In previous experiments it was seen that as for 3-methoxy compound **12**, also the 2-benzyloxy derivative **24** resulted not to be a suitable intermediate for iodination step. Thus, compound **22** was catalytically reduced (Pd/C 10%, H_2)[37] producing the 2,17-dihydroxylic derivative **25** (93%) that was submitted to the successful iodination to compound **26** with NIS, $(CF_3SO_3)_3In$ in CH_3CN for 8h.[38] Bromination had previously been carried out on 3-methoxy-estrone **1** (scheme 1) but it was slightly region-selective (data not shown) and mainly with the 2-Br-derivatives the cross-coupling did not take place later in the synthesis. The iodination of compound **25** with NIS yielded the desired 2-iodinated product **26** (51%) and a little amount of 4-iodinated and 2,4-diiodinated as deduced from ^1H NMR spectrum of the reaction mixture. Therefore, iodinating with NIS and $(CF_3SO_3)_3In$ proved to be more region-selective compared with the other methods carried out (data not shown). It is worth to underline that the chromatographic purification of **26** in presence of other two iodinated compounds was only feasible when the two phenolic and alcoholic hydroxyls were free. Unfortunately, for compound **26** 16-17 double bond formation was no longer possible. Preliminarily, the S-M cross-coupling reaction of compound **26** was accomplished with three boronic acids of different hindrance and following two different methods: conventional synthesis[38] and MW added organic synthesis.[39] The first one provided only complex mixtures, while the second one was found to be successful due to the following advantages: shorter reaction times, higher yields, less by-products and thus easier to process mixtures. After flash chromatography purification, compounds **27-29** were obtained in good yields 26%, 33%, 42%, respectively.

Finally, the three methyl esters **27-29** were transformed into the corresponding acids by treatment with MeOH-NaOH 10% giving the compounds **30** (99%), **31** (98%) and **32** (97%).[40] For all the synthesized compounds, complete characterization was carried out by mono-dimensional ^1H- ^{13}C- and bi-dimensional HSQC, HMBC and COSY NMR experiments.

Scheme 4. Synthesis of compounds **30-32**

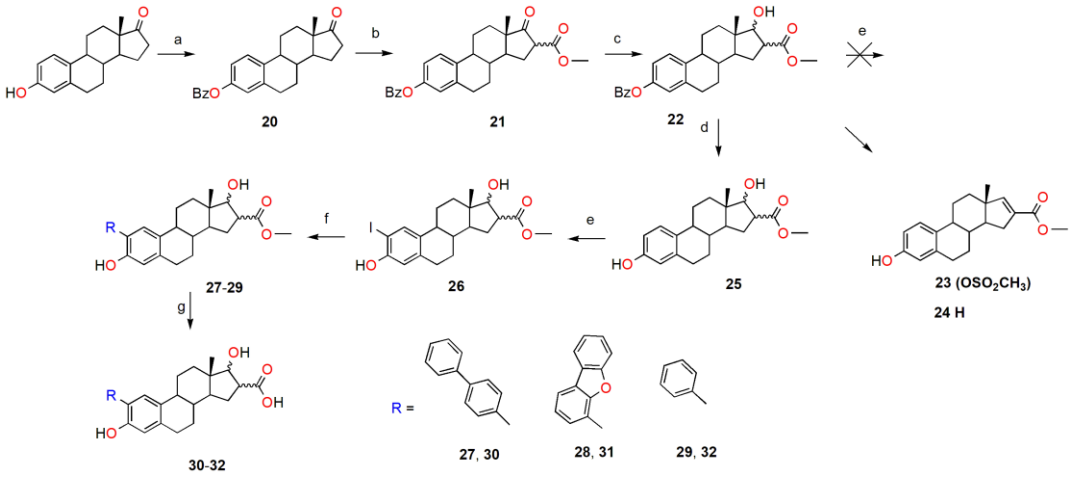

Reagents and conditions: a) BzCl, $Bu_4N^+I^-$, CH_2Cl_2, NaOH 10%, rif., 3h, 99%; b) $C_3H_6O_3$, NaH, rif., 3h, 31%; c) $NaBH_4$, THF/CH_3OH 9:1, 1h, 68%; d) Pd/C, H_2, EtOAc, r.t., 8h, 93%; e) NIS, $(CF_3SO_3)_3In$, CH_3CN, 8h, 51%; f) 1. $C_{12}H_{11}BO_2$, $Pd(PPh_3)_4$, K_2CO_3, $C_4H_8O_2$, MW (160° C), 30 min, 33%; 2. $Pd(PPh_3)_4$, K_2CO_3, $C_4H_8O_2$, MW (160° C), 30 min, 42%; 3. $C_6H_7BO_2$, $Pd(PPh_3)_4$, K_2CO_3, $C_4H_8O_2$, MW (160° C), 30 min, 26%; g) MeOH, NaOH 10%, rif, 1h, 99%.

Furthermore, it is noted that the synthesis described in Scheme 4, despite the successful S-M cross-coupling on the iodinated **26**, presents a strong restriction due to the impracticality to obtain the designed compounds with 16-17 double bond. Indeed, iodination reaction with NIS did not work with compounds **12** and **24** and additionally the chromatographic purification of the 2-iodinated derivative was achievable only with the di-hydroxylic compound **26** that however was not suitable for the removal of 17-alcoholic OH by the method reported before.

Table 2. Structure of compounds tested for cytotoxic and estrogenic activity

Compound	Structure	Compound	Structure
7	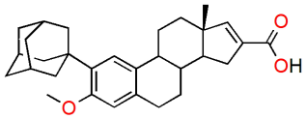	**8**	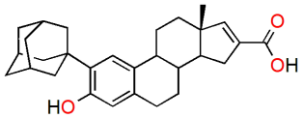

19a	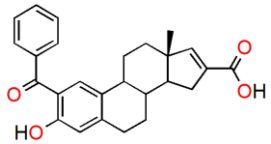	**30**	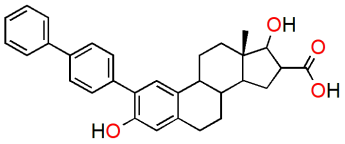
31	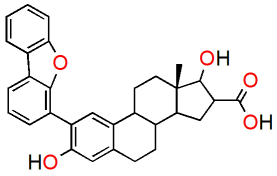	**32**	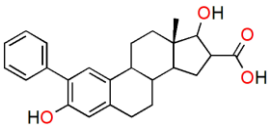

Biology

Effect of compounds 7, 8, 19a, 30-32 on cell viability.

In order to verify whether the synthetic RORγt inverse agonists had any effect on cell growth and survival, MTT assay was performed on HepG2 cells. As shown in Figure 6, compound **19a** was found to be toxic at the highest concentrations tested (25 μM, $p<0.01$ *vs* vehicle; 50 μM, $p<0.001$ *vs* vehicle), whereas compounds **30** and **32** caused a significant decrease of cell viability even at lower concentrations. No cytotoxic effects were observed on after incubation of HepG2 cells with compounds **7**, **8** and **31**.

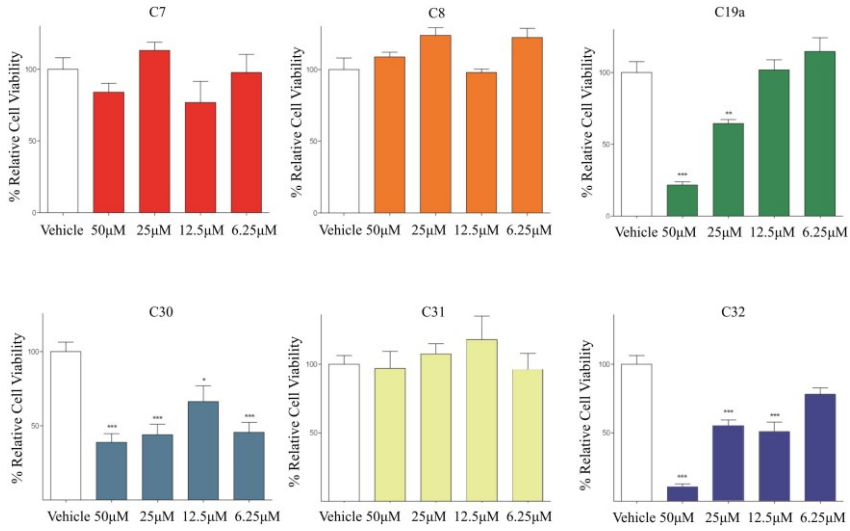

Figure 6. Cell viability assay on HepG2 cells treated with the synthetic compounds **7, 8, 19a** and **30-32**, reported as percentage of viable cells with respect to control treated with medium. Results are mean ± SEM. * $p<0.05$, ** $p<0.01$ and *** $p<0.001$ vs vehicle, one-way ANOVA followed by Dunnett post hoc test. Three independent experiments were performed in quadruplicate.

Estrogenic activity of the synthetic compounds 7, 8, 19a and 30-32.

Estrogenic activity of the novel steroidal compounds **7**, **8**, **19a** and **30-32** was evaluated because of the molecular structure being derived from estrone, a known estrogenic agent. Real time PCR analysis was performed on RNA extracts from an estrogen-receptors (ERs) expressing cell line (MCF-7). Cells were treated with the compounds in order to test whether the expression of GREB1 and CXCL12, two target genes for ERs, was altered. Figure 7 shows that the expression of both GREB1 and CXCL12 was increased by compound **8** ($p<0.05$ and $p<0.001$ for GREB and CXCL12 mRNA expression *vs* vehicle, respectively), **30** ($p<0.001$ for GREB and CXCL12 mRNA expression *vs* vehicle), **31** ($p<0.001$ for GREB and CXCL12 mRNA expression *vs* vehicle) and **32** ($p<0.001$ and $p<0.05$ for GREB and CXCL12 mRNA expression *vs* vehicle, respectively), while neither compound **7** nor **19a** display any estrogenic activity.

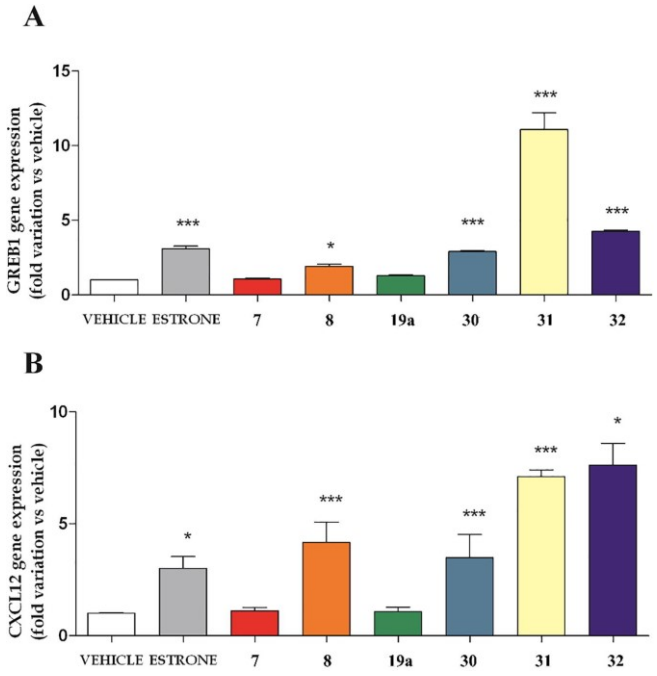

Figure 7. Gene expression of GREB1 (A) and CXCL12 (B) in MCF-7 cells treated with the synthetic compounds **7, 8, 19a** and **30-32**. All the compounds were tested at 2 μM concentration. Results are mean ± SEM. * $p<0.05$ and *** $p<0.001$ vs vehicle, one-way ANOVA followed by Dunnett post hoc test. Three independent experiments were performed in triplicate.

Evaluation of inverse-agonist activity of compounds 7, 8, 19a and 31 on RORγt

Based on the MTT assay results, where compounds **7**, **8** and **31** did not display any cytotoxic activity, and compound **19a** was cytotoxic only at the highest concentrations

(25-50 μM), compounds **7**, **8**, **19a** and **31** were selected for evaluating their ability to modulate the *in vitro* RORγt activity in a cellular environment by means of a Gal UAS-Luc co-transfection system taken ursolic acid as reference compound. Since the absence of *in vitro* cytotoxicity at low concentrations is a promising feature for candidate drugs designed for lifetime lasting diseases such as autoimmune diseases, no further *in vitro* characterization of **30** and **32** was performed. To ascertain whether HEK-293 cells had been successfully transfected with the plasmids, RORγt protein expression was evaluated by means of Western Blot analysis. As shown in Figure 8, the cells transfected with all three plasmids (RORγ-Gal4, UAS-Luc, NanoGlo) express RORγt, whereas the cells transfected with the plasmids UAS-Luc and NanoGlo do not express the protein containing the RORγt LBD. Densitometric analysis confirmed that RORγt is not expressed in lanes 2 and 3 (Data not shown).

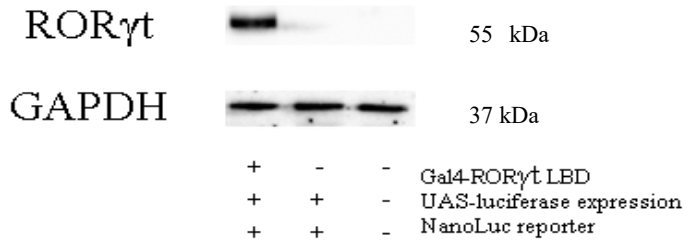

Figure 8. Western blot analysis of RORγt (58 kDa) protein in whole protein extracts of HEK-293 cells transfected with Gal4-RORγ LBD plasmid, UAS-luc and NanoLuc reporter plasmid (+) or not-transfected cells (-). GAPDH (43 KDa) was used as loading control.

Figure 9 shows the ability of the tested compounds to decrease activity, as luminescence lessening, at various concentrations. After 2 μM treatment only compound **19a** displayed a slight but significant activity, at 5 μM both compounds **8** and **19a** decreased activity in a significant amount, at 10 μM a dramatic decrease in RORγ activity could be observed after addition for all the tested compounds ($p<0.001$), and finally, at 20 μM all compounds showed an inhibitory effect comparable to that of ursolic acid. Fig. 9 shows that compounds **7**, **8**, **19a** and **31** displayed a concentration-dependent activity. Extrapolated IC_{50} values were similar for compounds **19a** and **31** (4,4 μM and 4,7 μM, respectively), and increased for compounds **7** and **8** (6,8 and 6,5 μM, respectively). The most relevant outcome of the *in vitro* RORγt inhibitory activity by the selected

compounds was that compound **19a** significantly reduced RORγt activity at low concentrations (2-5 μM, $p<0.05$ *vs* vehicle).

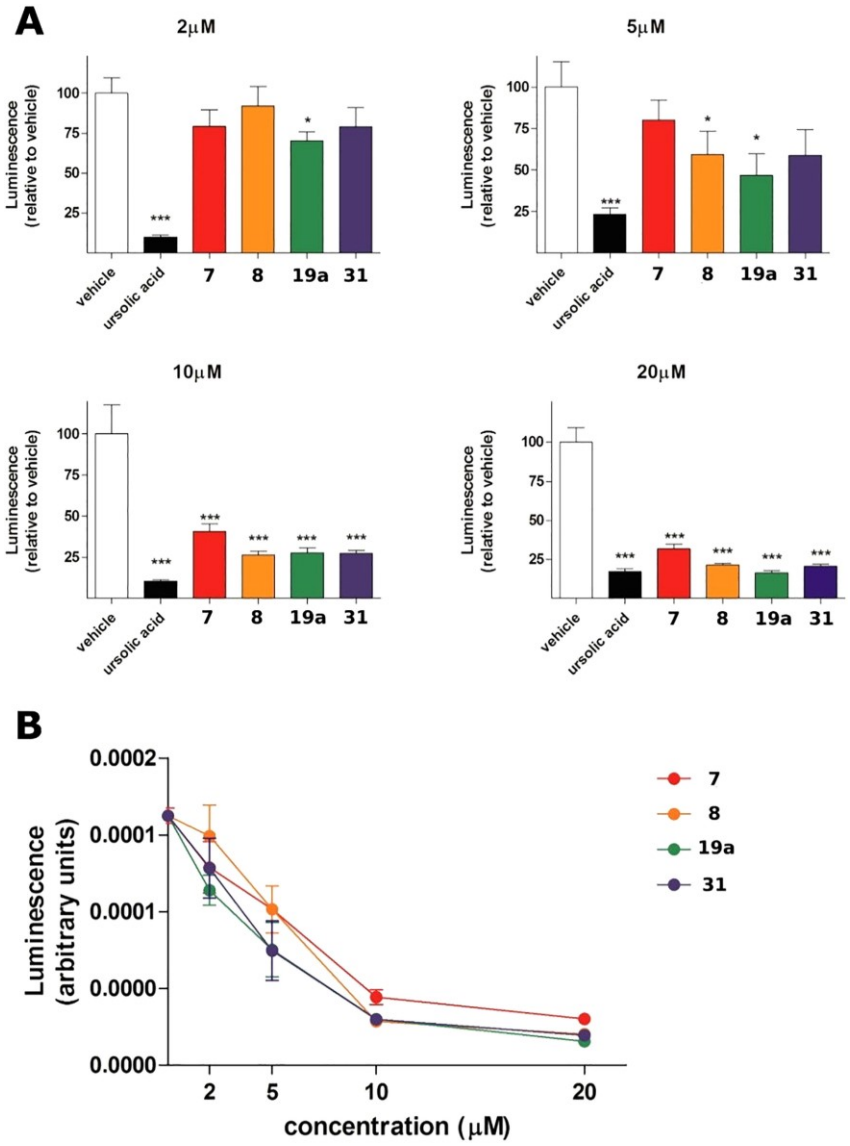

Figure 9. Evaluation of inverse-agonist activity of compounds **7, 8, 19a** and **31** on RORγt (A) and dose-dependent efficacy (B). Results are mean Â± SEM. * $p<0.05$ and *** $p<0.001$ vs vehicle, one-way ANOVA followed by Dunnett post hoc test. Three independent experiments were performed in triplicate.

Effect of compounds 7, 8, 19a and 31 on cell cycle distribution

In order to complete the characterization of the selected synthetic compounds, we analysed their effect on cell cycle distribution both in HepG2 and HEK-293 cells. Fig. 10 shows the effect of compounds **7**, **8**, **19a** and **31** on both cell viability of HepG2 and HEK-293 either transfected or not with RORγt- Gal4 plasmid, and cell cycle distribution. After confirming the absence of cytotoxicity of the selected synthetic compounds on both

cell lines, we also demonstrated that cell cycle distribution was not affected even after incubation with the highest concentrations (10 and 20 μM) tested previously.

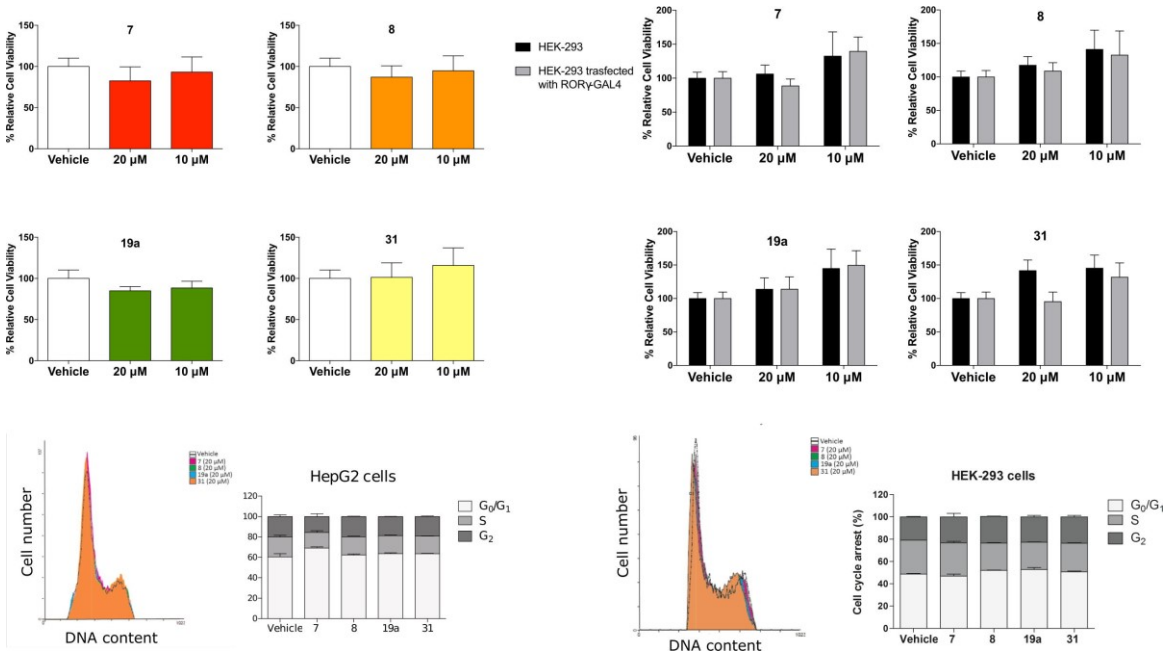

Fig. 10. Cell viability of HepG2 (left) and HEK-293 (right) cells after incubation with compounds **7**, **8**, **19a** and **31** at 10 and 20 μM. Below, cell cycle distribution analysis at 20 μM. The results are expressed as mean ± SEM. Three independent experiments were performed in duplicate.

Docking study of compound 19a

Compound **19a** was docked using the crystal structure of RORγt in complex with digoxin (PDB code 3B0W).[27] Computer docking simulation of **19a** was performed using Maestro 10.5 Glide software SP precision. The most favoured pose of **19a** (Figure 11) in the presumptive binding site is similar to the one found for **8** (Figure 5). Compound **19a** could be readily accommodated in the pocket, but also in this case, no significant interactions with residues responsible for digoxin binding were found.[15] Again, we can suggest the possibility that the substituent in position 2 (benzoyl group in this case), could perturb the interactions necessary for RORγt activity.[15,17]

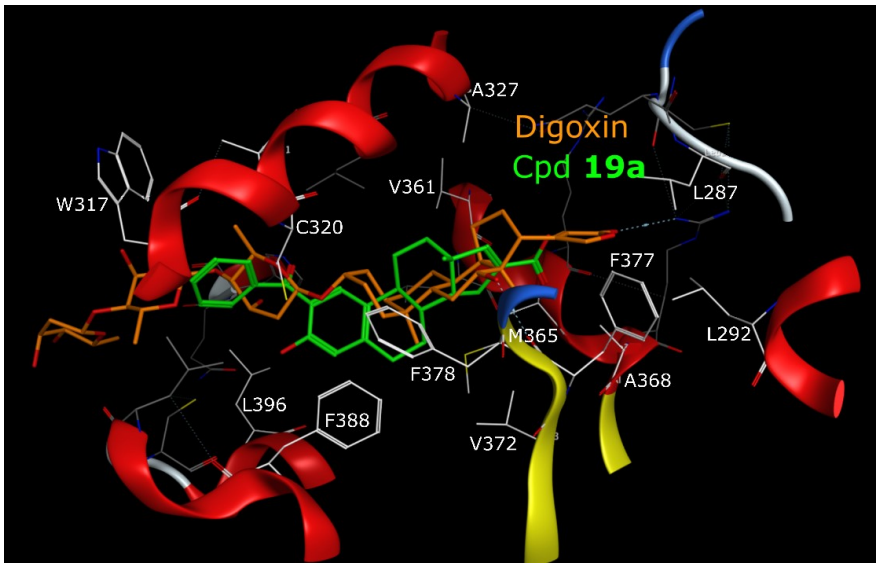

Figure 11. Comparison of the crystallographic structure of digoxin (in orange) in complex with RORγt ligand binding domain (Protein Data Bank code 3B0W) and the energetically most favourable pose of **19a** (in green) obtained by molecular docking simulation. Hydrophobic residues are shown in white. Hydrogen atoms are omitted.

Conclusion

Looking the NRs natural ligands structure through, representative arotinoids ligands and RORs ligands, by means of a structure-based approach founded on hybridization of chemical structures, a lead compound **8** (MG 2778) was identified, synthesized and chemically modified in order to obtain a small series of novel steroidal compounds acting as RORγ inverse agonists. Docking simulations of compounds **8** and 1**9a** into RORγt LBD in complex with digoxin showed a potential binding affinity.

The four non-cytotoxic compounds **7**, **8**, **19a** and **31** were tested by means of a Gal UAS-Luc co-transfection system taken ursolic acid as reference compound, resulting to act as RORγt inverse agonists in a dose dependent manner. Considering these preliminary biological results, we can propose that using the tetracyclic scaffold is an appropriate approach for the further design of RORγt inverse agonists. Regarding the bound groups at 2, 3 and 16 positions, we can deduce that a bulky alkyl or aryl group in the 2 position is necessary in order to reduce estrogenic activity, although low estrogenic activity is maintained in presence of the free 3-phenolic OH as for compound **8** with respect to compound **7** (3-OCH_3). However, no estrogenic activity was observed for compound **19a**

having the free 3-OH. In this case, we suggest the existence of a H-bond, between the carbonyl of the flexible benzoyl group and the phenolic OH. Probably, this event could hamper the interaction of the OH itself at the ER, however, at the docking simulation of **19a** in RORγt LBD (Figure 10) we did not see it. The polar terminus (16-COOH) is essential for activity while the 16-17 double bond not as noted for compound **31** that was active as well as compounds showing the double bond at that position. The potency of our compounds is lower than that of ursolic acid, the strongest known RORγt inverse agonist, but their efficacy is similar. In particular, compound **19a** was the most active, causing a significant reduction of RORγt activity at low micromolar concentrations. From the above considerations, we can conclude that **19a** may represent a suitable candidate for further *in vitro* and *in vivo* characterization and may serve as a useful tool for developing RORγt inverse agonists.

Experimental section

Melting points were determined on a Buchi M-560 capillary melting point apparatus and are uncorrected. ^{1}H NMR spectra were determined on Bruker 300 and 400 MHz spectrometers, with the solvents indicated; chemical shifts are reported in δ (ppm) downfield from tetramethylsilane as internal reference. Coupling constants are given in hertz. In the case of multiplets, chemical shifts were measured starting from the approximate centre. Integrals were satisfactorily in line with those expected based on compound structure. Mass spectra were obtained on a Mat 112 Varian Mat Bremen (70 eV) mass spectrometer and Applied Biosystems Mariner System 5220 LC/MS (nozzle potential 140 eV). Column flash chromatography was performed on Merck silica gel (250−400 mesh ASTM); chemical reactions were monitored by analytical thin-layer chromatography (TLC) on Merck silica gel 60 F-254 glass plates. Microwave assisted reactions were performed on a CEM Discover® monomode reactor with a built-in infrared sensor assisted-temperature monitoring and automatic power control; all reactions were performed in closed devices under pressure control. Solutions were concentrated on a rotary evaporator under reduced pressure. The purity of new tested compounds was checked by HPLC using the instrument HPLC VARIAN ProStar model 210, with detector DAD VARIAN ProStar 335. The analysis was performed with a flow of 1 mL/min, a C-8 column of dimensions 250 mm X 4.6 mm, a particle size of 5 mm,

and a loop of 10 mL. The detector was set at 254 nm. The mobile phase consisted of phase A (Milli-Q H_2O, 18.0 MU, TFA 0.05%) and phase B (95% MeCN, 5% phase A). Gradient elution was performed as reported: 0 min, % B = 10; 0-20 min, % B = 90; 25 min, % B = 90; 26 min, % B = 10; 31 min, % B = 10.

Starting materials were purchased from Sigma-Aldrich and Alfa Aesar, and solvents were from Carlo Erba, Fluka and Lab-Scan. DMSO was obtained anhydrous by distillation under vacuum and stored on molecular sieves.

Dulbecco's modified Eagle's medium (DMEM), was obtained from Sigma-Aldrich Italy (Milan, Italy). Dulbecco's modified Eagle's medium (DMEM), was obtained from Sigma-Aldrich Italy (Milan, Italy). Foetal bovine serum (FBS), glutamine and penicillin-streptomycin (pen-strep) solutions were obtained from Gibco (Life Technologies Italia, Monza, Italy).

Chemical Synthesis

*General procedure for the synthesis of of-protected estrone derivatives **1** and **20**.* As a typical procedure, the synthesis of the-3-methoxy-estrone derivative is described in detail. A mixture of commercial estrone (1.00 g, 3.70 mmol) and tetrabutylammonium iodide (0.068 g, 0.185 mmol) was suspended in CH_2Cl_2 (18 mL). Methyl iodide (0.875 mL, 14.06 mmol) and a 10% NaOH solution (18 mL) were added. The mixture was refluxed at 70°C for 3 h. The reaction was monitored by TLC analysis (eluent chloroform/methanol 95:5). At the end of the reaction, the two phases were clearly transparent and were separated. The aqueous phase was extracted with CH_2Cl_2 (30 mLx3) and the combined organic phases were washed with brine, dried over sodium sulphate, filtered and evaporated under vacuum to give a white solid product (1.045 g).

(8R,9S,13S,14S)-7,8,9,11,12,13,15,16-octahydro-3-methoxy-13-methyl-6-H-cyclopenta[a]phenanthren-17(14H)-one (**1**).

Yield 99%; R_f = 0.88 (chloroform/methanol, 95:5); mp = 177-178°C; ^{1}H NMR (300 MHz, $CDCl_3$): δ 0.84 (s, 3H), 1.49 (m, 1H), 1.50 (m, 1H), 1.52 (m, 1H), 1.53 (m, 1H), 1.61 (m, 1H), 1.65 (m, 1H), 1.97 (m, 1H), 2.05 (m, 1H), 2.09 (m, 1H), 2.27 (m, 1H), 2.42 (m, 1H), 2.51 (m, 1H), 2.53 (m, 1H), 2.93 (m, 2H), 3.80 (s, 3H), 6.67 (d, *J* = 2.73 Hz, 1H), 6.75 (dd, *J* = 8.61 Hz, *J* = 2.73 Hz, 1H), 7.23 ppm (d, *J* = 8.61 Hz, 1H); ^{13}C NMR (75 MHz, $CDCl_3$): δ 13.86, 21.60, 25.94, 26.57, 29.68, 31.60, 35.88, 38.39, 43.99, 48.03, 50.43, 55.22, 111.59, 113.89, 126.35, 132.03, 137.77, 157.91, 220.94 ppm. HRMS (ESI-MS, 140 eV): m/z [M + H^+] calculated for $C_{19}H_{25}O_2^+$, 285.1855; found, 285.1865.

(8R,9S,13S,14S)-3-(benzyloxy)-7,8,9,11,12,13,15,16-octahydro-13-methyl-6H-cyclopenta[a]phenanthren-17(14H)-one (**20**).

Compound **20** was prepared as for compound **1** by reacting estrone (2.50 g, 9.25 mmol), tetrabutylammonium iodide (0.178 g, 0.462 mmol), benzyl bromide (4.18 mL, 35.14 mmol) in a mixture of CH_2Cl_2 /10% NaOH solution (45 mL each). After the workup, the obtained residue was washed with hexane to remove excess benzyl bromide yielding 3.301 g of yellow solid. Yield 99%; R_f =0.38 (n-hexane/ethyl acetate, 8:2); mp = 128-129°C; ^{1}H NMR (400 MHz, $CDCl_3$): 0.91 ppm (s, 3H), 1.50 (m, 1H), 1.52 (m, 1H), 1.53 (m, 1H), 1.56 (m, 1H), 1.62 (m, 1H), 1.65 (m, 1H), 1.99 (m, 1H), δ 2.04 (m, 1H), 2.09 (m, 1H), 2.17 (m, 1H), 2.29 (m, 1H), 2.43 (m, 1H), 2.51 (m, 1H), 2.88 (m, 2H), 5.04 (s, 2H), 6.73 (d, *J* = 2.7 Hz, 1H), 6.79 (dd, *J* = 8.6, 2.8 Hz, 1H), 7.20 (d, *J* = 8.4 Hz, 1H), 7.34 – 7.29 (m, 1H), 7.40 – 7.35 (m, 2H), 7.45 – 7.41 ppm (m, 2H); ^{13}C NMR (101 MHz, $CDCl_3$): δ 13.89, 21.62, 25.95, 26.58, 29.69, 31.63, 35.90, 38.40, 44.04, 48.04, 50.47, 70.00, 112.42, 114.94, 126.37, 127.45, 127.88, 128.57, 132.36, 137.29, 137.82, 156.90, 220.94 ppm. HRMS (ESI-MS, 140 eV): m/z [M + H^+] calculated for $C_{25}H_{29}O_2^+$, 361.2168; found, 361.2149.

(8R,9S,13S,14S)-7,8,9,11,12,13,15,16-octahydro-2-adamantyl-3-methoxy-13-methyl-6H-cyclopenta[a]phenanthrene-17(14H)-one (**2**).

Into a two-necked 100 mL round-bottomed flask, compound **1** (1.08 g, 3.80 mmol) and 1-adamantanol (0.70 g, 4.60 mmol) were placed and stirred for 15 min in hexane at 0°C. Under N_2 atmosphere, BF_3 Et_2O (1.6 mL, 12.74 mmol) was added dropwise with a syringe. The mixture was stirred at room temperature for 4 h. The reaction was monitored by TLC analysis (eluent cyclohexane/ethyl acetate, 8:2). At the end of the reaction, the mixture was transferred to a single-necked round-bottomed flask and the solvent was removed under vacuum. The obtained residue was treated with water to obtain a yellowish solid. The solid was filtrated and dried overnight under vacuum to yield 1.55 g of yellow powder. Yield 95%; R_f = 0.50 (cyclohexane/ethyl acetate, 8:2); mp = 253°C; ^{1}H NMR (400 MHz, $CDCl_3$): δ 0.93 (s, 3H), 1.47 (m, 1H), 1.53 (m, 1H), 1.54 (m, 1H), 1.56 (m, 1H), 1.64 (m, 1H), 1.65 (m, 1H), 1.76 (6H), 1.97 (m, 1H), 2.01 (m, 1H), 2.06 (m, 1H), 2.11 (3H), 2.20-2.08 (6H), 2.30 (m, 1H), 2.47 (m, 1H), 2.53 (m, 2H), 2.92 (m, 2H), 3.83 (s, 3H), 6.63 (s, 1H), 7.18 ppm (s, 1H); ^{13}C NMR (101 MHz, $CDCl_3$): δ 13.90, 21.61, 26.04, 26.63, 29.17, 29.30, 31.60, 35.92, 36.94, 37.16, 38.55, 40.79, 44.36, 48.08, 50.42, 55.03, 112.09, 123.68, 131.03, 134.72, 136.07, 156.87, 221.12 ppm. HRMS (ESI-MS, 140 eV): m/z [M + H^+] calculated for $C_{29}H_{39}O_2^+$, 419.2950; found, 419.2932.

(8R,9S,13S,14S)-7,8,9,11,12,13,15,16-octahydro-2-benzoyl-3-methoxy-13-methyl-6H-cyclopenta[a]phenanthrene-17(14H)-one (**14**).

In a dried round-bottomed flask, a suspension of anhydrous $AlCl_3$ (1.260 g, 9.453 mmol) in 15 mL of anhydrous CH_2Cl_2 was prepared. The mixture was cooled to 0°C and benzoyl chloride (0.880 mL, 7.574 mmol) was added dropwise. The mixture turned pink and was stirred for 1 h at room temperature. After this period, the mixture was cooled again at 0°C and then a solution of compound **1** (1.077 g, 3.787 mmol) in anhydrous CH_2Cl_2 (10 mL) was added dropwise. The reaction mixture turned yellow immediately and it was kept at 0°C for all the duration. The progression of the reaction was monitored by TLC analysis (hexane/ethyl acetate 6:4). At the end of the reaction, the suspension was poured into an ice/water mixture and it was acidified with concentrated HCl. The two phases were separated: the aqueous phase was extracted with CH_2Cl_2 and the resulting organic phase was washed with saturated sodium bicarbonate solution, brine and dried over sodium sulphate. The mixture was filtered, and the solvent evaporated under vacuum to yield 1.344 g of white solid. Yield 58% **14a**, 31% **14b**, 2%; **14c**; R_f = 0.49 (hexane/ethyl acetate, 6:4); mp = 229°C; ^{1}H NMR (300 MHz, $CDCl_3$): δ 0.91 (s, 3H), 1.45 (m, 1H), 1.49 (m, 1H), 1.50 (m, 1H), 1.55 (m, 1H), 1.59 (m, 1H), 1.60 (m, 1H), 1.92 (m, 1H), 2.05 (m, 1H), 2.05 (m, 1H), 2.06 (m, 1H), 2.25 (m, 1H), 2.32 (m, 1H), 2.51 (m, 1H), 2.97 (m, 2H), 3.68 (s, 3H), 6.70 (s,1H), 7.30 (s, 1H), 7.39-7.46 (m, 2H); 7.50-7.57 (m, 1H), 7.81 ppm (dd, *J* = 8.3, 1.3 Hz, 2H); ^{13}C NMR (400 MHz, $CDCl_3$): δ 13.83, 21.56, 25.77, 26.40, 29.94, 31.45, 35.81, 38.26, 43.80, 47.94, 50.35, 55.64, 111.79, 126.47, 127.07, 128.08, 129.77, 131.98, 132.64, 138.20, 140.97, 155.54, 196.47, 220.60 ppm. HRMS (ESI-MS, 140 eV): m/z [M + H^+] calculated for $C_{26}H_{29}O_3^+$, 389.2117; found, 389.2212.

General procedure for the synthesis of derivatives (**3**, **9**, **15**, **21**). As a typical procedure, the synthesis of the methyl 2-adamantyl-3-methoxy-16-carboxylate estrone derivative **3** is described in detail. Compound **2** (0.640 g, 1.53 mmol) was suspended in dimethyl carbonate (11.2 mL, 132.91 mmol) and NaH (0.320 g, 13.33 mmol) was added. A catalytic amount of CH_3OH was added. The mixture was refluxed for 3h at controlled temperature (85°C). The reaction was monitored by TLC analysis (eluent cyclohexane/ethyl acetate, 8:2). At the end of the reaction, the mixture was cooled at room temperature and quenched with CH_3OH (1 mL). The mixture was acidified with glacial acetic acid and poured into water (150-200 mL). The suspension was stirred and once the precipitate was formed, filtrated to obtain a yellow precipitate that was dried overnight under vacuum to yield 0.511 g of yellow powder.

(8R,9S,13S,14S)-methyl-7,8,9,11,12,13,14,15,16,17-decahydro-2-adamantyl-3-methoxy-13-methyl-17-oxo-6H-cyclopenta[a]phenanthrene-16-carboxylate (**3**).

Yield 93%; R_f = 0.30 (cyclohexane/ethyl acetate, 8:2); mp = 180-181°C; ^{1}H NMR (300 MHz, $CDCl_3$): δ 0.98 (s, 3H), 1.37 (m, 1H), 1.51 (m, 1H), 1.52 (m, 1H), 1.57 (m, 1H), 1.63 (m, 1H), 1.65 (m, 1H), 1.76 (6H), 1.85 (m, 1H), 1.99 (m, 1H), 2.03 (m, 1H), 2.11 (3H), 2.20-2.08 (6H), 2.29 (m, 1H), 2.44 (m, 1H), 2.88 (m, 2H), 3.21 (dd, *J* = 9.9, 8.5 Hz, 1H), 3.76-3.79 (s, 3H), 3.80 (s, 3H), 6.61 (s, 1H), 7.14 ppm (s, 1H); ^{13}C NMR (75 MHz, $CDCl_3$): δ 13.31, 25.90, 26.40, 29.17, 29.30, 32.50, 36.90, 36.94, 37.16, 38.40, 40.79, 44.80, 47.87, 50.42, 52.50, 54.10, 55.03, 112.09, 124.20, 131.03, 134.72, 136.07, 156.87, 169.87, 212.05 ppm. HRMS (ESI-MS, 140 eV): m/z [M + H^+] calculated for $C_{31}H_{41}O_4^+$, 477.3005; found, 477.3015.

(8R,9S,13S,14S)-methyl7,8,9,11,12,13,14,15,16,17-decahydro-3-methoxy-13-methyl-17-oxo-6H-cyclopenta[a]phenanthrene-16-carboxylate (**9**).

Compound **9** was prepared as for compound **3** by reacting compound **1** (1.045 g; 3.674 mmol) with dimethyl carbonate (26.9 mL, 319 mmol) and NaH (0.768 g, 32.01 mmol). Yield 93%; R_f = 0.33 (hexane/ethyl acetate, 8:2); ^{1}H-NMR (300 MHz, $CDCl_3$): δ 0.98 (s, 3H), 1.37 (m, 1H), 1.51 (m, 1H), 1.52 (m, 1H), 1.57 (m, 1H), 1.63 (m, 1H), 1.65 (m, 1H), 1.85 (m, 1H), 1.99 (m, 1H), 2.03 (m, 1H), 2.29 (m, 1H), 2.44 (m, 1H), 2.88 (m, 2H), 3.21 (dd, *J* = 9.9, 8.5 Hz, 1H), 3.76-3.79 (s, 3H), 3.80 (s, 3H), 6.67 (d, *J* = 2.73 Hz, 1H), 6.75 (dd, *J* = 8.61 Hz, 2.73 Hz, 1H), 7.23 ppm (d, *J* = 8.61 Hz, 1H).

(8R,9S,13S,14S)-methyl-7,8,9,11,12,13,14,15,16,17-decahydro-2-benzoyl-3-methoxy-13-methyl-17-oxo-6H-cyclopenta[a]phenanthrene-16-carboxylate (**15**).

Compound **15** was prepared as for compound **3** by reacting compound **14** (1.259 g; 3.241 mmol) with dimethyl carbonate (23.7 mL, 281.5 mmol) and NaH (0.677 g, 28.23 mmol). An amount of 1.290 g of a crude product was obtained, and this was purified by silica gel flash column chromatography (hexane/ethyl acetate) to give 0.430 g of compound **15**. Yield 33%; R_f = 0.35 (hexane/ethyl acetate, 2:1); mp = 114°C; ^{1}H NMR (400 MHz, $CDCl_3$): δ 0.99-0.96 (m, 3H), 1.40(m, 1H), 1.41 (m, 1H), 1.42 (m, 1H), 1.45 (m, 1H), 1.52 (m, 1H), 1.90 (m, 1H), 2.07 (m, 1H), 2.07 (m, 1H), 2.24 (m, 1H), 2.26 (m, 1H), 2.27 (m, 1H), 2.91 (m, 2H), 3.22 (dd, *J* = 9.9, 8.4 Hz, 1H), 3.68 (s, 3H), 3.77 (s, 3H), 6.70 (s,1H), 7.29 (s, 1H), 7.39-7.46 (m, 2H); 7.50-7.57 (m, 1H), 7.81 ppm (dd, *J* = 8.3, 1.3 Hz, 2H); ^{13}C NMR (101 MHz, $CDCl_3$): δ 13.27/14.34, 25.70, 26.31, 26.39, 30.05, 31.57/31.77, 37.82, 43.78, 47.82, 48.89, 52.61, 54.01, 55.62, 111.75, 126.49, 127.05, 128.09, 129.77, 131.75, 132.69, 138.14, 140.91, 155.54/155.56, 169.80/170.32, 196.48,

211.79 ppm. HRMS (ESI-MS, 140 eV): m/z [M + H^+] calculated for $C_{28}H_{31}O_5^+$, 447.2171; found, 447.2157.

(8R,9S,13S,14S)-methyl-3-(benzyloxy)-7,8,9,11,12,13,14,15,16,17-decahydro-13-methyl-17-oxo-6H-cyclopenta[a]phenanthrene-16-carboxylate (**21**).

Compound **21** was prepared as for compound **3** by reacting compound **20** (3.301 g; 9.157 mmol) with dimethyl carbonate (67.03 mL, 795.46 mmol) and NaH (1.914 g, 79.78 mmol) to yield 3.104 g of yellow powder. Yield 81%; R_f = 0.27 (hexane/ethyl acetate, 8:2); mp = 155°C; ^{1}H NMR (300 MHz, $CDCl_3$): δ 0.98 ppm (s, 3H), 1.45 (m, 1H), 1.46 (m, 1H), 1.48 (m, 1H), 1.51 (m, 1H), 1.62 (m, 1H), 1.63 (m, 1H), 1.98 (m, 1H), 2.03 (m, 1H), 2.07 (m, 1H), 2.25 (m, 1H), 2.40 (m, 1H), 2.89 (m, 2H), 3.21 (dd, *J* = 9.9, 8.5 Hz, 1H), 3.76 (s, 3H), 5.04 (s, 2H), 6.74 (d, *J* = 2.6 Hz, 1H), 6.79 (dd, *J* = 8.6, 2.7 Hz, 1H), 7.20 (d, *J* = 8.5 Hz, 1H), 7.32 (t, *J* = 7.1 Hz, 1H), 7.38 (t, *J* = 7.3 Hz, 2H), 7.43 ppm (d, *J* = 6.9 Hz, 2H); ^{13}C-NMR (75 MHz, $CDCl_3$): δ 13.29, 25.78, 26.54, 29.56, 31.94, 36.90, 37.94, 43.99, 47.95, 48.94, 52.57,54.07, 69.97, 112.47, 114.92, 126.32, 127.42, 127.87, 128.55, 132.00,137.22, 137.67, 156.94, 169.85, 212.90 ppm. HRMS (ESI-MS, 140 eV): m/z [M + H^+] calculated for $C_{27}H_{31}O_4^+$, 419.2222; found, 419.2237.

General procedure for the synthesis of derivatives (**4**, **10**, **16**, **22**). As a typical procedure, the synthesis of methyl 17-hydroxy-2-adamantyl-3-methoxy-13-methyl-16-carboxylate **4** is described in detail. Compound **3** (1,711g, 3.59 mmol) was suspended in a mixture THF/CH_3OH 9:1 (20 mL). The mixture was cooled and stirred for 15 min at 0°C, then $NaBH_4$ (0.156 g, 4.12 mmol) was added carefully in portions. The temperature was maintained at 0°C and the reaction was monitored by TLC analysis (eluent cyclohexane/ethyl acetate, 2:1). The reaction was completed in 0.5h. The mixture was acidified with HCl 2N solution and extracted with ethyl acetate. The combined organic phases were washed with brine, dried over sodium sulphate, filtered and evaporated to dryness to yield 1.725 g of spongy solid. The crude product was purified by silica gel flash column chromatography (hexane/ethyl acetate) to give 1.53 g of white solid.

(8R,9S,13S,14S)-methyl-7,8,9,11,12,13,14,15,16,17-decahydro-17-hydroxy-2-adamantyl-3-methoxy-13-methyl-6H-cyclopenta[a]phenanthrene-16-carboxylate (**4**).

Yield 90%; R_f = 0.57 (hexane/ethyl acetate, 2:1); mp = 210-211°C; ^{1}H NMR (300 MHz, $CDCl_3$): δ 0.83 (s, 3H), 1.18 (m, 1H), 1.32 (m, 1H), 1.35 (m, 1H), 1.45 (m, 1H), 1.55 (m,1H), 1.68 (m, 1H), 1.76 (6H), 1.91 (m, 1H), 1.80 (m, 1H), 2.02 (m, 1H), 2.02 (3H), 2.10 (6H), 2.32 (m, 1H), 2.35 (m, 1H), 2.83 (m, 2H), 3.14 (dd, *J* = 18.7, 9.1 Hz, 1H), 3.72 (s, 3H), 3.80 (s, 3H), 3.89 (d, *J* = 10.0 Hz, 1H), 6.59 (s, 1H), 7.16 ppm (s, 1H); ^{13}C NMR

(300 MHz, $CDCl_3$): δ 11.67, 26.71, 27.25, 27.74, 29.48, 29.71, 37.24, 37.49, 37.62, 38.72, 41.11, 44.44, 44.57, 44.69, 48.96, 52.04, 55.10, 82.16, 112.39, 124.03, 131.70, 135.07, 136.25, 156.87, 175.94 ppm. HRMS (ESI-MS, 140 eV): m/z [M + H^+] calculated for $C_{31}H_{43}O_4^+$, 479.3161; found, 479.3149.

(8R,9S,13S,14S)-methyl-7,8,9,11,12,13,14,15,16,17-decahydro-17-hydroxy-3-methoxy-13-methyl-6H-cyclopenta[a]phenanthrene-16-carboxylate (**10**).

Compound **10** was prepared as for compound **4** by reacting compound **9** (1.195, 3.49 mmol) with $NaBH_4$ (0.151 g, 4.005 mmol) for 0.5 h, to give 1.166 g of spongy solid. The crude product was purified by silica gel flash column chromatography (hexane/ethyl acetate) to give 0.717 g of white solid. Yield 60%; R_f = 0.53 (hexane/ethyl acetate, 2:1); ^{1}H NMR (300 MHz, $CDCl_3$): δ 0.83 (s, 3H), 1.18 (m, 1H), 1.32 (m, 1H), 1.35 (m, 1H), 1.45 (m, 1H), 1.57 (m, 1H), 1.63 (m, 1H), 1.68 (m, 1H), 1.85 (m, 1H), 1.99 (m, 1H), 2.02 (m, 1H), 2.32 (m, 1H), 2.35 (m, 1H), 2.83 (m, 2H), 3.14 (dd, *J* = 18.7, 9.1 Hz, 1H), 3.72 (s, 3H), 3.80 (s, 3H), 3.88 (d, *J* = 10.0 Hz, 1H), 6.67 (d, *J* = 2.73 Hz, 1H), 6.75 (dd, *J* = 8.61 Hz, 2.73 Hz, 1H), 7.23 ppm (d, *J* = 8.61 Hz, 1H).

(8R,9S,13S,14S)-methyl 2-benzoyl-7,8,9,11,12,13,14,15,16,17-decahydro-17-hydroxy-3-methoxy-13-methyl-6H-cyclopenta[a]phenanthrene-16-carboxylate (**16**).

Compound **16** was prepared as for compound **4** by reacting compound **15** (0.564g, 1.263 mmol) with $NaBH_4$ (0.055 g, 1.449 mmol) for 0.25 h, to give 0.553 g of spongy solid. Yield 97%; R_f = 0.54 (hexane/ethyl acetate, 1:1); mp = 250°C; ^{1}H NMR (400 MHz, $CDCl_3$): δ 0.84 (s, 3H), 1.23 (m, 1H), 1.31(m, 1H), 1.31 (m, 1H), 1.47 (m, 1H), 1.70 (m, 1H), 1.87 (m, 1H), 1.87 (m, 1H), 1.93 (m, 1H), 2.01 (m,1H), 2.17 (m, 1H), 2.98 (m, 2H), 3.14 (dd, *J* = 18.8, 9.1 Hz, 1H), 3.67 (s, 3H), 3.72 (s, 3H), 3.87 (d, *J* = 10.0 Hz, 1H), 6.68 (s,1H), 7.30 (s, 1H), 7.42 (t, *J* = 7.5 Hz, 2H), 7.54 (t, *J* = 7.3 Hz, 1H), 7.83 – 7.77 ppm (m, 2H); ^{13}C-NMR (101 MHz, $CDCl_3$): δ 11.28, 27.19, 27.44, 29.67/29.25, 30.01, 37.16/37.07, 38.14, 43.75, 44.05, 44.38, 48.65, 51.86, 55.64, 81.71, 111.76, 126.41, 127.16, 128.11/128.07, 129.79, 132.33, 132.59, 138.27, 141.02, 155.47, 175.41, 196.53 ppm. HRMS (ESI-MS, 140 eV): m/z [M + H^+] calculated for $C_{28}H_{33}O_5^+$, 449.2328; found, 449.2548.

(8R,9S,13S,14S)-methyl-3-(benzyloxy)-7,8,9,11,12,13,14,15,16,17-decahydro-17-hydroxy-13-methyl-6H-cyclopenta[a]phenanthrene-16-carboxylate (**22**).

Compound **22** was prepared as for compound **4** by reacting compound **21** (3.104 g, 7.42 mmol) with $NaBH_4$ (0.322 g, 8.52 mmol) for 0.5 h, to give 3.586 g of orange solid. The crude product was purified by silica gel flash column chromatography (cyclohexane/ethyl

acetate) to give 2.44 g of white solid. Yield 68%; R_f = 0.45 (cyclohexane/ethyl acetate, 2:1); mp = 186°C; ^{1}H NMR (300 MHz, $CDCl_3$): δ 0.84 ppm (s, 3H), 1.38 (m, 1H), 1.41 (m, 1H), 1.55 (m, 1H), 1.56 (m, 1H), 1.77 (m, 1H), 1.90 (m, 1H), 2.05 (m, 1H), 2.12 (m, 1H), 2.26 (m, 1H), 2.36 (m, 1H), 2.89 (m, 2H), 3.13 (m, 1H), 3.73 (s, 3H), 3.88 (d, 1H), 5.03 (s, 2H), 6.72 (d, *J* = 2.7 Hz, 1H), 6.78 (dd, *J* = 8.4, 2.6 Hz, 1H), 7.20 (d, *J* = 8.5 Hz, 1H), 7.31 (dd, *J* = 8.5, 5.9 Hz, 1H), 7.37 (dd, *J* = 8.1, 6.5 Hz, 2H), 7.43 ppm (d, *J* = 6.9 Hz, 2H); ^{13}C-NMR (75 MHz, $CDCl_3$): δ 11.29, 26.24, 27.32, 29.33, 29.69, 37.16, 38.19, 43.90, 44.04, 48.62, 51.88, 69.93, 81.76, 112.29, 114.79, 126.35, 127.43, 127.84, 128.53, 132.64, 137.25, 137.81, 156.74, 175.57 ppm. HRMS (ESI-MS, 140 eV): m/z [M + H^+] calculated for $C_{27}H_{33}O_4^+$, 421.2379; found, 421.2364.

General procedure for the synthesis of derivatives (**6**, **12**, **18**). As a typical procedure, the synthesis of methyl 2-adamantyl-3-methoxy-16-carboxylate derivative **6** is described in detail. In a double-necked round bottomed flask compound **4** (0.659g, 1.377 mmol) was dissolved in anhydrous CH_2Cl_2. Under a N_2 atmosphere, triethylamine (0.273mL, 1.956 mmol) was added dropwise to the solution and then methanesulfonyl chloride (0.112 mL, 1.456mmol) was poured into the mixture. The obtained solution was stirred overnight. The mixture was then washed with water, saturated $NaHCO_3$ solution, brine, filtered and evaporated under vacuum to yield a yellow solid (**5**). The obtained residue (0.741 g, 1.331 mmol) was then dissolved in benzene (20 mL), and DBU (0.397 mL, 2.662 mmol) was added. Under a N_2 atmosphere, the reaction mixture was refluxed for 5 h. The progress of the reaction was monitored by TLC analysis (hexane/ethyl acetate 2:1). Even though the reaction was not completed, the mixture was cooled and washed with equivalent volumes of 5% HCl solution, brine and saturated $NaHCO_3$ solution. The organic phase was evaporated to dryness under vacuum and the obtained crude product was purified by silica gel flash column chromatography (hexane/ethyl acetate) to give 0.179 g of white solid correspondent to the desired product (**6**) and 0.287 g of starting material.

(8S,9S,13S,14S)-methyl-7,8,9,11,12,13,14,15-octahydro-2-adamantyl-3-methoxy-13-methyl-6H-cyclopenta [a] phenanthrene-16-carboxylate (**6**).

Yield 60%; R_f = 0.80 (hexane/ethyl acetate, 2:1); mp = 179°C; ^{1}H NMR (300 MHz, $CDCl_3$): δ 0.88 (s, 3H), 1.50 (m, 1H), 1.63 (m, 1H), 1.65 (m, 1H), 1.70 (m, 1H), 1.77 (6H), 1.91 (m, 1H), 1.97 (m, 1H), 2.05 (3H), 2.09-2.06 (6H), 2.10 (m, 1H), 2.27 (m, 1H), 2.37 (m, 1H), 2.42 (m, 1H), 2.58 (m, 1H), 2.86 (m, 2H), 3.76 (s, 3H), 3.81 (s, 3H), 6.62 (s, 1H), 6.92 (d, *J* = 1.7 Hz, 1H), 7.14 (s, 1H); ^{13}C-NMR (75 MHz, $CDCl_3$): δ 16.48, 26.68, 28.13, 29.48, 29.55, 31.51, 35.38, 37.24, 37.49, 37.73, 41.11, 44.90, 47.50, 51.73,

55.30, 55.34, 112.44, 123.60, 131.85, 135.14, 135.26, 136.16, 155.12, 157.02, 166.78 ppm. HRMS (ESI-MS, 140 eV): m/z [M + H^+] calculated for $C_{31}H_{41}O_3^+$, 461.3056; found, 461.3067.

(8S,9S,13S,14S)-methyl-7,8,9,11,12,13,14,15-octahydro-3-methoxy-13-methyl-6H-cyclopenta[a]phenanthrene-16-carboxylate (**12**).

Compound **12** was prepared as for compound **6** by reacting compound **10** (0.660 g, 1.916 mmol) with triethylamine (0.379 mL, 2.722 mmol) and methanesulfonyl chloride (0.119 mL, 2.026 mmol). The obtained crude product **11** (0.659 g, 1.560 mmol) was treated with DBU (0.466 mL, 3.120 mmol) and after the work-up, it was purified by silica gel flash column chromatography (hexane/ethyl acetate) to give 0.523 g of white solid. Yield 84%; R_f = 0.83 (hexane/ethyl acetate, 2:1); ^{1}H NMR (300 MHz, $CDCl_3$): δ 0.88 (s, 3H), 1.50 (m, 1H), 1.63 (m, 1H), 1.65 (m, 1H), 1.70 (m, 1H), 1.91 (m, 1H), 1.97 (m, 1H), 2.10 (m, 1H), 2.27 (m, 1H), 2.37 (m, 1H), 2.42 (m, 1H), 2.58 (m, 1H), 2.86 (m, 2H), 3.76 (s, 3H), 3.81 (s, 3H), 6.67 (d, 1H), 6.75 (d, *J* = 1.7 Hz, 1H), 7.23 ppm (d, 1H).

(8S,9S,13S,14S)-methyl-7,8,9,11,12,13,14,15-octahydro-2-benzoyl-3-methoxy-13-methyl-6H-cyclopenta[a]phenanthrene-16-carboxylate (**18**).

Compound **18** was prepared as for compound **6** by reacting compound **16** (0.656 g, 1.462 mmol) with triethylamine (0.289 mL, 2.077 mmol) and methanesulfonyl chloride (0.119 mL, 1.546 mmol). The obtained crude product **17** (0.495 g, 0.940 mmol) was treated with DBU (0.317 mL, 2.126 mmol) and after the work-up, it was purified by silica gel flash column chromatography (hexane/ethyl acetate) to give 0.104 g of white solid. Yield **21**%; R_f = 0.66 (hexane/ethyl acetate, 2:1); mp = 107°C; ^{1}H NMR (300 MHz, $CDCl_3$): δ 0.91 (s, 3H), 1.54 (m, 1H), 1.61 (m, 1H), 1.68 (m, 1H), 1.72 (m, 1H), 1.74 (m, 1H), 1.90 (m,1H), 2.04 (m, 1H), 2.35 (m, 1H), 2.38 (m,1H), 2.39 (m, 1H), 2.60 (m, 1H), 2.89 (m, 2H), 3.68 (s, 3H), 3.71 (s, 3H), 6.65 (s, 1H), 6.85 (d, *J* = 1.8 Hz, 1H), 7.22 (s, 1H), 7.44 (t, *J* = 7.4 Hz, 2H), 7.58 – 7.50 (m, 1H), 7.84 – 7.77 (m, 2H); ^{13}C-NMR (75 MHz, $CDCl_3$): δ 15.95, 26.04, 27.65, 29.99, 31.23, 34.78, 37.10, 43.95, 46.99, 51.54, 54.88, 55.60, 111.57, 126.47, 126.79, 128.09, 129.83, 132.52, 132.59, 132.60, 134.72, 141.27, 154.60, 155.43, 166.51, 196.63 ppm. HRMS (ESI-MS, 140 eV): m/z [M + H^+] calculated for $C_{28}H_{31}O_4^+$, 431.2222; found, 419.2473.

(8S,9S,13S,14S)-7,8,9,11,12,13,14,15-octahydro-2-adamantyl-3-methoxy-13-methyl-6H-cyclopenta[a]phenanthrene-16-carboxylic acid (**7**).

In a round bottomed flask, compound **6** (0.166g, 0.360 mmol) was dissolved in a mixture of CH_2Cl_2/CH_3OH (9:1), and then 2 mL of 3M methanolic NaOH solution were added.

The mixture was stirred at room temperature for 96 h. The progression of the reaction was monitored by TLC analysis (hexane/ethyl acetate 2:1). At the end of the reaction, 1M HCl solution was added and the organic phase was extracted with $CHCl_3$. The combined organic phases were washed with 1M HCl solution, brine and dried over sodium sulphate. After filtration, the organic phase was evaporated to dryness to yield 0.153 g of white solid. Yield 95%; R_f = 0.49 (hexane/ethyl acetate, 2:1); mp = over 300°C; ^{1}H NMR (300 MHz, $CDCl_3$): δ 0.89 (s, 3H), 1.46 (m, 1H), 1.58 (m, 1H), 1.65 (m, 1H), 1.72 (m, 1H), 1.77 (6H), 1.81 (m, 1H), 1.95 (m, 1H), 2.03 (m, 1H), 2.05 (3H), 2.09-2.06 (6H), 2.27 (m, 1H), 2.36 (m, 1H), 2.37 (m, 1H), 2.56 (m, 1H), 2.88 (m, 2H), 3.80 (s, 3H), 6.61 (s, 1H), 7.05 (d, *J* = 1.7 Hz, 1H), 7.14 (s, 1H); ^{13}C-NMR (75 MHz, $CDCl_3$): δ 16.38, 26.65, 28.13, 29.46, 29.59, 31.19, 35.20, 37.22, 37.47, 37.72, 41.09, 44.85, 47.79, 55.27, 55.35, 112.43, 123.62, 131.77, 134.74, 135.15, 136.19, 157.03, 157.88, 170.75 ppm. HRMS (ESI-MS, 140 eV): m/z [M + H^+] calculated for $C_{30}H_{39}O_3^+$, 447.2899; found, 447.2878. RP-C8 HPLC: t_R = 19.80 min, 98.9% (A%).

(8S,9S,13S,14S)-7,8,9,11,12,13,14,15-octahydro-2-adamantyl-3-hydroxy-13-methyl-6H-cyclopenta[a]phenanthrene-16-carboxylic acid (**8**).

Compound **6** (0.103 g, 0.217 mmol) was dissolved in 5 mL of NMP and treated with a suspension of $NaSCH_3$ (0.092 g, 1.32 mmol) in 5 mL of NMP. The mixture was refluxed for 5 h and monitored by TLC analysis. Once the starting material spot disappeared on TLC, a mixture of water and ice was added, and then 1M HCl solution until pH=1. The mixture was extracted with ethyl acetate, washed with water, brine and dried over sodium sulphate. The solvent was evaporated under vacuum and the black residue obtained was dissolved with diluted NH_3 solution. The solution was acidified again with 1M HCl until pH=1 to obtain a subtle precipitate. The suspension was centrifugated and the supernatant discarded. The obtained powder was dried to yield 0,057 g of final product. Yield 56%; R_f = 0.49 (hexane/ethyl acetate, 2:1); mp = over 300°C; ^{1}H NMR (400 MHz, $CDCl_3$): δ 0.89 (s, 3H), 1.46 (m, 1H), 1.72 (m,1H), 1.75 (m, 1H), 1.76 (m, 1H), 1.77 (6H), 1.93 (m, 1H), 1.97 (m, 1H), 2.06 (m, 1H), 2.07 (3H), 2.11 (6H), 2.30 (m, 1H), 2.31 (m, 1H), 2.42 (m, 1H), 2.66 (m, 1H), 2.88 (m, 2H), 6.39 (s, 1H), 7.03 (d, *J* = 1.7 Hz, 1H), 7.12 ppm (s, 1H). ^{13}C-NMR (101 MHz, $CDCl_3$): δ 16.98, 26.16, 28.91, 29.46, 29.59, 32.06, 34.85, 36.45, 37.47, 37.65, 40.07, 44.52, 47.39, 55.15, 116.3, 123.74, 131.74, 133.69, 134.19, 134.73, 151.14, 157.60, 168.99 ppm. HRMS (ESI-MS, 140 eV): m/z [M + H^+] calculated for $C_{29}H_{37}O_3^+$, 433.2743; found, 433.2761. RP-C8 HPLC: t_R = 16.59 min, 99.1% (A%).

(8S,9S,13S,14S)-7,8,9,11,12,13,14,15-octahydro-2-benzoyl-3-hydroxy-13-methyl-6H-cyclopenta[a]phenanthrene-16-carboxylic acid (**19a**).

Compound **18** (0.124 g, 0.289 mmol) was dissolved in 5 mL DMF and treated with $NaSCH_3$ (0.123 g, 1.759 mmol). The mixture was refluxed for 1 h and monitored by TLC analysis (hexane/ethyl acetate 1:1). Once the starting material spot disappeared on TLC, DMF was evaporated under vacuum and the residue was acidified with 1M HCl. The mixture was extracted with ethyl acetate, washed with water, brine and dried over sodium sulphate. The solvent was evaporated under vacuum to give 0.074 g of a spongy yellow solid. The crude product was purified by RP-C18 flash column chromatography (tetrahydrofuran/water 8:2) to give a solid correspondent to the products: 25% **19a**, 37,5% **19b** and 37% **19c** as approximately evaluated by ^{1}H-NMR. The mixture was further separated by a flash column chromatography (Ethyl acetate/hexane 8:2) yielding the desired compound 0.0185 g. Overall yield 16%; mp = over 300°C; ^{1}H NMR (300 MHz, $CDCl_3$): δ 0.87 (s, 3H), 1.56 (m, 1H), 1.66 (m, 1H), 1.68 (m, 1H), 1.70 (m, 1H), 1.71 (m, 1H), 1.91 (m,1H), 2.02 (m, 1H), 2.31 (m, 1H), 2.31 (m,1H), 2.36 (m, 1H), 2.58 (m, 1H), 2.91 (m, 2H), 6.69 (s, 1H), 6.90 (d, J = 1.7 Hz, 1H), 7.28 (s, 1H), 7.42 (t, J = 7.4 Hz, 2H), 7.57 – 7.50 (m, 1H), 7.83 – 7.78 (m, 2H); ^{13}C-NMR (75 MHz, $CDCl_3$): δ 16.09, 26.11, 27.56, 29.98, 31.16, 34.81, 37.12, 43.99, 47.10, 55.62, 111.77, 126.27, 126.78, 128.07, 129.79, 132.52, 132.61, 132.61, 134.88, 141.17, 154.67, 155.45, 166.40, 196.66 ppm. HRMS (ESI-MS, 140 eV): m/z [M + H^+] calculated for $C_{26}H_{27}O_4^+$, 403.1909; found, 403.1889. RP-C8 HPLC: t_R = 17.75 min, 98.7% (A%).

(8R,9S,13S,14S)-methyl-7,8,9,11,12,13,14,15,16,17-decahydro-3,17-dihydroxy-13-methyl-6H-cyclopenta[a]phenanthrene-16-carboxylate (**25**).

Into a double-necked round bottomed flask, previously dried in oven, about 0.300 g of Pd/C 10% and approximately 40 ml of ethyl acetate were placed. After connecting the flask to an elastomer balloon containing hydrogen gas, the mixture was stirred at room temperature for 1h to saturate the suspension of Pd/C with hydrogen. Then, compound 22 (2.121 g, 5.04 mmol) in 20 mL of ethyl acetate was added dropwise to the suspension, and the mixture was stirred under hydrogen at atmospheric pressure and heated by means of an oil bath at 50 °C for 8 h, monitoring the progression of the reaction by TLC analysis (cyclohexane/ethyl acetate 2:1). At the end of the reaction the mixture was filtered, and the solution was concentrated to dryness on a rotavapor to give 1.550 g of white solid. Yield 93%; R_f = 0.20 (cyclohexane/ethyl acetate, 2:1); mp = 125°C ^{1}H NMR (300 MHz, DMSO-d6): δ 0.76 (s, 3H), 1.14 (m, 1H), 1.21 (m, 1H), 1.24 (m, 1H), 1.25 (m, 1H), 1.32

(m, 1H), 1.41 (m, 1H), 1.81 (m, 1H), 1.82 (m, 1H), 1.83 (m, 1H), 2.11 (m, 1H), 2.26 (m, 1H), 2.71 (m, 2H), 3.04 (q, *J* = 8.7 Hz, 1H), 3.60 (s, 3H), 3.77 (s, 1H), 5.00 (dd, *J* = 8.8, 5.4 Hz, 1H), 6.43 (d, *J* = 2.6 Hz, 1H), 6.50 (dd, *J* = 8.4, 2.5 Hz, 1H), 7.03 (d, *J* = 8.3 Hz, 1H), 8.99 ppm (s, 1H); ^{13}C-NMR (75 MHz, DMSO-d6): δ 12.11, 26.62, 27.46, 28.59, 29.63, 37.08, 38.71, 43.88, 44.53, 46.82, 48.94, 51.72, 80.89, 113.32, 115.38, 126.64, 130.85, 137.71, 155.37, 175.70 ppm. HRMS (ESI-MS, 140 eV): m/z [M + H^+] calculated for $C_{20}H_{27}O_4^+$, 331.1909; found, 331.1901.

(8R,9S,13S,14S)-methyl 7,8,9,11,12,13,14,15,16,17-decahydro-3,17-dihydroxy-2-iodo-13-methyl-6H-cyclopenta[a]phenanthrene-16-carboxylate (**26**).

Compound **25** (1.550 g, 4.69 mmol), N-iodosuccinimide (1.161 g, 5.160 mmol), Indium (III) trifluoromethanesulfonate (0.264 g, 0.47 mmol) were mixed together and dissolved in acetonitrile. The mixture was stirred overnight in the dark (wrapped in foil) at room temperature. The progression of the reaction was monitored by TLC analysis (cyclohexane/ethyl acetate 1:1). At the end of the reaction water was added and the organic phase was extracted with ethyl acetate. The combined organic phases were washed with brine and dried over sodium sulphate. After filtration, the solvent was evaporated under vacuum to yield 2.183 g of yellow product. The product was purified by silica gel column chromatography (*d* = 3 cm, *l* = 35 cm, 230-400 mesh, eluent cyclohexane/ ethyl acetate 1:1) to yield 0.639 g of white product. Yield 30%; R_f = 0.66 (cyclohexane/ethyl acetate, 1:1); mp = 179°C ^{1}H NMR (300 MHz, $CDCl_3$): δ 0.82 (s, 3H), 1.16 (m, 1H), 1.31 (m, 1H), 1.32 (m, 1H), 1.48 (m, 1H), 1.51 (m, 1H), 1.76 (m, 1H), 1.88 (m, 1H), 2.05 (m, 1H), 2.09 (m, 1H), 2.16 (m, 1H), 2.24 (m, 1H), 2.78 (m, 2H), 3.13 (dd, *J* = 18.7, 9.2 Hz, 1H), 3.72 (s, 3H), 3.88 (d, *J* = 10.1 Hz, 1H), 5.74 (s br, 1H), 6.68 (s, 1H), 7.51 ppm (s, 1H); ^{13}C NMR (75 MHz, $CDCl_3$): δ 11.33, 26.28, 27.10, 29.23, 29.28, 37.02, 37.94, 43.52, 44.15, 45.99, 48.53, 51.99, 81.68, 82.23, 115.00, 134.75, 135.20, 138.94, 152.83, 175.63 ppm. HRMS (ESI-MS, 140 eV): m/z [M + H^+] calculated for $C_{20}H_{26}IO_4^+$, 457.0876; found, 457.0853.

*General procedure for the synthesis of derivatives (***27**, **28**, **29**). As a typical procedure, the synthesis of (8R,9S,13S,14S)-methyl 7,8,9,11,12,13,14,15,16,17-decahydro-3,17-dihydroxy-13-methyl-2-(4-byphenyl)-6*H*-cyclopenta[*a*]phenanthrene-16-carboxylate **27** is described in detail. Compound **26** (0.200 g, 0.438 mmol) was dissolved in dioxane (2 mL) and then biphenyl boronic acid (0.174 g, 0.880 mmol), potassium carbonate (0.243 g, 1.760 mmol) and tetrakis(triphenylphosphine)palladium (0) (0.050 g, 0.045 mmol) were added. The mixture was microwave irradiated at 160°C (power set point 250 W,

ramp time 60 sec, hold time 30 min). The reaction progression was monitored by TLC analysis (hexane/ethyl acetate 1:1). At the end of the reaction, the mixture was diluted with water (10 mL) and extracted with ethyl acetate. The combined organic phases were dried over sodium sulphate, filtered and the solvent removed under vacuum. The crude product was purified by silica gel flash-column chromatography (hexane/ethyl acetate) to give 0.081 g of compound **27**.

(8R,9S,13S,14S)-methyl-7,8,9,11,12,13,14,15,16,17-decahydro-3,17-dihydroxy-13-methyl-2-(4-byphenyl)-6H-cyclopenta[a]phenanthrene-16-carboxylate (**27**).

Yield 33%; R_f = 0.54 (hexane/ethyl acetate, 1:1); mp = 232°C; ^{1}H NMR (400 MHz, MeOD-d_4): δ 0.94 (s, 3H), 1.46 (m, 1H), 1.65 (m, 1H), 1.69 (m, 1H), 1.79 (m, 1H), 1.81 (m, 1H), 1.85 (m, 1H), 1.90 (m, 1H), 1.91 (m, 1H), 1.93 (m, 1H), 2.03 (m, 1H), 2.65 (m, 1H), 2.74 (m, 1H), 2.76 (m, 1H), 2.95 (m, 1H), 3.70 (s, 3H), 3.82 (d, *J* = 10.5 Hz, 1H), 6.75 (s, 1H), 7.39 (s, 1H), 7.41 (m, AA'BB', 2H), 7.45 (m, AA'BB', 2H), 7.62 (m, 1H), 7.68 (m, 2H), 7.65 (m, 2H) ppm. ^{13}C-NMR (101 MHz, MeOD-d4): δ 11.64, 24.70, 26.41, 29.32, 34.27, 36.48, 39.02, 42.54, 44.97, 47.91, 53.39, 55.64, 84.23, 114.35, 127.01, 127.28, 127.50, 127.61, 127.67, 128.78, 129.03, 137.41, 138.56, 139.34, 140.25, 142.65, 158.70, 174.60 ppm. HRMS (ESI-MS, 140 eV): m/z [M + H^+] calculated for $C_{32}H_{35}O_4^+$, 483.2535; found, 483.2547.

(8R,9S,13S,14S)-methyl-7,8,9,11,12,13,14,15,16,17-decahydro-3,17-dihydroxy-13-methyl-2-(4-dibenzofuranyl)-6H-cyclopenta[a]phenanthrene-16-carboxylate (**28**).

Compound **28** was prepared as for compound **27** by reacting compound **26** (0.308 g, 0.675 mmol) with 4-(dibenzofuranyl)-boronic acid (0.287 g, 1.356 mmol), potassium carbonate (0.375 g, 2.710 mmol) and tetrakis(triphenylphosphine)palladium (0) (0.078 g, 0.068 mmol). The obtained crude product was purified by silica gel flash column chromatography (hexane/ethyl acetate) to give 0.129 g of white solid. Yield 42%; R_f = 0.53 (hexane/ethyl acetate, 1:1); mp = 215°C; ^{1}H NMR (400 MHz, MeOD-d_4): δ 0.80 (s, 3H), 1.14 (m, 1H), 1.15 (m, 1H), 1.24 (m, 1H), 1.31 (m, 1H), 1.42 (m, 1H), 1.43 (m, 1H), 1.52 (m, 1H), 1.72 (m, 1H), 1.94 (m, 1H), 2.07 (m, 1H), 2.24 (m, 1H), 2.82 (m, 2H), 3.16 (q, *J* = 6.82 Hz, 1H), 3.70 (s, 3H), 3.91 (d, *J* = 5.07 Hz, 1H), 7.13 (d, *J* = 9.04 Hz, 1H), 7.59 (d, *J* = 2.24 Hz, 1H), 7.65 (dd, *J* = 9.12, 1.94 Hz, 1H), 7.88 (m, *J* = 7.54, 1.12 Hz, 1H), 7.98 (m, *J* = 7.45, 0.98 Hz, 1H), 8.08 (d, *J* = 8.94 Hz, 1H), 8.15 (d, *J* = 9.14 Hz, 1H), 8.22 (s, 1H), 8.55 ppm (s, 1H). ^{13}C-NMR (101 MHz, MeOD-d4): δ 10.45, 27.02, 27.76, 29.53, 30.01, 32.31, 38.45, 44.12, 45.02, 47.54, 47.35, 55.72, 82.01, 113.06, 124.23, 125.08, 125.10, 126.11, 126.40, 127.21, 128.05, 128.86, 130.09, 131.20, 134.89, 138.55,

139.71, 142.89, 149.81, 154.89, 159.11, 169.81 ppm. HRMS (ESI-MS, 140 eV): m/z [M + H^+] calculated for $C_{32}H_{33}O_5^+$, 497.2328; found, 497.2341.

(8R,9S,13S,14S)-methyl-7,8,9,11,12,13,14,15,16,17-decahydro-3,17-dihydroxy-13-methyl-2-phenyl-6H-cyclopenta[a]phenanthrene-16-carboxylate (**29**).

Compound **29** was prepared as for compound **27** by reacting compound **26** (0.131 g, 0.287 mmol) with phenyl boronic acid (0.070 g, 0.577 mmol), potassium carbonate (0.158 g, 1.150 mmol) and tetrakis(triphenylphosphine)palladium (0) (0.033 g, 0.029 mmol). The obtained crude product was purified by silica gel flash column chromatography (hexane/ethyl acetate) to give 0.081 g of white solid. Yield 26%; R_f = 0.47 (hexane/ethyl acetate, 1:1); mp = 240°C; ^{1}H NMR (400 MHz, MeOD-d_4): δ 0.89 (s, 3H), 1.22 (m, 1H), 1.34 (m, 1H), 1.37 (m, 1H), 1.54 (m, 1H), 1.55 (m, 1H), 1.91 (m, 1H), 1.94 (m, 1H), 1.97 (m, 1H), 2.23 (m, 1H), 2.36 (m, 1H), 2.41 (m, 1H), 2.85 (m, 2H), 3.18 (q, *J* = 8.8 Hz, 1H), 3.71 (s, 3H), 3.96 (d, *J* = 10.5 Hz, 1H), 6.62 (s, 1H), 7.14 (s, 1H), 7.29 – 7.27 (m, 1H), 7.41 – 7.38 (m, 2H), 7.54 – 7.51 ppm (m, 2H); ^{13}C NMR (101 MHz, MeOD-d_4): δ 10.74, 26.17, 27.23, 28.30, 28.94, 37.36, 38.51, 43.91, 46.43, 48.30, 48.85, 50.78, 82.90, 115.51, 125.89, 126.08, 127.17, 127.65, 129.12, 131.38, 136.76, 139.31, 151.47, 176.20 ppm. ^{13}C-NMR (101 MHz, MeOD-d4): δ 10.74, 26.17, 27.23, 28.30, 28.94, 37.36, 38.51, 43.91, 46.43, 48.30, 48.85, 50.78, 82.90, 115.51, 125.89, 126.08, 127.17, 127.65, 129.12, 131.38, 136.76, 139.31, 151.47, 176.20 ppm. HRMS (ESI-MS, 140 eV): m/z [M + H^+] calculated for $C_{26}H_{31}O_4^+$, 407.2222; found, 407.2234.

General procedure for the synthesis of derivatives (**30**, **31**, **32**). As a typical procedure, the synthesis of (8R,9S,13S,14S)-7,8,9,11,12,13,14,15,16,17-decahydro-3,17-dihydroxy-13-methyl-2-(4-byphenyl)-6*H*-cyclopenta[*a*]phenanthrene-16-carboxylic acid **30** is described in detail. Compound **27** was dissolved in 8 mL of methanol and then 4 mL of 10% NaOH solution were added. The mixture was heated to reflux for 1 h and monitored by TLC analysis (hexane/ ethyl acetate, 2:1). As the starting reagent spot disappeared, the solvent was reduced with rotavapor and the mixture acidified with concentrated HCl until pH=1. The suspension was centrifugated and the supernatant discarded. The obtained powder was dried to yield 0,069 g of final product.

(8R,9S,13S,14S)-7,8,9,11,12,13,14,15,16,17-decahydro-3,17-dihydroxy-13-methyl-2-(4-byphenyl)-6H-cyclopenta[a]phenanthrene-16-carboxylic acid (**30**).

Yield 98%; mp = over 300°C; ^{1}H NMR (400 MHz, MeOD-d_4): δ 0.94 ppm (s, 3H), 1.46 (m, 1H), 1.65 (m, 1H), 1.69 (m, 1H), 1.79 (m, 1H), 1.81 (m, 1H), 1.85 (m, 1H), 1.90 (m, 1H), 1.91 (m, 1H), 1.93 (m, 1H), 2.03 (m, 1H), 2.65 (m, 1H), 2.74 (m, 1H), 2.76 (m, 1H),

2.95 (m, 1H), 3.82 (d, 1H), 6.77 (s, 1H), 7.39 (s, 1H), 7.41 (m, AA'BB', 2H), 7.45 (m, AA'BB', 2H), 7.64 (m, 1H), 7.68 (m, 2H), 7.69 ppm (m, 2H); ^{13}C-NMR (101 MHz, MeOD-d4): δ 11.12, 25.94, 26.17, 29.23, 34.16, 36.72, 38.98, 42.57, 44.89, 47.95, 53.47, 79.66, 114.12, 127.07, 127.34, 127.54, 127.69, 127.82, 128.87, 128.92, 137.42, 138.43, 139.24, 140.32, 142.68, 158.76, 177.55 ppm. HRMS (ESI-MS, 140 eV): m/z [M + H^+] calculated for $C_{31}H_{33}O_4^+$, 469.2379; found, 469.2354. RP-C8 HPLC: t_R = 18.89 min, 99.23% (A%).

(8R,9S,13S,14S)-7,8,9,11,12,13,14,15,16,17-decahydro-3,17-dihydroxy-13-methyl-2-(4-dibenzofuranyl)-6H-cyclopenta[a]phenanthrene-16-carboxylic acid (**31**).

Compound **31** was prepared as for compound **30.** Yield 97%; mp = over 300°C; ^{1}H NMR (400 MHz, DMSO-d_6): δ 0.81 (s, 3H), 1.14 (m, 1H), 1.15 (m, 1H), 1.24 (m, 1H), 1.31 (m, 1H), 1.42 (m, 1H), 1.43 (m, 1H), 1.52 (m, 1H), 1.72 (m, 1H), 1.94 (m, 1H), 2.07 (m, 1H), 2.24 (m, 1H), 2.82 (m, 2H), 3.16 (q, *J* = 6.82 Hz, 1H), 3.91 (d, *J* = 5.07 Hz, 1H), 7.13 (d, *J* = 9.04 Hz, 1H), 7.59 (d, *J* = 2.24 Hz, 1H), 7.65 (dd, *J* = 9.12, 1.94 Hz, 1H), 7.89 (m, *J* = 7.54, 1.12 Hz, 1H), 7.98 (m, *J* = 7.45, 0.98 Hz, 1H), 8.08 (d, *J* = 8.94 Hz, 1H), 8.15 (d, *J* = 9.14 Hz, 1H), 8.22 (s, 1H), 8.59 ppm (s, 1H); ^{13}C-NMR (101 MHz, DMSO-d_6): δ 10.94, 26.98, 27.88, 29.72, 30.04, 32.24, 38.74, 44.17, 45.09, 47.53, 47.88, 82.04, 113.12, 124.12, 125.06, 125.07, 126.15, 126.34, 127.93, 128.01, 128.92, 130.14, 131.24, 134.93, 138.56, 139.72, 142.82, 149.82, 154.83, 159.14, 169.87 ppm. HRMS (ESI-MS, 140 eV): m/z [M + H^+] calculated for $C_{31}H_{31}O_5^+$, 483.2171; found, 483.2161. RP-C8 HPLC: t_R = 14.32 min, 98.8% (A%).

(8R,9S,13S,14S)-7,8,9,11,12,13,14,15,16,17-decahydro-3,17-dihydroxy-13-methyl-2-phenyl-6H-cyclopenta[a]phenanthrene-16-carboxylic acid (**32**).

Compound **32** was prepared as for compound **30.** Yield 90%; mp = over 300°C; ^{1}H NMR (400 MHz, MeOD-d_4): δ 0.94 (s, 3H), 1.46 (m, 1H), 1.65 (m, 1H), 1.69 (m, 1H), 1.79 (m, 1H), 1.81 (m, 1H), 1.85 (m, 1H), 1.90 (m, 1H), 1.91 (m, 1H), 1.93 (m, 1H), 2.03 (m, 1H), 2.65 (m, 1H), 2.74 (m, 1H), 2.76 (m, 1H), 2.95 (m, 1H), 3.82 (d, 1H), 6.88 (s, 1H), 7.38 (s, 1H), 7.40 (m, 1H), 7.42 (m, 2H), 7.45 ppm (m, 2H); ^{13}C-NMR (101 MHz, MeOD-d4):δ 11.48, 26.12, 26.17, 29.42, 34.16, 36.72, 39.65, 42.57, 44.12, 47.93, 53.47, 79.66, 113.01, 127.69, 127.81, 128.87, 128.92, 129.04, 137.42, 138.76, 139.24, 158.76, 177.52 ppm. HRMS (ESI-MS, 140 eV): m/z [M + H^+] calculated for $C_{25}H_{29}O_4^+$, 393.2066; found, 393.2973. RP-C8 HPLC: t_R = 11.81 min, 99.1% (A%).

Biology

Cell viability assay

Cell viability was determined by the 3-(4,5-dimethyl- thiazole-2-yl)-2,5-diphenyltetrazolium bromide (MTT, Sigma-Aldrich, St Louis, MO, USA) assay, as previously described.[41] Briefly, HepG2 cells were cultured in DMEM supplemented with 1% glutamine, pen-strep and 10% FBS; cells were seeded in 96-multiwells culture plates at a concentration of (5000 cells/well) and treated with compounds **7**, **8**, **19a**, **30**, **31** and **32** (6.25, 12.5, 25, 50 μM) for 24 h. The formazan absorbance was measured at 570 nm, using a Multilabel Plate Reader VICTOR™ X3 (Wallac Instruments, Turku, Finland). Three independent experiments were performed in quadruplicate.

Cell cycle distribution analysis

Cell cycle distribution analysis was evaluated by flow cytometry (Epics XL, Beckmann Coulter) with CXP software, according to an already described method.[42] Cells (200000 per well), 24 hours after seeding into 6 well-plates, were treated with compounds 7, 8, 19a, 31 at 20 μM for 24 h. The cells were washed with PBS and fixed with ethanol 70%. After 15 min of incubation, cells were resuspended with RNase A (0,1 mg/mL) and 25 μL of propidium iodide (1 mg/mL) for 15 min at room temperature. The results of the different experiments were analysed with CXP software. Three independent experiments were performed in duplicate.

Evaluation of the estrogenic activity by qRT-PCR

The estrogenic activity of the compounds **7**, **8**, **19a**, **30**, **31** and **32** was evaluated in the human breast adenocarcinoma cell line MCF-7 which highly expresses estrogen receptor (ER).[43] MCF-7 cells were cultured in high glucose DMEM without phenol red supplemented with 1% glutamine, pen-strep and 10% FBS, and seeded in 6-well culture plates at a concentration of (250000 cells/well). Samples were treated with compounds **7**, **8**, **19a**, **30**, **31** and **32** (2 μM) for 24 h. Estrone (2 μM) was used as positive control. At the end of the incubation period, MCF-7 were scraped away from cell culture dishes and total RNA was extracted and purified by means of the SV Total RNA Isolation System (Promega Corporation, Madison, WI), as already described.[44] Integrity and quantity of RNA were evaluated by an RNA 6000 Nano assay in an Agilent BioAnalyser (Agilent Technologies Inc., Palo Alto, CA, USA). The relative expression of GREB-1 and CXCL12, two genes which increase their transcription after the activation of ER[45] was determined by real-time PCR (Eco™ Illumina, Real-Time PCR system, San Diego, CA, USA) using One Step SYBR PrimeScript RT-PCR Kit (Takara Bio, Inc., Otsu, Shiga,

Japan). PCR amplifications were tested for linearity and efficiency using standard curves obtained with serial dilution of cDNA; the specificity of amplification and absence of dimers were confirmed by melt-curve analysis. All genes were normalized to Glyceraldehyde-3-phosphate dehydrogenase (GAPDH). The primers used in this study are listed in Table 3. Expression levels of GREB-1 and CXCL12 genes were calculated by the ΔΔCt method using the Eco™ Software v4.0.7.0. Modifications of mRNA levels were expressed as fold variation compared with that of untreated cells. Three independent experiment were performed in triplicate.

Gene	Forward primer	Reverse primer	RefSeq	Size(bp)
GREB-1	5'-gtt-ctg-aag-cta-gac-acg-ga-3'	5'-ttg-agc-aatcgg-tcc-acc-aa-3'	NM_014668.3	185
CXCL12	5'-tac-aga-tgc-cca-tgc-cga-tt-3'	5'-gaa-tcc-act-tta-gct-tcg-gg-3'	NM_000609.6	157
GAPDH	5'-aca-tca-aga-agg-tgg-tga-agc-a-3'	5'-gtc-aaa-ggt-gga-gga-gtg-ggt-3'	NM_001289746.1	119

Table . Primer sequences used in this study, NCBI reference sequences and amplicon sizes (base pairs).

Cell transient transfection assays

HEK293 cells were maintained in DMEM supplemented with 10% FBS, 1% penicillin and streptomycin. Cells were plated at a concentration of 30000/well in 96-well plates, according to an already described method.[26] HEK293 cells were transiently transfected in OPTIMEM (Gibco) medium using lipofectamine 2000 (Invitrogen) following manufacturer instructions. Each plate was co-transfected with 0,2 μg of Gal4-RORγ LBD plasmid (Gal4-driven reporter assays), 0.1 μg UAS-luciferase expression plasmid (both plasmids were kindly furnished by prof. Griffin) and 0.01 μg of NanoLuc reporter plasmid (Promega, Italy). 6 h after transfection medium was replaced with DMEM supplemented with 1% FBS. The following day compounds **7**, **8, 19a** and **32** were added at different concentrations (2, 5, 10, 20 μM). Ursolic acid was used as a positive control. 48 h after transfection luminescence emission was measured using Nano-glo dual-luciferase reporter assay system (Promega) following manufacturer instructions with a

Perkin Elmer en-vision system. All the assays were performed in triplicate, and the standard errors were calculated accordingly.

Western blot analysis.

Protein expression levels of RORγt in transient transfected HEK293 cells was evaluated by Western blot analysis, as already described.[46] Briefly, 20 µg per lane of proteins were subjected to sodium dodecylsulfate polyacrylamide gel electrophoresis (SDS-PAGE) on 10% polyacrylamide gels (100 mV for 15' and 150 mV for 90') and transferred to a 0.45µm nitrocellulose membrane (Bio-Rad Laboratories S.r.l., Segrate, Milan, Italy) at 250 mA for 90 min in the presence of 25 mM Tris - 192 mM glycine. Mouse monoclonal anti-RORγ (Millipore, Billerica, MA, USA) and rabbit polyclonal anti-GAPDH (Santa Cruz Biotechnology, Dallas, TX, USA) primary antibodies (both diluted 1:500) were used to detect RORγt and GAPDH (used as a loading control). Signal intensity of immunoreactive bands was analyzed by the Quantity One software (Bio-Rad Laboratories S.r.l.).

Statistical analysis

Comparison of the experimental data obtained from control cell cultures and those treated with the synthetic compounds was made by one-way analysis of variance (ANOVA). In the case of significant differences ($\alpha = 0.05$), the analysis of variance was followed by the Dunnett *post-hoc* test. $P < 0.05$ was considered statistically significant. If not otherwise stated, data are presented as mean ± standard deviation.

Molecular docking simulations

The 3D structure of orphan nuclear receptor RORγt in complex with the inverse agonists, digoxin, was retrieved from the Protein Data Bank (www.rcsb.org, PDB code 3B0W).

Prior to docking simulation, protein structure was processed with Maestro 10.5 Protein Preparation tool using OPLS-2005 force field. Maestro 10.5[47] Receptor Grid tool was used for the docking site identification, indicating bound digoxin as the grid centre and a length of 10 Å. Molecular structures of compounds **8** and **19a** used for virtual docking were designed using the Builder tool of MOE 2015.10[48] and prepared for the docking simulation with Maestro 10.5[47] Ligand Preparation tool using OPLS-2005 force field. The docking simulations were performed with Maestro 10.5[47] Glide software SP precision, using flexible ligand sampling and performing post-docking minimization.

Acknowledgements

Synthesis and molecular modelling by M. Dal Prà, D. Carta, M.G. Ferlin and biological evaluation by G. Szabadkai, M. Suman, Y. Frión-Herrera, N. Paccagnella, G. Castellani, S. De Martin were supported by financial grants from the University of Padova, Italy.

References

[1] M. Pawlak, P. Lefebvre, B. Staels, General Molecular Biology and Architecture of Nuclear Receptors, Curr. Top. Med. Chem. 12 (2012) 486–504. doi:10.2174/156802612799436641.

[2] A.A. Bogan, F.E. Cohen, T.S. Scanlan, Natural ligands of nuclear receptors have conserved volumes, Nat. Struct. Mol. Biol. 5 (1998) 679–681. doi:10.1038/1372.

[3] C. Zhong, J. Zhu, Small-Molecule RORγt Antagonists: One Stone Kills Two Birds, Trends Immunol. 38 (2017) 229–231. doi:10.1016/j.it.2017.02.006.

[4] R. Mohan, R.A. Heyman, Orphan nuclear receptor modulators., Curr. Top. Med. Chem. 3 (2003) 1637–1647. doi:10.2174/1568026033451709.

[5] J.R. Huh, D.R. Littman, Small molecule inhibitors of RORγt: Targeting Th17 cells and other applications, Eur. J. Immunol. 42 (2012) 2232–2237. doi:10.1002/eji.201242740.

[6] B.P. Fauber, S. Magnuson, Modulators of the nuclear receptor retinoic acid receptor-related orphan receptor-γ (RORγ or RORc), J. Med. Chem. 57 (2014) 5871–5892. doi:10.1021/jm401901d.

[7] L.A. Solt, T.P. Burris, Action of RORs and their ligands in (patho)physiology, Trends Endocrinol. Metab. 23 (2012) 619–627. doi:10.1016/j.tem.2012.05.012.

[8] N. Kumar, L.A. Solt, J.J. Conkright, Y. Wang, M.A. Istrate, S.A. Busby, R.D. Garcia-Ordonez, T.P. Burris, P.R. Griffin, The benzenesulfoamide T0901317 [N-(2,2,2-trifluoroethyl)-N-[4-[2,2,2-trifluoro-1-hydroxy-1-(trifluoromethyl)ethyl] phenyl]-benzenesulfonamide] is a novel retinoic acid receptor-related orphan receptor-α/γ inverse agonist, Mol. Pharmacol. 77 (2010) 228–236. doi:10.1124/mol.109.060905.

[9] N. Mitro, L. Vargas, R. Romeo, A. Koder, E. Saez, T0901317 is a potent PXR ligand: Implications for the biology ascribed to LXR, FEBS Lett. 581 (2007) 1721–1726. doi:10.1016/j.febslet.2007.03.047.

[10] L.A. Solt, N. Kumar, Y. He, T.M. Kamenecka, P.R. Griffin, T.P. Burris, Identification of a selective RORγ ligand that suppresses TH17 cells and stimulates T regulatory cells, ACS Chem. Biol. 7 (2012) 1515–1519. doi:10.1021/cb3002649.

[11] N. Kumar, B. Lyda, M.R. Chang, J.L. Lauer, L.A. Solt, T.P. Burris, T.M. Kamenecka, P.R. Griffin, Identification of SR2211: A potent synthetic RORγ-selective modulator, ACS Chem. Biol. 7 (2012) 672–677. doi:10.1021/cb200496y.

[12] Y. Wang, N. Kumar, P. Nuhant, M.D. Cameron, M.A. Istrate, W.R. Roush, P.R. Griffin, T.P. Burris, Identification of SR1078, a synthetic agonist for the orphan nuclear receptors RORα and RORγ, ACS Chem. Biol. 5 (2010) 1029–1034. doi:10.1021/cb100223d.

[13] S. Xiao, N. Yosef, J. Yang, Y. Wang, L. Zhou, C. Zhu, C. Wu, E. Baloglu, D. Schmidt, R. Ramesh, M. Lobera, M.S. Sundrud, P.Y. Tsai, Z. Xiang, J. Wang, Y. Xu, X. Lin, K. Kretschmer, P.B. Rahl, R.A. Young, Z. Zhong, D.A. Hafler, A. Regev, S. Ghosh, A. Marson, V.K. Kuchroo, Small-molecule RORγt antagonists inhibit T helper 17 cell transcriptional network by divergent mechanisms, Immunity. 40 (2014) 477–489. doi:10.1016/j.immuni.2014.04.004.

[14] J. Kallen, J.M. Schlaeppi, F. Bitsch, I. Delhon, B. Fournier, Crystal Structure of the Human RORα Ligand Binding Domain in Complex with Cholesterol Sulfate at 2.2 Å, J. Biol. Chem. 279 (2004) 14033–14038. doi:10.1074/jbc.M400302200.

[15] S. Fujita-Sato, S. Ito, T. Isobe, T. Ohyama, K. Wakabayashi, K. Morishita, O. Ando, F. Isono, Structural basis of digoxin that antagonizes RORgamma t receptor activity and suppresses Th17 cell differentiation and interleukin (IL)-17 production., J. Biol. Chem. 286 (2011) 31409–17. doi:10.1074/jbc.M111.254003.

[16] T. Xu, X. Wang, B. Zhong, R.I. Nurieva, S. Ding, C. Dong, Ursolic acid suppresses interleukin-17 (IL-17) production by selectively antagonizing the function of RORgamma t protein., J. Biol. Chem. 286 (2011) 22707–10. doi:10.1074/jbc.C111.250407.

[17] J.R. Huh, M.W.L. Leung, P. Huang, D.A. Ryan, M.R. Krout, R.R. V. Malapaka, J. Chow, N. Manel, M. Ciofani, S. V. Kim, A. Cuesta, F.R. Santori, J.J. Lafaille, H.E. Xu, D.Y. Gin, F. Rastinejad, D.R. Littman, Digoxin and its derivatives suppress TH17 cell differentiation by antagonizing RORγt activity, Nature. 472 (2011) 486–490. doi:10.1038/nature09978.

[18] Y. Wang, N. Kumar, L.A. Solt, T.I. Richardson, L.M. Helvering, C. Crumbley, R.D. Garcia-Ordonez, K.R. Stayrook, X. Zhang, S. Novick, M.J. Chalmers, P.R. Griffin, T.P. Burris, Modulation of retinoic acid receptor-related orphan receptor alpha and gamma activity by 7-oxygenated sterol ligands., J. Biol. Chem. 285 (2010) 5013–25. doi:10.1074/jbc.M109.080614.

[19] L. Jin, D. Martynowski, S. Zheng, T. Wada, W. Xie, Y. Li, Structural Basis for Hydroxycholesterols as Natural Ligands of Orphan Nuclear Receptor RORγ, Mol. Endocrinol. 24 (2010) 923–929. doi:10.1210/me.2009-0507.

[20] B.P. Fauber, O. René, G. de Leon Boenig, B. Burton, Y. Deng, C. Eidenschenk, C. Everett, A. Gobbi, S.G. Hymowitz, A.R. Johnson, H. La, M. Liimatta, P. Lockey, M. Norman, W. Ouyang, W. Wang, H. Wong, Reduction in lipophilicity improved the solubility, plasma–protein binding, and permeability of tertiary sulfonamide RORc inverse agonists, Bioorg. Med. Chem. Lett. 24 (2014) 3891–3897. doi:10.1016/J.BMCL.2014.06.048.

[21] B.P. Fauber, G. de Leon Boenig, B. Burton, C. Eidenschenk, C. Everett, A. Gobbi, S.G. Hymowitz, A.R. Johnson, M. Liimatta, P. Lockey, M. Norman, W. Ouyang, O. René, H. Wong, Structure-based design of substituted hexafluoroisopropanol-arylsulfonamides as modulators of RORc, Bioorg. Med. Chem. Lett. 23 (2013) 6604–6609. doi:10.1016/J.BMCL.2013.10.054.

[22] T. Yang, Q. Liu, Y. Cheng, W. Cai, Y. Ma, L. Yang, Q. Wu, L.A. Orband-Miller, L. Zhou, Z. Xiang, M. Huxdorf, W. Zhang, J. Zhang, J.-N. Xiang, S. Leung, Y. Qiu, Z. Zhong, J.D. Elliott, X. Lin, Y. Wang, Discovery of Tertiary Amine and Indole Derivatives as Potent RORγt Inverse Agonists, ACS Med. Chem. Lett. 5 (2014) 65–68. doi:10.1021/ml4003875.

[23] Y. Wang, N. Kumar, C. Crumbley, P.R. Griffin, T.P. Burris, A second class of nuclear receptors for oxysterols: Regulation of RORα and RORγ activity by 24S-hydroxycholesterol (cerebrosterol), Biochim. Biophys. Acta - Mol. Cell Biol. Lipids. 1801 (2010) 917–923. doi:10.1016/J.BBALIP.2010.02.012.

[24] A.R. de Lera, W. Bourguet, L. Altucci, H. Gronemeyer, Design of selective nuclear receptor modulators: RAR and RXR as a case study, Nat. Rev. Drug Discov. 6 (2007) 811–820. doi:10.1038/nrd2398.

[25] S. Xia, Z.Y. Cai, L.L. Thio, J.S. Kim-Han, L.L. Dugan, D.F. Covey, S.M. Rothman, The estrogen receptor is not essential for all estrogen neuroprotection: New evidence from a new analog, Neurobiol. Dis. 9 (2002) 282–293.

doi:10.1006/nbdi.2002.0478; A.B. Petrone, J.W. Gatson, J.W. Simpkins, M.N. Reed, Non-feminizing estrogens: A novel neuroprotective therapy, Mol. Cell. Endocrinol. 389 (2014) 40–47. doi:10.1016/J.MCE.2013.12.017; M. Qian, E.B. Engler-Chiurazzi, S.E. Lewis, N.P. Rath, J.W. Simpkins, D.F. Covey, Structure–activity studies of non-steroid analogues structurally-related to neuroprotective estrogens, Org. Biomol. Chem. 14 (2016) 9790–9805. doi:10.1039/C6OB01726F.

[26] M.R. Chang, V. Dharmarajan, C. Doebelin, R.D. Garcia-Ordonez, S.J. Novick, D.S. Kuruvilla, T.M. Kamenecka, P.R. Griffin, Synthetic RORγt Agonists Enhance Protective Immunity, ACS Chem. Biol. 11 (2016) 1012–1018. doi:10.1021/acschembio.5b00899.

[27] H.M. Berman, J. Westbrook, Z. Feng, G. Gilliland, T.N. Bhat, H. Weissig, I.N. Shindyalov, P.E. Bourne, The Protein Data Bank., Nucleic Acids Res. 28 (2000) 235–42.

[28] C. Li, W. Qiu, Z. Yang, J. Luo, F. Yang, M. Liu, J. Xie, J. Tang, Stereoselective synthesis of some methyl-substituted steroid hormones and their *in vitro* cytotoxic activity against human gastric cancer cell line MGC-803, Steroids. 75 (2010) 859–869. doi:10.1016/J.STEROIDS.2010.05.008.

[29] W.H.W. Lunn, E. Farkas, The adamantyl carbonium ion as a dehydrogenating agent, its reactions with estrone, Tetrahedron. 24 (1968) 6773–6776. doi:10.1016/S0040-4020(01)96851-6.

[30] U. Gozzi, G. Marnini. Cleavage of the D ring in 16-substituted steroids. Gazz. Chim. Ital., 1977; 107: 75-81.

[31] N. Vicker; L. Harshani Rithma Ruchi; M.A. Allan, C. Bubert, D.S.M Fischer, A. Purohit, M.J. Reed, B.V.L Potter. Inventors: Sterix Ltd, N. Vicker, L.Harshani, Rithma Ruchi; M.A. Allan, C. Bubert; D.S.M Fischer, A, Purohit, M.J. Reed, B.V.L Potter, Assignee. 17beta-hydroxysteroid dehydrogenase inhibitors. WO2004085457 A2 2004

[32] L.A. Paquette, K. Dahnke, J. Doyon, W. He, K. Wyant, D. Friedrich, Regioselective conversion of cycloalkanones to vinyl bromides with 1,2-functionality transposition. A general stratagem, J. Org. Chem. 56 (1991) 6199–6205. doi:10.1021/jo00021a044.

[33] V. Theodorou, K. Skobridis, A.G. Tzakos, V. Ragoussis, A simple method for the alkaline hydrolysis of esters, Tetrahedron Lett. 48 (2007) 8230–8233. doi:10.1016/J.TETLET.2007.09.074.

[34] B. Charpentier, J.-M. Bernardon, J. Eustache, C. Millois, B. Martin, S. Michel, B. Shroot, Synthesis, Structure-Affinity Relationships, and Biological Activities of Ligands Binding to Retinoic Acid Receptor Subtypes, J. Med. Chem. 38 (1995) 4993–5006. doi:10.1021/jm00026a006.

[35] G. Göndös, G. Dombi, Novel Friedel-Crafts Alkylation of Estrogens in the Presence of Anhydrous $FeCl_3$ or $FeCl_3$-Graphite as Catalyst, Monatshefte Fűr Chemie / Chem. Mon. 133 (2002) 1279–1283. doi:10.1007/s007060200106.

[36] A. Suzuki, Carbon–carbon bonding made easy, Chem. Commun. 0 (2005) 4759. doi:10.1039/b507375h.

[37] G.M. Allan, H.R. Lawrence, J. Cornet, C. Bubert, D.S. Fischer, N. Vicker, A. Smith, H.J. Tutill, A. Purohit, J.M. Day, M.F. Mahon, M.J. Reed, B.V.L. Potter, Modification of estrone at the 6, 16, and 17 positions: Novel potent inhibitors of 17β-hydroxysteroid dehydrogenase type 1, J. Med. Chem. 49 (2006) 1325–1345. doi:10.1021/jm050830t.

[38] C.Y. Zhou, J. Li, S. Peddibhotla, D. Romo, Mild arming and derivatization of natural products via an In(OTf) 3-catalyzed arene iodination, Org. Lett. 12 (2010) 2104–2107. doi:10.1021/ol100587j.

[39] J. Lee, J.Y. Kim, K.S. Song, J. Kim, K.W. Ahn, Y. Kong; (+)-3-hydroxymorphinan derivatives as neuroprotectants. US 2012/0122848 2012.

[40] D. Catanzaro, R. Filippini, C. Vianello, M. Carrara, E. Ragazzi, M. Montopoli, Chlorogenic Acid Interaction with Cisplatin and Oxaliplatin: Studies in Cervical Carcinoma Cells., Nat. Prod. Commun. 11 (2016) 499–502.

[41] D. Catanzaro, E. Ragazzi, C. Vianello, L. Caparrotta, M. Montopoli, Effect of Quercetin on Cell Cycle and Cyclin Expression in Ovarian Carcinoma and Osteosarcoma Cell Lines., Nat. Prod. Commun. 10 (2015) 1365–8.

[42] L. Ponnusamy, P.K.S. Mahalingaiah, K.P. Singh, European Journal of Pharmaceutical Sciences Treatment schedule and estrogen receptor-status in fl uence acquisition of doxorubicin resistance in breast cancer cells, Eur. J. Pharm. Sci. 104 (2017) 424–433. doi:10.1016/j.ejps.2017.04.020.

[43] G. Castellani, G. Paliuri, G. Orso, N. Paccagnella, C. D'Amore, L. Facci, F. Cima, F. Caicci, P. Palatini, S. Bova, S. De Martin, An intracellular adrenomedullin system reduces IL-6 release via a NF-kB-mediated, cAMP-independent transcriptional mechanism in rat thymic epithelial cells, Cytokine. 88 (2016) 136–143. doi:10.1016/j.cyto.2016.09.003.

[44] C.-Y. Lin, A. Ström, V. Vega, S. Li Kong, A. Li Yeo, J.S. Thomsen, W. Chan, B. Doray, D.K. Bangarusamy, A. Ramasamy, L.A. Vergara, S. Tang, A. Chong, V.B. Bajic, L.D. Miller, J.-Å. Gustafsson, E.T. Liu, Discovery of estrogen receptor α target genes and response elements in breast tumor cells, Genome Biol. 5 (2004) R66. doi:10.1186/gb-2004-5-9-r66.

[45] S. De Martin, D. Gabbia, G. Albertin, M.M. Sfriso, C. Mescoli, L. Albertoni, G. Paliuri, S. Bova, P. Palatini, Differential effect of liver cirrhosis on the pregnane X receptor-mediated induction of CYP3A1 and 3A2 in the rat, Drug Metab. Dispos. 42 (2014) 1617–1626. doi:10.1124/dmd.114.058511.

[46] Schrödinger Release 2016-1: MS Jaguar, Schrödinger, LLC, New York, NY, 2016.

[47] Molecular Operating Environment (MOE), 2015.10; Chemical Computing Group ULC, 1010 Sherbooke St. West, Suite #910, Montreal, QC, Canada, H3A 2R7, 2017.

CHAPTER 4

In silico screening as a tool to identify new anticancer agents acting in the Notch pathway

Synopsis

Finding new effective anticancer agents still represent a challenge for the scientific community. Notch signalling pathway represents one of the major driver in the pathogenesis and progression of several cancer diseases, but still no agent able to interfere with its activity is proceeding in the drug development process. A virtual screening of commercially available drug-like compounds (over 3 million) was performed on the Notch1-Jagged1 and NRR binding sites of the Notch1 receptor. 62 compounds were selected for biological screening, and 29 of them revealed cytotoxic activity against a panel of four T-ALL leukemia cell lines. To assess direct interference with Notch1 signalling pathway, western blot analysis and real-time PCR were performed, and two compounds have been selected and identified as hit compounds for Notch1 inhibition. These compounds interfere with Notch1 activity by blocking the release of intracellular Notch1 domain and downregulate the mRNA levels of HES1, a direct Notch1 target gene. Thus, these hit compounds are proposed as candidates for Notch1 inhibition and will be further evaluated, and their structure optimized to develop Notch1 modulators as anticancer agents.

Introduction

Notch signalling pathway is part of a small group of evolutionarily highly conserved signalling mechanisms which are crucial for development and homeostasis. Notch signalling pathway was primarily discovered a century ago by T. H. Morgan during his studies on mutated *Drosophila melanogaster*. After that discovery, several studies were conducted leading to the comprehension of Notch biological implications in reasonable details.[1] Notch signalling plays a pivotal role in important processes such as cell proliferation, apoptosis, activation of differentiation programs of specific cell fates, and its gain or loss of functionality has been related to the development of several diseases

such as leukemia, breast cancer, Alagille syndrome and CADASIL syndrome.[2] The first evidence of Notch involvement in malignancies was determined in T-cell acute lymphoblastic leukemia (T-ALL).[3]

Notch receptor is at the centre of a cell-cell communication system, based on the interaction with Notch ligands on another cell.[1] The receptor is a single pass trans-membrane protein and in mammals, four closely related Notch receptors exist (1-4), while Notch ligands belongs to two different but closed families: Delta-like family (DLL1, DLL3 and DLL4) and Jagged family (Jag1, Jag2).[1] The existence of various specific Notch receptors and ligands allows fine-tuning of the amplitude and duration of Notch activity to generate context- and tissue-specific signals.[2]

At first sight, Notch signalling pathway appears simple: events start when a ligand binds to the Notch receptor expressed on another cell surface. Ligand binding leads to the exposure of the extracellular protease cleavage site (S2) which is cleaved by ADAM-proteases ("A Disintegrin And Metalloproteinase"). Then another cleavage at site S3 occurs by γ-secretase complex to release Notch intracellular domain (NICD) which migrates to the nucleus and forms a transcriptional activation complex with the DNA binding factor RBPJ (Recombining Binding Protein suppressor of hairless) of the CSL family (an acronym for *C*BF-1/RBPJ-κ in *Homo sapiens*/*Mus musculus* respectively, *S*uppressor of Hairless in *Drosophila melanogaster*, *L*ag-1 in *Caenorhabditis elegans*) and coactivators of the Mastermind-like family (MAML).[4] Once this complex is activated, transcription of target genes can start.

Physiologically, Notch regulates different target genes in distinct cell types through complex interactions with multiple regulators, thus the network of different biological events which are affected by its action is very intricate. Basically, Notch functions as a signalling hub, cross-talking with and influencing other signalling pathways.

The best-characterised Notch-targets are HES family members involved in the repression of cell-fate determinants and cell-cycle regulators; the Notch-related ankyrin repeat protein (Nrarp) which can regulate cancer cells self-renewal and angiogenesis; and c-Myc that highly affects cell proliferation.[5]

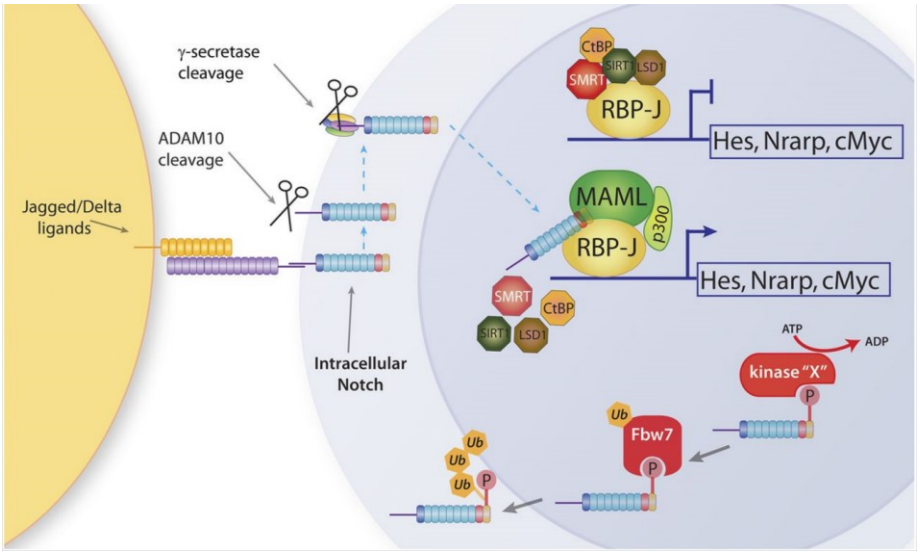

Figure 1. Notch signalling pathway[6]

Notch1 Structure

Notch receptor is a single pass trans-membrane protein and its complete quaternary structure has still to be exhaustively determined. At first glance, it can be divided in extracellular domains, responsible for ligand binding and in intracellular domains, which translocate in the nucleus after cleavage by specific enzymes. Structure of the ectodomain remains unsolved but since it mainly comprises Epidermal Growth factor-like domains, 36 for being precise, it is reasonable to hypothesize a structural model based on the features of this domain type. Indeed, the receptor is predicted to have a rigid near-linear architecture but with some sites of flexibility. Regarding the domains mainly involved in ligand binding, it has been demonstrated that Jagged and DLL ligands bind Notch-1 primarily through EGF 11-12[7] and this is also demonstrated by recently solved crystal structures.[8] However, it is possible that additional sites may contribute for the specificity in ligand recognition. Moreover, molecular force measurements show that Jag1 and DLL4 have different tension thresholds for receptor activation, and both form 'catch bonds', or bonds whose lifetimes are prolonged upon the application of tensile forces and this seems to be the basis on which discrimination of Notch ligands occurs.[8]

Following the EGF-like domains, there is a portion called Negative Regulatory Region (NRR), adjacent to the cell membrane. The NRR is composed by three LNR repeats (Lin-12/Notch) and a hydrophobic region called the heterodimerisation domain (HD). The NRR prevents ligand-independent activation by maintaining Notch in a non-active

conformation, which cannot be cleaved by metalloproteases and thus cannot release the intracellular domain. For its part, the intracellular domain NICD contains a RAM domain, seven ankyrin repeats (ANK), a transcription activation domain and a PEST domain (Figure 2). When Notch signalling starts and NICD is cleaved from its extracellular counterpart, this domains cooperatively bind to coactivators inducing gene transcription.[9]

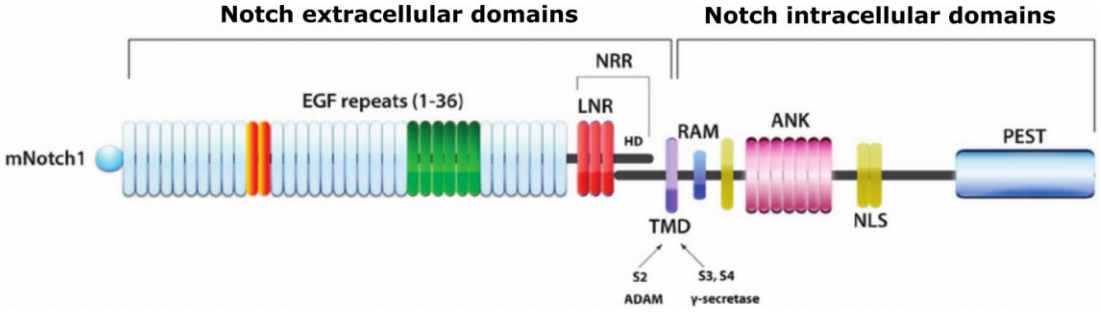

Figure 2. Notch structural domains

Notch-1 ligand binding site

Structural studies of Notch-1-ligand interactions are made difficult because of the low affinity between Notch-1 and its ligands of the Jagged or DLL families. From the first mutational studies performed in order to understand how ligand recognition occurs, Notch-1 EGF-11 and -12 were recognised as fundamental for ligand binding. Some authors then determined the dissociation constant (K_D) between Jag1 ligand, as representative of the Jagged family, with Notch-1 EGF domains 8 to 12, which resulted to be of 0.81 μM, and with Notch-1 EGF domains 11-12 obtaining a K_D of 5.4 μM. This difference in affinity demonstrated that EGF 8-10 domains contributes to Notch-1-Jag1 binding energetics. On the other hand, regarding DLL binding event, Notch-1 EGF 8-12 and Notch-1 EGF 11-12 bound to DLL4 showed a K_D of 9.7 μM and of 12.8 μM, respectively, indicating that in this case EGF 8-10 have minimal impact on the affinity. Thus, it seems that the two different families of ligands have different energetic requirements, and this might account for tuning and regulating the sensitivity towards each of them.[8]

The crystal structures of the complex between Notch-1 and ligands DLL4 (PDB code 4XL1) and Jag1 (PDB code 5UK5) have been solved recently.[8-9] In our study, we

decided to focus on the interaction between Notch-1 and Jag1, because of the major affinity compared to DLL family.[10]

Notch-1 negative regulatory region[11]

Notch-1 Negative Regulatory Region is the area of Notch proximal to cell membrane and it is well-characterised compared to the EGF-repeats region. The key role for NRR is to protect Notch receptor from proteolytic cleavage at S2 site, which would liberate the intracellular domain. Indeed, NRR is considered as the regulatory switch that control activation of the receptor. Crystal structure of Notch-1 NRR has been completely solved (PDB code 3ETO) and structural determinants have been identified. The overall architecture is composed by three LNR repeats which wrap around a highly hydrophobic region called Heterodimerisation domain (HD) (see Figure 3). This peculiar structure serves to cover and protect the S2 cleavage site. Each LNR module is characterised by 3 disulphide bonds and a calcium coordinating site, which is fundamental for the maintenance of the overall structure. The LNR modules tightly stabilize the fold of the HD domain and in particular, LNR-A and LNR-B form a hydrophobic plug for the protection of S2 site. Thus, for the activation of the receptor this hydrophobic plug has to be displaced to expose the S2 site (Figure 3).

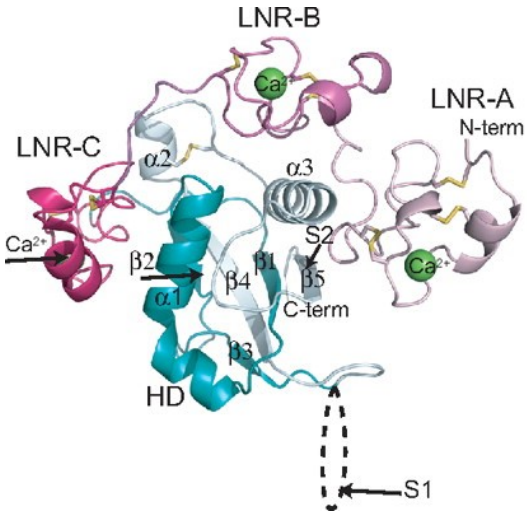

Figure 3. Overall structure of the human Notch1 NRR, shown in ribbon representation. Shades of pink and purple represent LNR modules; shades of light and dark cyan, HD domain (on N- and C-terminal sides of the furin cleavage loop, respectively). Disulphide bonds are rendered as yellow sticks, and calcium ions as green spheres. Arrows denote positions of the S1 and S2 cleavage sites.[11]

This plug consists of 3 residues that envelop the amide bond sterically precluding metalloprotease access to S2. A leucine residue (L1482) extending from the LNR A-B linker packs tightly against the valine residue (V1722) that lies immediately terminal to the scissile bond. A hydrogen bond from the main chain carbonyl group of the leucine residue to the main chain amide group protects the scissile bond. Another polar interaction between the carbonyl group of the glutamic acid residue (E1720) preceding the scissile bond and the side chain of asparagine (N1483) stabilizes the orientation of the long-range interactions, and a hydrophobic cap provided by phenylalanine (F1484) is also buried within contact distance of both the valine residue following the S2 cleavage site and an aliphatic side chain from helix 3.

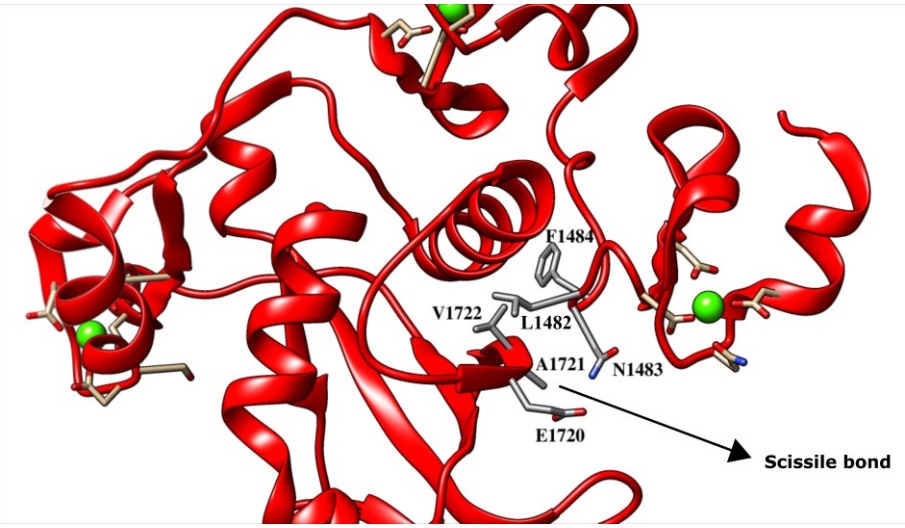

Figure 4. S2 site and selected amino acids residues

This region is usually associated with mutations that lead to ligand-independent Notch-1 activation which account, in most cases, for the development or exacerbation of cancer disease. Thus, the determination of the molecular structures and features of NRR components provides a template for the development of agents designed to stabilise or destabilise its conformation in order to interfere with cancer.

Notch in cancer

Notch pathway, as already mentioned before, is deeply involved in the development of several tissues and organs. Briefly, its signalling pathway controls or regulates at various levels: growth, proliferation and differentiation of cells belonging to vasculature, hematopoietic system, heart, liver, skin. From a pharmaceutical point of view, the interest

towards Notch signalling as a pharmacological target relies on its demonstrated role as tumour trigger in several types of cancer disease. Indeed, functional studies implicate Notch signalling in all the hallmarks of cancer (Figure 5) but clearly show that it can switch from oncogenic to tumour-suppressor depending on context.[12]

As an oncogene, Notch plays a key role in solid tumour biology, including regulation of tumour growth, malignant cell survival, endothelial function, angiogenesis, and normal stem cell differentiation and development. Its aberrant constitutive activation in most type of leukemia and lymphomas has been clearly highlighted.[13] Proposed mechanisms for upregulation of Notch pathway activity include activating mutations of the Notch receptor; loss of Notch negative regulators; and indirect activation of Notch through other pathways. In line with this concept, the inhibition of Notch signalling represents a new promising opportunity in cancer therapy, as Notch pathway regulates and sustains a wide range of tumorigenic processes and interacts with a high number of pathways. Moreover, a co-targeting approach that simultaneously inhibits these processes can eventually results in more effective and durable cancer therapies.[14]

The pathological role of Notch in the development of cancer has been related to the following mechanisms:

- Sustained proliferative signalling. Notch strongly stimulates the progression of the cell cycle by induction of the expression of cyclin D1[15] and of the activity of CDK2. Moreover, cMyc, one of the most powerful driver of cell cycle entry, was identified as direct downstream target of Notch1.[16] Notch is also able to enhance PI3K-Akt signalling, probably through multiple mechanism.[17]
- Decreased apoptosis. Notch 1 inhibits production and activation of transcriptional repressors such as p27 and p57,[18] but it also increases the transcription of anti-apoptotic genes like B-cell lymphoma 2 (Bcl-2) and of the inhibitor of apoptosis survivin.[19]
- Angiogenesis. Notch indirectly potentiates the production of Vascular endothelial growth factor (VEGF) by modulating the activity of hypoxia-inducible factors (HIF-1A), which cause the formation of new vessels and in turn, increases the expression of DLL4 Notch ligand. In this way the process is self-sustaining.[20]
- Controls cancer stemness.[21]
- Induction of a pro-metastatic phenotype with development of aggressive diseases. Notch/Jagged 1 activation in epithelial and endothelial cells is involved in the

Epithelial-to-Mesenchymal transition (EMT) process, which in turn seems to be fundamental for the transformation to malignant phenotypes.[22] Moreover, this transition can promote the acquisition of drug resistance.

- Promotion of chemo- and radio-resistance. In several types of cancer (ovarian, colon, hepatocellular), the blockage of Notch signalling restore sensitivity towards chemo- and radiotherapy.[23]

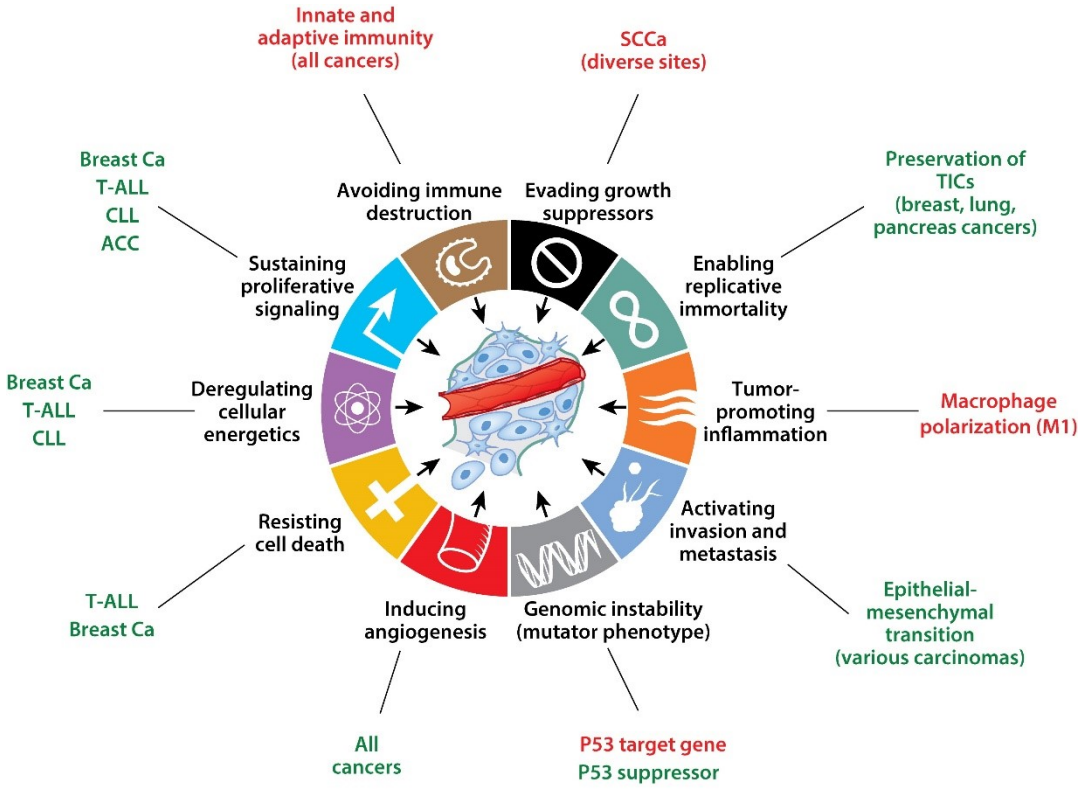

Figure 5. Cancer hallmarks proposed to be influenced by Notch signalling. Positive (oncogenic) effects (*green*) and tumor suppressive effects (*red*) are shown. Abbreviations: ACC, adenoid cystic carcinoma; breast Ca, breast carcinoma; CLL, chronic lymphocytic leukemia; SCCa, squamous cell carcinoma; T-ALL, T cell acute lymphoblastic leukemia; TIC, tumor-initiating cell.[12]

From a clinical point of view, hyperactivation of Notch signalling was identified in 50-60% of T-cell acute lymphoblastic leukemia (T-ALL) cases examined, establishing Notch1 activity as the main oncogenic lesion in T-ALL.[24] Furthermore, Notch1 is also involved in chronic lymphocytic leukemia (CLL), the most frequent adult leukemia and even though its role is less important compared to T-ALL disease, it is usually associated with poor prognosis. In addition, aberrant activation of Notch pathway is associated with all the types of breast cancer.[25]

Despite its very-well characterised oncogenic role, recently, some tumour-suppressor's aspects were found and demonstrated for Notch, furnishing the details for a complete but more complex situation. Some authors reported that conditional loss of function of Notch resulted in a myeloproliferative syndrome which rapidly evolved to acute myeloid leukemia (AML) characterised by an increased number of granulocytes and monocytes invading tissues.[6] Other studies reported that activation of Notch pathway, mainly through administration of peptides mimicking Notch ligands, would inhibit AML cell propagation and survival.[26] Great attention merits also the case of development and progression of squamous cell carcinoma which is usually associated with Notch loss-of-function mutations, representing the most recurrent mutations in this type of solid cancer. Also, some *in vivo* data suggest this onco-suppressor role.[27] Thus, it seems that in some cases activation of Notch signalling might result in onco-suppressor activity, especially in myeloid malignancies, indeed some *in vitro* and *in vivo* evidences suggest that Notch suppresses myeloid differentiation, and basically it could prevent uncontrolled proliferation and transformation of myeloid cells during hematopoietic development.[26]
Despite the increase in the comprehension of its biological role and implications in several types of cancer, only a small group of molecules have been discovered with the ability to interfere with its activity, and none of them is progressing in the drug development process. Additionally, the complexity related to its capacity of modulating cancer progression, where Notch can act as oncogenic or as tumour suppressor in a context-dependent way, renders it a challenging target.

Results and Discussion

Molecular Modelling: hit identification

From a molecular modelling point of view, two potential binding sites were explored in order to find small molecules able to activate or to block the Notch pathway. For our studies, Notch1 structure was taken in consideration, as its role in cancer, especially in some type of leukemia is well-documented and understood. The selected sites were Notch-1/Jagged1 binding site and the NRR region.
Two different virtual screening approaches have been used for the initial selection of potential hit compounds: a structure-based virtual screening (for both the binding sites) and a ligand-based virtual screening (only for NRR region). While the first approach

takes into consideration the protein structure to filter a library of molecules through docking simulations, the ligand-based methodology compares the shapes of known ligands with unknown ones, evaluating two-dimensional similarities (i.e. same functional groups) or three-dimensional similarities (molecule occupational volume) without considering the protein structure. The molecules selected with the two methods were then subjected to different molecular docking evaluations described below.

Structure-based virtual screening on Notch1-Jagged1 binding site

Since no crystal structure was available in the literature at the time of the experiment, a reliable model of the interaction between Notch1 and its ligand Jagged1 was built. The main binding site of Jagged1 is located within Notch1 surface, in the area that comprises EGF 11-13 domains.[10] In order to obtain a model of the interaction between Notch1 EGF 11-13 (PDB code 2VJ3) and Jagged1 DSL and EGF 1-3 (PDB code 2VJ2), their crystallographic structures were retrieved from the Protein Data Bank. The structures were imported into MOE[28] and unrelated entities such as unnatural dimerization of Jagged1, water and sodium atoms were removed for docking purposes via MOE sequence editor. Both proteins were reprocessed, and protonation was performed with protonate3D tool in MOE. Partial charges were calculated using Amber99 forcefield, adjusting hydrogens and lone pairs. Lastly, an energy minimization procedure was conducted to orientate the atoms to their optimal positions. The minimization was performed by using Amber99 forcefield, commonly used for large proteins. Then, the two structures were docked by using protein-protein docking tool in MOE, using standard parameters. A hundred poses were obtained and visual inspected by looking at the number of hydrogen interactions and orientation, and then one pose was selected as the best.

The selected model was used to perform a structure-based virtual screening of the SPECS library, a database of ~300,000 commercially available compounds,[29] using Maestro 10.5 Glide software High Throughput Virtual Screening tool.[30] All default parameters were kept allowing one output pose per ligand input. The top 20% best performing compounds (53,165) were docked again in the same site using Maestro 10.5 Glide software Standard Precision tool.[30] This is a more reliable and accurate procedure which gave three output poses per ligand input. The obtained conformations (486,325) were submitted to a Rescoring study by employing the following docking software: Maestro 10.5 Glide software Extra Precision tool, FlexX module in LeadIT 2.1.8 and PLANTS.[30-32] All the scores obtained from the different docking programs were exported in Excel

where a Consensus score was performed. We obtained a selection of 3,580 unique compounds. The compounds were visual inspected to give a final selection of 19 compounds.

Ligand-based virtual screening on NRR binding site

The NRR region acts as an activation switch for Notch1 receptor, thus interfering with it means also influencing Notch1 activity. Recently, N-methylhemeanthidine chloride (NMHC, see Figure 6), a compound isolated from *Zephyranthes candida*, was shown to promote Notch1 proteolytic cleavage and therefore its activation in AML cell line by interacting with NRR region.[26] This compound could be considered a Notch1 agonist. As consequence, the NRR region seems a good target for a molecular modelling study in order to find small molecules that can either activate Notch1, by disrupting the NRR region and allow the S2 cleavage and therefore Notch1 activation, or block Notch1 by stabilising the NRR region and not allowing the S2 cleavage.

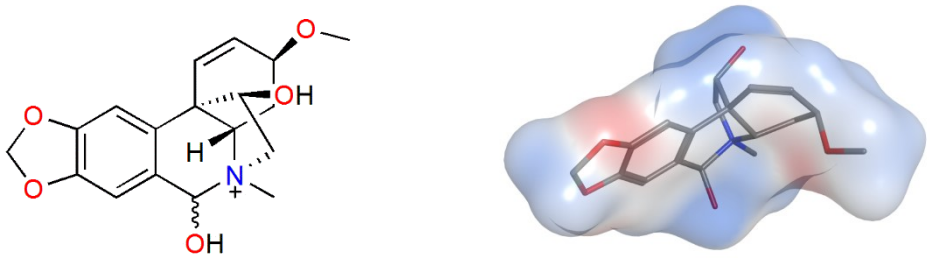

Figure 6. NMHC molecular structure and occupied volume

In this case, we preliminarily studied and evaluated NMHC from a molecular point of view. Firstly, a conformational study search on this compound was performed in order to find the most likely compound conformation to be used in the next steps. The presumptive binding site in the NRR was obtained from literature.[26] (see figure below)

A virtual screening of more than 3 million compounds (SPECS, Enamine, LifeChemicals databases)[29,33,34] was performed using ROCS software,[35] which compared the shape of the active NMHC with the ones of commercial compounds. The best 3% compounds were selected for the second step. The selected compounds were docked using Maestro 10.5 Glide software Standard Precision tool,[30] which lead to the generation of a library of 248,216 entries. A Rescoring study was performed again with Maestro 10.5 Glide software Extra Precision tool, FlexX module in LeadIT 2.1.8 and PLANTS.[30-32] A

Consensus score was performed to obtain a selection of 6,820 compounds. After fingerprint clustering and visual inspection, 22 compounds were selected for purchasing.

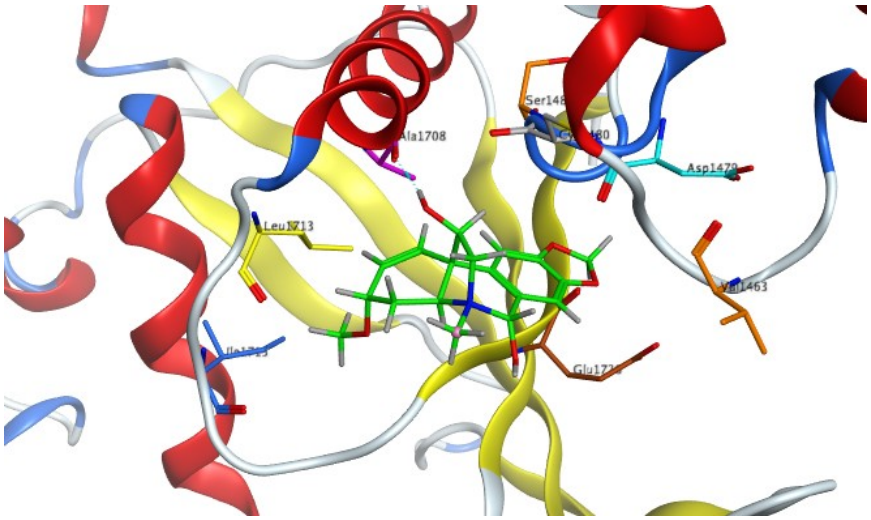

Figure 7. Presumptive NMHC binding site in the Notch1 NRR region

Structure-based virtual screening on NRR binding site

A High Throughput virtual screening of a library of commercially available compounds (3 million structures taken from three different databases: SPECS, Enamine, LifeChemicals)[29,33,34] was performed in the NMHC binding site by using Maestro 10.5 Glide software High Throughput Virtual Screening tool.[30] The best performing 5% (249,648 entries) was selected for further evaluation. The results were then filtered performing a docking simulation using Maestro 10.5 Glide software Standard Precision, to generate a library of 745,700 poses.[30] A consensus score study was performed using three different docking software: Maestro 10.5 Glide software Extra Precision, FlexX and PLANTS.[30-32] The consensus score was performed to obtain a library of 14,844 entries. The molecules were visual inspected and 21 of them were selected to be purchased.

The selected compounds were divided into two sets characterised by the following code:

- Compounds targeting the Notch1/Jagged1 binding site: AB1521-AB1537
- Compounds targeting the NRR: AB1674-AB1715

Biological Screening. Two candidates affects Notch pathway

The selected 62 compounds were screened in order to evaluate the cytotoxic activity with the 3-(4,5-dimethylthiazol-2-yl)-2,5-diphenyltetrazolium bromide (MTT) assay against a panel of 4 T-ALL cell lines (ALL-SIL, TALL1, DND41, Jurkat). RO4929097, a commercially available γ-secretase inhibitor, acting in the Notch pathway, was used as reference compound.[36] Compounds were tested at concentrations ranging from 100 μM to 0.1 nM for 72 h. Of the 62 screened compounds, one showed to be insoluble, thirty-two were not toxic and twenty-nine showed cytotoxic activity in at least one cell lines. These last derivatives showed the following ranges of GI_{50}s: two compounds showed $GI_{50} < 1$ μM, five with GI_{50}s between 1 μM and 20 μM, twelve with GI_{50}s between 20 μM and 50 μM and ten with GI_{50}s > 50 μM (see Figure 8). Our interest in conducting cytotoxicity testing was to rule out compounds which did not affect cancer cell growth ($GI_{50} > 100$ μM). We decided to set this rather generous cut off since also established Notch1 inhibitors such as γ-secretase inhibitors (GSIs) show GI_{50} values around 30μM or higher.[2]

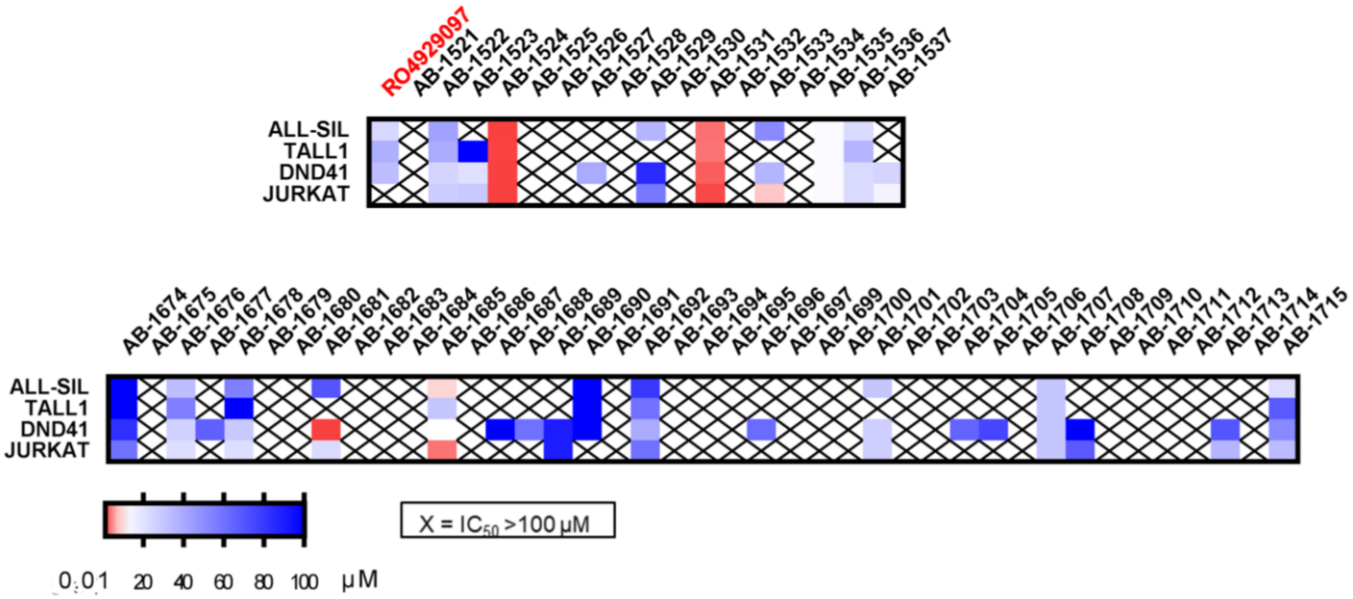

Figure 8. Heat map showing growth inhibitory concentrations (GI_{50}) on 4 T-ALL cell lines of the tested compounds.

To exclude the inhibition of other cellular pathway and to select only the compounds affecting Notch signalling, the compounds were assayed by means of Western Blot analysis to detect intracellular protein levels of cleaved Notch1 in DND41 cells after 48h

of exposure. Most interesting results are shown in Figure 9. Cells were treated at sub lethal doses (one-third GI_{50}).

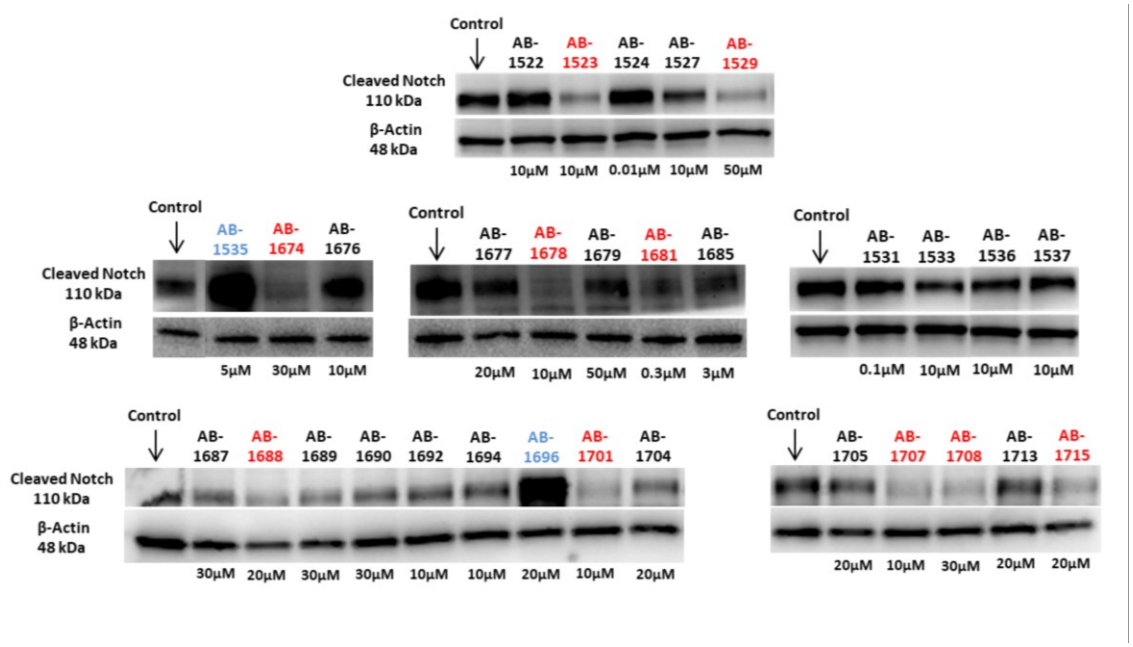

Figure 9. Western Blot data showing in red compounds which downregulate the intracellular protein levels of cleaved Notch1 and in blue, compounds which upregulate the intracellular protein levels of cleaved Notch1 in DND41 cells after 48h of exposure.

From the results, it is clear that twelve compounds affect the protein levels of Notch1 intracellular domain. In particular, compounds AB1523, 1529, 1674, 1678, 1681, 1688, 1701, 1707, 1708 and 1715 (in red) decreased the level of cleaved Notch1, while compounds AB1535 and 1696 enhance the level of intracellular Notch1 domain. In the first case, this means that compounds are blocking the release of Notch1 intracellular domain, thus they are inhibiting its activity. In the case of compounds highlighted in blue, the upregulation of Notch1 intracellular domain means that they are working as Notch activators.

Focusing our attention on compounds able to inhibit Notch1 activity and to further validate the influence on this signalling pathway, we decided to evaluate the reduction in expression of HES1, a direct Notch1 target gene by means of a Real-Time PCR (qPCR) analysis. The assay was performed with two cell lines (DND41 and ALL-SIL) by exposing cells at sub lethal doses (one-third GI_{50}) of selected compounds for 72 h and using GSI X, a commercially available γ-secretase inhibitor as reference compound.[37] Figure 10 shows compounds able to reduce the expression of HES1 mRNA levels.

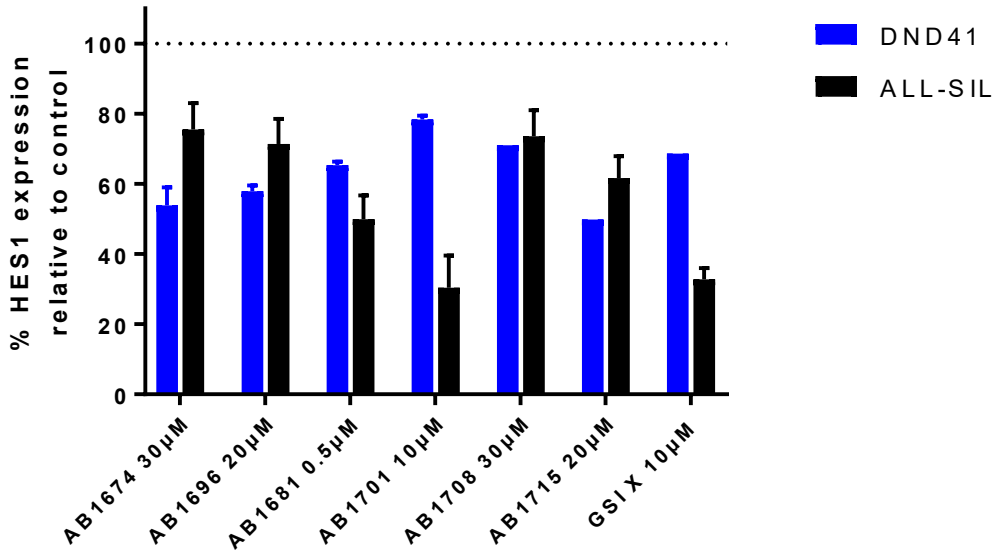

Figure 10. Real-Time PCR (qPCR) data showing the compounds which downregulated the mRNA levels of HES1, a direct Notch1 target gene. mRNAs derive from DND41 (blue) and ALL-SIL (black) treated for 72h with test compounds. The effect on HES1 levels of GSI X, a commercially available gamma secretase inhibitor was included as a reference.

From the above results, compounds AB1674, 1696, 1681, 1701, 1708 and 1715 are able to reduce the expression of HES1 mRNA. The compounds which showed the best activity profile are AB1681 and AB1701 that are able to reduce the expression of HES1 target gene in both DND41 and ALL-SIL cell lines, similarly to GSI X, the reference compound. In particular, AB1681 is able to reduce the production of HES1 mRNA by 50-40% at low micromolar concentration (0.5 μM, see Figure 10), while AB1701 is particularly effective in the case of ALL-SIL cell line, downregulating the levels of HES1 mRNA by 70% at low micromolar concentration (10 μM, see Figure 10). Taking together the results obtained by cytotoxic assays, western blot and PCR analysis, both AB1681 and AB1701 can be considered as hit compounds targeting Notch signalling pathway. Molecular structure of discovered hit compounds cannot be shown due to patentability reasons.

Conclusions and future works

Exploiting both Structure-based and Ligand-based approaches, a virtual screening study of commercially available drug-like compounds (over 3 million) was performed on the

Notch1-Jagged1 and NRR binding-sites of the Notch1 receptor. Selected compounds (n = 62) were examined for growth inhibition ability on four cancer cell lines using the MTT test. Thirty-one cytotoxic compounds were further evaluated by means of a Western Blot analysis and twelve of them demonstrated activity towards Notch1 pathway by reducing or increasing the protein levels of Notch1 intracellular domain. Focusing on Notch1 inhibition, six compounds were evaluated for their capacity to downregulate the expression of HES1 mRNA, a direct Notch1 target gene. Two compounds revealed promising activity, at low micromolar concentrations, in a comparable fashion with reference compound GSI X and could be identified as hit compounds.

In conclusion, two novel hit compounds were found to be effective inhibitor of Notch1 signalling pathway. The in-silico studies demonstrated to be predictive and reliable in finding new structures able to interfere with Notch1 pathway. More experiments are required to definitely confirm and validate the biological outcome of these two compounds. Anyway, these compounds represent a promising starting point for further hit-to-lead optimization studies, in order to improve potency, understand structure-activity relationships and determine specificity profile in the search for a new and better anticancer agent.

Experimental

Molecular Modelling

All the in-silico studies were performed on Vigle genie processor Intel®core i7-4790 CPU@ 3.60 GHz x 8 running Linux Ubuntu 16.04. Molecular Operating Environment (MOE) 2015.10, Maestro (Schrodinger Release 2016–1), LeadIT (version 2.1.8) and PLANTS were used as molecular modelling software. Shape-comparison screening was performed with ROCS version 3.2.1.4. Output conformations were ranked according to the Tanimoto combo score and the shape Tanimoto score. Three libraries of commercially available compounds were purchased from SPECS, Enamine and LifeChemicals in sdf format and prepared using the Conformational Search tool in MOE for the screening. Notch crystal structures were downloaded from Protein Data Bank (PDB) (http://www.rcsb.org/); PDB code 2VJ3 (Notch-1 EGF 11-13), PDB code 2VJ2 (Jagged1 DSL and EGF 1-3), PDB code 3ETO (Notch-1 NRR region) and prepared with the MOE Protein Preparation tools for the screening and docking studies.

Maestro Glide docking simulations for the virtual screening were performed using a grid: binding site centre of coordinates [22.527, -21.830, -27.731] for Notch1 NRR crystal and [-19.057, 13.570, -23.056] for Notch1-Jagged1 binding site. The docking results obtained were then re-docked using Glide SP. The results were submitted to a rescoring study using Glide XP, PLANTS and FlexX scoring functions. The docking output database was saved as mol2 file and the docking poses visually inspected for their binding mode in MOE. The visual inspection process, conducted as last step of the structure-based and the ligand-based virtual screening, was performed using MOE 2016.10. The docking poses of the compounds obtained from the *consensus* score procedure were evaluated considering the ability of a compound to occupy the binding site and to establish significant interactions with the target protein (H-bonds, π-π interactions, etc.); the coverage of different chemical scaffolds, discarding similar structural features; the chemical instability and presence of potential toxic groups (multiple halogen atoms, aldehyde, etc.).

Cell culture

Human leukemia cell lines were cultured in RPMI 1640 (Gibco) with 10% (DND41 and Jurkat) or 20% (ALL-SIL, TALL-1) FBS (Gibco), glutamine (2 mM/L; Gibco), penicillin (100 U/mL; Gibco), and streptomycin (100 mg/mL; Gibco) and were maintained at 37°C in a humidified atmosphere with 5% CO_2. All cell lines were periodically tested for mycoplasma infection.

***In vitro* treatments**

For the viability assay cells were treated at doses starting from 100 μM to 0.1 nM for 72 h. Cells were treated at sub lethal doses (one-third GI_{50}) for 48 h (protein assays, Western blots) or 72 h (gene expression analysis, Real Time PCR).

Cell viability assay

Cells were seeded in 96-well round bottom plates (Falcon Plymouth, England) and, following overnight incubation, treated for 72h with test compounds. Cell viability was assessed by MTT assay: 10 μL of MTT solution (3-(4,5-Dimethyl-2-thiazolyl)-2,5-diphenyl-2H-tetrazolium bromide, 5 mg/mL in Hank's salt solution) were added to each well and plates were incubated at 37°C in a humidified atmosphere with 5% CO_2. After 4 h, 100 μL of acid-isopropanol solution (0.08 M HCl in isopropanol) were added to each well and mixed thoroughly to dissolve the formazan crystals. The plate was read on a Victor (Perkin Elmer) plate reader using a test wavelength of 570 nm and a reference wavelength of 630 nm. Absorbances were corrected by subtracting the mean value

obtained from cell-free wells. Results were expressed as percentage of live cells setting at 100 % of vitality the absorbance obtained from the control wells (untreated cells).

Western Blot Analysis

After incubation, cells were collected, centrifuged, and washed two times with ice cold phosphate buffered saline (PBS). The pellet was then resuspended in lysis buffer. Cells were lysed on ice for 30 min and lysates were centrifuged at 15000 *g* at 4 °C for 10 min. The protein concentration in the supernatant was determined using the BCA protein assay reagents (Pierce, Italy). Equal amounts of protein (10 μg) were resolved using sodium dodecyl sulfate−polyacrylamide gel electrophoresis (SDS−PAGE) (7.5−15% acrylamide gels) and transferred to a PVDF Hybond-p membrane (GE Healthcare). Membranes were blocked with BSA 3% for 2h at room temperature. Membranes were then incubated with primary antibodies against cleaved Notch1 (rabbit, 1:1000, Cell Signaling), or β-actin (mouse, 1:10,000, Sigma) overnight at 4 °C. Membranes were next incubated with peroxidase-labeled goat antirabbit IgG (1:100000, Sigma) or peroxidase-labeled goat antimouse IgG (1:100000, Sigma) for 1 h. All membranes were visualized using ECL Advance (GE Healthcare) and exposed to Hyperfilm MP (GE Healthcare).

RNA isolation and reverse transcriptase polymerase chain reaction (RT-PCR)

Total cellular RNA from cell lines was extracted with TRIzol reagent (Invitrogen). RNA quality and quantity was controlled using Nanodrop spectrophotometer. Subsequently, 1 μg of total RNA was reversely transcribed using random hexamers and Superscript II (Invitrogen), according to the manufacturer's instructions.

Real-time quantitative RT-PCR (RQ-PCR) was performed on an Applied Biosystems 7900 HT Sequence Detection System using SYBR Green PCR Master Mixture Reagents (Applied Biosystems; Forest City, CA). Experiments were performed minimum as triplicate and used for relative quantity studies. Primers used for RQ-PCR analysis were for *HES1* (F: 5′-CTCTCTTCCCTCCGGACTCT-3′, R: 5′-AGGCGCAATCCAATATGAAC -3′).All expression values were normalized using expression of GAPDH as an endogenous control. The relative expression levels were calculated using the ddCt method.

Acknowledgements

Molecular modelling by M. Dal Prà, S. Ferla, A. Brancale and biological evaluation by R. Fatlum, R. Bortolozzi, G. Viola were supported by financial grants from Cardiff University, UK and University of Padova, Italy.

References

[1] E.R. Andersson, U. Lendahl, Therapeutic modulation of Notch signalling-are we there yet?, Nat. Rev. Drug Discov. 13 (2014) 357–378. doi:10.1038/nrd4252.

[2] R. Kumar, L. Juillerat-Jeanneret, D. Golshayan, Notch Antagonists: Potential Modulators of Cancer and Inflammatory Diseases, J. Med. Chem. 59 (2016) 7719–7737. doi:10.1021/acs.jmedchem.5b01516.

[3] L.W. Ellisen, J. Bird, D.C. West, A.L. Soreng, T.C. Reynolds, S.D. Smith, J. Sklar, TAN-1, the human homolog of the Drosophila Notch gene, is broken by chromosomal translocations in T lymphoblastic neoplasms, Cell. 66 (1991) 649–661. doi:10.1016/0092-8674(91)90111-B.

[4] T. Borggrefe, R. Liefke, Fine-tuning of the intracellular canonical Notch signaling pathway, Cell Cycle. 11 (2012) 264–276. doi:10.4161/cc.11.2.18995.

[5] A.P. Weng, J.M. Millholland, Y. Yashiro-Ohtani, M.L. Arcangeli, A. Lau, C. Wai, C. Del Bianco, C.G. Rodriguez, H. Sai, J. Tobias, Y. Li, M.S. Wolfe, C. Shachaf, D. Felsher, S.C. Blacklow, W.S. Pear, J.C. Aster, c-Myc is an important direct target of Notch1 in T-cell acute lymphoblastic leukemia/lymphoma, Genes Dev. 20 (2006) 2096–2109. doi:10.1101/gad.1450406.

[6] C. Lobry, P. Oh, M.R. Mansour, A. Thomas Look, I. Aifantis, Notch signaling: Switching an oncogene to a tumor suppressor, Blood. 123 (2014) 2451–2459. doi:10.1182/blood-2013-08-355818.

[7] I. Rebay, R.J. Fleming, R.G. Fehon, L. Cherbas, P. Cherbas, S. Artavanis-Tsakonas, Specific EGF repeats of Notch mediate interactions with Delta and serrate: Implications for notch as a multifunctional receptor, Cell. 67 (1991) 687–699. doi:10.1016/0092-8674(91)90064-6.

[8] V.C. Luca, B.C. Kim, C. Ge, S. Kakuda, D. Wu, M. Roein-Peikar, R.S. Haltiwanger, C. Zhu, T. Ha, K.C. Garcia, Notch-Jagged complex structure implicates a catch bond in tuning ligand sensitivity, Science (80-.). 355 (2017) 1320–1324. doi:10.1126/science.aaf9739.

[9] V.C. Luca, K.M. Jude, N.W. Pierce, M. V. Nachury, S. Fischer, K.C. Garcia, Structural basis for Notch1 engagement of Delta-like 4, Science (80-.). 347 (2015) 847–853. doi:10.1126/science.1261093.

[10] C.R. Chillakuri, D. Sheppard, S.M. Lea, P.A. Handford, Notch receptor-ligand binding and activation: Insights from molecular studies, Semin. Cell Dev. Biol. 23 (2012) 421–428. doi:10.1016/j.semcdb.2012.01.009.

[11] W.R. Gordon, M. Roy, D. Vardar-Ulu, M. Garfinkel, M.R. Mansour, J.C. Aster, S.C. Blacklow, Structure of the Notch1-negative regulatory region: Implications for normal activation and pathogenic signaling in T-ALL, Blood. 113 (2009) 4381–4390. doi:10.1182/blood-2008-08-174748.

[12] J.C. Aster, W.S. Pear, S.C. Blacklow, The Varied Roles of Notch in Cancer, Annu. Rev. Pathol. Mech. Dis. 12 (2017) 245–275. doi:10.1146/annurev-pathol-052016-100127.

[13] M.J. Malecki, C. Sanchez-Irizarry, J.L. Mitchell, G. Histen, M.L. Xu, J.C. Aster, S.C. Blacklow, Leukemia-Associated Mutations within the NOTCH1 Heterodimerization Domain Fall into at Least Two Distinct Mechanistic Classes, Mol. Cell. Biol. 26 (2006) 4642–4651. doi:10.1128/MCB.01655-05.

[14] M. Locatelli, G. Curigliano, Notch inhibitors and their role in the treatment of triple negative breast cancer: Promises and failures, Curr. Opin. Oncol. 29 (2017) 411–427. doi:10.1097/CCO.0000000000000406.

[15] H. Ling, J.R. Sylvestre, P. Jolicoeur, Notch1-induced mammary tumor development is cyclin D1-dependent and correlates with expansion of pre-malignant multipotent duct-limited progenitors, Oncogene. 29 (2010) 4543–4554. doi:10.1038/onc.2010.186.

[16] V.M. Sharma, J.A. Calvo, K.M. Draheim, L.A. Cunningham, N. Hermance, L. Beverly, V. Krishnamoorthy, M. Bhasin, A.J. Capobianco, M.A. Kelliher, Notch1 Contributes to Mouse T-Cell Leukemia by Directly Inducing the Expression of c-myc, Mol. Cell. Biol. 26 (2006) 8022–8031. doi:10.1128/MCB.01091-06.

[17] E. Calzavara, R. Chiaramonte, D. Cesana, A. Basile, G. V. Sherbet, P. Comi, Reciprocal regulation of Notch and PI3K/Akt signalling in T-ALL cells *in vitro*, J. Cell. Biochem. 103 (2008) 1405–1412. doi:10.1002/jcb.21527.

[18] J. Murata, T. Ohtsuka, A. Tokunaga, S. Nishiike, H. Inohara, H. Okano, R. Kageyama, Notch-Hes1 pathway contributes to the cochlear prosensory formation potentially through the transcriptional down-regulation of p27Kip1, J. Neurosci. Res. 87 (2009) 3521–3534. doi:10.1002/jnr.22169.

[19] Y. Chen, D. Li, H. Liu, H. Xu, H. Zheng, F. Qian, W. Li, C. Zhao, Z. Wang, X. Wang, Notch-1 signaling facilitates survivin expression in human non-small cell

lung cancer cells, Cancer Biol. Ther. 11 (2011) 14–21. doi:10.4161/cbt.11.1.13730.

[20] C. Mailhos, U. Modlich, J. Lewis, A. Harris, R. Bicknell, D. Ish-Horowicz, Delta4, an endothelial specific Notch ligand expressed at sites of physiological and tumor angiogenesis, Differentiation. 69 (2001) 135–144. doi:10.1046/j.1432-0436.2001.690207.x.

[21] J. Sjölund, M. Johansson, S. Manna, C. Norin, A. Pietras, S. Beckman, E. Nilsson, B. Ljungberg, H. Axelson, Suppression of renal cell carcinoma growth by inhibition of Notch signaling *in vitro* and *in vivo*, J. Clin. Invest. 118 (2008) 217–228. doi:10.1172/JCI32086.

[22] I. Espinoza, L. Miele, Deadly crosstalk: Notch signaling at the intersection of EMT and cancer stem cells, Cancer Lett. 341 (2013) 41–45. doi:10.1016/j.canlet.2013.08.027.

[23] Z. Wang, Y. Li, A. Ahmad, A.S. Azmi, S. Banerjee, D. Kong, F.H. Sarkar, Targeting Notch signaling pathway to overcome drug resistance for cancer therapy, Biochim. Biophys. Acta - Rev. Cancer. 1806 (2010) 258–267. doi:10.1016/j.bbcan.2010.06.001.

[24] A.P. Weng, A.A. Ferrando, W. Lee, J.P. Morris IV, L.B. Silverman, C. Sanchez-Irizarry, S.C. Blacklow, A.T. Look, J.C. Aster, Activating mutations of NOTCH1 in human T cell acute lymphoblastic leukemia, Science (80-.). 306 (2004) 269–271. doi:10.1126/science.1102160.

[25] A. Acar, B.M. Simões, R.B. Clarke, K. Brennan, A Role for Notch Signalling in Breast Cancer and Endocrine Resistance, Stem Cells Int. 2016 (2016) 2498764. doi:10.1155/2016/2498764.

[26] Q. Ye, J. Jiang, G. Zhan, W. Yan, L. Huang, Y. Hu, H. Su, Q. Tong, M. Yue, H. Li, G. Yao, Y. Zhang, H. Liu, Small molecule activation of NOTCH signaling inhibits acute myeloid leukemia, Sci. Rep. 6 (2016) 26510. doi:10.1038/srep26510.

[27] D. Nassar, M. Latil, B. Boeckx, D. Lambrechts, C. Blanpain, Genomic landscape of carcinogen-induced and genetically induced mouse skin squamous cell carcinoma, Nat. Med. 21 (2015) 946–954. doi:10.1038/nm.3878.

[28] Molecular Operating Environment (MOE), 2016.10; Chemical Computing Group ULC, 1010 Sherbooke St. West, Suite #910, Montreal, QC, Canada, H3A 2R7, 2017.

[29] http://www.specs.net

[30] Schrödinger Release 2016-1: MS Jaguar, Schrödinger, LLC, New York, NY, 2016.

[31] B. Kramer, M. Rarey, T. Lengauer, Evaluation of the FlexX incremental construction algorithm for protein- ligand docking, Proteins Struct. Funct. Genet. 37 (1999) 228–241. doi:10.1002/(SICI)1097-0134(19991101)37:2<228:AID-PROT8>3.0.CO;2-8.

[32] Korb, O., Stutzle, T. & Exner, T. E. PLANTS: Application of ant colony optimization to structure-based drug design. In: Ant Colony Optimization and Swarm Intelligence, 5th International Workshop, ANTS. Brussels, Belgium, Springer Berlin Heidelberg, pp, 245‑258 September 4‑7, 2006.

[33] https://www.enamine.net

[34] http://www.lifechemicals.com

[35] OpenEye Scientific Software, Santa Fe, NM. www.eyesopen.com

[36] L. Luistro, W. He, M. Smith, K. Packman, M. Vilenchik, D. Carvajal, J. Roberts, J. Cai, W. Berkofsky-Fessler, H. Hilton, M. Linn, A. Flohr, R. Jakob-Røtne, H. Jacobsen, K. Glenn, D. Heimbrook, J.F. Boylan, Preclinical profile of a potent γ-secretase inhibitor targeting notch signaling with *in vivo* efficacy and pharmacodynamic properties, Cancer Res. 69 (2009) 7672–7680. doi:10.1158/0008-5472.CAN-09-1843.

[37] A. Geling, H. Steiner, M. Willem, L. Bally-Cuif, C. Haass, A γ-secretase inhibitor blocks Notch signaling *in vivo* and causes a severe neurogenic phenotype in zebrafish, EMBO Rep. 3 (2002) 688–694. doi:10.1093/embo-reports/kvf124.

CHAPTER 5

Rational design and synthesis of 2,3,4,9-tetrahydro-1H-β-carboline derivatives as trypanothione reductase inhibitors

Synopsis

The neglected tropical Chagas disease, caused by the protozoan parasite *Trypanosoma cruzi*, is a relevant social and economic problem in many Latin American countries. The current treatment and control of Chagas disease depend on the chemotherapeutic agents benznidazole and nifurtimox. However, they have limited efficacy and produce severe side effects. Trypanothione disulphide-reductase (TryR), the glutathione reductase analog of *T.cruzi,* is the only parasite's defense toward oxidative damage caused by benznidazole and nifurtimox and represents a new promising pharmacological target. A structure-based virtual screening was performed with the TryR protein structure, and again the β-carboline nucleus was confirmed as a key scaffold for the rational design of new potential inhibitors of TryR. Some derivatives of 2,3,4,9-tetrahydro-1*H*-β-carboline-3-carboxylate acid were proposed as good candidates to inhibit TryR. Accordingly, the new derivatives exhibit structural features such as long hydrophobic chains bound to pH-dependent or permanent positively charged groups, represented by branched or bulky quaternary alkyl amines. The synthesized compounds are currently under biological investigation at the UMCE, Santiago (Chile).

Introduction

Recognized by WHO as one of the world's 13 most neglected tropical diseases, Chagas disease, also known as American trypanosomiasis, is a relevant social and economic problem in many Latin American countries. It was discovered in 1909 by the physician Carlos Chagas and nowadays is considered endemic in 21 countries, with a number of infection cases between 6 and 8 million, and a consequent number of deaths of approximately 12,000 per year worldwide.[1] Furthermore, it results in the largest burden of disease in disability-adjusted-life-years of any parasitic disease in the Americas and the

morbidity and mortality associated with this infection produce an astonishing annual global economic burden of 7.2 billion US $.[2]

Chagas disease originally stroke the poorest sections of the population of the rural areas of Southern and Central America, however, the recent influx of immigrants from these countries has meant that Chagas disease is becoming an important health issue also in the USA, Canada and in many parts of Europe.[3] From the etiopathological point of view, Chagas disease, is caused by the protozoan parasite *Trypanosoma cruzi*. *T.cruzi* is transmitted to human beings and to animals mainly by bloodsucking reduviid bugs of the Triatominae subfamily, which in turn becomes infected by feeding on the blood of infected people or animals. Other mechanisms of transmission are transfusion of whole blood or blood derivatives, congenital transmission in children from chagasic mothers and oral transmission through contaminated food in some cases.[4]

Phases of infection and clinical manifestations

In human, Chagas disease occurs in two main stages:

1. Acute phase: symptoms appear 1-2 weeks after the infection and last for 4-8 weeks. Acute phase is in general asymptomatic or with self-limiting states of illness, such as fever, muscle pain, nausea and vomit. In the case of vector-borne transmission a local swelling on the skin, called *chagoma*, or a periorbital swelling, namely *Romaña sign*, can be recognized during the physical examination of the patient. They both represents the site of entrance of the parasite on the body.[3] Serious manifestations, such as myocarditis or meningoencephalitis have a high risk of death but are rare.[5] In fact, in most of the cases, the disease resolves spontaneously without any treatment, but for the 30-40% of infected people, the acute phase can turn chronic.

2. Chronic phase: usually developed 10-30 years after the initial infection, it targets specifically two main sites: heart and digestive system. Because of this reason it can be classified in different form (digestive, cardiac or cardio-digestive), depending on the major clinical manifestation. The digestive form is characterized mainly by gastrointestinal dysfunctions, such as megacolon, megaesophagus or both, but the cardiac form is the most frequent and the most dangerous one. Affected patients show a chronic inflammatory process that involves all heart chambers and conduction system damage.[6] The typical clinical manifestations

are related to heart rhythm abnormalities (bradyarrhythmia and tachyarrhythmia), high-degree heart block, pulmonary and systemic thromboembolic phenomena which can exasperate in progressive dilated cardiomyopathy with congestive heart failure, and a considerable risk of death. The association of megacolon or megaesophagus with cardiac manifestation defines the cardio-digestive form.[3]

Current treatment

The drugs currently used to treat Chagas disease were discovered to have anti-*T.cruzi* activity over four decades ago. They are nitroheterocycles compounds: benznidazole, a nitro-imidazole derivative and nifurtimox, a nitrofuran derivative[7].

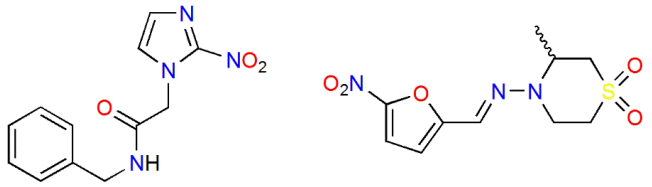

Benznidazole Nifurtimox

Figure 1. Molecular structures of benznidazole and nifurtimox

The recommended dose in the acute phase is 8–10 mg/kg/day for nifurtimox and 5 mg/kg/day for benznidazole. The average duration of treatment is about 60 days, but when chronic disease is reactivated, such as in immunocompromised patients, treatment can last 5 months or longer.[8]

The two compounds behave as prodrugs because to exert cytotoxic activity they should be metabolized by enzymes of the nitroreductases class (NTRs). Their actual mechanism of action has been debated for long time, and it still has not been completely clarified. Both drugs act through the formation of free radicals or electrophilic metabolites, which damage the parasite's cells. The reactivity center is the nitro group which is reduced by *T. cruzi* cytochrome P450-related nitroreductases. In the case of nifurtimox, the generated free radicals may undergo redox cycling with oxygen and then H_2O_2 can be produced by the action of superoxide dismutase. In this way, the obtained free radicals and electrophilic metabolites can damage macromolecules inside the cells. On the other hand, benznidazole activity seems not to be dependent on oxygen radicals' production, but instead its reduced metabolites may be involved in covalent binding of macromolecules.[9]

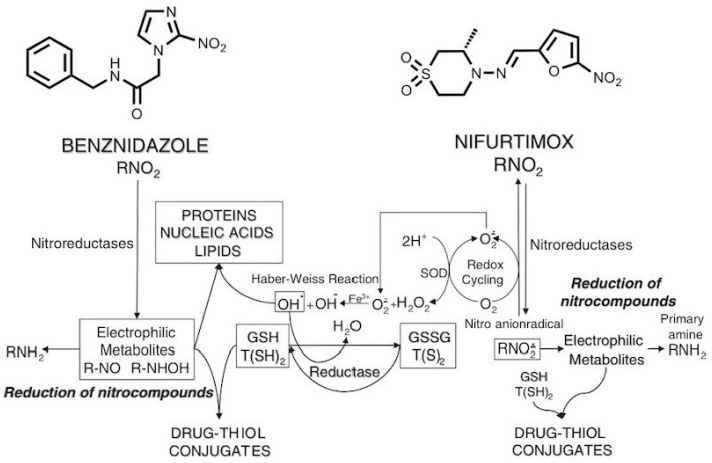

Figure 2. General benznidazole and nifurtimox mechanisms of action

Asides from the exact mechanism of action, nifurtimox and benznidazole are trypanocidal to all forms of the parasite, but because of its better tolerance, benznidazole is considered as the first-line treatment.[10] The two drugs are effectively used to treat the acute phase of Chagas disease, however the use in the chronic phase remains controversial and still raises perplexities.[11] The major problem is related to their modest or sometimes very low antiparasitic activity in the chronic form, resulting in 80% of not parasitologically cured patients.[12] Furthermore, chemotherapeutic efficiency varies in patients coming from different geographic areas highlighting the fact that different strains of *T. cruzi* have different response to the drug. Toxicities and side effects are not negligible and frequently force the physician to stop the treatment. The most frequent undesirable effects are anorexia, nausea, vomiting and nervous problems that can also be aggravated with other patient conditions such as immunodeficiency and advanced age. With nifurtimox the central nervous system side effects are emphasized, while with benznidazole, skin manifestations are considerable, often combined with lymphadenopathy, articular and muscular pain. Also, polyneuropathy, paraesthesia and polyneuritis of peripheral nerves are reported.[11] Recently, some antifungal agents such as posaconazole and ravuconazole have been tested as clinical alternatives to benznidazole. These agents are well-known and should cause less side effects, but the efficacy results from different clinical trials were not satisfactory.[13] Thus, there is an urgent need to discover new compounds as starting point for the development of potent drugs with less side effects, preferably interfering with unique essential pathways of this parasite.

Trypanothione reductase as drug target for *T.cruzi* infection

Several studies have been conducted to discover new molecular targets to develop specific antiparasitic drugs. The main pursued concept was the exploitation of metabolic differences between the pathogen and the host. In particular, the target should be essential for the survival of the parasite and should have no counterpart in the host or should be sufficiently different from its counterpart in the host to allow selective inhibition.

In the case of Trypanosomatidae, one of the most important distinctions regards the redox defence system. In facts, in mammalians, the defence towards oxidative stress is based on the glutathione/Glutathione Reductase (GR) couple, which in trypanosomatids is replaced by an analogous but different system which involves the flavoenzyme Trypanothione Reductase (TryR) and the substrate trypanothione.[14] Trypanothione has strong structural similarities with glutathione, in fact it is constituted by the same amino acids (γ-glutamic acid, cysteine and glycine), but the two small peptides in trypanothione are also linked by a spermidine cross-link between the two glycyl carboxyl groups, that confers it different physico-chemical properties and specificity.

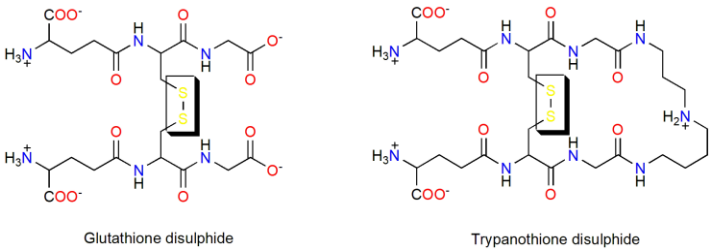

Figure 3. Molecular structures of Glutathione disulphide and Trypanothione disulphide

From a physiological point of view, TryR has the role to maintain an intracellular reducing environment by scavenging free radicals and reactive oxygen species produced by the host during *T.cruzi* infection.[15] In particular, TryR catalyses the NADPH-dependent reduction of trypanothione disulphide to the dithiol trypanothione [bis(glutathionyl)spermidine].

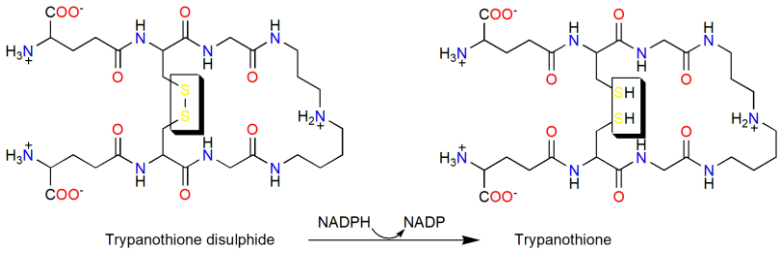

Figure 4. Reaction catalyzed by Trypanothione Reductase

Human GR and TryR are both flavin-containing disulphide oxidoreductases and they share about 30% sequence identity. The interesting fact is that the key residues involved in catalysis are conserved (Cys 58 and 63 in GR; Cys 53 and 58 in TryR) but each enzyme is specific for its cognate substrate and this suggests the chance to inhibit the parasite enzyme without affecting the host GR.[15] In particular, in GR a group of positive residues (Arg 37, Arg 38 and Arg 347) create a positive charged site able to properly interact with the negatively charged carboxylate groups of glutathione (see Figure 5). The corresponding residues in TryR are Leu 18, Trp 22, Tyr 111 and Met 114 which are mainly involved in hydrophobic interactions with both glycyl carboxamide groups of Trypanothione disulphide. Additionally, mutagenesis studies suggested an interaction of the hydrophobic region of spermidine chain of Trypanothione disulphide with Trp 22, besides a negatively charged active site that binds to the extra protonated secondary amino group present in the spermidine component of Trypanothione, which promotes significant steric and electrostatic difference in relation to GR.[16]

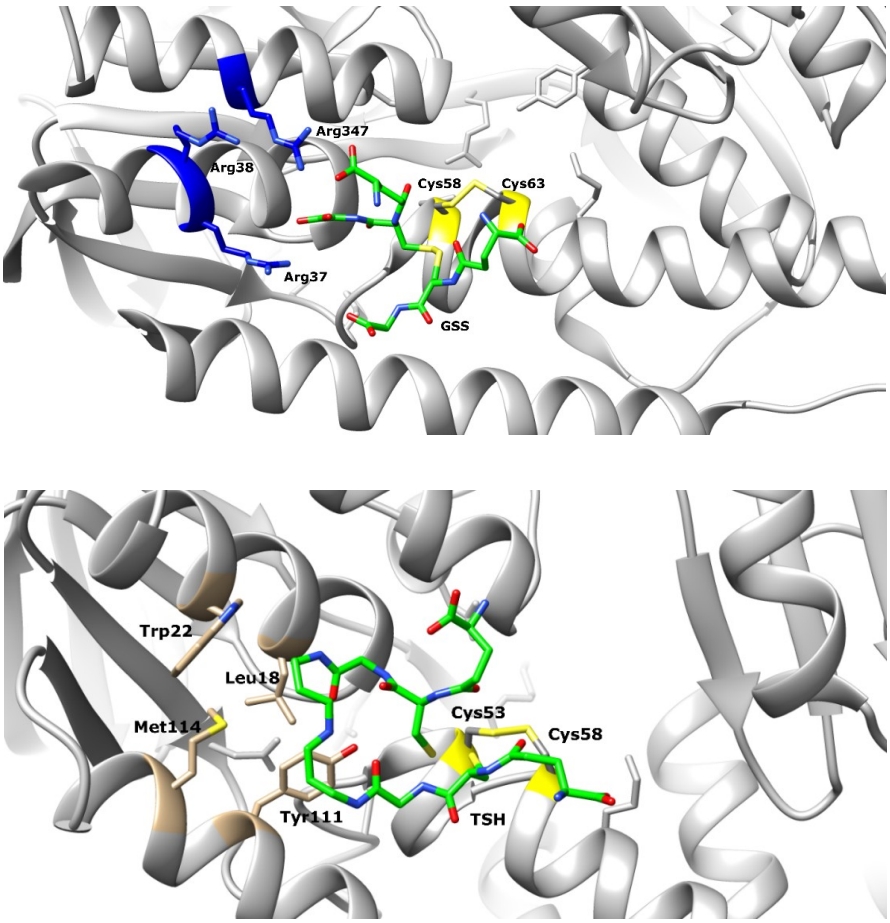

Figure 5. a) Crystallographic structure of oxidized Glutathione GSS (in green) in complex with GR (PDB code 1GRA). The catalytic couple Cys 58 and Cys 63 (in yellow) and the basic residues Arg 37, Arg 38 and

Arg 347 (in blue) are shown. b) Crystallographic structure of Trypanothione disulfide TSH (in green) in complex with TryR (PDB code 1BZL). The catalytic couple Cys 53 and Cys 58 (in yellow) and the residues Leu 18, Trp 22, Tyr 111 and Met 114 (in white) are shown.

Moreover, it has been demonstrated that TryR is essential for survival of *T. cruzi* both *in vitro* and in the human host.[17] All together these facts validate TryR and trypanothione metabolism as a target for structure-based drug design of molecules able to interfere with its activity. These new structures have the potentialities to exert trypanocidal activity by their own right or at least may be capable of increasing the susceptibility of *T.cruzi* toward anti-Chagas drugs in a synergistic way, allowing lower doses and probably major success in treating the disease.

State of the art

The first rationally designed non-peptide inhibitors are represented by the class of the tricyclic phenothiazines and related structures. These compounds have been demonstrated to act as competitive inhibitors of TryR and some of them are commercial drugs such as chlorpromazine, trifluopromazine, thioridazine and promethazine.

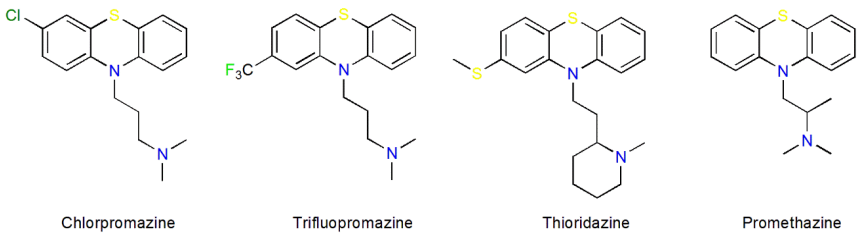

Figure 6. Structures of known phenothiazines inhibitors of TryR

These molecules are all characterised by the same structural features: a tricyclic scaffold represented by the phenothiazine core and an alkyl amino group. Some authors suggested that these compounds bound to the enzyme with their tricyclic moiety lodged against the hydrophobic surface formed by Trp 22 and Met 114, with the aminopropyl side chain protruding towards Glu 466 and Glu 467.[18] Additional modelling studies have indicated the possibility to enhance the affinity of these compounds by exploiting another hydrophobic cavity near the two glutamic residues. This site was called Z-site and is not implicated in trypanothione disulphide binding. The main residues responsible for its nature are Phe 396, Pro 398 and Leu 399. Thus, the consequent step was trying to gain additional binding interactions through Z-site and to introduce a permanent positive

charge able to interact with Glu 466 and/or Glu 467. The results obtained by enzyme inhibition assays reported in this work, showed an improved TryR inhibition of about 20-fold compared to chlorpromazine, for the compounds with quaternary ammonium salts with a benzyl substituent. In the same study, it has also been suggested that the positive charged group helps in the specificity of interaction with TryR over GR.[19]

Although tricyclic compounds have been extensively studied for their capacity to inhibit TryR, the study of molecules with a β-carboline scaffold remains underexplored, and only a few examples have been reported in the literature.[20-22] Thus, the aim of this work was to use the knowledge about the structure and interaction mode of reported TryR inhibitors and to exploit it by designing new β-carboline inhibitors.

Results and Discussion

Molecular modelling

A pharmacophore model[23]

For the generation of a TryR inhibitors pharmacophore model, a library of TryR inhibitor reported in the literature was constructed using the information available in the ChEMBL database.[24] The model was built by using the structures of the eight TryR inhibitors with the lowest known IC_{50} using the flexible alignment function implemented in MOE. The obtained model is characterised by six features (F1 to F6): F1-F4 were considered to be essential, while F5 and F6 were judged as desirable. As reported in Figure 7, the pharmacophore model features are the following: F1, aromatic ring centre, F2 and F3, aliphatic hydrophobic centre, F4, cationic heavy atoms and hydrogen bond donor, F5, aliphatic hydrophobic centre and F6, aromatic ring centre or aliphatic hydrophobic centre.

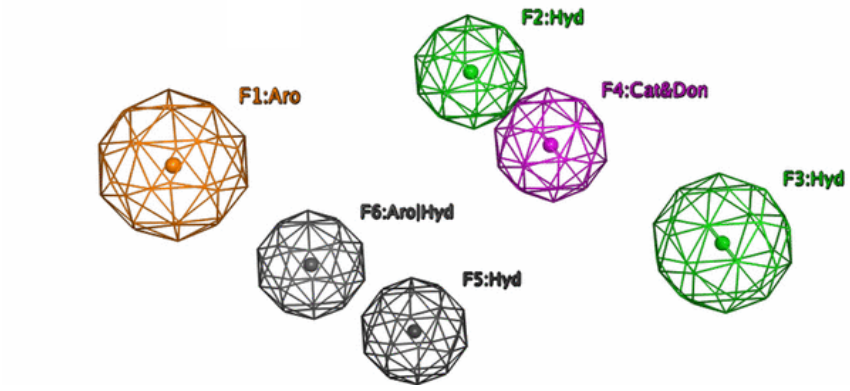

Figure 7. Pharmacophore spheres: F1, aromatic ring centre (Aro); F2, F3 and F5, aliphatic hydrophobic

centre (Hyd); F4, cationic heavy atoms (Cat) and hydrogen bond donor (Don); F6, aromatic ring centre (Aro) or aliphatic hydrophobic centre (Hyd). The radiuses of the spherical regions were adjusted manually: F1 and F3 were adjusted to 1.5 Å, while F2, F4, F5 and F6 were adjusted to 1.2 Å

This model was used for the selection of new β-carboline derivatives, after the virtual screening and docking studies, to be proposed as new TryR inhibitors.

Virtual screening and chemical space analysis

A molecular modelling study was completed with the aim to explore the chemical space of commercial β-carboline derivatives versus known TryR inhibitors. A virtual library of amides derived from 2,3,4,9-tetrahydro-1H-β-carboline-3-carboxylate acid (THBCA) was designed and generated by acylating selected nucleophiles standards, purchased by Sigma-Aldrich, with THBCA, employing the software Reactor.[25]

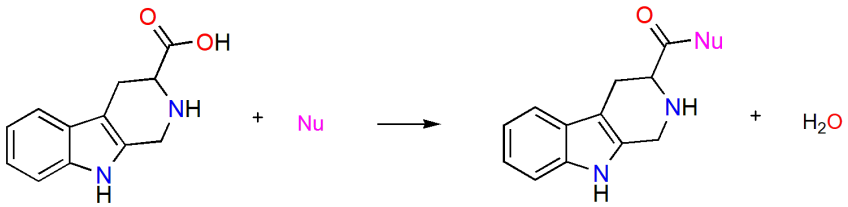

Figure 8. Acylation of THBCA with nucleophiles standard

The obtained library was standardised using the protocol already described by Becerra et all[23] and explored using drug-like filters (Ghose Filter, Veber Filter and Muegge Filter)[26-28] and a lead-like filter[29] implemented in Instant Jchem. Then all the structure were clustered using chemical fingerprints, similarity matrices and a Tanimoto Combo of 0.70, which are all implemented in MOE.[30]

A virtual screening study was performed on the structure of TryR (PDB code 1AOG), using an optimized virtual screening method for computer-aided discovery of new TryR inhibitors[23] by employing the AutoDock 4.2 software.[31] The obtained binding energies were computed using a consensus score study which consider DSX-Online score function[32] and ASE and Affinity dG score functions implemented in MOE.[30]

This consensus scoring function was combined with the conformational search method implemented in Autodock-4.2.[31] Only the best scored conformation of each β-carboline derivative was considered for ranking, obtaining a small library of new potential β-carboline inhibitors of TryR. The best compounds were compared to the pharmacophore model and selected for the synthesis. Structurally speaking, new derivatives exhibit

common structural features with known TryR inhibitors, for instance, long hydrophobic chains bound to positively charged groups, represented by branched or bulky quaternary amines. In Figure 9, the general structures of compounds **4** and **34** (panel A) and of derivatives **23**, **24**, **28-30** (panel B) are depicted. The first two derivatives only differ for the tricyclic nucleus: tetrahydro-β-carboline scaffold for **4** and β-carboline scaffold for **34**, while both bear the di-octylamine lateral chain. Regarding the other five derivatives **23**, **24**, **28-30** the tetrahydro-β-carboline scaffold is always present but it is differently decorated with various di-amino chains.

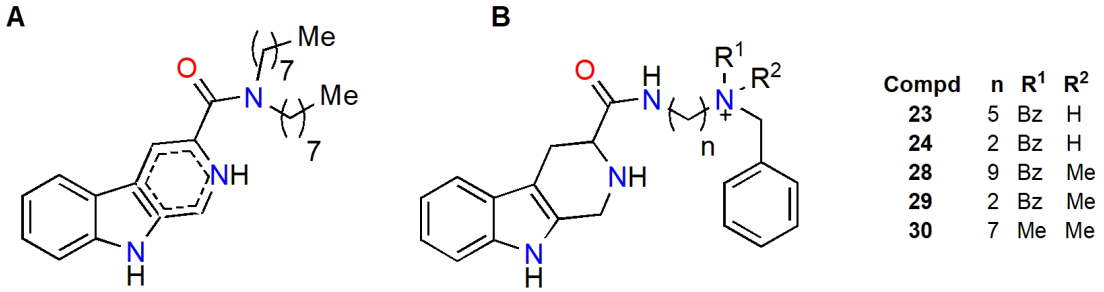

Figure 9. General structures of compounds **4** and **34** (A) and of derivatives **23**, **24**, **28-30** (B)

The chemical space (CS) for the small library of selected new THBCA derivatives was generated and compared to the one of commercial β-carboline derivatives and known TryR inhibitors using MACCS Structural Keys (MACCS) as chemical fingerprint, as already described by Becerra et all.[23] A structural similarity analysis was performed using the MACCS chemical fingerprints and the Tanimoto Coefficient (TC) implemented in MOE. Then, a similarity matrix for the studied compounds was calculated, and the R Software was applied to conduct a Principal Component Analysis (PCA).[33] The obtained results showed that both commercial and designed β-carboline derivatives contribute to extend the chemical space of TryR inhibitors already described in literature.

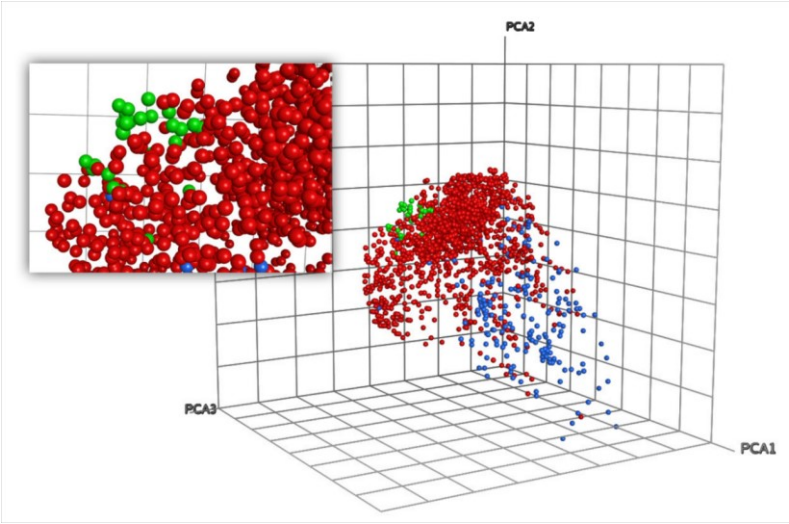

Figure 10. Representation of the chemical space of TryR inhibitors (blue color), commercial β-carboline derivatives (red color) and designed β-carboline derivatives (green color). Chemical space using MACCS fingerprint with the Tanimoto coefficient as similarity metrics.

Figure 10 shows the position of the chemical space occupied by TryR inhibitors obtained from literature (blue colour), commercial β-carboline derivatives (red colour) and designed β-carboline derivatives (green colour). This displays that there is no significant overlapping of the areas, indicating that the designed β-carboline derivatives have topological features that have not been yet considered in TryR inhibitors reported. Therefore, the study of new β-carboline derivatives, as potential inhibitors of TryR, would allow the exploration of new areas of chemical space, currently not considered in this topic.

Chemical synthesis

For the synthesis of new β-carboline derivatives we followed a multistep convergent pathway. The preparation of tetrahydro-*β*-carboline scaffold was performed by classical Pictet-Spengler reaction. In Scheme 1 starting from commercial tryptophan, the final *N*-dioctyl-amide derivative **4** was obtained in good yields. The starting amino acid was submitted to Pictet-Spengler reaction by treatment with formaldehyde in water solution, obtaining the tricyclic structure in excellent yield (95%). The amino group was then protected with carboxybenzyl group, which proved to be the best in terms of yields and ease of workup, by using benzyl chloroformate and sodium carbonate in a mixture 1:1 water/THF for 16 h at room temperature, giving the desired product in very good yield

(85%). Following a previously described procedure[34] the obtained compound **2** was then submitted to amidic coupling reaction by using commercial di-octylamine in presence of the coupling reagents HOBt and EDC, by treatment with Et_3N in DMF at room temperature overnight. The final derivative **4** was obtained by removal of CBz protecting group with a catalytic hydrogenation reaction and precipitation by treatment with concentrated hydrochloric acid.

Scheme 1. Synthesis of compound **4**

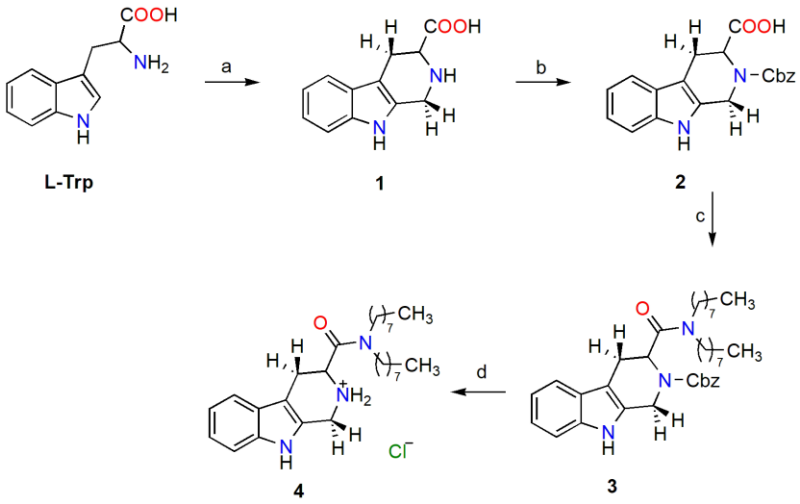

Reagents and conditions: a. HCHO, $NaHCO_3$, H_2O, rt 2h, ref. 3h, 95%; b. CbzCl, Na_2CO_3, H_2O/THF 1:1, rt, 16h, 83%; c. Di-N-Octylamine, HOBt, EDC, Et_3N, DMF, rt, 16h, 70%; d. H_2, Pd/C 10%, EtOAc, rt, 16h, 56%.

In Scheme 2, part A and B respectively, the preparation of dibenzyl- and methyl-benzyl-diamino derivatives **11-13** and **17** is described. Compound **5** was obtained by reacting commercial 1,8-dibromoottane with sodium cyanide in DMF for 2 h.[35] The bromo-cyanide derivatives **5-7** were submitted to substitution reaction with dibenzylamine in presence of K_2CO_3, KI in DMF at 80°C for 16 h,[36] while in the case of compound **16**, methyl-benzyl amine **15** was firstly prepared in a two-steps procedure by reacting commercial benzaldehyde with methylamine and $NaBH_4$,[37] and then substitution reaction was performed as reported for compounds **8-10**. The free amine derivatives **11-13** and **17** were obtained by treating compounds **8-10** and **16** with $LiAlH_4$ in Et_2O or THF for 2h.[38]

Scheme 2A. Synthesis of dibenzyl-diamino derivatives **11-13**

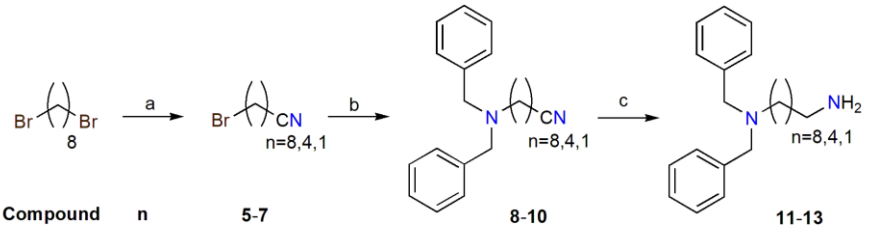

Compound	n	5-7	8-10	11-13
5, 8, 11	8			
6, 9, 12	4			
7, 10, 13	1			

Reagents and conditions: a. NaCN, DMF, 35°C, 2h, 90%; b. K_2CO_3, KI, DMF, 80°C, 18h, 95-65%; c. $LiAlH_4$, Et_2O, rt, 2h, 88-75%.

Scheme 2B. Synthesis of benzyl-methyl-diamino derivative **17**

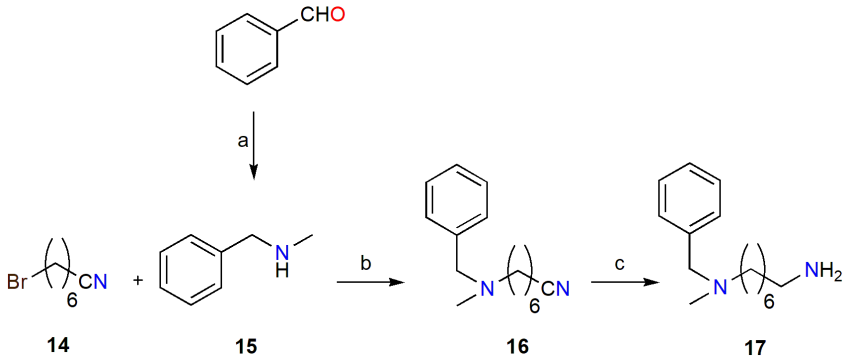

14 **15** **16** **17**

Reagents and conditions: a.1.$MeNH_2$ 40%, MeOH, rt, 15 min. 2. $NaBH_4$, rt, 1h, 88%; b. K_2CO_3, KI, DMF, 80°C, 18h, 82%; c. $LiAlH_4$, THF, rt, 2h, 95%.

In Scheme 3 the synthesis of final derivatives **23**, **24** and **28-30** is described. Firstly, compound **1** was protected at the amino group with BOC by treatment with di-tert-butyl dicarbonate and Na_2CO_3 to obtain compound **18** and then submitted to amidic coupling reaction with previously synthesised amines **11-13** and **17**.[34] The reaction was performed with HOBt, EDC and Et_3N in DMF for 16 h at room temperature leading to the amidic derivatives **19-22** in good yields (55-87%).

Compounds **20** and **21** were then submitted to acidic treatment by using gaseous HCl in ethanol to deprotect the amino group and retrieve the final derivatives **23** and **24** as hydrochloride salts. Derivatives **19**, **21** and **22** were methylated at the amino group in the lateral chain, using methyl iodide to obtain ammonium salts **25-27** in good yields (62-77%).[39] This methylated derivatives were then reacted for the deprotection of the amino

group using the same conditions reported for compounds **23** and **24**, furnishing compounds **28-30** as hydrochloride salts.

Scheme 3. Synthesis of tetrahydro-β-carboline derivatives **23**, **24**, **28-30**

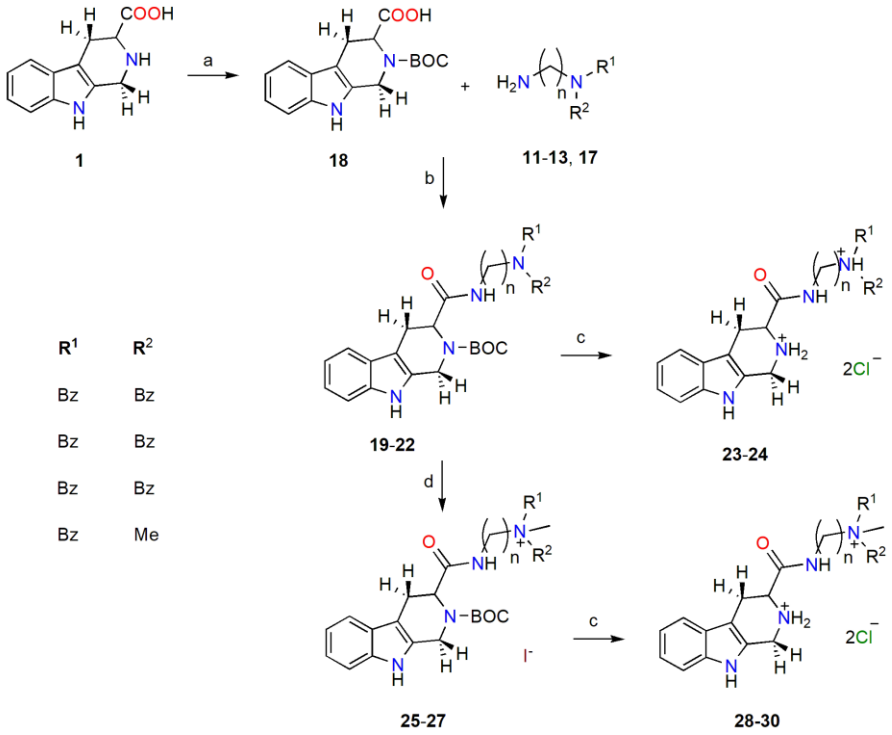

Compound	n	R^1	R^2
11; **19**; **25**; **28**	9	Bz	Bz
12; **20**; **23**	5	Bz	Bz
13; **21**; **24**; **26**; **29**	2	Bz	Bz
17; **22**; **27**; **30**	7	Bz	Me

Reagents and conditions: a. BOC_2O, Na_2CO_3, H_2O, THF, rt, 16h, 73%; b. HOBt, EDC, Et_3N, DMF, rt, 16h, 87-55%; c. HCl, EtOH, rt, 16h, 92-84%; d. CH_3I, rt, 18h, 62-77%

In the last scheme (Scheme 4), the synthesis of the fully aromatic carboline derivative **34** is described. Firstly, already synthesised compound **1** was transformed into the ester derivative **31** by treatment with ethanol and concentrated HCl.[40] The obtained ester was submitted to oxidation reaction employing MnO_2 in toluene for 24 h at reflux to retrieve the carboline derivative **32**.[41] The ethyl ester moiety was then hydrolysed by alkaline treatment,[40] and the carboxylic acid **33** coupled with commercial di-octylamine using HOBt and EDC as coupling reagents in presence of Et_3N in DMF for 16 h at room temperature.[34] Final derivative **34** was obtained in good yield (56%).

Scheme 4. Synthesis of derivative **34**

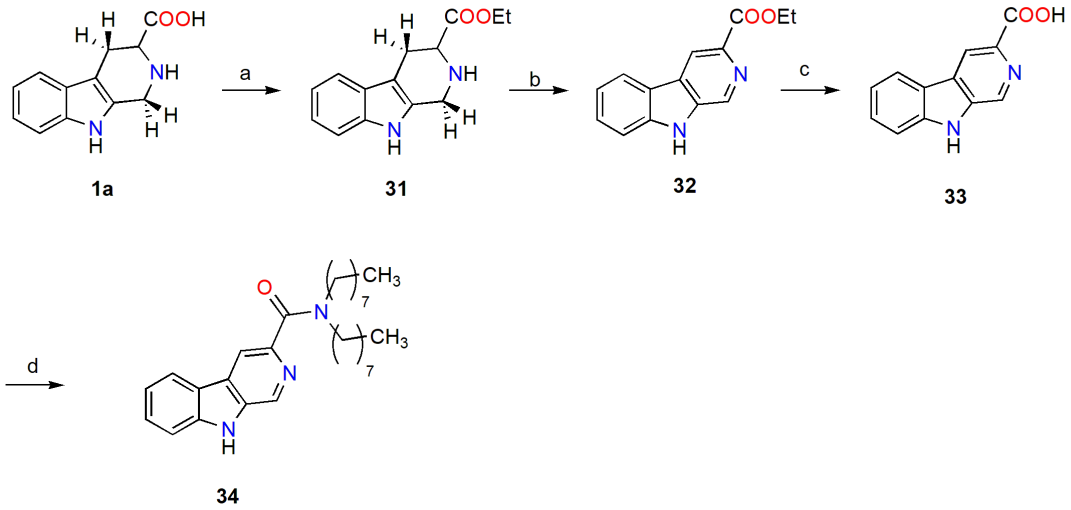

Reagents and conditions: a. HCl, EtOH, 0°C, 2h, 87%; b. MnO_2, toluene, ref., 24h, 65%; c. NaOH 10%, EtOH, ref., 1h, 94%; d. Di-N-Octylamine, HOBt, EDC, Et_3N, DMF, rt, 16h, 56%.

These new compounds are presently being tested at the Universidad Metropolitana de Ciencias de la Educación, Santiago (Chile) to assess possible effects on *Trypanosoma cruzi* viability and TryR inhibition.

Experimental section

Molecular modelling

The virtual library of new β-carbolines was constructed using the amines building blocks offered by Sigma-Aldrich Company and 2,3,4,9-tetrahydro-1-β-carboline-3-carboxylate acid (THBCA). All molecular structures were imported in SDF format and standardized using the Standardizer software[42] and the protocol as previously described.[23] The β-carboline library was generated from reactants of building blocks and THBCA using the reaction of acylation of nucleophiles with carboxylic acids implemented in software Reactor.[25] Parameters employed were combinatorial for reactant combination and with 1:1 molar ratio. The obtained β-carbolines were subsequently compiled into the library.

The libraries of β-carbolines and TryR inhibitors were analysed using the Instant JChem software and filters were used to classify chemicals as drug-like or lead-like. The stereoisomers detected were considered as duplicates and only tautomeric forms were preserved. New β-carboline and TryR inhibitors were explored using drug-like filters

(Ghose Filter, Veber Filter and Muegge Filter)[26-28] and a lead-like filter[29] implemented in Instant Jchem. Polarity, flexibility and molecular size descriptors were obtained computing the Cumulative Distribution Function (CDF) for molecular descriptors within the Muegge filter (HBD, HBA, logD, PSA, RB, MW, AC and RC). Clustering was performed using the method described by Jarvis-Patrick,[43] using chemical fingerprints, similarity matrices and a TC of 0.70, which are all implemented in MOE.[30] The chemical space (CS) of each standardized library was generated using the following chemical fingerprints: MACCS Structural Keys (MACCS). The chemical fingerprints were implemented in the MOE software package and used to compute Topological Molecular Descriptors. A structural similarity analysis was performed using the MACCS chemical fingerprints and the Tanimoto Coefficient (TC) implemented in MOE. Then, a similarity matrix for the studied compounds was calculated, and the R Software was applied to conduct a Principal Component Analysis (PCA).[33] The first three PCs were used to plot the chemical space of TR inhibitors and β-CDs. Molecular docking calculations for TR inhibitors and β-CDs were performed using the AutoDock 4.2 software.[31] All ligands were considered with their major microspecies at pH 7.4 for the ligand preparation process. These ligands were exported in SDF format using Instant Jchem and subjected to a conformational search using the stochastic method implemented in MOE.[30] The selected conformers were exported, with their respective atomic partial charges (ESP charge), in MOL2 format. During the TryR preparation process, all molecules of flavin adenine dinucleotide (FAD), maleic acid and water were removed from the PDB input file (1AOG, RCSB Protein Data Bank Code).[44] Pre-calculated grid maps were generated using Autogrid, with one map for each atom type present in the ligand being docked into TryR (A, BR, C, Cl, F, H, HD, HS, N, NA, OA, S, SA). The grid maps were built using a three-dimensional lattice with a size of 126 Å x 126 Å x 126 Å, with a grid point spacing of 0.204 Å and centred on the TryR active site. The coordinates of the carbonyl oxygen of the amino acid Glu19 (23,495x, 18,935y, and -4,912z; PDB Code: OE1) were used.[31]

In the AutoDock software 4.2,[31] we used the Lamarckian Genetic Algorithm (LGA)[45] to explore the conformational states of a flexible ligand and the empirical free energy scoring function to evaluate conformations during the docking process. The parameters employed for the docking process were: i) number of automated docking runs, 200, and ii) maximum number of energy evaluations and maximum number of generations

performed during each LGA run, 25,000,000 and 50,000, respectively. The other parameters were taken from the default settings in AutoDock 4.2.

The binding energies were computed using the triple consensus scoring function, which consider: DSX-Online score function[32] and ASE and Affinity dG score functions implemented in MOE.[30] This consensus scoring function was combined with the conformational search method implemented in Autodock-4.2[31] to provide a list of ligands sorted by simple scoring and consensus scoring adopting the rank-by-rank method. For each conformation, the final ranking was calculated as the average ranking obtained using the three scoring functions. Only the best scored conformation of each β-carboline derivative was considered for ranking. The Spearman coefficient (ρ) was used to assess the correlation interval between the IC_{50} values and the binding energies computed for the calibration library previously reported by our group.[23]

Chemical synthesis

^1H NMR spectra were determined on Bruker 300 and 400 MHz spectrometers, with the solvents indicated; chemical shifts are reported in δ (ppm) downfield from tetramethylsilane as internal reference. Coupling constants are given in hertz. In the case of multiplets, chemical shifts were measured starting from the approximate centre. Integrals were satisfactorily in line with those expected based on compound structure. Mass spectra were obtained on a Mat 112 Varian Mat Bremen (70 eV) mass spectrometer and Applied Biosystems Mariner System 5220 LC/MS (nozzle potential 140 eV). Column flash chromatography was performed on Merck silica gel (250−400 mesh ASTM); chemical reactions were monitored by analytical thin-layer chromatography (TLC) on Merck silica gel 60 F-254 glass plates. The purity of new tested compounds was checked by HPLC using the instrument HPLC VARIAN ProStar model 210, with detector DAD VARIAN ProStar 335. The analysis was performed with a flow of 1 mL/min, a C-18 column of dimensions 250 mm X 4.6 mm, a particle size of 5 mm, and a loop of 10 mL. The detector was set at 254 nm. The mobile phase consisted of phase A (Milli-Q H_2O, 18.0 MU, TFA 0.05%) and phase B (95% MeCN, 5% phase A). Gradient elution was performed as reported: 0 min, % B = 20; 0 and 20 min, % B = 90; 25 min, % ; B = 90; 26 min, % B = 20; 31 min, % B = 20. Starting materials were purchased from Sigma-Aldrich and Alfa Aesar, and solvents were from Carlo Erba, Fluka and Lab-Scan. DMSO was obtained anhydrous by distillation under vacuum and stored on molecular sieves.

(3S)-1H,2H,3H,4H,9H-pyrido[3,4-b]indole-3-carboxylic acid (**1**).

5 g (24.48 mmol) of Tryptophan were suspended in 250 mL of water and 2.05 g (24.48 mmol) of sodium bicarbonate were added. The mixture was stirred to give a clear solution and 2.00 g (66.61 mmol) of 37% formaldehyde solution were added. The mixture was stirred for 2 hours at room temperature, then refluxed for 3 hours. The hot solution was poured into 50 mL of water and, with vigorous stirring, the pH was adjusted to 5 with 6M HCl, giving a precipitate. The slurry was stirred for 18 hours, filtered, and the solid dried in vacuo. Yield: 95%; ^{1}H NMR (400 MHz, DMSO-d_6): δ 10.99 (s, 1H), 9.89 (s, 1H), 7.30 (t, J = 7.5 Hz, 1H), 7.22 (t, J = 8.0 Hz, 1H), 7.01 (d, J = 8.0 Hz, 1H), 6.81 (d, J = 7.5 Hz, 1H), 4.01 (t, J = 4.8 Hz, 1H), 3.75 (dd, J = 10.5 Hz, J = 5.0 Hz, 1H), 3.64 (dd, J = 10.5 Hz, J = 2.4 Hz, 1H), 2.91 (d, J = 10.5 Hz, 2H), 2.86 (s, 1H) ppm; HRMS (ESI-MS, 140 eV): m/z $[M+H]^+$ calculated for $C_{12}H_{13}N_2O_2^+$, 217.0972; found, 217.0969.

(3S)-2-[(benzyloxy)carbonyl]-1H,3H,4H,9H-pyrido[3,4-b]indole-3-carboxylic acid (**2**).

5 g (23.12 mmol) of compound **1** were suspended in a mixture water/THF 1:1 and 5.15 g (48.59 mmol) of sodium carbonate were added. After 5 minutes stirring, 3.94 g (23.10 mmol) of benzyl chloroformate were added and the mixture was stirred overnight. The THF was evaporated under vacuum and the aqueous residue was acidified with 1 M HCl. The resulting solid was extracted with ethyl acetate. The organic solution was washed with 1 M HCl, water, brine, and dried over sodium sulfate. The solution was evaporated, and the residue crystallized from toluene to give pure protected compound **2**. Yield: 83%; ^{1}H NMR (400 MHz, DMSO-d_6) δ: 12.89 (s, 1H), 10.85 (d, J = 33.5 Hz, 1H), 7.46 – 7.27 (m, 7H), 7.08 – 7.02 (m, 1H), 6.97 (m, 1H), 5.21 (s, 2H), 5.19 (m, 1H), 4.82 (dd, J = 21.5, 16.3 Hz, 1H), 4.48 (dd, J = 40.7, 16.3 Hz, 1H), 3.32 (m, 1H), 3.06 – 2.95 (m, 1H) ppm. HRMS (ESI-MS, 140 eV): m/z $[M+H]^+$ calculated for $C_{20}H_{19}N_2O_4^+$, 351.1339; found, 351.1376.

Benzyl (3S)-3-(dioctylcarbamoyl)-1H,3H,4H,9H-pyrido[3,4-b]indole-2-carboxylate (**3**).

1.00 g (2.85 mmol) of compound **2**, 0.758 g (3.14 mmol) of di-*N*-Octylamine, 0.424 g (3.14 mmol) of HOBt and 0.602 g (3.14 mmol) of EDC were dissolved in 4 mL of DMF. Then, 0.854 mL (6.14 mmol) of triethylamine were added, and the mixture was stirred at room temperature overnight. After evaporating the DMF, the residue was dissolved with ethyl acetate and washed with 10% acid citric solution, 10 % sodium carbonate solution, water, brine, and dried over sodium sulfate. The solution was filtered, evaporated and the crude product was purified by silica gel flash column chromatography on silica gel (eluent *n*-hexane/EtOAc 6:4). Yield: 70%; R*f* 0.77 (eluent *n*-hexane/EtOAc 6:4); ^{1}H-NMR [300 MHz, $CDCl_3$] δ: 8.03 ppm (s, 1H), 7.43 – 7.33 (m, 6H), 7.23 (d, J = 8.1 Hz,

1H), 7.13 – 7.01 (m, 2H), 5.63 (d, *J* = 7.1 Hz, 1H), 5.29 – 5.10 (m, 2H), 5.06-4.78 (m, 2H), 3.49-2.94 (m, 6H), 1.47-1.04 (m, 24H), 0.91 (t, *J* = 6.9 Hz, 3H), 0.83 (t, *J* = 6.9 Hz, 3H) ppm; HRMS (ESI-MS, 140 eV): m/z $[M+H]^+$ calculated for $C_{36}H_{52}N_3O_3^+$, 574.4003; found, 574.4043.

(3S)-3-(dioctylcarbamoyl)-1H,2H,3H,4H,9H-pyrido[3,4-b]indol-2-ium hydrate chloride (**4**).

0.556 g (0.97 mmol) of compound **3** were dissolved in 50 mL of ethyl acetate and this solution was added to a suspension of Pd/C 10% in ethyl acetate. The mixture was stirred under H_2 at atmospheric pressure for 5 hours, filtered and the residue was precipitated with HCl 12 M. Yield: 56%; ^{1}H NMR (400 MHz, DMSO-d_6) δ 11.22 (s, 1H, NH pyrrole), 10.10 (s, 1H, NH amine), 9.57 (s, 1H, NH amine), 7.47 (d, *J* = 7.8 Hz, 1H, H-5), 7.39 (d, *J* = 8.1 Hz, 1H, H-8), 7.12 (ddd, *J* = 8.2, 7.0, 1.2 Hz, 1H, H-7), 7.02 (ddd, *J* = 8.0, 7.0, 1.0 Hz, 1H, H-6), 4.63 (dd, *J* = 11.7, 4.6 Hz, 1H, H-3), 4.43 (d, *J* = 15.5 Hz, 1H, H-1), 4.31 (d, *J* = 15.4 Hz, 1H, H-1), 3.58 – 3.49 (m, 1H, H-4), 3.38 - 3.17 (m, 4H, CONCH_2), 2.89 – 2.78 (m, 1H, H-4), 1.68 – 1.46 (m, 4H, CONCH$_2$CH_2), 1.36 – 1.16 (m, 20H, CH_2CH_2CH_2CH_2CH_2CH$_3$), 0.91 – 0.81 (m, 6H, CH_3) ppm; ^{13}C NMR (400 MHz, DMSO-d_6) δ 168.40, 136.70, 126.96, 126.22, 122.14, 119.45, 118.31, 111.87, 105.05, 53.67, 47.37, 45.42, 40.80, 31.69, 31.65, 29.17, 29.16, 29.09, 29.07, 27.38, 26.69, 26.50, 23.48, 22.56, 22.51, 14.42, 14.37 ppm; HRMS (ESI-MS, 140 eV): m/z $[M+H]^+$ calculated for $C_{28}H_{46}N_3O^+$, 440.3635; found, 440.3628; RP-C18 HPLC: t_R = 18.59 min, 96.22%.

9-bromononanenitrile (**5**).

To a stirred solution of 2 g (7.35 mmol) of commercial 1,8-dibromoottane in 6 mL of DMF, 0.360 g (7.35 mmol) of NaCN were added and the reaction mixture was stirred for 2 h at 35°C. After cooling to r.t., the mixture was poured into water, and the aqueous layer was extracted with ethyl acetate. The combined organic layers were washed with brine and water and dried over sodium sulfate. Evaporation of the solvent gave the product as a yellow oil. Yield: 90%; ^{1}H-NMR [300 MHz, $CDCl_3$] δ: 3.40 (t, 2H), 2.34 (t, 2H), 1.85 (m, 2H), 1.66 (m, 2H), 1.33-1.46 (m, 8H) ppm.

N-benzylmethylamine (**15**).

To a solution of 2 g (18.82 mmol) of benzaldehyde in MeOH, 1.86 g (23.95 mmol) of 40% aqueous solution of methylamine were added. After stirring at room temperature for 15 min, the solution was cooled to 0°C and 0.356 g (9.41 mmol) of sodium borohydride were added portion wise. The resulting solution was stirred at room temperature for 1 h. After addition of water (25 mL), methanol was evaporated under vacuum and the

resulting aqueous phase extracted with CH_2Cl_2. The combined organic layers were dried ($MgSO_4$) and evaporated, affording **15** as a colorless oil. The product was used in the next step without any further purification. Yield: 88%; ^{1}H-NMR [300 MHz, $CDCl_3$] δ: 7.29-7.35 (m, 4H), 7.22-7.28 (m, 1H), 3.75 (s, 2H), 2.46 (s, 3H), 1.54 (s br, 1H) ppm.

General procedure for the synthesis of amino-nitrile derivatives (**8-10** and **16**). As a typical procedure, the synthesis of 9-(dibenzylamino)nonanenitrile (**8**) is described in detail. To a solution of dibenzylamine (1.72 g, 8.73 mmol) in 2.5 mL of anhydrous DMF, compound **5** (1.91 g, 8.73 mmol), potassium carbonate (2.65 g, 19.20 mmol) and potassium iodide (0.158 g, 0.958 mmol) were added. The resulting mixture was heated at 80°C overnight. The slurry was partitioned with water and ethyl acetate. The aqueous layer was extracted twice with ethyl acetate and the combined organic layers washed with water, dried over sodium sulfate and evaporated under vacuum to give the crude product.

9-(dibenzylamino)nonanenitrile (**8**).

The crude product was purified by silica gel flash-column chromatography (eluent *n*-hexane/EtOAc, 8:2).Yield: 65%; ^{1}H-NMR [300 MHz, $CDCl_3$] δ: 7.36 (m, 4H), 7.31 (m, 4H), 7.23 (m, 2H), 3.55 (s, 4H), 2.40 (t, J=7.04 Hz), 2.31 (t, J=7.10 Hz, 2H), 1.62 (m, 2H), 1.50 (m, 2H), 1.40 (m, 2H), 1.15-1.30 (m, 6H) ppm; HRMS (ESI-MS, 140 eV): m/z $[M+H]^+$ calculated for $C_{23}H_{31}N_2^+$, 335.2482; found, 335.2456.

5-(dibenzylamino)pentanenitrile (**9**).

Compound **9** was prepared as for compound **8** by reacting 0.59 g (5 mmol) of commercial 5-chlorovaleronitrile **6,** 0.99 g (5 mmol) of dibenzylamine, 1.38 g (10 mmol) of potassium carbonate and 0.083 g (0.5 mmol) of potassium iodide. After workup procedure, compound **9** was used for the next step without any further purification. Yield: 84%; ^{1}H-NMR [300 MHz, $CDCl_3$] δ: 7.24-7.36 (m, 10H), 3.55 (s, 4H), 2.44 (t, J = 6.22 Hz, 2H), 2.13 (t, J = 7.02 Hz, 2H), 1.58-1.68 (m, 4H) ppm; HRMS (ESI-MS, 140 eV): m/z $[M+H]^+$ calculated for $C_{19}H_{23}N_2^+$, 279.1856; found, 279.1877.

2-(dibenzylamino)acetonitrile (**10**).

Compound **10** was prepared as for compound **8** by reacting 0.6 g (5 mmol) of commercial bromo-acetonitrile **7**, 0.99 g (5 mmol) of dibenzylamine, 1.38 g (10 mmol) of potassium carbonate and 0.083 g (0.5 mmol) of potassium iodide. After workup procedure, compound **10** was used for the next step without any further purification. Yield: 95%; ^{1}H-NMR [300 MHz, $CDCl_3$] δ: 7.28-7.42 ppm (m, 10H), 3.75 (s, 4H), 3.37 (s, 2H) ppm; HRMS (ESI-MS, 140 eV): m/z $[M+H]^+$ calculated for $C_{16}H_{17}N_2^+$, 237.1386; found, 237.1375.

7-(N-benzyl-N-methylamino)heptanenitrile (**16**).

Compound **16** was prepared as for compound **8** by reacting 0.5 g (2.63 mmol) of commercial 7-bromoheptanenitrile **14**, 0.319 g (2.63 mmol) of previously synthesised compound **15**, 0.73 g (5.26 mmol) of potassium carbonate and 0.083 g (0.5 mmol) of potassium iodide. After workup procedure, compound **16** was used for the next step without any further purification. Yield: 78%; ^{1}H NMR (300 MHz, $CDCl_3$) δ 7.34 - 7.17 (m, 5H), 3.43 (s, 2H), 2.35 – 2,25 (m, 4H), 2.15 (s, 3H), 1.68 – 1.55 (m, 2H), 1.53 – 1.27 (m, 6H) ppm; HRMS (ESI-MS, 140 eV): m/z $[M+H]^+$ calculated for $C_{15}H_{23}N_2^+$, 231.1856; found, 231.1878

General procedure for the synthesis of diamino derivatives (**11**-**13** and **17**). As a typical procedure, the synthesis of N1,N1-dibenzylnonane-1,9-diamine (**11**) is described in detail. 0.67 g (2 mmol) of compound **8** were dissolved in 20 mL of anhydrous diethyl ether and dropped to an ice-cold suspension of lithium aluminum hydride (0.113 g, 3 mmol). The suspension was stirred for 2 h at room temperature, and then quenched by addition of water, followed by 3 mL of a 10% aqueous sodium hydroxide solution. The formed precipitate was filtered, and the filtrate extracted with ethyl acetate. The combined organic phases dried in sodium sulfate and evaporated under vacuum.

N1,N1-dibenzylnonane-1,9-diamine (**11**).

Yield: 79%; ^{1}H-NMR [300 MHz, $CDCl_3$] δ: 7.36 (d, J=6.87 Hz, 4H), 7.30 (t, J= 7.60 Hz, 4H), 7.22 (m, 2H), 3.54 (s, 4H), 2.67 (t, J=7.08 Hz, 2H), 2.39 (t, J=7.09 Hz, 2H), 1.61 (s br, 2H), 1.38-1.56 (m, 4H)**,** 1.13-1.30 (m, 10H) ppm; HRMS (ESI-MS, 140 eV): m/z $[M+H]^+$ calculated for $C_{23}H_{35}N_2^+$, 339.5369; found, 339.5388.

N1,N1-dibenzylpentane-1,5-diamine (**12**).

Compound **12** was prepared as for compound **11** by reacting 0.631 g (2.27 mmol) of compound **9** with 0.129 g (3.40 mmol) of lithium aluminum hydride. Yield: 75%; ^{1}H NMR (300 MHz, $CDCl_3$): δ 7.40 – 7.24 (m, 10H), 3.56 (s, 4H), 2.64 (t, *J* = 7.6 Hz, 2H), 2.43 (t, *J* = 7.2 Hz, 2H), 1.64 (s, 2H), 1.53 (m, 2H), 1.38 – 1.26 (m, 4H) ppm; HRMS (ESI-MS, 140 eV): m/z $[M+H]^+$ calculated for $C_{19}H_{27}N_2^+$, 283.2169; found, 283.2145.

N1,N1-dibenzylethane-1,2-diamine (**13**).

Compound **13** was prepared as for compound **11** by reacting 1.02 g (4.33 mmol) of compound **10** with 0.246 g (3.40 mmol) of lithium aluminum hydride. Yield: 88%; ^{1}H-NMR [300 MHz, $CDCl_3$] δ: 7.29-7.36 (m, 8H), 7.24 (tt, J=6.90, 2.45, 2 H), 3.58 (s, 4H), 2.74 (t, J = 5.76 Hz, 2H), 2.51 (t, J = 6.13 Hz, 2H), 1.70 (s br, 2H) ppm; HRMS (ESI-MS, 140 eV): m/z $[M+H]^+$ calculated for $C_{16}H_{21}N_2^+$, 241.1699; found, 241.1687.

N1-benzyl-N1-methylheptane-1,7-diamine (**17**).

Compound **17** was prepared as for compound **11** by reacting 0.238 g (1.03 mmol) of compound **16** with 0.059 g (1.55 mmol) of lithium aluminum hydride. Yield: 95%; ^{1}H NMR (300 MHz, $CDCl_3$) δ 7.24 - 7.19 (m, 5H), 3.41 (s, 2H), 2.62 (t, *J* = 7.0 Hz, 2H), 2.28 (t, *J* = 8.6 Hz, 2H), 2.15 (s, 2H), 2.10 (s, 3H), 1.41 (m,4H), 1.29 – 1.19 (s, 6H) ppm; HRMS (ESI-MS, 140 eV): m/z $[M+H]^+$ calculated for $C_{15}H_{27}N_2^+$, 235.2169; found, 235.2177.

2-(tert-butoxycarbonyl)-1H,3H,4H,9H-pyrido[3,4-b]indole-3-carboxylic acid (**18**).

2.91 g (13.33 mmol) of di-tert-butyl dicarbonate and 2.88 g (23.12 mmol) of compound **1** were dissolved together in 50 mL of THF and 1.84 g (48.59 mmol) of sodium carbonate were added along with 50 mL of water. The mixture was stirred vigorously overnight. THF was evaporated under vacuum and the aqueous residue was acidified with 1 M HCl. The residue was extracted with ethyl acetate and the organic solution washed with brine, dried over sodium sulfate, filtered and evaporated. Yield: 73%; ^{1}H NMR (400 MHz, DMSO) δ 12.72 (s, 1H), 10.87 (d, *J* = 18.6 Hz, 1H), 7.41 (d, *J* = 7.7 Hz, 1H), 7.29 (dd, *J* = 8.0, 5.0 Hz, 1H), 7.07 – 7.02 (m, 1H), 6.96 (m, 1H), 5.10 (dd, 1H), 4.72 (t, *J* = 16.4 Hz, 1H), 4.39 (dd, 1H), 3.29 (dd, *J* = 15.6, 5.7 Hz, 1H), 2.95 (m, 1H), 1.58 – 1.35 (m, 9H); HRMS (ESI-MS, 140 eV): m/z $[M+H]^+$ calculated for $C_{17}H_{21}N_2O_4^+$, 317.1496; found, 317.1469.

General procedure for the synthesis of amidic derivatives (**19-22**). As a typical procedure, the synthesis of tert-butyl 3-(9-(dibenzylamino)nonylcarbamoyl)-3,4-dihydro-1*H*-pyrido[3,4-b]indole-2(9*H*)-carboxylate (**19**) is described in detail. 0.452 g (1.43 mmol) of compound **18** were mixed with 0.532 g (1.57 mmol) of diamino derivatives **11**, 0.212 g (1.57 mmol) of HOBt and 0.301 g (1.57 mmol) of EDC in 4 mL of DMF. 0.311 g (3.07 mmol) of triethylamine were added, and the mixture was stirred at room temperature overnight. After evaporating the DMF under vacuum, the residue dissolved with ethyl acetate and washed with 10% acid citric solution, 10 % sodium carbonate solution, water, brine, and dried over sodium sulfate. The solution was filtered and evaporated under vacuum.

Tert-butyl-3-(9-(dibenzylamino)nonylcarbamoyl)-3,4-dihydro-1H-pyrido[3,4-b]indole-2(9H)-carboxylate (**19**).

The crude product was purified by silica gel flash-column chromatography (eluent n-hexane/EtOAc, 8:2). Yield: 82%; ^{1}H NMR (300 MHz, $CDCl_3$) δ 7.89 (m, 1H), 7.50 (d, *J* = 7.4 Hz, 1H), 7.42 – 7.20 (m, 11 H), 7.16 – 7.04 (m, 2H), 5.84 (d, 14 Hz, 1H), 5.18 (d, *J*

= 55.9 Hz, 1H), 5.01 – 4.80 (m, 1H), 4.49 – 4.26 (m, 1H), 3.54 (s, 4H), 3.42 (m, 1H), 3.15 (m, 2H), 2.99 (m, 1H), 2.37 (m, 2H), 1.43 (s, 9H), 1.14 (s, 10H) ppm; HRMS (ESI-MS, 140 eV): m/z $[M+H]^+$ calculated for $C_{40}H_{53}N_4O_3^+$, 637.4112; found, 637.4139.

Tert-butyl-3-(5(dibenzylamino)pentylcarbamoyl)-3,4-dihydro-1H-pyrido[3,4-b]indole-2(9H)-carboxylate (**20**).

Compound **20** was prepared as for compound **19** by reacting 0.365 g (1.16 mmol) of compound **18** with 0.359 g (1.27 mmol) of compound **12**, 0.172 g (1.27 mmol) of HOBt and 0.244 g (1.27 mmol) of EDC, 0.251 g (2.48 mmol) of triethylamine in 4 mL of DMF. After the same workup reported for compound **19**, the crude product was purified by silica gel flash-column chromatography (eluent n-hexane/EtOAc, 6:4). Yield: 87%; ^{1}H NMR (300 MHz, $CDCl_3$) δ 7.48 (d, *J* = 7.5 Hz, 1H), 7.41 – 7.19 (m, 11 H), 7.09 (m, 2H), 5.80 (s, 1H), 5.31 – 4.79 (m, 2H), 4.32 (m, 1H), 3.51 (m, 5H), 3.22 – 2.89 (m, 3H), 2.29 (m, 2H), 1.52 (s, 9H), 1.39 – 1.21 (m, 4H), 1.08 (s, 2H) ppm; HRMS (ESI-MS, 140 eV): m/z $[M+H]^+$ calculated for $C_{36}H_{45}N_4O_3^+$, 581.3486; found, 581.3476.

Tert-butyl-3-(2(dibenzylamino)ethylcarbamoyl)-3,4-dihydro-1H-pyrido[3,4-b]indole-2(9H)-carboxylate (**21**).

Compound **21** was prepared as for compound **19** by reacting 0.567 g (1.79 mmol) of compound **18** with 0.474 g (1.97 mmol) of compound **13**, 0.267 g (1.97 mmol) of HOBt and 0.344 g (1.97 mmol) of EDC, 0.390 g (3.86 mmol) of triethylamine in 4 mL of DMF. After the same workup reported for compound **19**, the product was used for the next step without any further purification. Yield: 70%; ^{1}H NMR (400 MHz, $CDCl_3$) δ 7.65 (s, 1H), 7.48 (d, *J* = 7.4 Hz, 1H), 7.39 – 7.33 (m, 4H), 7.32 - 7.27 (m, 6H), 7.25 – 7.17 (m, 1H), 7.10 (dt, *J* = 14.9, 7.0 Hz, 2H), 6.35 (s, 1H), 5.20 (m, 1H), 5.05 – 4.80 (m, 1H), 4.34 – 4.11 (m, 1H), 3.54 (m, 4H), 3.36 (d, *J* = 13.2 Hz, 1H), 3.24 (m, 2H), 2.98 (m, 1H), 2.63 – 2.41 (m, 2H), 1.57 (s, 9H) ppm; HRMS (ESI-MS, 140 eV): m/z $[M+H]^+$ calculated for $C_{33}H_{39}N_4O_3^+$, 539.3017; found, 539.3005.

Tert-butyl-3-(7-(N-benzyl-N-methylamino)heptylcarbamoyl)-3,4-dihydro-1H-pyrido[3,4-b]indole-2(9H)-carboxylate (**22**).

Compound **22** was prepared as for compound **19** by reacting 0.282 g (0.89 mmol) of compound **18** with 0.230 g (0.98 mmol) of compound **17**, 0.133 g (0.98 mmol) of HOBt and 0.188 g (0.98 mmol) of EDC, 0.194 g (1.92 mmol) of triethylamine in 4 mL of DMF. After the same workup reported for compound **19**, the crude product was purified by silica gel flash-column chromatography (eluent chloroform/methanol, 93:7). Yield: 55%; ^{1}H NMR (300 MHz, $CDCl_3$) δ 8.92 (s, 1H), 7.56 – 7.45 (m, 1H), 7.39 – 7.28 (m, 5H),

7.24 (m, 1H), 7.14 – 6.99 (m, 2H), 5.88 (s, 1H), 5.36 – 4.83 (m, 2H), 4.40 (t, *J* = 21.4 Hz, 1H), 3.67 (s, 2H), 3.61 (m, 1H), 3.25 (dt, *J* = 13.2, 6.6 Hz, 1H), 3.12 (dt, *J* = 13.2, 6.3 Hz, 1H), 2.99 (d, *J* = 16.8 Hz, 1H), 2.44 (m, 2H), 2.28 (s, 3H), 1.53 (s, 9H), 1.46 – 0.96 (m, 10H) ppm; HRMS (ESI-MS, 140 eV): m/z $[M+H]^+$ calculated for $C_{32}H_{45}N_4O_3^+$, 553.3486; found, 553.3499.

General procedure for the synthesis of N-methylated derivatives (**25**-**27**). As a typical procedure, the synthesis of tert-butyl 3-(9-([dibenzyl-(methyl)-ammonio]nonyl})-3,4-dihydro-1H-pyrido[3,4-b]indole-2(9H)-carboxylate (**25**) is described in detail. 0.415 g (0.65 mmol) of derivative **25** were mixed with 1.85 g (13.03 mmol) of methyl iodide and stirred for 18 h. At the end of the reaction, the remaining methyl iodide was evaporated.

Tert-butyl-3-(9-([dibenzyl-(methyl)-ammonio]nonyl})-3,4-dihydro-1H-pyrido[3,4-b]indole-2(9H)-carboxylate (**25**).

The crude residue was purified by silica gel flash column chromatography (eluent EtOAc/methanol, 95:5). Yield: 77%; ^{1}H NMR (400 MHz, $CDCl_3$) δ 8.91 (s, 1H), 7.61 - 7.53 (m, 4H), 7.50 – 7.39 (m, 8H), 7.06 – 6.96 (m, 2H), 6.15 (d, *J* = 25.5 Hz, 1H), 5.30 – 4.72 (m, 6H), 4.46 (d, *J* = 16.8 Hz, 1H), 3.60 – 3.35 (m, 1H), 3.31 – 2.85 (m, 9H), 1.88 (s, 2H), 1.63 (s, 2H), 1.51 (s, 9H), 1.41 – 1.31 (m, 2H), 1.29 – 1.06 (m, 4H) ppm; HRMS (ESI-MS, 140 eV): m/z $[M+H]^+$ calculated for $C_{41}H_{55}N_4O_3^+$, 651.4269; found, 651.4255.

Tert-butyl-3-(2-([dibenzyl-(methyl)-ammonio]ethyl})-3,4-dihydro-1H-pyrido[3,4-b]indole-2(9H)-carboxylate (**26**).

Compound **26** was prepared as for compound **25** by reacting 0.702 g (1.30 mmol) of compound **21** with 3.70 g (26 mmol) of methyl iodide. The crude residue was purified by silica gel flash column chromatography (eluent EtOAc/methanol, 9:1). Yield: 65%; ^{1}H NMR (400 MHz, DMSO-d_6) δ 11.15 (s, 1H), 10.15 (d, *J* = 10.6 Hz, 1H), 9.79 (d, *J* = 8.1 Hz, 1H), 9.39 (t, *J* = 5.9 Hz, 1H), 7.71 – 7.63 (m, 4H), 7.55 (m, 6H), 7.42 (d, *J* = 7.9 Hz, 1H), 7.38 (d, *J* = 8.1 Hz, 1H), 7.12 (t, *J* = 8.2 Hz, 1H), 7.06 – 7.00 (m, 1H), 4.82 (dd, *J* = 12.7, 6.0 Hz, 2H), 4.60 (dd, *J* = 15.5, 12.8 Hz, 2H), 4.41 (m, 1H), 4.36 – 4.23 (m, 2H), 3.86 (q, *J* = 6.2 Hz, 2H), 3.37 (m, 2H), 3.34 (m, 1H), 2.98 (s, 3H), 2.88 (dd, *J* = 15.4, 11.2 Hz, 1H) ppm; HRMS (ESI-MS, 140 eV): m/z $[M+H]^+$ calculated for $C_{34}H_{41}N_4O_3^+$, 553.3173; found, 553.3166.

Tert-butyl-3-(7-(N-benzyl-N-methylamino)heptylcarbamoyl)-3,4-dihydro-1H-pyrido[3,4-b]indole-2(9H)-carboxylate (**27**).

Compound **27** was prepared as for compound **25** by reacting 0.134 g (0.253 mmol) of compound **22** with 0.064 g (0.451 mmol) of methyl iodide. Yield: 62%; ^{1}H NMR (400

MHz, $CDCl_3$) δ 9.63 (s, 1H), 7.61 – 7.30 (m, 7H), 7.10 – 6.93 (m, 2H), 6.37 (d, *J* = 35.2 Hz, 1H), 5.39 – 4.98 (m, 2H), 4.60 - 4.38 (m, 3H), 3.44 – 3.22 (m, 3H), 2.86 (m, 4H), 1.64 - 1.46 (m, 12H), 1.41 – 0.96 (m, 9H) ppm; HRMS (ESI-MS, 140 eV): m/z $[M+H]^+$ calculated for $C_{33}H_{47}N_4O_3^+$, 547.3643; found, 547.3629.

General procedure for the synthesis of deprotected derivatives (**23**, **24**, **28**-**30**). As a typical procedure, the synthesis of 3-({5-[dibenzyl-ammonio]pentyl}carbamoyl)-1*H*,2*H*,3*H*,4*H*,9*H*-pyrido[3,4-b]indol-2-ium dichloride (**23**) is described in detail. In a round-bottomed flask, derivative **23** was dissolved in 5 mL of absolute EtOH. Gaseous HCl was bubbled inside the flask for 2 minutes and the mixture was stirred at room temperature overnight. The solvent was evaporated under vacuum and the residue was treated with diethyl ether. The obtained precipitate was filtered and dried to afford the final compound.

3-({5-[Dibenzyl-ammonio]pentyl}carbamoyl)-1H,2H,3H,4H,9H-pyrido[3,4-b]indol-2-ium dichloride (**23**).

Yield: 92%; ^{1}H NMR (300 MHz, DMSO) δ 11.40 (s, 1H, NH amine), 11.25 (s, 1H, NH pyrrole), 10.06 (d, *J* = 8.7 Hz, 1H, NH-2), 9.75 (d, J = 8.6 Hz, 1H, NH-2), 8.85 (t, *J* = 5.4 Hz, 1H, NH amide), 7.77 - 7.64 (m, 4H, *ortho*-H benzylic groups), 7.50 – 7.40 (m, 7H, *meta*-, *para*-H benzylic groups, H-5), 7.37 (d, *J* = 8.0 Hz, 1H, H-8), 7.14 – 7.06 (m, 1H, H-7), 7.06 – 6.98 (m, 1H, H-6), 4.39 (m, 1H, H-1), 4.35 – 4.26 (m, 5H, H-1, NCH_2Phe), 4.20 (dd, *J* = 10.2, 6.1 Hz, 1H, H-3), 3.37 (m, 1H, H-4), 3.20 – 3.09 (m, 2H, H-3'), 2.86 (m, 3H, H-4, H-7'), 1.88 – 1.73 (m, 2H, H-6'), 1.46 – 1.35 (m, 2H, H-4'), 1.21 (m, 2H, H-5') ppm; ^{13}C NMR (75 MHz, DMSO-d_6) δ 167.91, 136.24, 131.39, 130.06, 129.34, 128.73, 126.50, 125.68, 121.67, 119.05, 117.63, 111.39, 104.63, 64.85, 55.87, 54.93, 50.97, 38.31, 28.10, 23.52, 23.20, 22.17, 15.16 ppm; HRMS (ESI-MS, 140 eV): m/z $[M+H]^{++}$ calculated for $C_{31}H_{38}N_4O_2^{++}$, 241.1518; found, 241.1535; RP-C18 HPLC: t_R = 12.12 min, 98.67%.

3-({2-[Dibenzyl-ammonio]acetyl}carbamoyl)-1H,2H,3H,4H,9H-pyrido[3,4-b]indol-2-ium dichloride (**24**).

Yield: 88%; ^{1}H NMR (400 MHz, DMSO-d_6) δ 11.43 (s, 1H, NH amine), 11.18 (s, 1H, NH pyrrole), 9.97 (s, 1H, NH-2) 9.89 (s, 1H, NH-2), 9.20 (s, 1H, NH amide), 7.70 – 7.61 (m, 3H,), 7.56 – 7.18 (m, 10H), 7.15 – 7.08 (m, 1H), 7.07 – 6.99 (m, 1H), 4.53 – 4.10 (m, 7H), 3.77 (s, 1H), 3.65 (d, *J* = 22.6 Hz, 2H), 3.09 (s, 2H), 2.86 – 2.78 (m, 1H) ppm; ^{13}C NMR (100 MHz, DMSO-d_6) δ 169.01, 136.75, 132.01, 130.03, 129.95, 129.29, 126.89, 126.13, 122.20, 119.59, 118.15, 111.93, 105.00, 56.87, 55.50, 50.85, 40.81, 39.84, 23.32

ppm; HRMS (ESI-MS, 140 eV): m/z $[M+H]^{++}$ calculated for $C_{31}H_{38}N_4O_2^{++}$, 220.1283; found, 220.1312; RP-C18 HPLC: t_R = 11.37 min, 97.6%.

3-({9-[Dibenzyl-(methyl)-ammonio]nonyl}carbamoyl)-1H,2H,3H,4H,9H-pyrido[3,4-b]indol-2-ium dichloride (**28**).

Yield: 92 %; ^{1}H NMR (400 MHz, DMSO-d_6) δ 11.15 (s, 1H, NH pyrrole), 9.89 (s, 1H, NH amine), 9.71 (s, 1H, NH amine), 8.74 (t, *J* = 5.6 Hz, 1H, NH amide), 7.61 – 7.57 (m, 4H, *ortho*-H benzylic groups), 7.53 (dd, *J* = 8.1, 5.9 Hz, 6H, *meta*-, *para*-H benzylic groups), 7.44 (d, *J* = 8.0 Hz, 1H, H-5), 7.37 (d, *J* = 8.1 Hz, 1H, H-8), 7.14 – 7.08 (m, 1H, H-7), 7.05 – 6.98 (m, 1H, H-8), 4.67 (d, *J* = 12.7 Hz, 2H, NCH_2Ph), 4.51 (d, *J* = 12.7 Hz, 2H, NCH_2Ph), 4.42 (s, 1H, H-1), 4.30 (d, *J* = 14.9 Hz, 1H, H-1), 4.20 (s, 1H, H-3), 3.35 (m, 1H, H-4), 3.19 (dd, *J* = 13.4, 6.5 Hz, 2H, H-3'), 3.10 – 3.04 (m, 2H, H-11'), 2.89 (d, *J* = 17.2 Hz, 4H, NCH_3, H-4), 1.89 (s, 2H, H-10'), 1.49 (d, *J* = 6.5 Hz, 2H, H-4'), 1.31 - 1.24 (m, 10H, H-5', H-6', H-7', H-8', H-9') ppm; ^{13}C NMR (101 MHz, DMSO-d_6) δ 168.27, 133.56, 130.60, 129.33, 122.11, 119.47, 118.07, 111.86, 65.53, 65.08, 65.03, 60.40, 55.39, 40.80, 40.77, 39.11, 29.32, 29.11, 26.83, 26.35, 23.82, 23.68, 22.13 ppm; HRMS (ESI-MS, 140 eV): m/z $[M+H]^{++}$ calculated for $C_{36}H_{48}N_4O_2^{++}$, 276.1909; found, 276.2017; RP-C18 HPLC: t_R = 14.71 min, 95.70%.

3-({2-[Dibenzyl(methyl)ammonio]ethyl}carbamoyl)-1H,2H,3H,4H,9H-pyrido[3,4-b]indol-2-ium dichloride (**29**).

Yield: 89%; ^{1}H NMR (400 MHz, DMSO-d_6) δ 11.15 (s, 1H, NH pyrrole), 10.15 (d, *J* = 9.0 Hz, 1H, NH amine), 9.79 (d, *J* = 7.2 Hz, 1H, NH amine), 9.39 (t, *J* = 5.6 Hz, 1H, NH amide), 7.67 (dd, *J* = 7.7, 1.7 Hz, 4H, *ortho*-H benzylic groups), 7.59 – 7.50 (m, 6H, *meta*-, *para*-H benzylic groups), 7.42 (d, *J* = 7.9 Hz, 1H, H-5), 7.38 (d, *J* = 8.1 Hz, 1H, H-8), 7.14 – 7.09 (m, 1H, H-7), 7.05 – 7.00 (m, 1H, H-6), 4.82 (dd, *J* = 12.7, 6.0 Hz, 2H, NCH_2Phe), 4.60 (dd, *J* = 15.5, 12.8 Hz, 2H, NCH_2Phe), 4.42 (dd, *J* = 12.5, 10.7 Hz, 1H, H-1), 4.33 (s, 1H, H-1, H-1), 4.28 (d, *J* = 5.0 Hz, 1H, H-3'), 3.86 (dd, *J* = 12.4, 6.2 Hz, 2H, H-3'), 3.35 (m, 2H, H-4'), 3.34 (m, 1H, H-4'), 2.98 (s, 3H, NCH_3), 2.88 (dd, *J* = 15.8, 11.1 Hz, 1H, H-4) ppm; ^{13}C NMR (100 MHz, DMSO-d_6) δ 169.25, 136.74, 133.77, 130.91, 130.09, 129.51, 128.01, 126.85, 126.08, 122.27, 119.62, 118.03, 111.95, 104.91, 65.74, 55.35, 46.73, 40.77, 39.68, 33.21, 23.52 ppm; HRMS (ESI-MS, 140 eV): m/z $[M+H]^{++}$ calculated for $C_{29}H_{34}N_4O^{++}$, 227.1361; found, 227.1389; RP-C18 HPLC: t_R = 10.96 min, 96.13%.

3-({7-[Benzyl(dimethyl)ammonio]heptyl}carbamoyl)-1H,2H,3H,4H,9H-pyrido[3,4-b]indol-2-ium dichloride (**30**).

Yield: 84%; ^{1}H NMR (400 MHz, DMSO-d_6) δ 11.11 (s, 1H, NH pyrrole), 9.82 (d, J = 8.5 Hz, 1H, NH amine), 9.69 (d, J = 8.9 Hz, 1H, NH amine), 8.71 (t, J = 5.4 Hz, 1H, NH amide), 7.60 – 7.50 (m, 5H, benzylic H), 7.45 (d, J = 7.6 Hz, 1H, H-5), 7.38 (d, J = 8.1 Hz, 1H, H-8), 7.12 (t, J = 7.6 Hz, 1H, H-7), 7.02 (t, J = 7.5 Hz, 1H, H-6), 4.54 (s, 2H, NCH_2Ph), 4.42 (s, 1H, H-1), 4.31 (d, J = 13.1 Hz, 1H, H-1), 4.20 (td, J = 9.5, 4.1 Hz, 1H, H-3), 3.37 (m, 1H, H-4), 3.24 (m, 2H, H-9'), 3.20 (dd, J = 12.7, 6.4 Hz, 2H, H-3'), 2.94 (d, J = 14.9 Hz, 6H, NCH_3), 2.89 (dd, J = 14.3, 12.6 Hz, 1H, H-4), 1.87– 1.73 (m, 2H, H-8'), 1.55 – 1.45 (m, 2H, H-4'), 1.38 – 1.22 (m, 8H, H-5', H-6', H-7', H-8') ppm; ^{13}C NMR (100 MHz, DMSO-d_6) δ 168.37, 136.75, 133.40, 130.74, 129.39, 128.60, 126.95, 126.16, 122.17, 119.55, 118.19, 111.19, 105.17, 66.64, 63.96, 55.48, 49.62, 40.82, 39.16, 29.21, 28.60, 26.50, 26.23, 23.72, 22.23 ppm; HRMS (ESI-MS, 140 eV): m/z $[M+H]^{++}$ calculated for $C_{28}H_{40}N_4O^{++}$, 224.1596; found, 224.1660; RP-C18 HPLC: t_R = 10.75 min, 97.31%.

Ethyl 2,3,4,9-tetrahydro-1H-pyrido[3,4-b]indole-3-carboxylate (**31**).

Dry gaseous HCl was bubbled into a suspension of **1** (1.100 g, 5.09 mmol) in 50 mL of ethanol. The temperature was kept at 0°C. The mixture cleared slowly, and then a white precipitate formed readily. The reaction was monitored by TLC (*n*-BuOH/AcOH/H_2O, 4:1:1). The crystalline product was collected, washed sparingly with ethanol, stirred into H_2O, neutralized ($NaHCO_3$), and extracted with CH_2Cl_2. The combined CH_2Cl_2 extracts were dried (Na_2SO_4) and evaporated to yield 1.081 g of ester derivative. Yield: 87%; ^{1}H NMR (400 MHz, $CDCl_3$) δ 7.93 (s, 1H), 7.48 (dd, J = 7.6, 1.2 Hz, 1H), 7.30 (d, J = 7.8 Hz, 1H), 7.13 (dt, J = 20.2, 7.3 Hz, 2H), 4.26 (q, J = 7.1 Hz, 2H), 4.13 (m, 2H), 3.78 (dd, J = 9.7, 4.5 Hz, 1H), 3.13 (dd, J = 15.5, 4.3 Hz, 1H), 2.89 (dd, J = 15.3, 9.5 Hz, 1H), 2.17 (s, 1H), 1.32 (t, J = 7.1 Hz, 3H) ppm; HRMS (ESI-MS, 140 eV): m/z $[M+H]^{+}$ calculated for $C_{14}H_{17}N_2O_2^{+}$, 245.1285; found, 245.1267.

Ethyl 9H-pyrido[3,4-b]indole-3-carboxylate (**32**).

Into a round-bottomed flask, compound 31 (1.000 g, 4.09 mmol) and toluene (30 mL) were mixed. The solution was heated to reflux, at which time MnO_2 (1.00 g) was added to the flask. Additional quantities of MnO_2 were added until analysis by TLC (eluent EtOAc) indicated the absence of starting material. The hot solution was filtered through a Celite pad to remove the MnO_2 and the filter cake was washed with toluene. The organic layers were cooled to room temperature and the formed precipitate collected by vacuum filtration. Yield: 65%; ^{1}H NMR (400 MHz, $CDCl_3$) δ 10.28 (s, 1H), 9.15 (s, 1H), 8.90 (s, 1H), 8.21 (d, J = 7.9 Hz, 1H), 7.71 (d, J = 8.3 Hz, 1H), 7.61 (ddd, J = 8.3, 7.1, 1.2 Hz,

1H), 7.36 (ddd, *J* = 8.0, 7.1, 0.9 Hz, 1H), 4.55 (q, *J* = 7.1 Hz, 2H), 1.47 (t, *J* = 7.1 Hz, 3H) ppm; HRMS (ESI-MS, 140 eV): m/z $[M+H]^+$ calculated for $C_{14}H_{13}N_2O_2^+$, 241.0972; found, 241.0988.

9H-Pyrido[3,4-b]indole-3-carboxylic acid (**33**).

A mixture of compound **32** (0.500 g, 2.08 mmol), NaOH (0.333 g, 200 mmol), EtOH (25 mL), and H_2O (25 mL) was refluxed for 30 min, and then EtOH was removed on the rotary evaporator. The mixture was neutralized (pH 5) with HCl 6 M and cooled to room temperature. The precipitate was collected, washed with H_2O and MeOH, and dried in vacuo. Yield: 94%; ^{1}H NMR (400 MHz, DMSO-d_6) δ 13.39 (s, 1H), 9.32 (s, 1H), 9.20 (d, *J* = 0.7 Hz, 1H), 8.64 (d, *J* = 7.7 Hz, 1H), 7.86 (dt, *J* = 8.4, 1.0 Hz, 1H), 7.79 (ddd, *J* = 8.3, 7.0, 1.2 Hz, 1H), 7.47 (ddd, *J* = 8.0, 6.9, 1.0 Hz, 1H) ppm; HRMS (ESI-MS, 140 eV): m/z $[M+H]^+$ calculated for $C_{12}H_9N_2O_2^+$, 213.0659; found, 213.0632.

N,N-Dioctyl-9H-pyrido[3,4-b]indole-3-carboxamide (**34**).

Compound **34** was prepared by reacting 0.350 g (1.65 mmol) of compound **33** with 0.438 g (1.81 mmol) of commercial di-N-octylamine, 0.245 g (1.81 mmol) of HOBt and 0.348 g (1.81 mmol) of EDC, 0.550 g (5.44 mmol) of triethylamine in 4 mL of DMF. The mixture was stirred overnight. After evaporating the DMF under vacuum, the residue was dissolved in ethyl acetate and washed with 10% acid citric solution, 10 % sodium carbonate solution, water, brine, and dried over sodium sulphate. The solution was filtered and evaporated under vacuum. Yield: 64%; ^{1}H NMR (400 MHz, $CDCl_3$) δ 11.77 (s, 1H, NH pyrrole), 8.82 (d, *J* = 1.1 Hz, 1H), 8.33 (s, 1H), 8.30 (d, *J* = 7.9 Hz, 1H), 7.62 (d, *J* = 8.2 Hz, 1H), 7.56 (ddd, *J* = 8.2, 6.8, 1.2 Hz, 1H), 7.28 – 7.21 (m, 1H), 3.40 (dt, *J* = 20.4, 7.7 Hz, 4H), 1.66 – 1.57 (m, 2H), 1.49 (t, *J* = 7.4 Hz, 2H), 1.37 – 1.16 (m, 12H), 1.03 – 0.95 (m, 8H), 0.89 – 0.84 (m, 3H, CH_3), 0.69 (t, *J* = 6.9 Hz, 3H, CH_3) ppm; 13C NMR (100 MHz, $CDCl_3$) δ 170.32, 144.04, 141.23, 136.01, 131.96, 129.17, 128.69, 121.72, 121.33, 120.18, 114.71, 112.08, 49.17, 46.20, 31.83, 31.68, 29.43, 29.23, 29.09, 28.80, 27.71, 27.23, 26.62, 22.54, 14.08 ppm; HRMS (ESI-MS, 140 eV): m/z $[M+H]^+$ calculated for $C_{28}H_{42}N_3O^+$, 436.3322; found, 436.3355; RP-C18 HPLC: t_R = 18.59 min, 99.02%.

Acknowledgements

Molecular modelling by J. R. Becerra and synthesis by M. Dal Prà, D. Carta, M.G. Ferlin were supported by financial grants from UMCE, Chile and University of Padova, Italy.

References

[1] Z.M. Cucunubá, O. Okuwoga, M.-G. Basáñez, P. Nouvellet, Increased mortality attributed to Chagas disease: a systematic review and meta-analysis, Parasit. Vectors. 9 (2016) 42. doi:10.1186/s13071-016-1315-x.

[2] E.E. Conners, J.M. Vinetz, J.R. Weeks, K.C. Brouwer, A global systematic review of Chagas disease prevalence among migrants, Acta Trop. 156 (2016) 68–78. doi:10.1016/j.actatropica.2016.01.002.

[3] A. Rassi, A. Rassi, J.A. Marin-Neto, Chagas disease, Lancet. 375 (2010) 1388–1402. doi:10.1016/S0140-6736(10)60061-X.

[4] A. Prata, Clinical and epidemiological aspects of Chagas disease, Lancet Infect. Dis. 1 (2001) 92–100. doi:10.1016/S1473-3099(01)00065-2.

[5] F. Torrico, C. Alonso-Vega, E. Suarez, P. Rodriguez, M.C. Torrico, M. Dramaix, C. Truyens, Y. Carlier, Maternal Trypanosoma cruzi infection, pregnancy outcome, morbidity, and mortality of congenitally infected and non-infected newborns in Bolivia, Am. J. Trop. Med. Hyg. 70 (2004) 201–209. doi:70/2/201 [pii].

[6] C. Bern, S.P. Montgomery, B.L. Herwaldt, A. Rassi, J.A. Marin-Neto, R.O. Dantas, J.H. Maguire, H. Acquatella, C. Morillo, L. V. Kirchhoff, R.H. Gilman, P.A. Reyes, R. Salvatella, A.C. Moore, Evaluation and Treatment of Chagas Disease in the United States, JAMA. 298 (2007) 2171. doi:10.1001/jama.298.18.2171.

[7] J.A. Urbina, R. Docampo, Specific chemotherapy of Chagas disease: Controversies and advances, Trends Parasitol. 19 (2003) 495–501. doi:10.1016/j.pt.2003.09.001.

[8] J.A. Marin-Neto, E. Cunha-Neto, B.C. Maciel, M. V. Simões, Pathogenesis of chronic Chagas heart disease, Circulation. 115 (2007) 1109–1123. doi:10.1161/CIRCULATIONAHA.106.624296.

[9] J.D. Maya, B.K. Cassels, P. Iturriaga-Vásquez, J. Ferreira, M. Faúndez, N. Galanti, A. Ferreira, A. Morello, Mode of action of natural and synthetic drugs against Trypanosoma cruzi and their interaction with the mammalian host, Comp. Biochem. Physiol. - A Mol. Integr. Physiol. 146 (2007) 601–620. doi:10.1016/j.cbpa.2006.03.004.

[10] S.R. Wilkinson, J.M. Kelly, Trypanocidal drugs: Mechanisms, resistance and new targets, Expert Rev. Mol. Med. 11 (2009) e31. doi:10.1017/S1462399409001252.

[11] J.A. Castro, M.M. DeMecca, L.C. Bartel, Toxic Side Effects of Drugs Used to Treat Chagas' Disease (American Trypanosomiasis), Hum. Exp. Toxicol. 25 (2006) 471–479. doi:10.1191/0960327106het653oa.

[12] X. Coronado, I. Zulantay, M. Rozas, W. Apt, G. Sánchez, J. Rodríguez, S. Ortiz, A. Solari, Dissimilar distribution of Trypanosoma cruzi clones in humans after chemotherapy with allopurinol and itraconazole, J. Antimicrob. Chemother. 58 (2006) 216–219. doi:10.1093/jac/dkl192.

[13] I. Molina, J. Gómez i Prat, F. Salvador, B. Treviño, E. Sulleiro, N. Serre, D. Pou, S. Roure, J. Cabezos, L. Valerio, A. Blanco-Grau, A. Sánchez-Montalvá, X. Vidal, A. Pahissa, Randomized Trial of Posaconazole and Benznidazole for Chronic Chagas' Disease, N. Engl. J. Med. 370 (2014) 1899–1908. doi:10.1056/NEJMoa1313122.

[14] R. Perez-Pineiro, A. Burgos, D.C. Jones, L.C. Andrew, H. Rodriguez, M. Suarez, A.H. Fairlamb, D.S. Wishart, Development of a novel virtual screening cascade protocol to identify potential trypanothione reductase inhibitors, J. Med. Chem. 52 (2009) 1670–1680. doi:10.1021/jm801306g.

[15] C.S. Bond, Y. Zhang, M. Berriman, M.L. Cunningham, A.H. Fairlamb, W.N. Hunter, Crystal structure of Trypanosoma cruzi trypanothione reductase in complex with trypanothione, and the structure-based discovery of new natural product inhibitors, Structure. 7 (1999) 81–89. doi:10.1016/S0969-2126(99)80011-2.

[16] L.S.C. Bernardes, C.L. Zani, I. Carvalho, Trypanosomatidae Diseases: From the Current Therapy to the Efficacious Role of Trypanothione Reductase in Drug Discovery, Curr. Med. Chem. 20 (2013) 2673–2696. doi:10.2174/0929867311320210005.

[17] S. Krieger, W. Schwarz, M.R. Arlyanayagam, A.H. Fairlamb, R.L. Krauth-Siegel, C. Clayton, Trypanosomes lacking trypanothione reductase are avirulent and show increased sensitivity to oxidative stress, Mol. Microbiol. 35 (2000) 542–552. doi:10.1046/j.1365-2958.2000.01721.x.

[18] C. Chan, H. Yin, J. Garforth, J.H. McKie, R. Jaouhari, P. Speers, K.T. Douglas, P.J. Rock, V. Yardley, S.L. Croft, A.H. Fairlamb, Phenothiazine inhibitors of

trypanothione reductase as potential antitrypanosomal and antileishmanial drugs, J. Med. Chem. 41 (1998) 148–156. doi:10.1021/jm960814j.

[19] M.O.F. Khan, S.E. Austin, C. Chan, H. Yin, D. Marks, S.N. Vaghjiani, H. Kendrick, V. Yardley, S.L. Croft, K.T. Douglas, Use of an additional hydrophobic binding site, the Z site, in the rational drug design of a new class of stronger trypanothione reductase inhibitor, quaternary alkylammonium phenothiazines, J. Med. Chem. 43 (2000) 3148–3156. doi:10.1021/jm000156+.

[20] D. Horvath, A virtual screening approach applied to the search for trypanothione reductase inhibitors, J. Med. Chem. 40 (1997) 2412–2423. doi:10.1021/jm9603781.

[21] B.C. Galarreta, R. Sifuentes, A.K. Carrillo, L. Sanchez, M. del R.I. Amado, H. Maruenda, The use of natural product scaffolds as leads in the search for trypanothione reductase inhibitors, Bioorganic Med. Chem. 16 (2008) 6689–6695. doi:10.1016/j.bmc.2008.05.074.

[22] S.S. Chauhan, S. Pandey, R. Shivahare, K. Ramalingam, S. Krishna, P. Vishwakarma, M.I. Siddiqi, S. Gupta, N. Goyal, P.M.S. Chauhan, Novel β-carboline-quinazolinone hybrid as an inhibitor of Leishmania donovani trypanothione reductase: Synthesis, molecular docking and bioevaluation, Medchemcomm. 6 (2015) 351–356. doi:10.1039/c4md00298a.

[23] J. Rodríguez-Becerra, L. Cáceres-Jensen, J. Hernández-Ramos, L. Barrientos, Identification of potential trypanothione reductase inhibitors among commercially available β -carboline derivatives using chemical space, lead-like and drug-like filters, pharmacophore models and molecular docking, Mol. Divers. 21 (2017) 697–711. doi:10.1007/s11030-017-9747-6.

[24] https://www.ebi.ac.uk/chembl/.

[25] ChemAxon, Reactor, in, 2013, pp. Reactor was used for enumeration and reaction modeling.

[26] A.K. Ghose, V.N. Viswanadhan, J.J. Wendoloski, A knowledge-based approach in designing combinatorial or medicinal chemistry libraries for drug discovery. 1. A qualitative and quantitative characterization of known drug databases, J. Comb. Chem. 1 (1999) 55–68. doi:10.1021/cc9800071.

[27] I. Muegge, S.L. Heald, D. Brittelli, Simple selection criteria for drug-like chemical matter, J. Med. Chem. 44 (2001) 1841–1846. doi:10.1021/jm015507e.

[28] D.F. Veber, S.R. Johnson, H.Y. Cheng, B.R. Smith, K.W. Ward, K.D. Kopple, Molecular properties that influence the oral bioavailability of drug candidates, J. Med. Chem. 45 (2002) 2615–2623. doi:10.1021/jm020017n.

[29] T.I. Oprea, A.M. Davis, S.J. Teague, P.D. Leeson, Is There a Difference between Leads and Drugs? A Historical Perspective, J. Chem. Inf. Comput. Sci. 41 (2001) 1308–1315. doi:10.1021/ci010366a.

[30] Molecular Operating Environment (MOE), 2012.10; Chemical Computing Group Inc., 1010 Sherbooke St. West, Suite #910, Montreal, QC, Canada, H3A 2R7, 2012

[31] G.M. Morris, H. Ruth, W. Lindstrom, M.F. Sanner, R.K. Belew, D.S. Goodsell, A.J. Olson, Software news and updates AutoDock4 and AutoDockTools4: Automated docking with selective receptor flexibility, J. Comput. Chem. 30 (2009) 2785–2791. doi:10.1002/jcc.21256.

[32] G. Neudert, G. Klebe, DSX: A knowledge-based scoring function for the assessment of protein-ligand complexes, J. Chem. Inf. Model. 51 (2011) 2731–2745. doi:10.1021/ci200274q.

[33] R Development Core Team (2008). R: A language and environment for statistical computing. R Foundation for Statistical Computing, Vienna, Austria. ISBN 3-900051-07-0, URL http://www.R-project.org

[34] B. F. Molino, P. R. Darkes, W. R. Ewing; Tetrahydro-pyrido-indoles as cholecystokinin and gastrin antagonists. US 1990/5162336 1990

[35] F.E. Chen, J.L. Yuan, H.F. Dai, Y.Y. Kuang, Y. Chu, Synthetic Studies on d-Biotin, Part 6:1An Expeditious and Enantiocontrolled Approach to the Total Synthesis of d-Biotin via a Polymer-Supported Chiral Oxazaborolidine-Catalyzed Reduction of meso-Cyclic Imide Strategy, Synthesis (Stuttg). 2003 (2003) 2155–2160. doi:10.1055/s-2003-41051.

[36] A.L. Ruchelman, P.J. Houghton, N. Zhou, A. Liu, L.F. Liu, E.J. LaVoie, 5-(2-Aminoethyl)dibenzo[c,h][1,6]naphthyridin-6-ones: Variation of N-alkyl substituents modulates sensitivity to efflux transporters associated with multidrug resistance, J. Med. Chem. 48 (2005) 792–804. doi:10.1021/jm049447z.

[37] N. Philippe, F. Denivet, J.L. Vasse, J. Sopkova-De Olivera Santos, V. Levacher, G. Dupas, Highly stereoselective Friedel-Crafts type cyclization. Facile access to enantiopure 1,4-dihydro-4-phenyl isoquinolinones, Tetrahedron. 59 (2003) 8049–8056. doi:10.1016/S0040-4020(03)01236-5.

[38] B. Sadek, R. Alisch, A. Buschauer, S. Elz, Synthesis and dual histamine H1 and H2 receptor antagonist activity of cyanoguanidine derivatives, Molecules. 18 (2013) 14186–14202. doi:10.3390/molecules181114186.

[39] T. Ohshima, T. Shibuguchi, Y. Fukuta, M. Shibasaki, Catalytic asymmetric phase-transfer reactions using tartrate-derived asymmetric two-center organocatalysts, Tetrahedron. 60 (2004) 7743–7754. doi:10.1016/j.tet.2004.05.120.

[40] K.P. Lippke, W.G. Schunack, W. Wenning, W.E. Muller, β-Carbolines as Benzodiazepine Receptor Ligands. 1. Synthesis and Benzodiazepine Receptor Interaction of Esters of β-Carboline-3-carboxylic Acid, J. Med. Chem. 26 (1983) 499–503. doi:10.1021/jm00358a008.

[41] W. Yin, S. Majumder, T. Clayton, S. Petrou, M.L. Vanlinn, O.A. Namjoshi, C. Ma, B.A. Cromer, B.L. Roth, D.M. Platt, J.M. Cook, Design, synthesis, and subtype selectivity of 3,6-disubstituted β-carbolines at Bz/GABA(A)ergic receptors. SAR and studies directed toward agents for treatment of alcohol abuse, Bioorganic Med. Chem. 18 (2010) 7548–7564. doi:10.1016/j.bmc.2010.08.049.

[42] ChemAxon, Standardizer, in, 2013, pp. Standardizer was used for structure canonicalization and transformation.

[43] R.A. Jarvis, E.A. Patrick, Clustering Using a Similarity Measure Based on Shared Near Neighbors, IEEE Trans. Comput. C-22 (1973) 1025–1034. doi:10.1109/T-C.1973.223640.

[44] Y. Zhang, C.S. Bond, S. Bailey, M.L. Cunningham, A.H. Fairlamb, W.N. Hunter, The crystal structure of trypanothione reductase from the human pathogen Trypanosoma cruzi at 2.3 A resolution., Protein Sci. 5 (1996) 52–61. doi:10.1002/pro.5560050107.

[45] G.M. Morris, D.S. Goodsell, R.S. Halliday, R. Huey, W.E. Hart, R.K. Belew, A.J. Olson, Automated docking using a Lamarckian genetic algorithm and an empirical binding free energy function, J. Comput. Chem. 19 (1998) 1639–1662. doi:10.1002/(SICI)1096-987X(19981115)19:14<1639::AID-JCC10>3.0.CO;2-B.

Participation to congresses

- **Dal Prà, M**., Carta, D., Becerra, J. R., Ferlin, M. G. Rational design and synthesis of 2,3,4,9-tetrahydro-1*H*-β-carboline derivatives as *Trypanosoma cruzi* trypanothione reductase inhibitors. Poster presentation. XXIV National Meeting in Medicinal Chemistry & 10th Young Medicinal Chemists' Symposium, Perugia (Italy), 11-14 September 2016.

- **Dal Prà, M**., Carta, D., Suman, M., De Martin, S., Ferlin, M.G. Targeting NR RORs by novel synthetic steroidal inverse agonists for autoimmune diseases. Poster presentation. EFMC-ASMC'17, International Symposium on Advances in Synthetic and Medicinal Chemistry, Vienna (Austria), 27-31 August 2017.

- **Dal Prà, M.**, Ferlin, M.G., Brun, P., Bernabè, G., Castagliuolo, I., Carta, D. Assessing the anti-virulence effect of Diflunisal aza-analogs for combatting antibiotic resistance. Poster presentation. EFMC-ASMC'17, International Symposium on Advances in Synthetic and Medicinal Chemistry, Vienna (Austria), 27-31 August 2017.

- **Dal Prà, M**., Bortolozzi, R., Carta, D., Sturlese, M., Antoniazzi, G., Di Paolo, V., Moro, S., Hamel, E., Calderan, L., Quintieri, L., Viola, G., Ferlin, M.G. Potent *in vitro* and *in vivo* anticancer fluorinated 7-phenyl-pyrroloquinolinones. Poster presentation. VII European Workshop in Drug Synthesis, Siena (Italy), 20-24 May 2018.

- **Dal Prà, M**., Bortolozzi, R., Carta, D., Sturlese, M., Antoniazzi, G., Di Paolo, V., Moro, S., Hamel, E., Calderan, L., Quintieri, L., Viola, G., Ferlin, M.G. Fluorinated anti-tubulin phenyl-pyrroloquinolinones: in *vitro* and in *vivo* anticancer properties Poster presentation. 10th World Congress on Medicinal Chemistry and Drug Design, Barcelona (Spain), 14-15 June 2018.